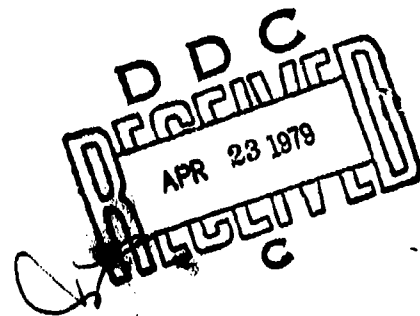USARTL-TR-78-55B

LEVEL

COMBUSTOR DESIGN CRITERIA VALIDATION
Volume II - Development Testing of Two Full-Scale Annular
Gas Turbine Combustors

H. Mongia, R. Reynolds, E. Coleman, T. Bruce
AiRESEARCH MANUFACTURING CO. OF ARIZONA
111 South 34th Street
Phoenix, Ariz. 85034

ADA067689

D D C

APR 23 1979

March 1979

Final Report for Period 2 July 1975 - 31 October 1978

Approved for public release;
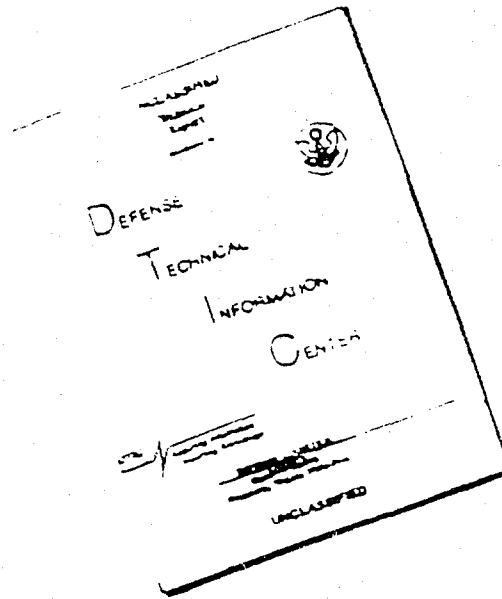distribution unlimited.

Prepared for

APPLIED TECHNOLOGY LABORATORY
U. S. ARMY RESEARCH AND TECHNOLOGY LABORATORIES (AVRADCOM)
Fort Eustis, Va. 23604

DDC FILE COPY

79 04 23 014

DISCLAIMER NOTICE

THIS DOCUMENT IS BEST
QUALITY AVAILABLE. THE COPY
FURNISHED TO DTIC CONTAINED
A SIGNIFICANT NUMBER OF
PAGES WHICH DO NOT
REPRODUCE LEGIBLY.

APPLIED TECHNOLOGY LABORATORY POSITION STATEMENT

This report describes an effort undertaken to improve small gas turbine combustor design techniques. This analytical procedure is viewed as a significant step toward reducing the design and development time and the cost associated with future Army gas turbine combustors while simultaneously achieving a more durable and fuel-efficient design. The reader is referred to the report documentation page for a description of each of the three volumes of this report. It is considered worthy of widespread application with the turbine industry. Any critique or other response regarding its use should be addressed to this agency.

Mr. Kent Smith of the Propulsion Technical Area, Aeronautical Technology Division, served as Project Engineer for this effort.

REPORT DOCUMENTATION PAGE		READ INSTRUCTIONS BEFORE COMPLETING FORM
1. REPORT NUMBER USARTL-TR-78-55B	2. GOVT ACCESSION NO.	3. RECIPIENT'S CATALOG NUMBER
4. TITLE (and Subtitle) COMBUSTOR DESIGN CRITERIA VALIDATION. VOLUME II — Development Testing of Two Full-Scale Annular Gas Turbine Combustors		5. TYPE OF REPORT & PERIOD COVERED Final Report, 2 July 1975-31 Oct 1978
		6. PERFORMING ORG. REPORT NUMBER 75-211682(38)-2
7. AUTHOR(s) H. Mongia, T. Bruce R. Reynolds, E. Coleman		8. CONTRACT OR GRANT NUMBER(s) DAAJ02-75-C-0044
9. PERFORMING ORGANIZATION NAME AND ADDRESS AiResearch Manufacturing Co. of Arizona 111 South 34th Street Phoenix, Arizona 85034		10. PROGRAM ELEMENT, PROJECT, TASK AREA & WORK UNIT NUMBERS 62209A 1F262209AH76 00 079 EK
11. CONTROLLING OFFICE NAME AND ADDRESS Applied Technology Laboratory, U.S. Army Research and Technology Laboratories (AVRADCOM) Fort Eustis, Virginia 23064		12. REPORT DATE Mar 1979
		13. NUMBER OF PAGES 253
14. MONITORING AGENCY NAME & ADDRESS(If different from Controlling Office)		15. SECURITY CLASS. (of this report) Unclassified
		15a. DECLASSIFICATION/DOWNGRADING SCHEDULE

16. DISTRIBUTION STATEMENT (of this Report)

Approved for public release; distribution unlimited.

17. DISTRIBUTION STATEMENT (of the abstract entered in Block 20, If different from Report)

18. SUPPLEMENTARY NOTES

Volume II of a three-volume report

19. KEY WORDS (Continue on reverse side if necessary and identify by block number)

Small Gas Turbines
Analytical Models

20. ABSTRACT (Continue on reverse side if necessary and identify by block number)

This report describes the development testing of two full-scale, reverse-flow, annular combustor systems that were designed based on the empirical/analytical design procedures described in Volume I. The baseline, Concept I, configuration met all design objectives with no hardware modifications. Concept II met the design objectives after only one major hardware modification design procedure for these two test concepts, the combustor-development

DD FORM 1473 EDITION OF 1 NOV 65 IS OBSOLETE

404 776

79 04 23

time was significantly reduced, meeting the main objective of
the USARTL Program. Volume III is the User's Manual for the
models and includes a description of the models and a listing
of the computer codes with instructions on usage.

TABLE OF CONTENTS

LIST OF ILLUSTRATIONS

LIST OF ILLUSTRATIONS (Contd.)

LIST OF ILLUSTRATIONS (Contd.)

6

LIST OF TABLES

14

I. INTRODUCTION

During Tasks II and III of the USARTL Program, two full-scale, reverse-flow, annular combustion systems were designed and tested based on the empirical/analytical design procedure. The Concept I combustor configuration employed 10 dome swirlers that created 10 discrete recirculation bubbles. Concept II (the second combustor configuration) had a continuous, one-sided primary zone, as established by 20 primary slots on the outer diameter liner, that injected the air toward the dome. Both concepts used 10 radial/tangential air-assist/airblast nozzles.

The baseline Concept I configuration met all design objectives, as summarized in Table 1, with no hardware modifications. Concept II met the design objectives after one major hardware modification. Consequently, by using the empirical/analytical design procedure for these two test concepts, the combustor-development time was significantly reduced, meeting the main objective of the USARTL Program.

The following six computer codes were developed and refined as described in Volume I.

- 3-D Combustor Performance Model
- Liner Cooling Model
- Transition Liner Mixing Model
- Gaseous Emissions Model
- Fuel Insertion Model
- Annulus Flow Model

The internal flow-field characteristics, including combustion efficiency, exhaust-temperature quality, and lean blowout are predicted by a 3-D recirculating (elliptic) reacting flow program. An accurate prediction of the practical cooling band performance and attendant liner temperature levels and gradients

15

TABLE 1. COMBUSTOR FLOW PARAMETERS, PERFORMANCE GOALS, AND ACHIEVED PERFORMANCE.

Performance Parameters	Performance Goal	Performance Concept I	Achieved Concept II
Engine airflow, kg/s	1.302	1.315	1.315
Combustor inlet pressure, MPa	1.01	1.01	1.01
Combustor inlet temperature, K	625	621	625
Combustor exit temperature, K	1533	1539	1528
Combustion efficiency, %			
Idle	98.0	98.08	99.57
Maximum power	99.5	99.99	99.99
Pressure drop, % P_{t3}	3.0	2.5	1.7
Pattern factor	0.23	0.17	0.22
Radial pattern factor	0.075	0.014	0.044
Maximum wall temperature, K	1144	1047	1144
Lean blowout, F/A	0.004	0.003	0.003
SAE smoke number	34	0	8.5
NO_x, kg/kw-hr/cycle	0.077	0.034	0.041

is essential for estimating the life of a new combustor. A 2-D parabolic program is used for analyzing near the wall flow regions. Appropriate initial and edge conditions are supplied by the combustor performance program. A 2-D parabolic program is used to predict the mixing rate in the transition liner of reverse-flow annular combustors.

In order to better estimate the gaseous pollutants emitted by a given combustor design, and to aid in the design of new combustion systems with minimal emissions, a 2-D parabolic program with a complex kinetic scheme was also developed. A fuel-insertion model provides a rough estimate of fuel nozzle system performance with respect to desirable or predicted combustor internal flow-field characteristics. A one-dimensional annulus-flow model is used to calculate the pressure losses and airflow distribution around the combustor liner. Information provided by this model on the jet velocities and efflux angles for the various orifices around the combustor liner is supplied to the combustor internal flow programs. Validation of these models was done with the experimental data obtained during Task I of the USARTL Program, as described in Volume I.

II. EMPIRICAL/ANALYTICAL DESIGN PROCEDURE

The conventional approach to the design and development of gas turbine combustion systems involves an extensive use of empirical correlations derived from experimental data, followed by a series of component-development tests. Through the years, a number of empirical and semi-empirical correlations have been developed by engine manufacturers to provide guidelines for the initial design of combustion systems and to predict attainable performance on the basis of experience trends. Consideration must be given to numerous combustor-design criteria including: combustion efficiency; pressure drop; lean flameout and ignition characteristics; exhaust-temperature quality; combustor life, size, and weight; and gaseous, particulate, and noise emissions. Many of these requirements are conflicting, and must be resolved through engineering compromises aided by component-development testing.

A number of design correlations are used including loading parameters, heat-release rate, combustor reference velocity and residence time, liner cooling-flow requirement and pressure drop, and dilution-zone length and residence time. Other factors requiring engineering judgement have not been amenable to simple quantitative correlations. These include combustor surface-to-volume ratio, number of fuel nozzles and their configuration (pressure atomizers including simplex/duplex or airblast) and mode of insertion (axial versus radial/tangential), nozzle spacing, axial location and orientation with respect to the recirculation zone, and interaction between fuel nozzle and flow-field characteristics. However, the empirical-design approach has historically been fairly successful in developing combustors that are based on proven design concepts.

In recent years, however, a trend of increasing time and cost required to fully develop combustors suitable for advanced gas turbine engines has been noted by industry as well as Government. Combustor performance is determined by its internal flow-field characteristics, which are strongly influenced by a number of variables. These include:

- Primary-zone volume

- Equivalence ratio

- Level and scale of mixedness

- Fuel-nozzle spray characteristics and orientation with respect to the recirculation zone

- Combustor-inlet pressure and temperature

- Combustor residence time.

Combustor analytical models can be used to provide a better understanding of the fluid mechanics and chemical kinetics involved in the overall combustion processes in gas turbine combustors. Although much more experimentation and modeling are required to further improve the accuracy of analytical models, as reported in Volume I, the models are developed to a stage where they can be effectively used to augment the empirical design procedure, and thereby can minimize combustor-development time and expenditures.

Good agreement was achieved with the model predictions and experimental measurements. This led to the conclusion that the models can be used for predicting the effects of detail design changes on combustor performance. The advanced combustor design

procedure, based upon empirical correlations and the use of analytical models, shows a potential for effecting a significant reduction in the development cycle time and cost, which is the main objective of the USARTL Program. This objective was realized in this program, as described in Section IV. A brief description of the advanced design procedure is given in the following paragraphs.

A.   Advanced Combustor Design Procedure Logic

A schematic of the empirical/analytical design procedure logic is outlined in Figure 1. After a new engine envelope has been defined with associated component constraints and an engine fuel schedule defined, a preliminary design of the combustor is executed in the usual fashion by utilizing various "experience" correlations. A number of preliminary design iterations are needed to satisfy conflicting performance objectives.

If the final empirically-designed combustor appears to be quite close to existing production combustor configurations (providing confidence in the applicability of the empirical correlations), an experienced combustion engineer may choose to bypass the analytical design path. Consequently, detail drawings are prepared and the combustor is fabricated and subjected to rig development testing with minimal support from analytical models. However, if the new engine envelope forces the consideration of combustor concepts that lie outside the designer's experience and/or empirical correlations, the models can be used to parametrically study the effects of detail design changes on combustor performance. The predicted effect of airflow distribution, jet velocities and efflux angles, spray characteristics, and geometrical relationships can be evaluated in light of the combustion engineer's development experience and intuitive grasp of the problem.

20
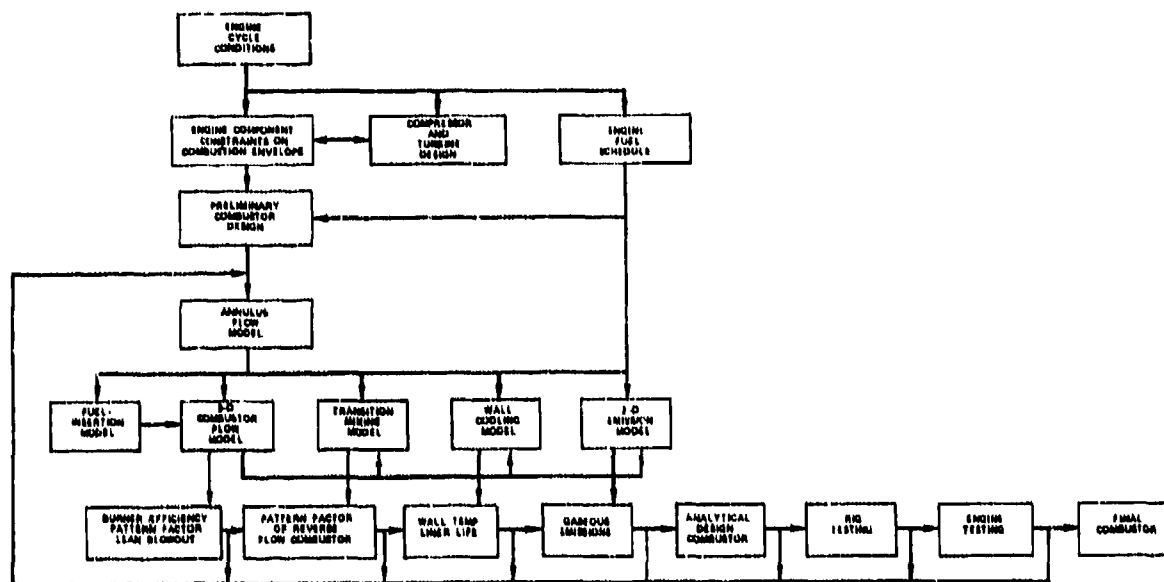
Figure 1.   Empirical/Analytical Combustor
Design Procedure Logic Chart.

21

Model predictions cannot be expected to provide an exact simulation of the complex combustor flow field because of less than satisfactory knowledge of various processes and the problem of specifying the boundary conditions. Consequently, while the models are useful guides for the combustion engineer, the final outcome is strongly determined by his ingenuity and development skill. It is, however, expected that the development time and cost will be significantly reduced by a judicious blend of development experience, models, and rig testing. Such a procedure was used in the design and development testing of two full-scale annular combustion systems under the USARTL Program, as described in Sections III and IV.

III. DESCRIPTION OF COMBUSTORS

The primary objective of the USARTL Program was to apply empirical/analytical combustor-design methodology to significantly reduce the design and development time of advanced, small, high-temperature-rise combustors for turbine engines in the 0.91 to 2.27 kg/s class. In addition to the usual design considerations common to all combustors, the design of advanced small combustion systems impose stringent design requirements in regard to liner cooling, fuel injection, discharge-temperature quality, liner carbon fouling, and idle combustion efficiency. The design requirement of a small, reverse-flow, annular combustor concept that results in a compact engine employing a centrifugal compressor, is even more demanding due in part to large surface-to-volume ratio and small combustor channel height.

The selected engine-flow conditions were such that the design combustor corrected flow rate (W_c) of 0.18 kg/s was approximately 60 percent less than that of the smallest AiResearch turbo-propulsion engine. Consequently, the scaling of the new combustor from a proven design was considered inappropriate. By not scaling, one was forced to rely more on the applicability of the analytical design tools in arriving at an optimum design. This, in turn, created an excellent test case for the validation of the advanced combustor-design approach. In addition, by having intentionally selected two radically different combustor-design concepts for the same engine envelope, the approach validation was made more thorough than possible with two slightly different designs. Both combustor concepts are described in Sections III.B and III.C. The design requirements and combustor-flow conditions are presented in Section III.A.

A. Combustor Design Objectives and Flow Conditions

The combustor design objectives and maximum power flow conditions were presented previously in Table 1.

The selected turbo-shaft engine combustor inlet flow conditions and exit temperatures at different power points from sea-level static to 6096 meters altitude are presented in Table 2.

A large number of combustion-system concepts were considered when defining the configuration that was most compatible with the compressor and turbine sections. A cross-section of a reference engine with the Concept I combustor is shown in Figure 2. Conceptual cross-sections of a reverse-flow combustor and four other basic design configurations (which utilized distinctively different flow paths) were considered during the preliminary design phase.

Application of the reverse-flow concept resulted in a compact engine; however, a major disadvantage in previous designs has been the high surface-to-volume ratio and small channel height of the combustor. These usually have required excessive amounts of cooling air, and also suffer from liner-wall fuel impingement with attendant carbon formation. Advanced cooling schemes, which showed potential for application in high-temperature-rise combustors, were not employed to minimize combustor fabrication cost.

A canted through-flow concept was evaluated, and was found to have approximately 30 percent less surface area to cool. However, this configuration required increased engine length, which in turn adds weight and potential shaft/bearing design problems. A radial-inflow combustor afforded a compromise between engine length and liner surface area required for the reverse-flow and canted through-flow concepts. However, the radial-inflow combustor resulted in an increased engine frontal area, which is considered unacceptable in turbo-propulsion applications. The problems of providing sufficient strength and durability to radial side-walls, adequate residence time for complete combustion in a strongly accelerating flow field, and adequate dilution-jet penetration were major design considerations for this concept.

24

TABLE 2. COMBUSTOR FLOW CONDITIONS FOR M = 0.

Altitude, Feet (m)	Maximum Power, %	$T_{3.1}$ °R (k)	$P_{3.1}$ psia (kPa)	$W_{a3.1}$ lb/sec (kg/s)	W_c lb/sec (kg/s)	Fuel/Air Ratio	T_4 °R (k)
0 (0)	100	1124.3 (624.6)	146.9 (1012.9)	2.696 (1.223)	0.397 (0.180)	0.0268	2759.6 (1533.3)
	75	1073.7 (596.5)	127.8 (881.2)	2.445 (1.109)	0.405 (0.184)	0.0238	2550.5 (1416.9)
	55	1025.4 (569.7)	110.3 (760.5)	2.197 (0.997)	0.412 (0.187)	0.0212	2363.0 (1312.8)
	35	963.4 (535.2)	90.0 (620.7)	1.891 (0.858)	0.421 (0.191)	0.0182	2135.5 (1186.4)
	6	816.4 (453.6)	53.6 (369.7)	1.256 (0.570)	0.432 (0.196)	0.0140	1720.6 (955.9)
5000 (1524)	100	1107.0 (615.0)	128.5 (886.0)	2.358 (1.070)	0.394 (0.179)	0.0271	2760.0 (1533.3)
	77	1057.6 (587.6)	112.6 (776.6)	2.151 (0.976)	0.401 (0.182)	0.0242	2560.0 (1422.2)
	54	1005.2 (558.4)	96.0 (662.4)	1.916 (0.869)	0.408 (0.185)	0.0215	2360.0 (1311.1)
	34	949.6 (527.6)	79.9 (551.5)	1.670 (0.757)	0.415 (0.188)	0.0189	2160.0 (1200.0)
	18	889.0 (493.9)	64.6 (446.0)	1.420 (0.644)	0.422 (0.191)	0.0166	1960.0 (1088.9)
	5	819.1 (455.1)	50.1 (435.6)	1.162 (0.527)	0.428 (0.194)	0.0148	1760.0 (977.8)

TABLE 2. COMBUSTOR FLOW CONDITIONS FOR M = 0. (Contd)

Altitude, Feet (m)	Maximum Power %	$T_{3.1}$ °R (k)	$P_{3.1}$ psia (kPa)	$W_{a3.1}$ lb/sec (kg/s)	W_c lb/sec (kg/s)	Fuel/Air Ratio	T_4 °R (k)
10000 (3048)	100	1089.1 (605.1)	111.5 (769.0)	2.046 (0.928)	0.391 (0.171)	0.0275	2760.0 (1533.3)
	78	1040.7 (578.2)	98.4 (678.9)	1.880 (0.853)	0.398 (0.181)	0.0246	2560.0 (1422.2)
	56	989.3 (549.6)	84.3 (581.8)	1.682 (0.763)	0.405 (0.184)	0.0218	2360.0 (1311.1)
	37	934.8 (519.3)	70.4 (485.7)	1.471 (0.667)	0.412 (0.187)	0.0193	2160.0 (1200.0)
	20	875.8 (486.5)	57.1 (393.8)	1.254 (0.569)	0.419 (0.190)	0.0170	1960.0 (1088.9)
	6	809.3 (449.6)	44.6 (307.6)	1.034 (0.469)	0.426 (0.193)	0.0152	1760.0 (977.8)
15000 (4572)	100	1070.8 (594.9)	95.9 (661.8)	1.761 (0.799)	0.387 (0.176)	0.0278	2760.0 (1533.3)
	79	1023.0 (568.3)	85.2 (587.7)	1.627 (0.738)	0.394 (0.179)	0.0249	2560.0 (1422.2)
	59	972.6 (540.3)	73.5 (507.2)	1.466 (0.665)	0.401 (0.182)	0.0220	2360.0 (1311.1)
	39	919.2 (510.7)	61.5 (424.6)	1.286 (0.584)	0.408 (0.185)	0.0197	2160.0 (1200.0)
	22	(487.6)	(435.2)	(0.498)	(0.189)		(1088.9)
	8	798.0 (443.3)	39.3 (271.3)	0.911 (0.413)	0.422 (0.191)	0.0158	1760.0 (977.8)

TABLE 2. COMBUSTOR FLOW CONDITIONS FOR M = 0. (Contd)

Altitude, Feet (m)	Maximum Power %	$T_{3.1}$ °R (k)	$P_{3.1}$ psia (kPa)	$W_{a3.1}$ lb/sec (kg/s)	W_c lb/sec (kg/s)	Fuel/Air Ratio	T_4 °F (k)
20000 (6096)	100	1051.7 (584.3)	81.5 (562.2)	1.496 (0.679)	0.384 (0.174)	0.0282	2760.0 (1533.3)
	81	1004.3 (557.9)	73.1 (504.1)	1.396 (0.633)	0.390 (0.177)	0.0253	2560.0 (1422.2)
	61	955.2 (530.7)	63.6 (438.6)	1.268 (0.575)	0.397 (0.180)	0.0226	2360.0 (1311.1)
	41	902.6 (501.4)	53.4 (368.3)	1.115 (0.506)	0.405 (0.184)	0.0202	21.60.0 (1200.0)
	24	846.4 (470.2)	43.5 (300.3)	0.956 (0.434)	0.412 (0.187)	0.0181	1960.0 (1088.9)
	10	784.5 (435.8)	34.2 (236.3)	0.794 (0.360)	0.419 (0.190)	0.0166	1760.0 (977.8)
	0	707.2 (392.9)	24.9 (172.2)	0.614 (0.279)	0.422 (0.191)	0.0165	1560.0 (866.7)

27
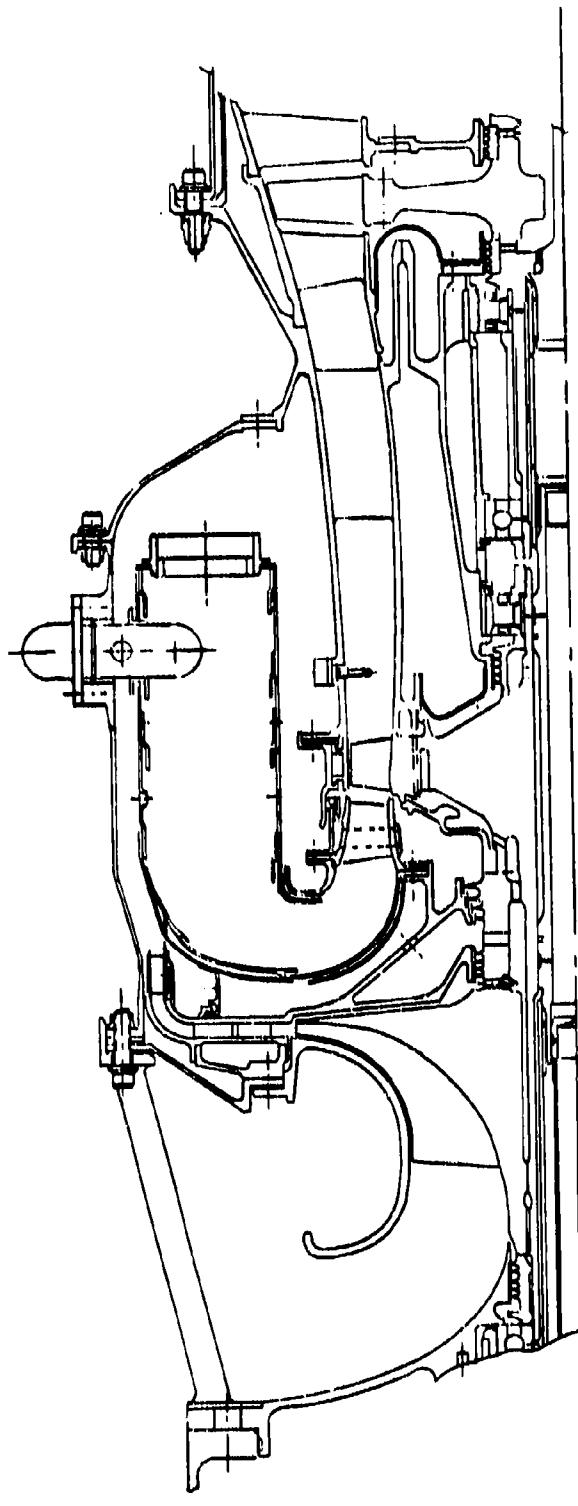
Figure 2. Army Combustor Engine Layout.

28

More advanced combustor concepts, such as a toroidal combustor, were not considered as potential candidates because of the inability of the analytical models to predict such a complex flow field. In order to minimize hardware expenses, it was necessary to use an existing rig with minimum modifications, and one set of fuel nozzles for both combustor concepts.

B. Design of Concept I

A schematic of the Concept I basic configuration is presented in Figure 3 along with the airflow distribution, as estimated by the annulus flow model. Ten individual recirculation bubbles are established by 10 equi-spaced 60-degree axial swirlers located at the combustion dome. These swirlers flow 12.01 percent of the combustor inlet total airflow (W_{a3}). An additional 8.68-percent W_{a3} air is used for cooling the dome region in between the dome swirlers, corresponding to a cooling flow rate of 0.56 g/s cm^2.

The liner outer wall uses 21.53 percent and the inner wall uses 15.08 percent of the compressor-discharge air for cooling, which correspond to 0.35 and 0.38 g/s cm^2 of surface area, respectively. An additional 5.80 percent of the total air is used for cooling the outer and inner transition liners. The first-stage stator and turbine rotor is cooled by 6.00 percent of the compressor-discharge air. This turbine cooling air is also used for convection cooling of the cold side of the outer transition liner (Figure 2). A total of 51 percent of the combustor air is used for cooling purposes to achieve a long-life combustor.

Ten equi-spaced air-assist/airblast fuel nozzles, with a flow number of 0.52 Kg/hr/(kPa)$^{1/2}$ per nozzle, injected the fuel radially into the combustor with a 35-degree down angle from the tangent and a 25-degree back angle from the liner circumference. Here, a 90-degree down angle is defined along-the-combustor-radius, whereas a 90-degree back angle indicates that the fuel is
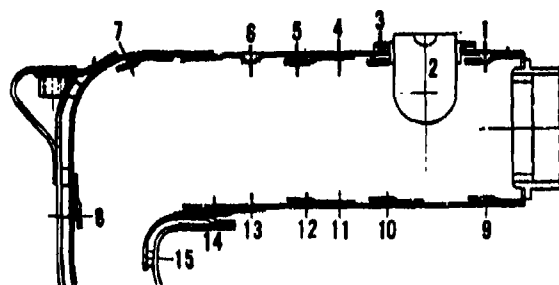
Row No.	Type of Orifice	Number of Orifices	Diameter mm	Total Area mm^2	Airflow % Total
Outside Diameter					
1	Cooling	86	2.2	340.5	9.67
		34	0.5		
2	Primary	20	4.0	251.4	7.21
3	Cooling	60	1.9	260.4	6.95
		20 slots	3.8 x 1.1		
4	Interme-diate	30	2.3	121.8	3.36
5	Cooling	90	1.6	189.7	4.91
6	Dilution	30	3.6	300.1	8.05
7	Cooling	90	1.2	98.6	2.15
8	Cooling	90	1.2	96.5	2.10
Inside Diameter					
9	Cooling	90	1.9	260.0	6.89
10	Cooling	90	1.6	178.1	4.50
11	Interme-diate	30	2.3	127.3	3.43
12	Cooling	60	1.3	83.8	2.15
13	Dilution	30	2.9	202.8	5.60
14	Cooling	60	1.1	60.2	1.54
15	Cooling	60	1.1	60.2	1.55

NOTE: 10 Swirlers: Area = 547.8 mm^2; Airflow = 12.02%
Air-Assist Airblast Nozzles: Airflow = 9.49%
Dome Louvers: Area = 301.3 mm^2; Airflow = 8.68%
Total Liner Cooling Air = 51.09%

Figure 3. Concept I Basic Configuration.

injected toward the dome. The spray origin is located 1.90 cm downstream from the dome, and 2.92 cm from the combustor inner diameter. The spray angular orientation is 9 degrees, whereas the swirler center is located 9 degrees downstream from the spray origin along the direction of the combustor inlet swirl.

The fuel nozzles are inserted through floating grommets to minimize air leakage. The grommet centerline is located 2.87 cm downstream from the combustor dome, and 10.14 degrees from the swirler centerline. The nozzle circumferential spacing, based upon the liner mean diameter, is 6.31 cm, giving a 1.44 h nozzle spacing; where h, the combustor channel height, is 4.4 cm. The combustor channel height between the cooling slots is 4.1 cm.

The primary-zone airflow rate, as defined by the summation of the air through the dome, fuel nozzles, and half of the primary orifices, is 33.8 percent, giving an equivalence ratio of 1.17 at the sea-level design point. The primary-zone equivalence ratio at sea-level, flight idle is 0.61.

The dilution orifices are located 7.75 cm downstream from the dome, giving a combustor length of 1.76 h to complete the combustion. This combustor length is considerably smaller than other AiResearch turbo-propulsion combustors so as to minimize the cooling-air requirement. Even with 51-percent cooling air, and approximately 40-percent combustion air, only a small fraction of the combustor air is left for dilution and for trimming the exhaust-temperature profile. Although approximately a 25-percent reduction in the cooling-air requirement was expected to be achieved by using an extended surface geometry, as demonstrated in Reference 1, a low-cost, less-efficient, conventional film band geometry was used instead to minimize hardware cost.

The compressor discharge Mach number and swirl angle down-
stream of the deswirl vanes were 0.15 and 35 degrees, respec-
tively. Due to relatively large manufacturing tolerances asso-
ciated with the sheet metal combustor liner and plenum, the com-
bustor annulus height was maintained at 0.95 cm. The annulus
inlet flow was decelerated to M=0.11, with a resultant decrease
in the heat-transfer rate from the cold side. Different empiri-
cal correlations for both Concepts I and II are presented in
Table 3. The major parameters of interest for both concepts,
i.e., heat release rate, loading parameter, residence time, and
pressure drop, are comparable with typical AiResearch advanced
reverse-flow combustors. Detail drawings of the Concept I com-
bustor liner (Dwg. 3551511), inner transition line (Dwg.
3551522), outer transition liner (Dwg. 3551527), combustor plenum
(Dwg. 3551513), dome swirler (Dwg. 3551540), and fuel nozzle
envelope (Dwg. SKP17134) are presented in Appendix A.

The Concept I performance was predicted by using different
combustor analytical models. The prediction of these models and
their correlation with measured data are discussed in Section V.
A qualitative discussion is given here for the approach taken in
attaining the optimum configuration in regard to combustion effi-
ciency, exhaust-temperature quality, fuel/air distribution, wall
temperature levels and gradients, and lean blowout. Fourteen
computer runs were made with the 3-D Combustor Performance
Model. Only a portion of the total combustor equivalent length
was analyzed in order to get the required field resolution within
acceptable computer time. One nozzle sector (comprised of 36-
degrees and 12.9 cm length) was divided into 28x17x13 nodes along
axial, radial, and circumferential directions, respectively.
Variations of the following baseline configuration were analyzed.

The baseline configuration was analyzed with fuel spray-
cone angle α = 90 degrees, Sauter Mean Diameter (SMD) = 30
microns, back angle β = 35 degrees, down angle = 25 degrees, and
dome swirler vane angle of 60 degrees. Different airflow splits

32

TABLE 3. COMPARISON OF CONCEPTS I AND II.

	Concept I	Concept II
Combustor inlet pressure, MPa	1.01	1.01
Combustor inlet temperature, K	625	625
Airflow rate, kg/s	1.22	1.22
Corrected flow, kg/s	0.18	0.18
Fuel flow, kg/h	117.98	117.98
Burner exit temperature, K	1533	1533
Burner OD, cm	24.5	24.4
Burner ID, cm	15.7	15.7
Burner length, cm	7.6	8.8
Burner volume, cm^3	2113	2276
Surface/volume ratio, cm^{-1}	0.46	0.46
Reference velocity, m/s	7.80	7.88
Heat release rate, $J/s\ m^3 P_a$	655	608
Loading parameter, $kg/s\ m^3$	1.03	0.96
Residence time, msec	9.77	10.51
Number of nozzles	10 (3 start)	10 (3 start)
Nozzle spacing S/H	1.44	1.45
Annulus Mach No., M	0.11	0.11
Swirl angle, degrees	35	35
$\Delta P/P$, %	2.5	1.70

around the primary zone were evaluated. In addition, the effects
of the following geometrical changes relative to the baseline
configuration on the combustor internal flow field were investi-
gated:

- Mod 1: Eliminate both O.D. and I.D. secondary orifices
  (Row numbers 4 and 11 of Figure 3) and add the corres-
  ponding amount of air through O.D. and I.D. dilution
  orifices.

- Mod 2: Eliminate O.D. secondary orifices and add an
  increased airflow rate through O.D. primary orifices.

- Mod 3: Move I.D. secondary orifice row number 11
  upstream inline with O.D. primary orifices.

- Mod 4: Reduce dome swirler vane angle to 45 degrees.

- Mod 5: Replace 10 dome swirlers with 10 dome louvers.

- Mod 6: Increase annulus air swirl angle from 35 to 60
  degrees.

- Mod 7: Decrease the fuel nozzle immersion by 6.9 mm.

- Mod 8: Vary nozzle spray-cone angle.

- Mod 9: Vary the spray Sauter mean diameter

- Mod 10: Vary the nozzle back angle and down angle.

Based on the above 14 computer modifications, the optimum
configuration (as presented in Figure 3) was selected. Detailed
internal flow-field predictions of this configuration are pre-
sented in Section V.A. Engineering drawings of the selected com-
bustor configuration, required rigs, and instrumentation were

prepared, fabricated, and tested as described in Section IV.B. The baseline combustor configuration, Figure 3, met all of the design objectives without any hardware modifications.

C. Design of Concept II

Application of a reverse-flow combustor (such as Concept I presented in Section III.B) results in a compact engine. However, a major disadvantage of conventional reverse-flow combustion systems has been the high surface-to-volume ratio, usually requiring excessive amounts of cooling air, particularly in small, high-temperature-rise combustors. Although the Concept I combustor length was considerably smaller than current technology combustors, it still required 51 percent of the combustor through-flow air for cooling, thus leaving only approximately 15 percent air for dilution and for trimming the exit profile. Consequently, the objective of achieving a low-pattern factor along with a low combustor-pressure drop and inlet distortion becomes a technically challenging objective.

A reduction in cooling air can be achieved, up to approximately 25 percent, by employing a film/extended surface cooling geometry. However, such a cooling scheme was not considered acceptable from cost and fabrication points of view. Therefore, a primary zone wherein the air is used effectively for both protecting the liner and for combustion was employed in Concept II, as shown in Figure 4. The combustor primary-zone flow field is established by the air injected through the orifices numbered 1, 2, 3, and 10 in Figure 4. A 13.19-percent air enters through 10 equi-spaced slots (Row number 3) at a 30-degree angle to the O.D. liner wall. Similarly, another 13.89-percent of the combustor air enters through 10 slots at Row number 2. All of these 20 inclined plane jets induce the flow toward the dome.
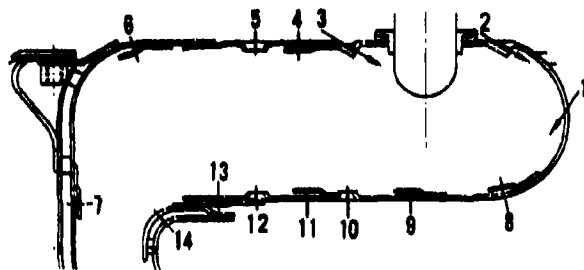
35

Row No.	Type of Orifice	Number of Orifices	Diameter mm	Total Area mm^2	Airflow % Total
Outside Diameter					
1	Dome	120	2.2	465.5	12.87
2	Primary Slot	10	64.3 x 0.76	490.0	13.89
3	Primary Slot	10	64.3 x 0.76	490.0	13.19
4	Cooling	90	1.6	189.7	4.63
5	Dilution	30	5.2	635.7	15.98
6	Cooling	90	1.2	98.6	2.04
7	Cooling	90	1.2	96.5	2.00
Inside Diameter					
8	Cooling	90	1.9	246.4	4.69
9	Cooling	90	1.5	166.9	3.21
10	Primary	30	3.3	258.9	5.68
11	Cooling	60	1.6	118.8	2.43
12	Dilution	30	3.8	344.3	8.47
13	Cooling	60	1.1	54.9	1.26
14	Cooling	60	1.1	60.2	1.38

Air-Assist Airblast Nozzles: Airflow = 8.30%
Total Liner Cooling Air = 21.64%

Figure 4. A Schematic of the Basic Concept II Configuration.

36

A semicircular dome is used with 120 orifices, 2.2 mm in diameter, eloxed tangentially to the surface of the dome to strengthen the flow field set up by the primary panel slots. The recirculation zone is terminated by 30 I.D. primary jets, indicated as Row No. 10 in Figure 4. The primary-zone cooling air is only 7.90 percent, compared to 36.70 percent in Concept I. A total of 51.10 percent air enters the primary reaction zone giving a primary-zone equivalence ratio of 0.77 at the sea-level, maximum power point.

It was expected that the air injected through Rows 1, 2, and 3 is used for protecting the primary panels as well as for taking an effective participation in combustion. Concept II uses 21.64 percent of the combustor air for cooling, compared to 51 percent used in Concept I. Consequently, 24.45 percent of the air is used for dilution and for trimming the exit-temperature profile.

Different empirical correlations for Concept II have previously been presented in Table 4. A detail drawing of the Concept II (Dwg. 3551512) liner is presented in Appendix A. It may be noticed that both combustor configurations used the same set of inner and outer transition liners, plenums, and fuel nozzles.

A number of combustor modifications were analytically assessed in regard to wall temperatures and combustor-performance parameters. In addition to studying the effect of airflow distribution around the liner, fuel nozzle axial location and orientation, and nozzle immersion (such as was done for the Concept I design), the effect of primary-jet angle on the flow field was studied. Figure 4 presents the best selected configuration. A comparison between predictions and measurement is given in Section V.B.

37

IV. COMBUSTOR TEST RESULTS

A. Test Rig Description

The test rig utilized in the performance mapping of both Concept I and II combustors to validate the predictions made by the 3-D Combustor Performance Model is shown in Figure 5. It was designed to simulate the flow from a centrifugal compressor into a reverse-flow combustor and exiting through an axial-turbine section. Combustor inlet pressures and temperatures were measured in twelve places around the plenulm annulus immediately upstream of the combustor inlet.

Combustor exit gases were monitored by an instrumentation rake, which was rotatable through 360 degrees, positioned in the plane of the leading edge of the first-stage turbine-stator to give a complete survey of the gas stream at this location. The assembled instrumentation rake, Figure 6, contains five platinum-platinum 10 percent rhodium thermocouples, three total-pressure probes, and a radially averaging water-cooled emission probe. The assembled test rig (Figure 7) was tested in a high-pressure combustion test facility.

B. Concept I Testing

1. Preliminary Testing

The basic Concept I hardware was assembled and the test rig was installed in the test facility as shown in Figure 7. Figure 8 shows the basic fuel nozzle, which had a spray cone angle of 45 degrees instead of the desired 90 degrees. The combustor inlet flow conditions, fuel-flow rates, and T_4, from sea level to 6069 meters altitude for different power settings, are tabulated in Table 2.
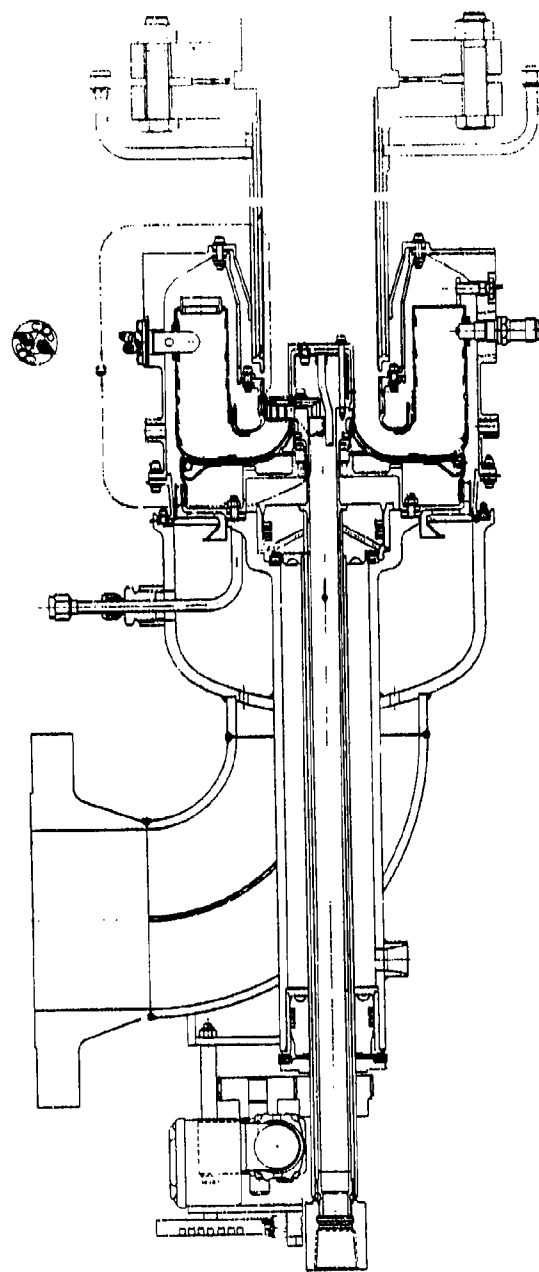
38

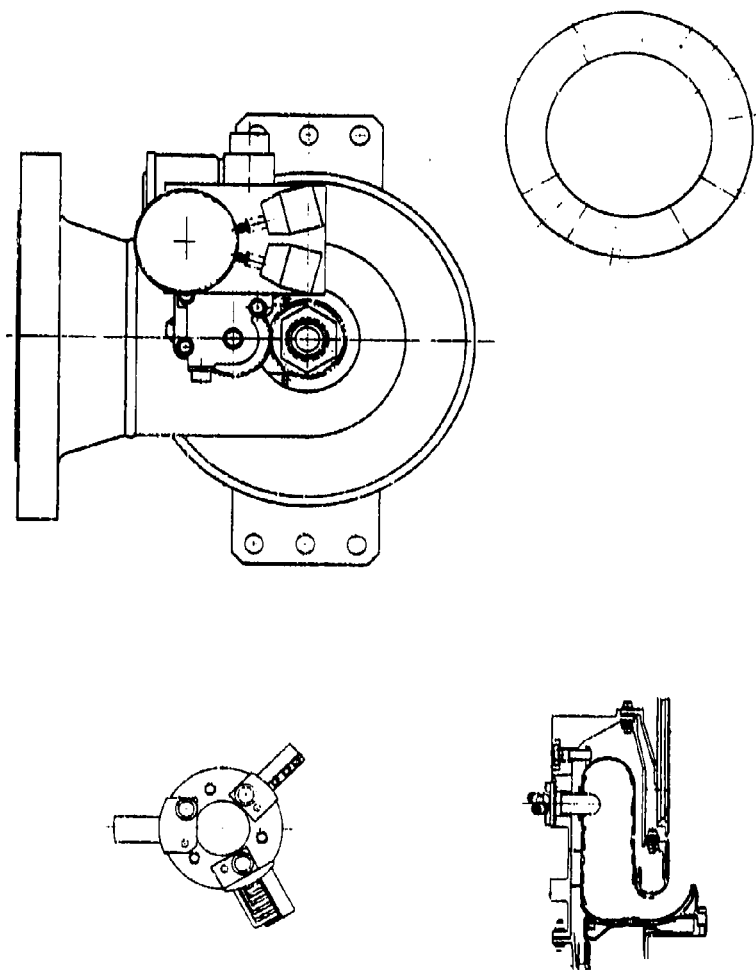Figure 5. Combustion Rig (Sheet 1 of 2).
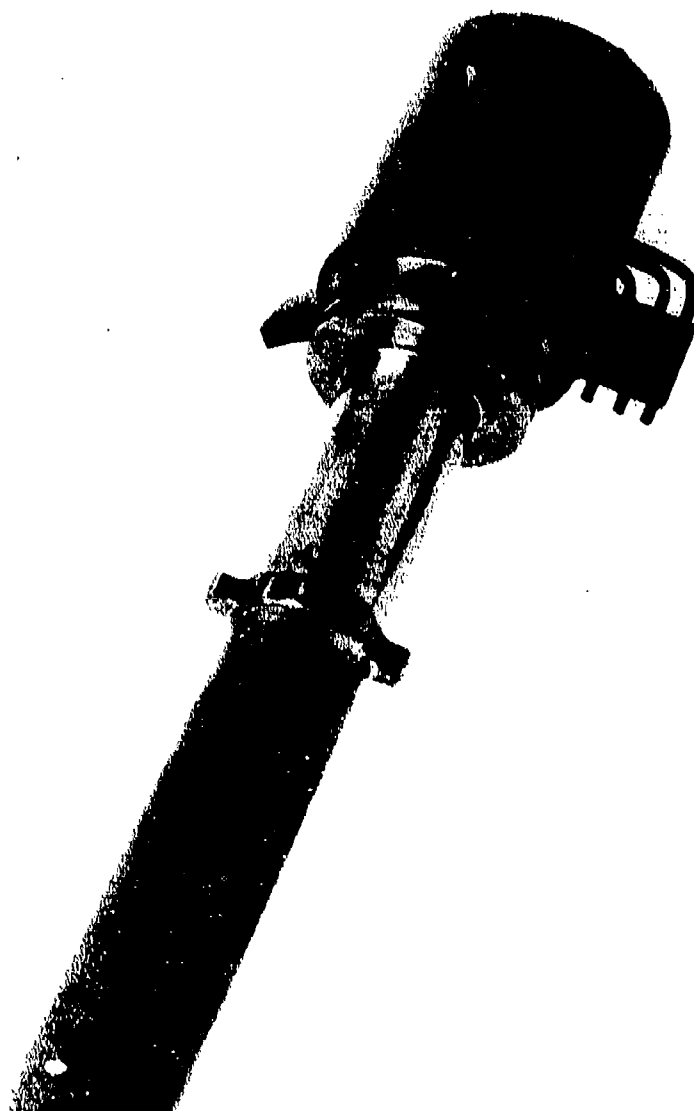
Figure 5. Combustion Rig (Sheet 2 of 2).

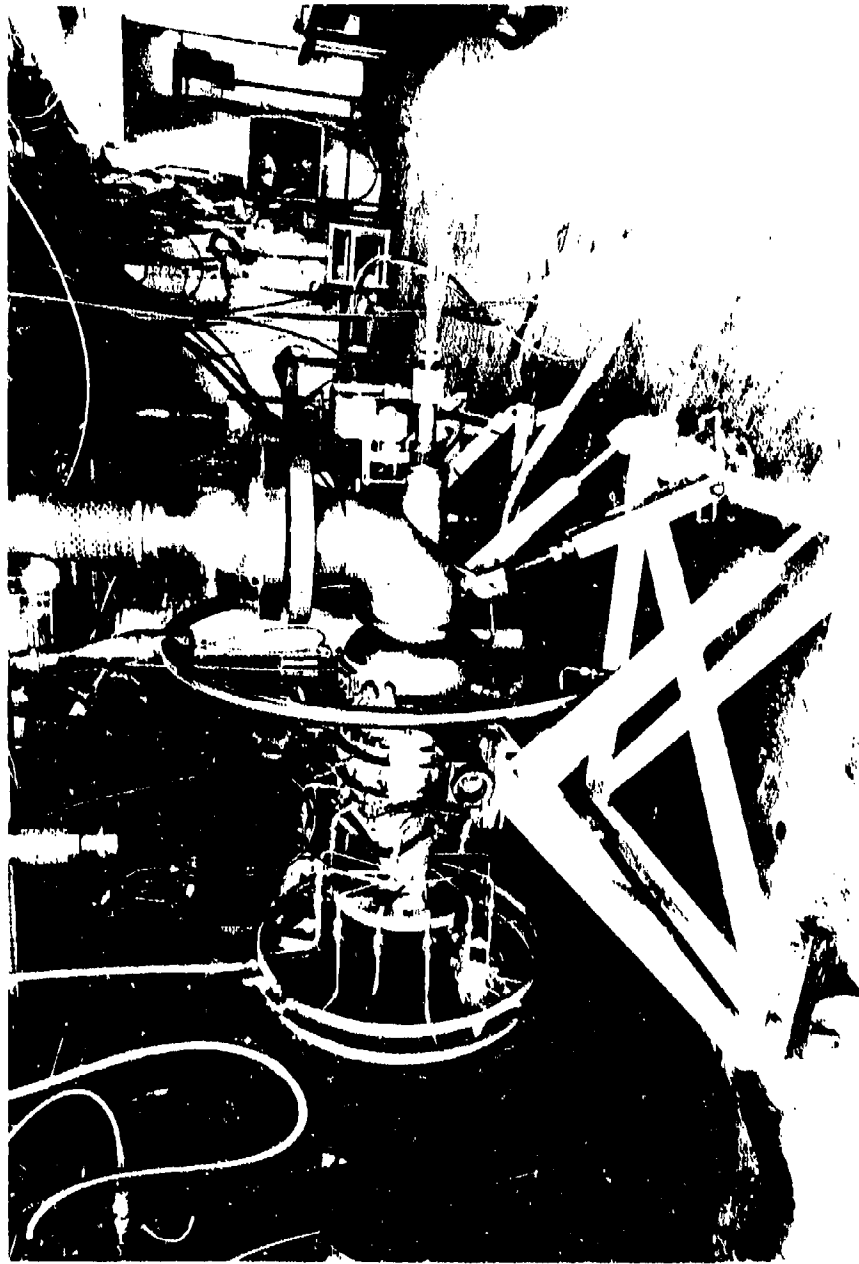Figure 6. USARTL Task II Instrumentation Drum.

41

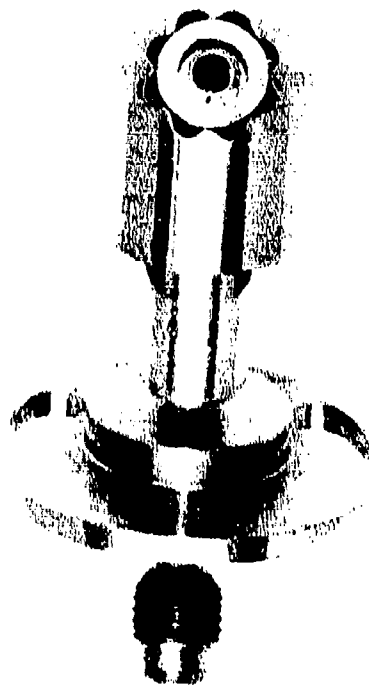Figure 7. USARTL Task II Combustor Test Rig.

42

Figure 8. Air Assist – Airblast Nozzle Used in Task II of Combustor Design Criteria Validation.

43

Results of the isothermal total pressure drop and liner static pressure drop are presented in Figure 9. At the maximum power condition the corrected flow is 0.180 Kg-per-second. The corresponding total pressure drop is 2.80 percent.

Included in the preliminary testing was the fuel nozzle immersion and back angle optimization. The test results indicated that the optimum back angle was 25 degrees, as was predicted for a 90-degree spray cone, and immersion was less than the nominal depth of 1.55 cm.

A typical discharge survey with optimum fuel nozzle positioning at the maximum power condition is presented graphically in Figures 10 and 11. Table 4 shows the same condition in tabular form. The circumferentially averaged temperature was 1470 K near the hub and the corresponding temperature near the tip was 1532 K. The circumferential pattern factor and radial pattern factors were 0.203 and 0.022, respectively, compared to the design objectives of 0.230 and 0.075.

Typical wall temperature characteristics, as indicated by OG-6 Thermindex temperature sensitive paint, are shown in Figure 12. The maximum wall temperature was 1061 K.

A preliminary evaluation of the Concept I lean blow-out characteristics was conducted at the sea-level idle and 10-percent power points at 6096 meter altitude. The blow-out fuel/air ratios of 0.010 and 0.012, respectively, with fuel flowing through all ten nozzles were unexpectedly high. The measured combustion efficiency, CO, and HC emission indices at the sea-level taxi-idle condition, but lower fuel-flow rate (f/a = 0.0107), were 95.03-percent, 79.0 and 35.5, respectively. This indicates either a highly mixed system with small-scale mixedness or the recirculation zone was not properly located with respect to the fuel nozzle. The blowout fuel/air ratio did not decrease with every other nozzle flowing, indicating good communication
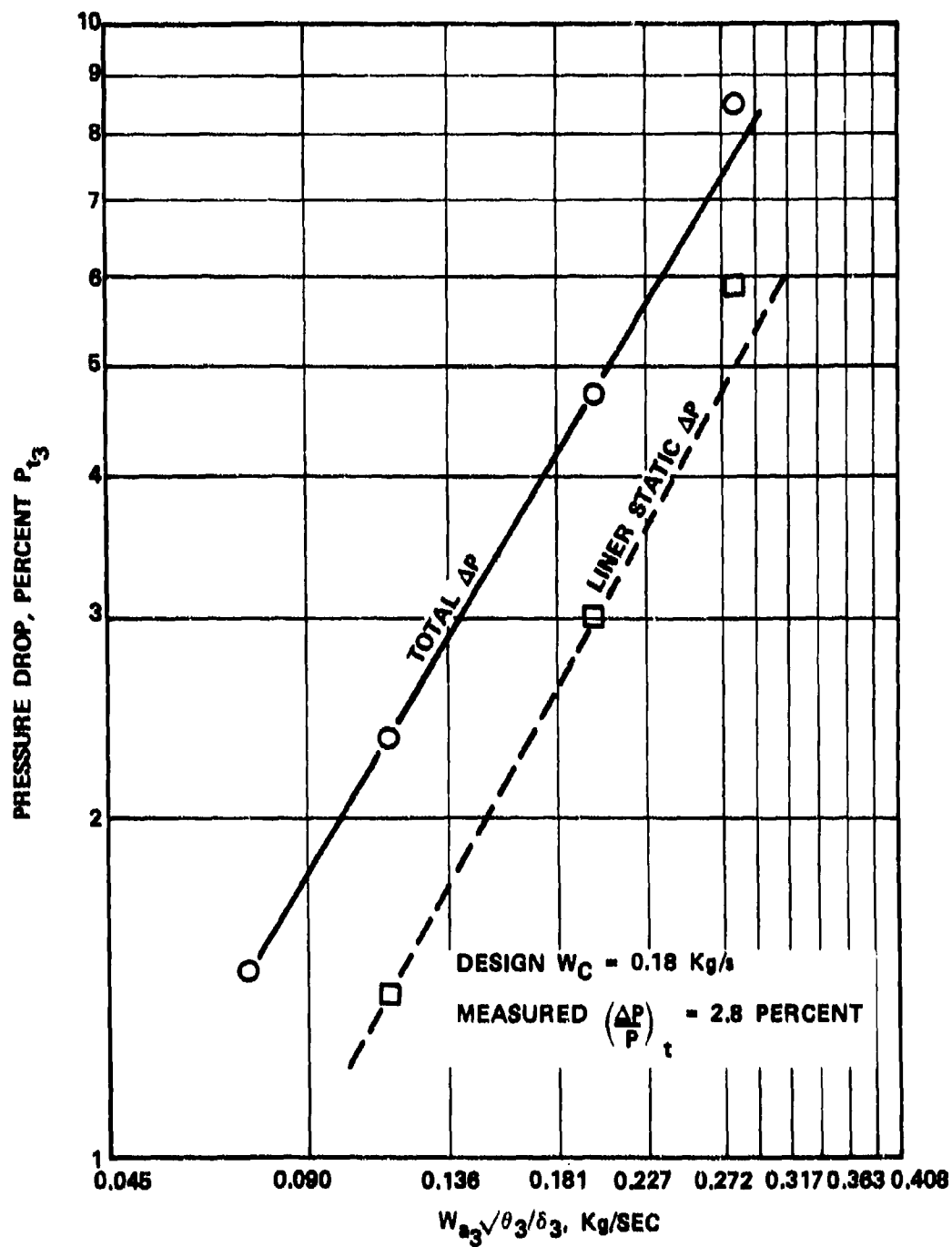
Figure 9. Measured Isothermal Pressure Drop of
Concept I.

45

WT AVG = 1529. WT TSF = 0.203 ST AVG = 1526. ST TSF = 0.208
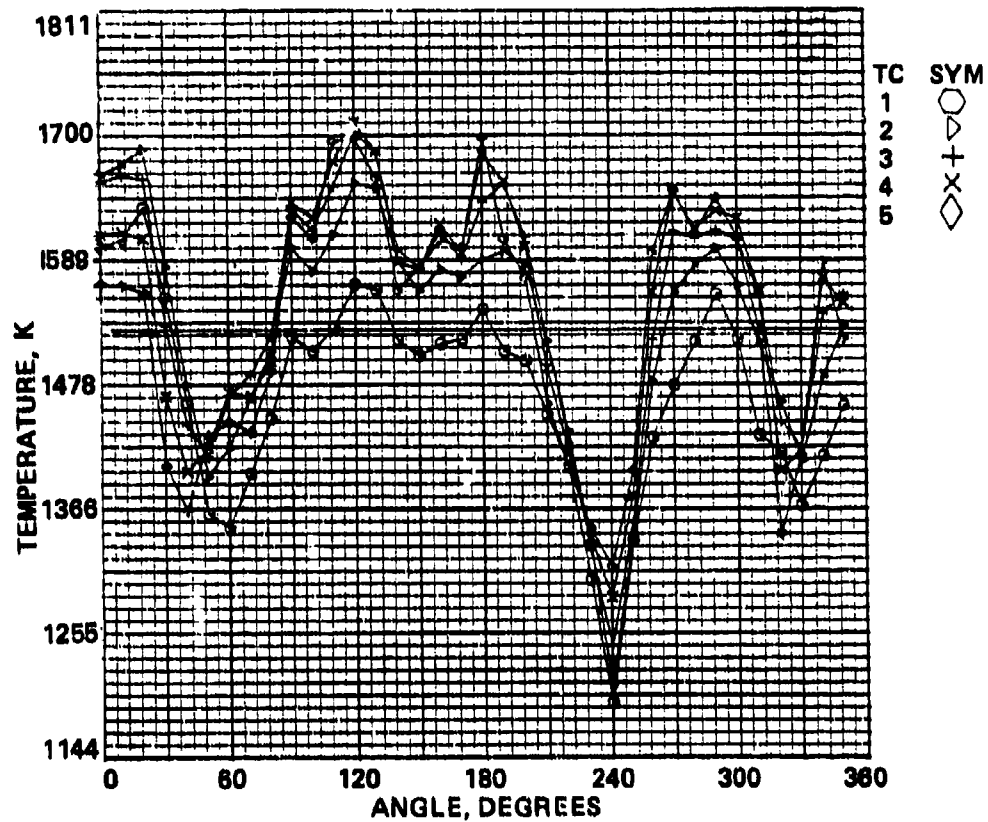

Figure 10.   Concept I Maximum Power Test with a 45-Degree
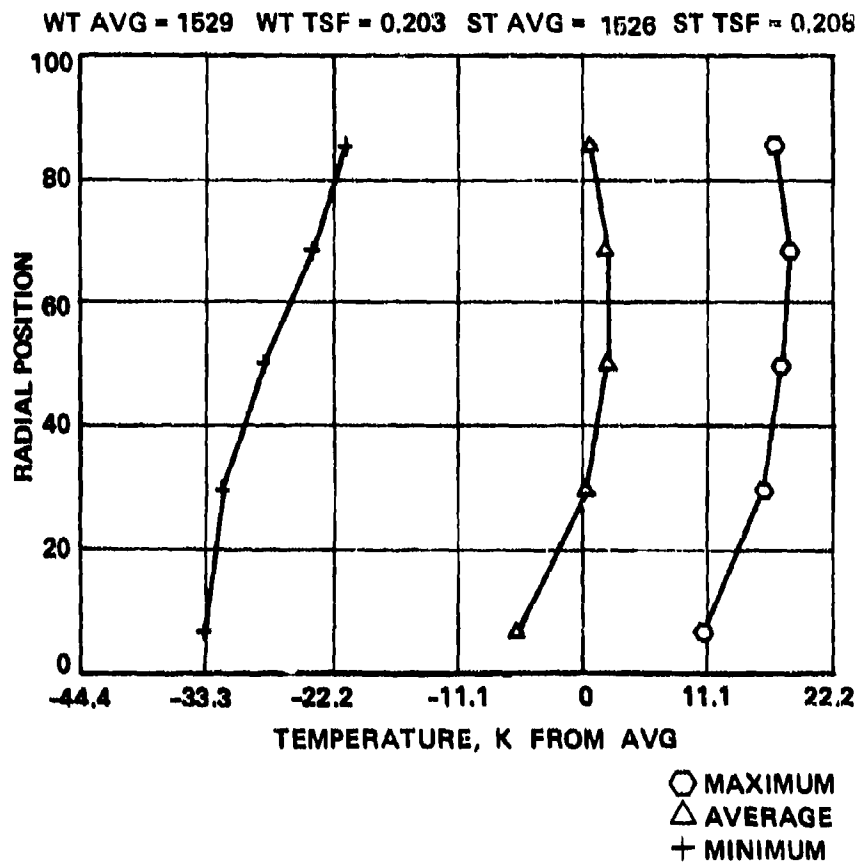   Spray Nozzle Air Assist ΔP = 689 kPa.

WT AVG = 1529   WT TSF = 0.203   ST AVG = 1526   ST TSF = 0.208

Figure 11.   Concept 1 Maximum Power Test Discharge Survey.

47

TABLE 4. T_4 TEMPERATURE SCAN OF CONCEPT I WITH REDUCED NOZZLE IMMERSION AND AIR-ASSIST ΔP = 689 kPa AT MAX POWER.

TEMPERATURES ARE IN °F

THERMOCOUPLE NO.

RADIAL VALUES—

RADIAL PATTERN FACTOR = $\dfrac{2327-2292}{2292-681}$ = 0.022

PATTERN FACTORS BASED ON INLET TEMP OF 681.

ALL TEMPS ARE FAHRENHEIT

THERMOCOUPLE JUNCTIONS ARE PLATINUM/PLATINUM 13 RHODIUM

PATTERN FACTOR = $\dfrac{2327-2292}{2292-681}$ = 0.022

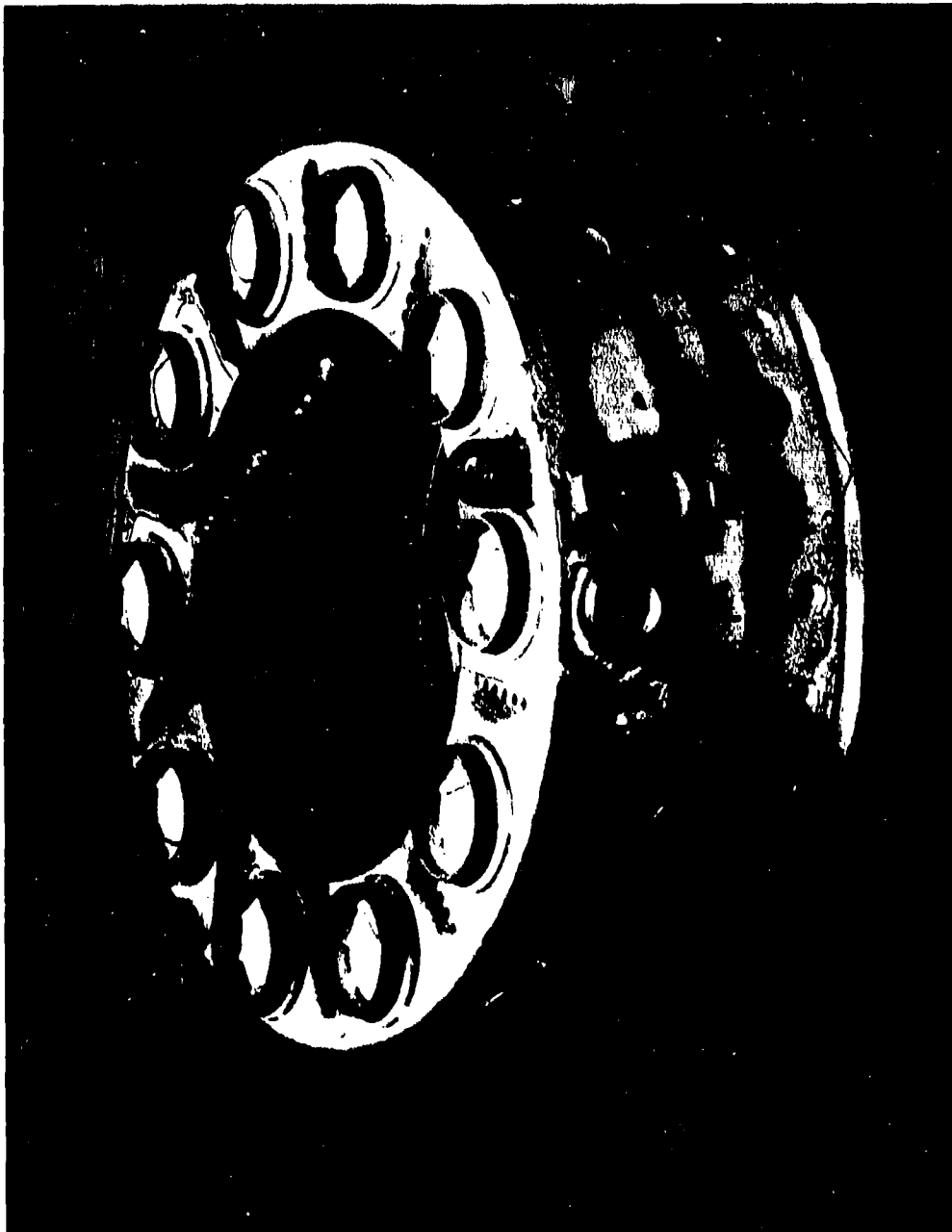|	STRAIGHT AVERAGE OF AREAS	WEIGHTED BY AREAS	INPUT AVG.
AVERAGE	2286.	2292.	2366.
MAXIMUM	****	2619.	****
MINIMUM	****	1685.	****
TOTAL SPREAD, MAX-MIN	****	933.	****
AVG TO PEAK SPREAD, MAX-AVG	333.	327.	319.
PATTERN FACTOR BASED ON SINGLE AVERAGE	.288	.283	.197
PATTERN FACTOR, (T MAX − RAKE AVG) / (INPUT AVG − T INLET)	.286	.283	.282

48

Figure 12. A Typical Wall Temperature Characteristic of Concept I at Maximum Power With a 45-Degree Spray Nozzle.

between recirculation zones established by individual dome swirlers. Subsequent to these tests, the airblast fuel nozzles were inspected to determine the manner in which the shroud air was entering the reaction zone. It was determined that the shroud air, which constituted approximately half of the nozzle air, entered the combustor with no swirl component. This explained why the nozzle spray cone angle was only 45 degrees instead of the desired 90-degree cone. Since each nozzle was located such that its cone passed through the center of the corresponding swirler, the shroud air was weakening the recirculation bubble established by the dome swirlers. Consequently, Concept I exhibited poor blowout characteristics. Since fabricating a swirler nut for the shroud air required major hardware modifications, shrouds without scallops were fabricated. The air previously injected into the reaction zone through the scallops was routed through a coarse-transpiration cooling film around the dome of the shrouds, which was an area of excessive heating. The modified nozzle set exhibited a normal cone angle of 90 degrees.

An acceptable pattern factor was obtained with the cooled unscalloped shrouds with air-assist $\Delta P = 0$, as shown in Figure 13. Previously, a significantly higher air-assist pressure was required with the original scalloped shrouds to obtain a comparable exhaust-temperature quality, as shown in Figure 10. The circumferential and radial pattern factors of 0.200 and 0.015, respectively, were within the program goals. Due to the increased spray-cone angle obtained with the unscalloped shrouds, the dome carbon-formation tendency was significantly reduced.

The liner wall-temperature characteristics of Concept I, shown in Figure 14, with cooled unscalloped shrouds at the sea-level, maximum power point, assured combustor life objectives. The combustion efficiency, as determined from gaseous emissions, was 99.99 percent. Preliminary testing indicated that the seal between the O.D. combustor liner and transition liner became
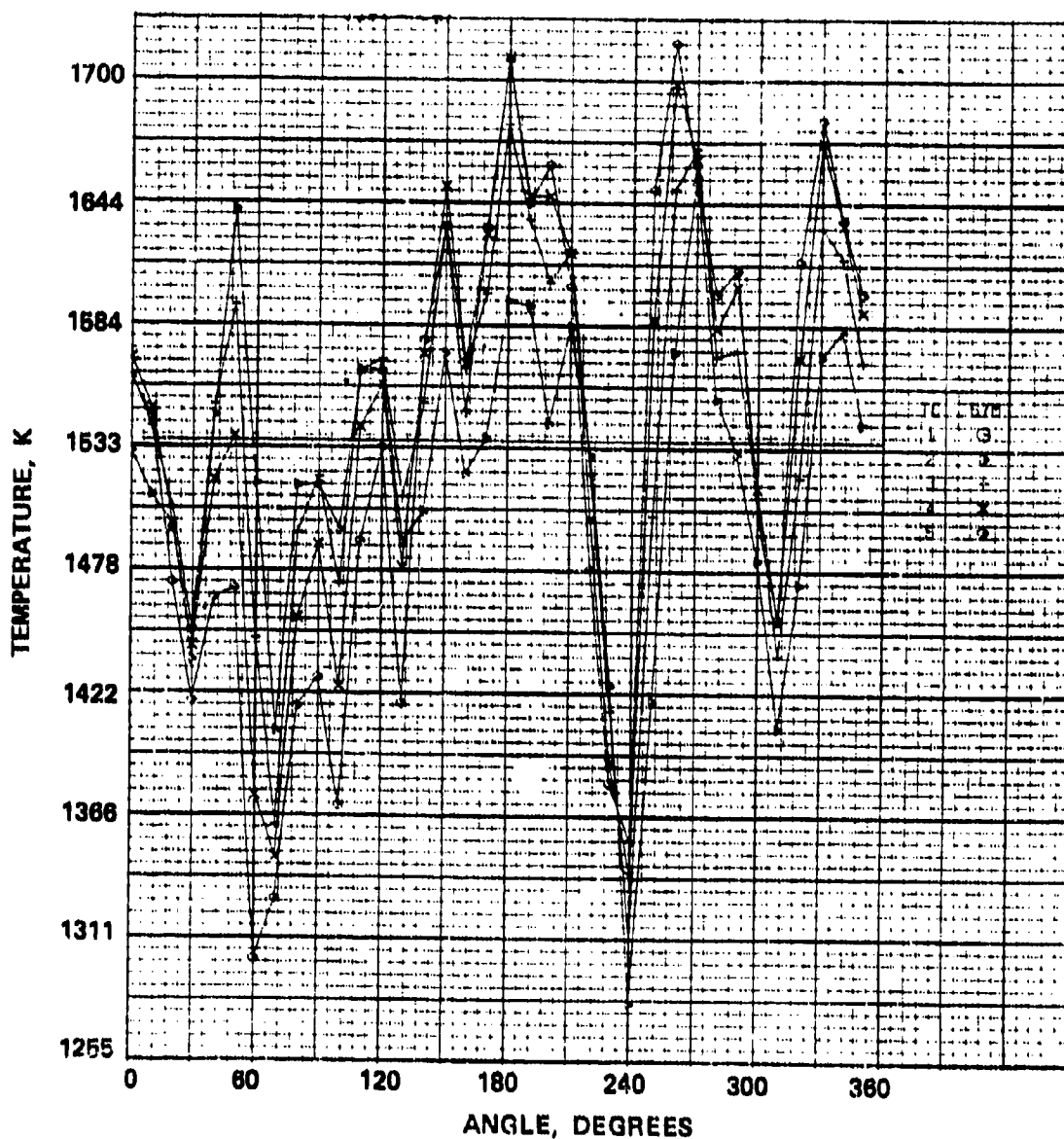
50

Figure 13. Concept I Exhaust-Temperature Scan at Sea-Level Maximum Power Point with the Modified Fuel Nozzle Set (90-Degree Spray), Nominal Nozzle Immersion.

51

NOTE: Isotherms written on combustor
liner are in degrees F. Convert
degrees F to degrees K as follows:

$$K = (5/9) (F+459.67)$$

Figure 14. Concept I, Liner Wall Temperature
Characteristics at Sea-Level Maximum
Power Point with the Modified Fuel
Nozzle (90-Degree Spray).

distorted and required local sizing to prevent deterioration of the pattern factor. A captive-type seal was installed on the combustor outer wall discharge to alleviate this problem prior to full scale testing.

Comparative tests were run between JP-4 and Jet-A (AK 640) fuel. A typical comparison, with the Concept I combustor, between the two fuels at sea-level and 6096 meters altitude representing the extremes of the performance map, is listed in Table 5. Performance data measured by gaseous emissions indicated that the HC index with JP-4 fuel was slightly higher than that with Jet-A fuel, and slightly less NO_x was produced with JP-4 fuel.

The effect of the number of thermocouple readings on the measured pattern factor has been a subject of many studies. It is important to take a sufficient number of points-per-unit-flow area of the stator inlet to make sure that none of the temperature peaks escape detection. The discharge survey, recorded during preliminary testing, was taken with 36 discrete circumferential scans spaced 10 degrees apart. Using five radial thermocouples, this resulted in a total of 180 points, giving approximately four readings/square centimeter of the flow area. The data was recorded only after the thermocouple readings had attained "steady-state" values. For comparison and per contract requirements, a continuous scan with 144 circumferential positions (giving 16 readings/square centimeter of flow area) was conducted.

A comparison with regard to the effect of the number of scans on both average T_4 and pattern factor is shown in Table 6. As can be seen, out of a total of 15 transverses taken at the maximum, intermediate, and idle power points from sea-level to 6096 meters altitude, the maximum difference in the circumferential pattern factor readings was approximately 11 percent (144 versus 36 scans), whereas the mean square error was only 2.4 percent.

TABLE 5. COMPARISON BETWEEN JET-A AND JP-4.

Fuel Type	Percent Power	Alt (m)	Circumferential PF	Radial PF	T_4 Avg (K)	Efficiency η
JP-4	100	SL	0.170	0.011	1558	100.0
	100	6096	0.213	0.020	1529	99.99
Jet-A	100	SL	0.203	0.015	1534	99.99
	100	6096	0.316	0.030	1457	

TABLE 6. EFFECT OF NUMBER OF CIRCUMFERENTIAL SCANS ON AVERAGE T$_4$ AND PF, CONCEPT I.

	Pattern Factor With					Average T$_4$ (K) With				
	144	72	48	36	24 Scans	144	72	48	36	24 Scans
SL maximum power	0.225	0.222	0.225	0.221	0.190	1521	1521	1521	1525	1527
1524 m altitude maximum power	0.249	0.248	0.249	0.226	0.249	1577	1577	1577	1577	1577
3048 m altitude maximum power	0.228	0.228	0.223	0.202	0.206	1542	1542	1542	1542	1542
4572 m altitude maximum power	0.212	0.213	0.213	0.213	0.212	1514	1514	1515	1515	1515
6096 m altitude maximum power	0.225	0.225	0.224	0.212	0.203	1531	1531	1531	1531	1531
SL 55-percent power	0.240	0.237	0.236	0.231	0.238	1380	1380	1380	1380	1380
1524 m altitude 54-percent power	0.297	0.297	0.298	0.284	0.298	1327	1328	1327	1327	1327
3048 m altitude 56-percent power	0.272	0.270	0.270	0.263	0.272	1332	1332	1332	1332	1331
4572 m altitude 59-percent power	0.229	0.229	0.229	0.206	0.231	1330	1330	1330	1330	1329
6096 m altitude 61-percent power	0.232	0.232	0.232	0.224	0.234	1361	1361	1361	1361	1360
SL 6-percent power	0.124	0.124	0.124	0.110	0.124	993	993	993	993	994
1524 m altitude 5-percent power	0.142	0.141	0.141	0.141	0.141	991	991	991	991	991
3048 m altitude 6-percent power	0.125	0.125	0.125	0.125	0.121	1000	1000	1006	1000	1000
4572 m altitude 8-percent power	0.124	0.124	0.124	0.123	0.123	1002	1002	1002	1002	1002
6096 m altitude 10-percent power	0.103	0.103	0.100	0.103	0.100	1025	1025	1025	1025	1025

2. Gaseous Emissions

Gaseous emissions were recorded at various power settings and altitudes by the use of a radially averaging water-cooled emission probe taking 36 discrete readings circumferentially around the transition liner discharge. Concept I performance at the sea-level idle power point, and the 6096 meter altitude 10-percent power point is summarized in Figures 15 through 20. Figure 15 shows that gaseous emission levels achieved with five fuel nozzles are comparable to 10 nozzles. Figure 16 shows that the taxi-idle emissions achieved with JP-4 fuel are slightly higher than that with Jet-A fuel at the same conditions, Figure 17. A combustion efficiency of 98.75 percent was obtained at the 6096 meter altitude, 10-percent power point with Jet-A fuel, as shown in Figure 18. The HC emission index decreased with increasing air-assist pressure drop (Figure 19). With 414 kPa air-assist pressure drop, the HC emissions index with JP-4 fuel was slightly higher than that with Jet-A fuel. The basic nozzle shrouds, because of a narrow spray cone angle, produced minimum unburned hydrocarbons. The performance with the uncooled unscalloped shrouds was slightly inferior. Similar performance was observed with regard to CO emissions as shown in Figure 20. The effect of air-assist pressure drop on the idle NO_x emission index is shown in Figure 21. The five-nozzle configuration produced NO_x levels comparable to 10 nozzles indicating good nozzle-to-nozzle communication. Slightly less NO_x was produced with JP-4 fuel due to its lower boiling point with attendant improvement in mixing, especially with higher air-assist pressure drops.

The NO_x emissions characteristics as a function of fuel/air ratio at sea-level (55-percent and maximum power conditions) and 6096 meters altitude (61-percent through maximum power conditions) are depicted in Figures 22 through 24. The scalloped fuel nozzle (basic) shrouds, due to smaller spray cone angle, produced the highest NO_x values as shown in Figures 22 and 23. The NO_x
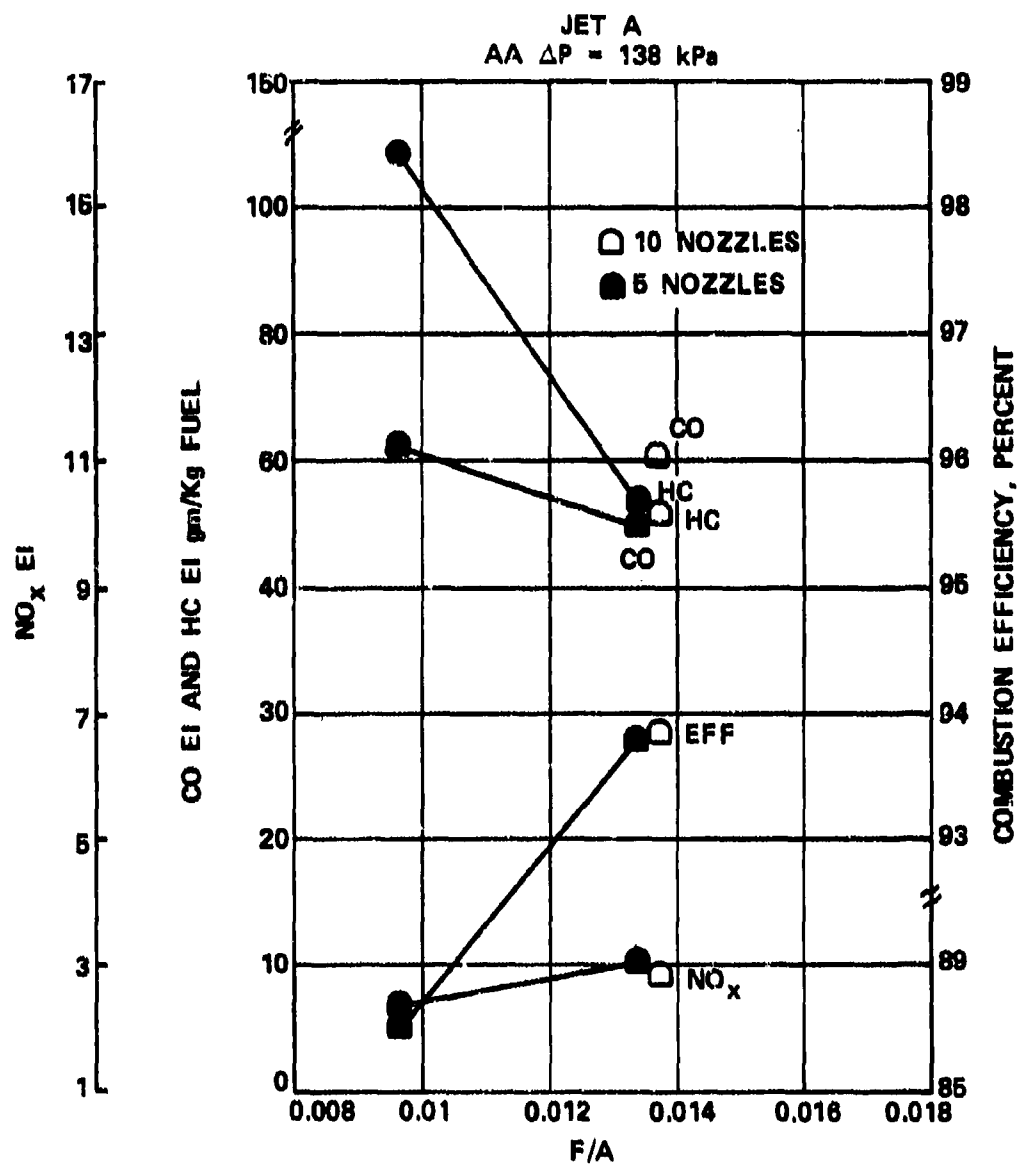
Figure 15. Effect of Fuel Nozzle Shaping on Concept I, Sea-Level, Taxi-Idle Gaseous Emissions.
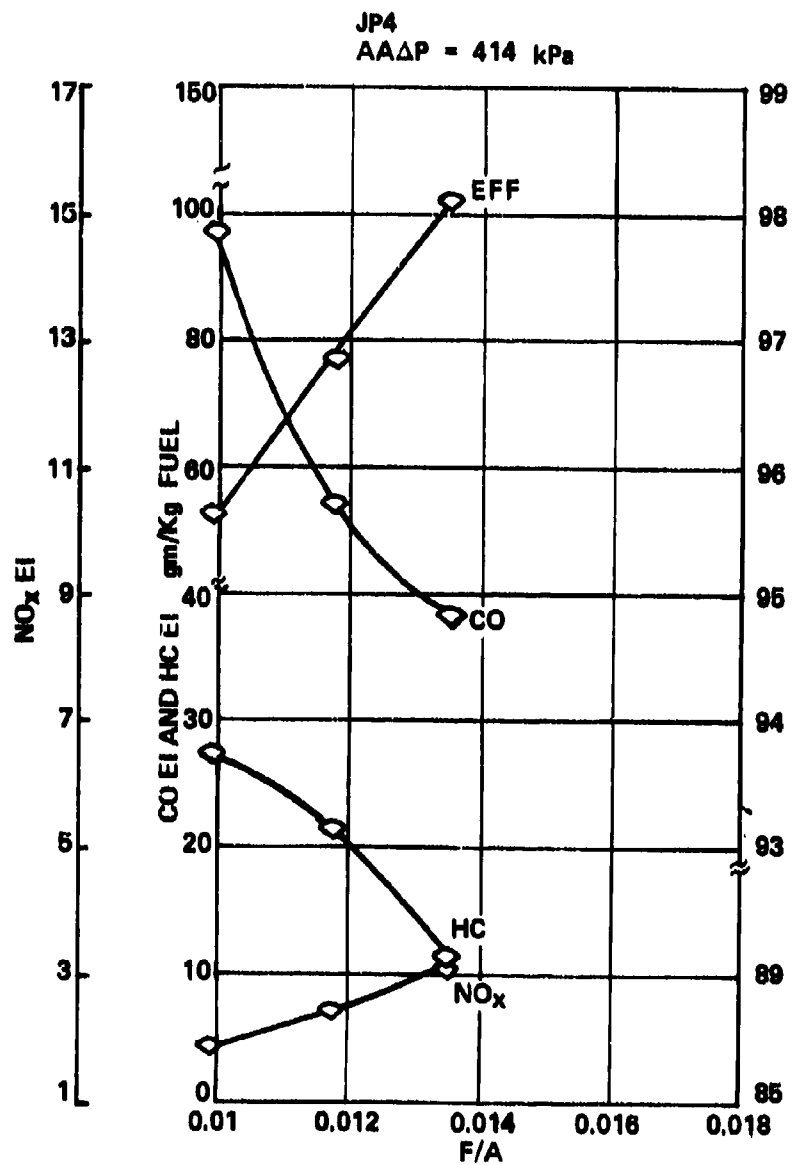
Figure 16. Concept I, Sea-Level, Taxi-Idle Gaseous Emissions Versus Fuel/Air Ratio.

58
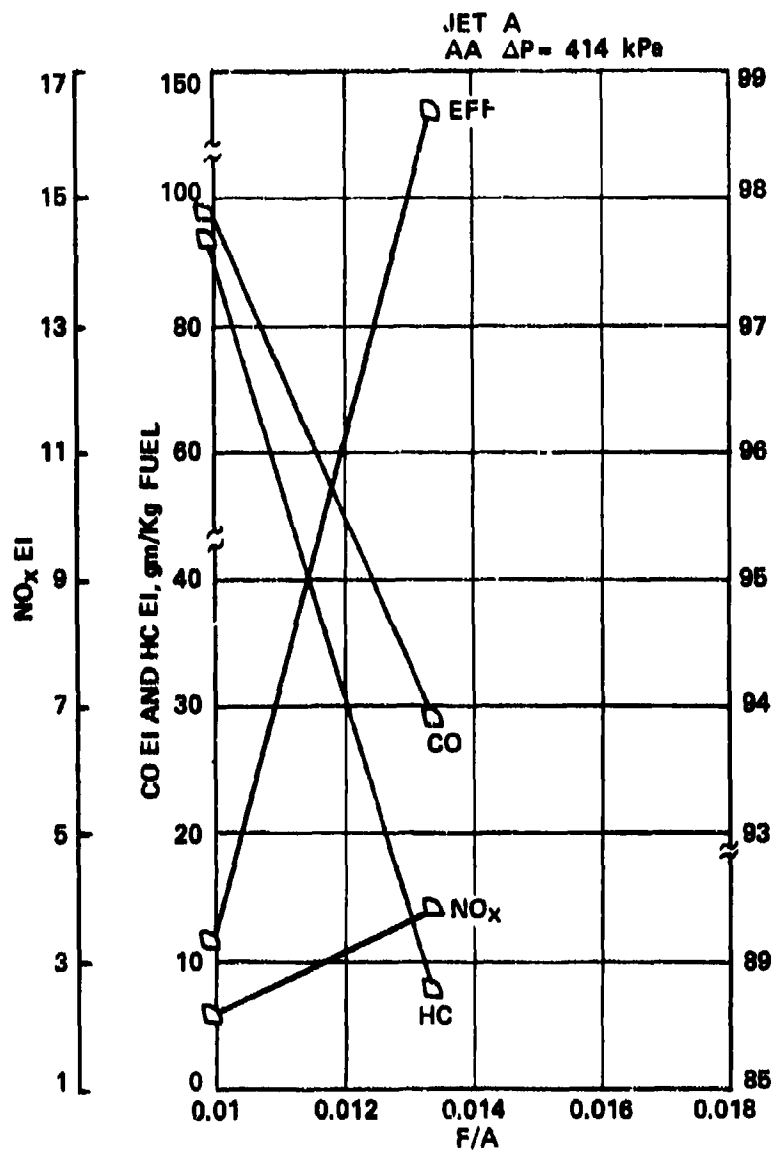
Figure 17.   Concept I Taxi-Idle Gaseous Emissions with
Jet A.
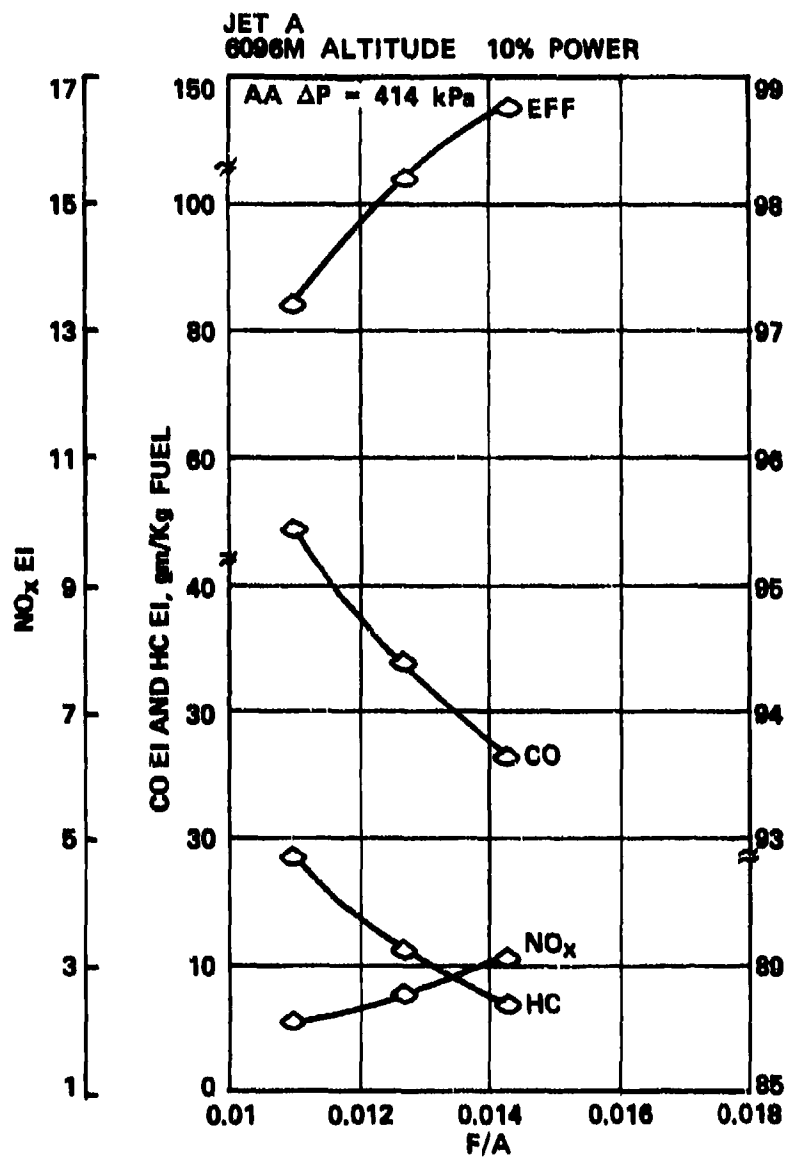
Figure 18. Concept I, 6096 Meter Altitude, 10-Percent Power
Point Gaseous Emissions.
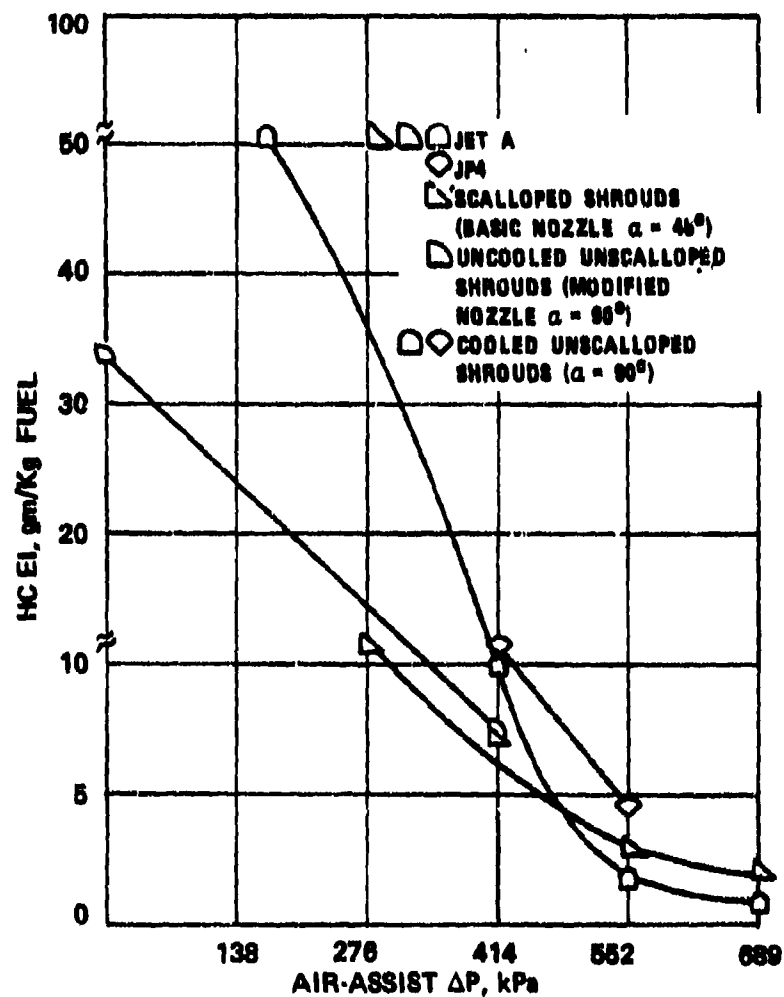
Figure 19.   Taxi-Idle HC Emission Index Versus
Air-Assist ΔP of Concept I.
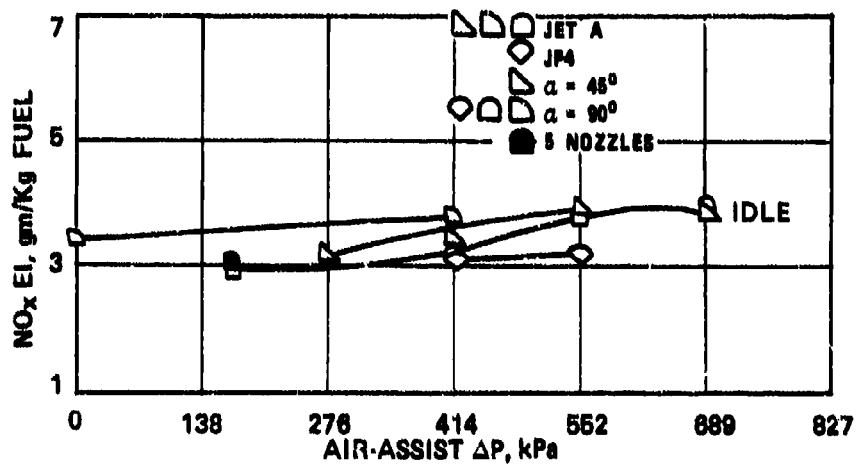
61
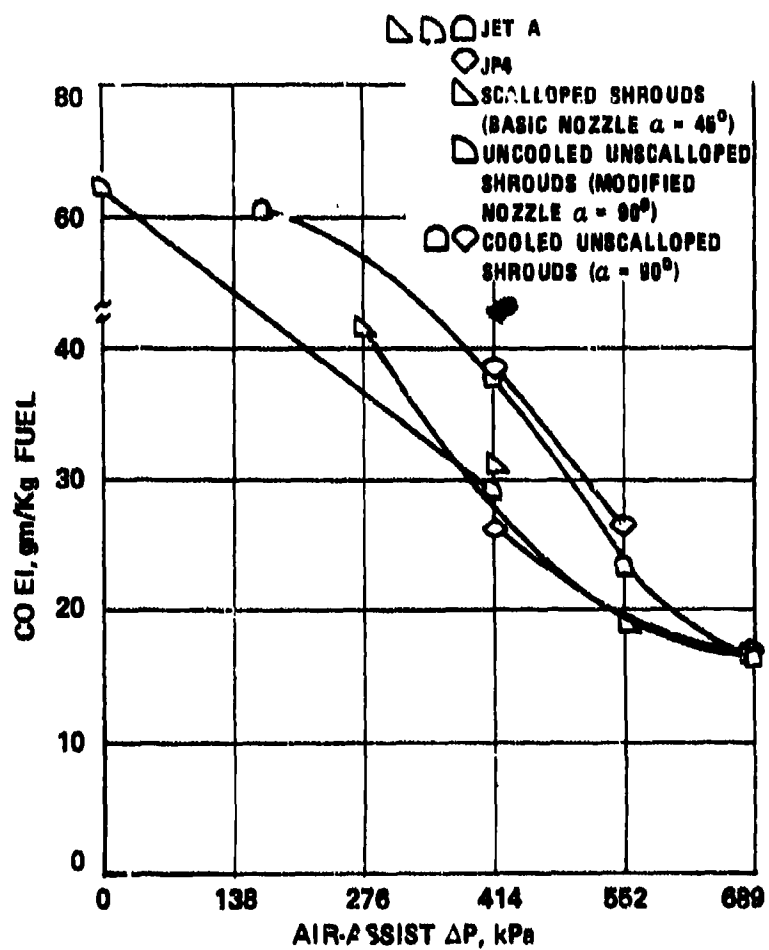
Figure 20. Taxi-Idle CO Emission Index Versus
Air-Assist ΔP of Concept I.

Figure 21. Taxi-Idle NO$_x$ Emission Index Versus Air-Assist ΔP of Concept I.

Figure 22. NO$_x$ Emission Index Versus Fuel/Air Ratio
of Concept I at Sea-Level, 55-Percent
Power point.

64
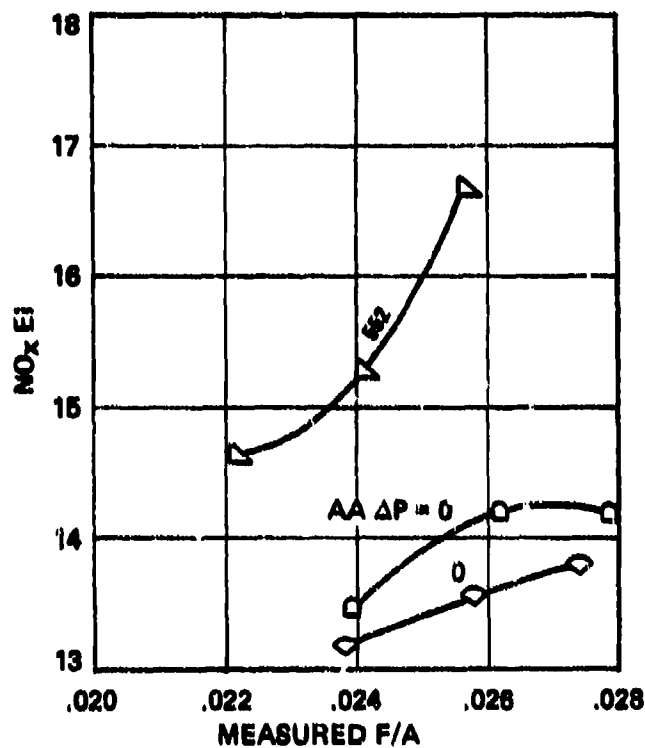
Figure 23. NO$_x$ Emission Index Versus Fuel/Air Ratio of Concept I at Sea-Level Maximum Power.

emission index increase with fuel/air ratio was more pronounced with the scalloped shrouds. Slightly less NO_x was produced with JP-4 compared to Jet-A fuel. Figure 24 shows the variation of the NO_x emission indices with fuel/air ratios at 61, 81, and 100-percent power points at 6096 meter altitude. The corresponding combustion efficiencies were 99.87, 99.97, and 99.98 percent.

3. Wall Temperature Characteristics

The Concept I combustor was run at sea-level, hot-day conditions, per contractual requirements. The combustor conditions were: P_{T3} = 880.5 kPa, T_3 = 646 K, W_{A3} = 1.08 Kg/sec, and f/a = 0.026. The results for the sea-level, hot-day, maximum power condition are shown in Figures 25 and 26. The measured circumferential pattern factor was 0.182 at an average discharge temperature of 1593 K. Wall temperature characteristics, as indicated by OG-6 Thermindex temperature sensitive paint, showed maximum wall temperatures of 922 K for the O.D. panel and 1074 K for the I.D. panel. The temperature gradients are within the desired 210 K/centimeter.

Tests were conducted to determine the effects of three different patterns of combustor inlet distortion on the discharge temperature quality.

The first inlet distortion pattern was generated by the placement of a 0.191-cm-thick (one-fourth of the channel height) band on the I.D. annulus wall, 1.78 cm downstream of the diffuser exit. The band extended from top dead center for 45 degrees in a clockwise direction, as viewed from the aft end of the test rig.

Figures 27 and 28 show the result for the sea-level maximum power test point. A deterioration in both discharge temperature quality (0.261 circumferential pattern factor) and O.D. liner temperature 1144 K O.D. hot spot) is evident. A comparison of the exhaust temperature plot (Figure 27) with the baseline scan,

66
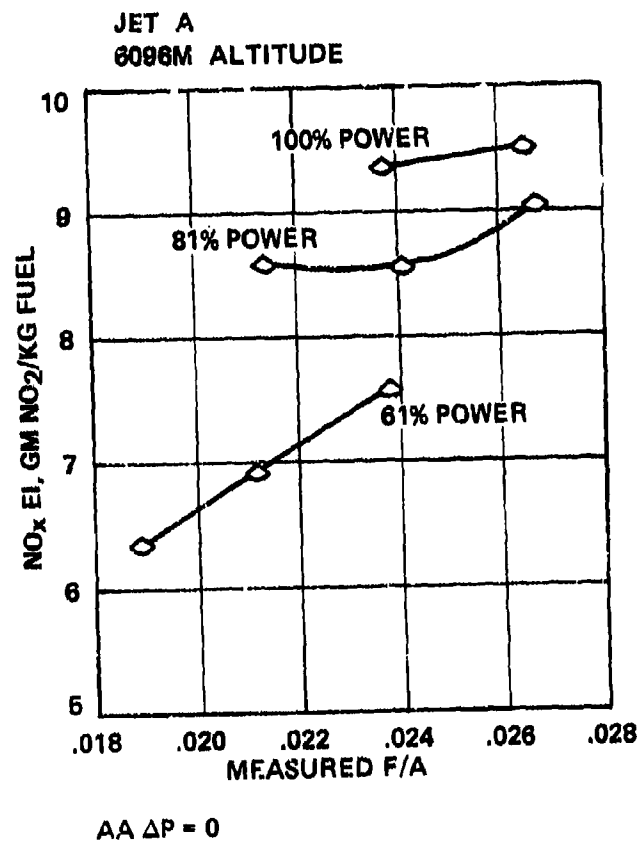
Figure 24. NO$_x$ Emicsion Index Versus Fuel/Air Ratio of Concept I at 6096 Meter Altitude.

67

WT AVG = 1593K. WT TSF = 0.182 ST AVG = 1592K. ST TSF = 0.183
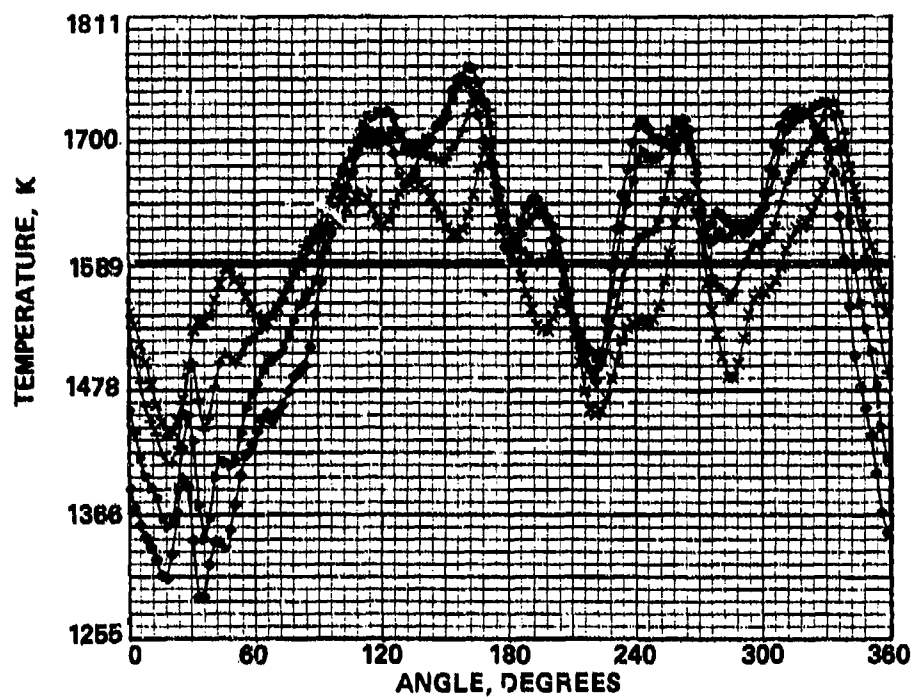
RADIAL PF = 0.0135

TC	SYM
1	⬡
2	▷
3	+
4	×
5	◇

Figure 25. Concept I Combustor Sea-Level,
Hot-Day Temperature Scan.

68

NOTE: Isotherms written on combustor liner are in degrees F. Convert degrees F to degrees K as follows:

$$K = (5/9)(F+459.67)$$

Figure 26. Concept I Combustor Sea-Level, Hot-Day Paint Run.
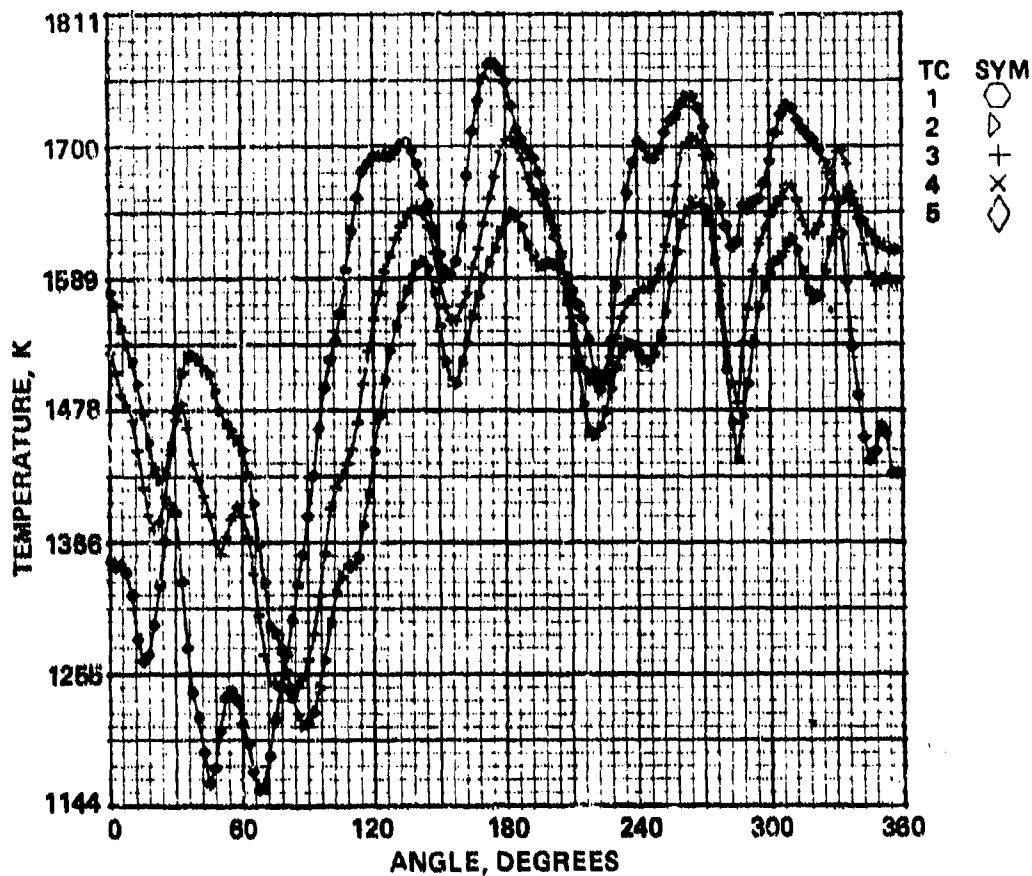
Figure 27. Effect of One 45-Degree Inlet Distortion on Concept I
Exhaust Temperature Scan at Sea-Level Maximum Power
Point.
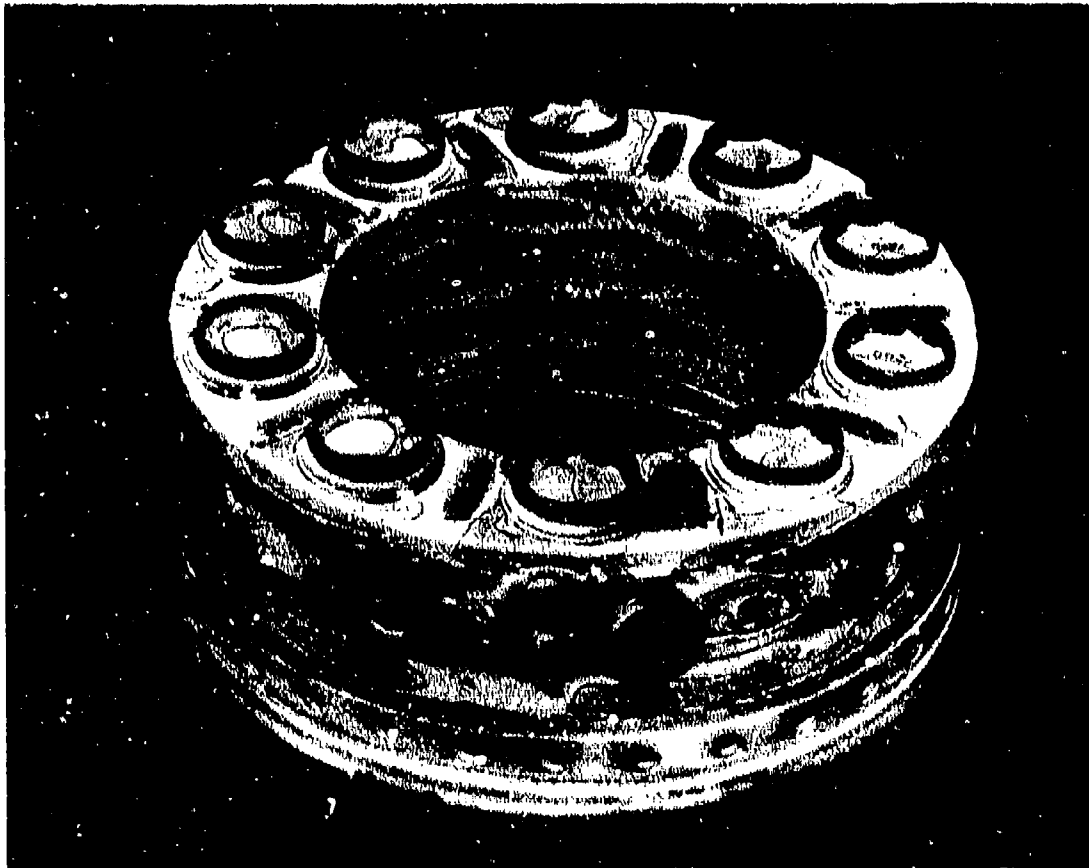
NOTE: Isotherms written on combustor liner are in
degrees F. Convert degrees F to degrees K
as follows:

$$K = (5/9)(F+459.67)$$

Figure 28. Effect of One 45-Degree Inlet Distortion on Concept I
Liner Wall-Temperature Characteristics at Sea-Level
Maximum Power Point.

71

at similar test conditions shown in Figure 13, indicates similar characteristics. However, the Number 5 outer thermocouple exhibits up to 333 K higher peaks, resulting in the increased pattern factor. The high temperature areas on the I.D., O.D. panels, and the dome (Figure 28) are limited to an area approximately 50 degrees on either side of the ignitor. This area is located approximately 180 degrees from the inlet distortion band.

For the second distortion pattern, a second band, diametrically opposite and of identical dimensions to the first, was added. Test results at the maximum power point are shown in Figures 29 and 30. The liner temperatures returned to levels similar to the baseline scan, while the circumferential pattern factor decreased to an acceptable level (0.201), but remained slightly higher than the baseline scan.

The third, and final, distortion pattern was generated by a band of identical dimensions and location to those used in the previous distortion tests, except that it extended for 360 degrees around the annulus.

The test results for the sea-level, maximum power condition are shown in Figures 31 and 32. The exhaust temperature quality (0.227 circumferential pattern factor), though below the program goal, was higher than the baseline. Liner wall temperatures, however, remained essentially unchanged.

An acceptable circumferential pattern factor (<0.23) was obtained for two of the three inlet distortion patterns tested (two 45-degree bands diametrically opposed, and a 360-degree band). The single 45-degree band pattern yielded a pattern factor slightly higher than design goals. The effect of inlet distortion on liner-wall temperature levels was minimal except in the single 45-degree pattern that yielded one hot spot 222 K higher than the baseline temperature at approximately 180 degrees from the inlet distortion band.

72
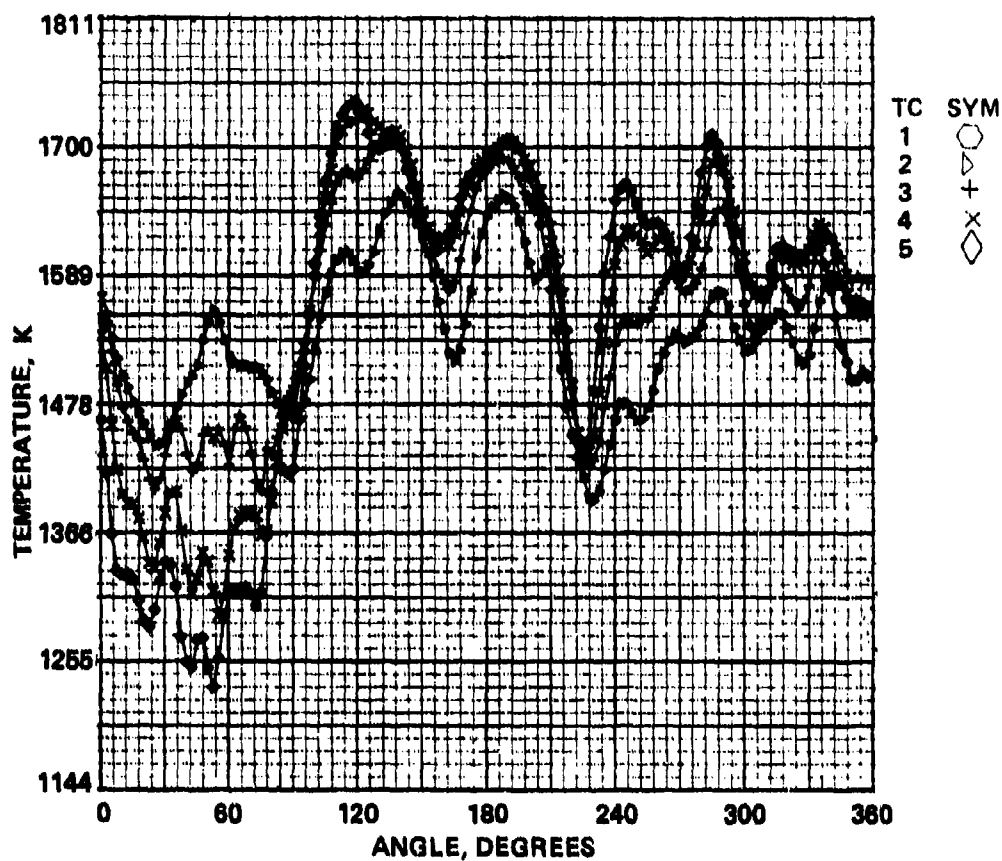
Figure 29. Effect of Two 45-Degree Inlet Distortions on Concept I
Exhaust Temperature Scan at Sea-Level Maximum Power
Point.
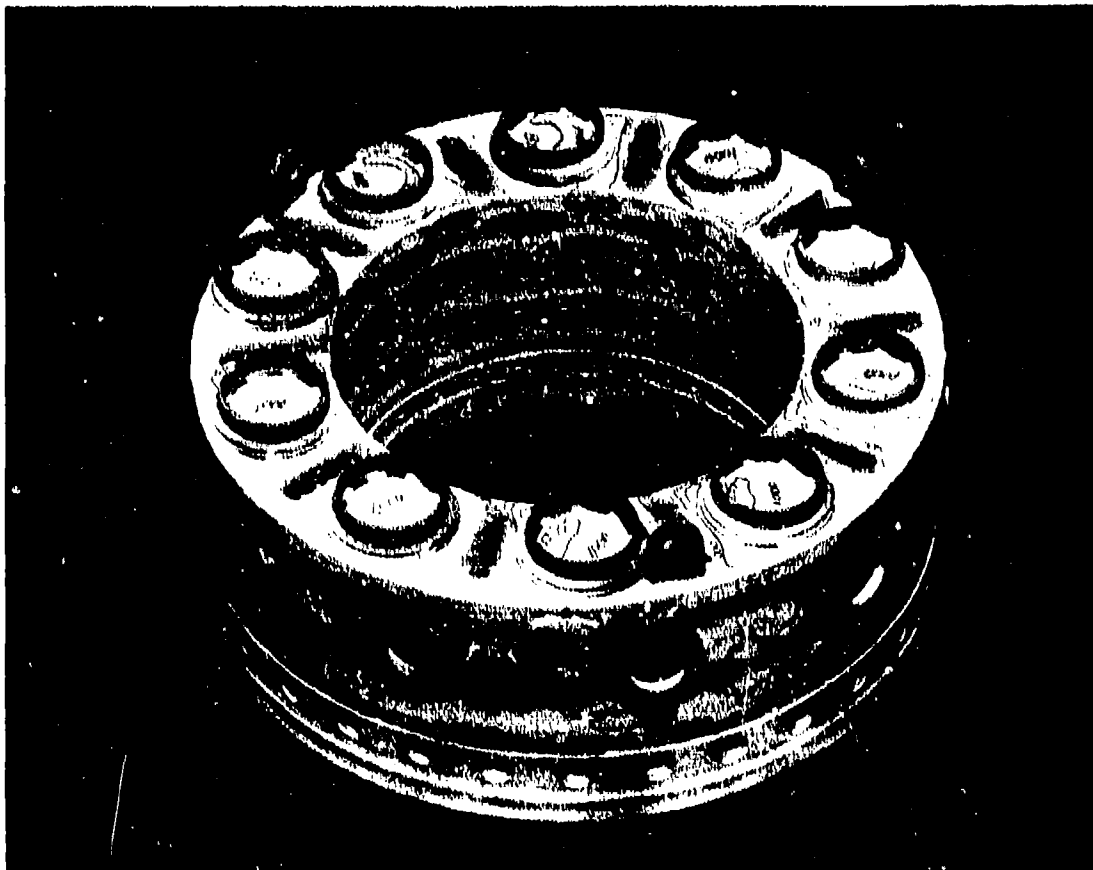
73

NOTE: Isotherms written on combustor liner are in
degrees F. Convert degrees F to degrees K
as follows:
$$K = (5/9)(F+459.67)$$

Figure 30. Effect of Two 45-Degree Inlet Distortions on Concept I
Liner Wall-Temperature Characteristics at Sea-Level
Maximum Power Point.

74

WT AVG = 1539   WT TSF = 0.227   ST AVG = 1542   ST TSF = 0.223
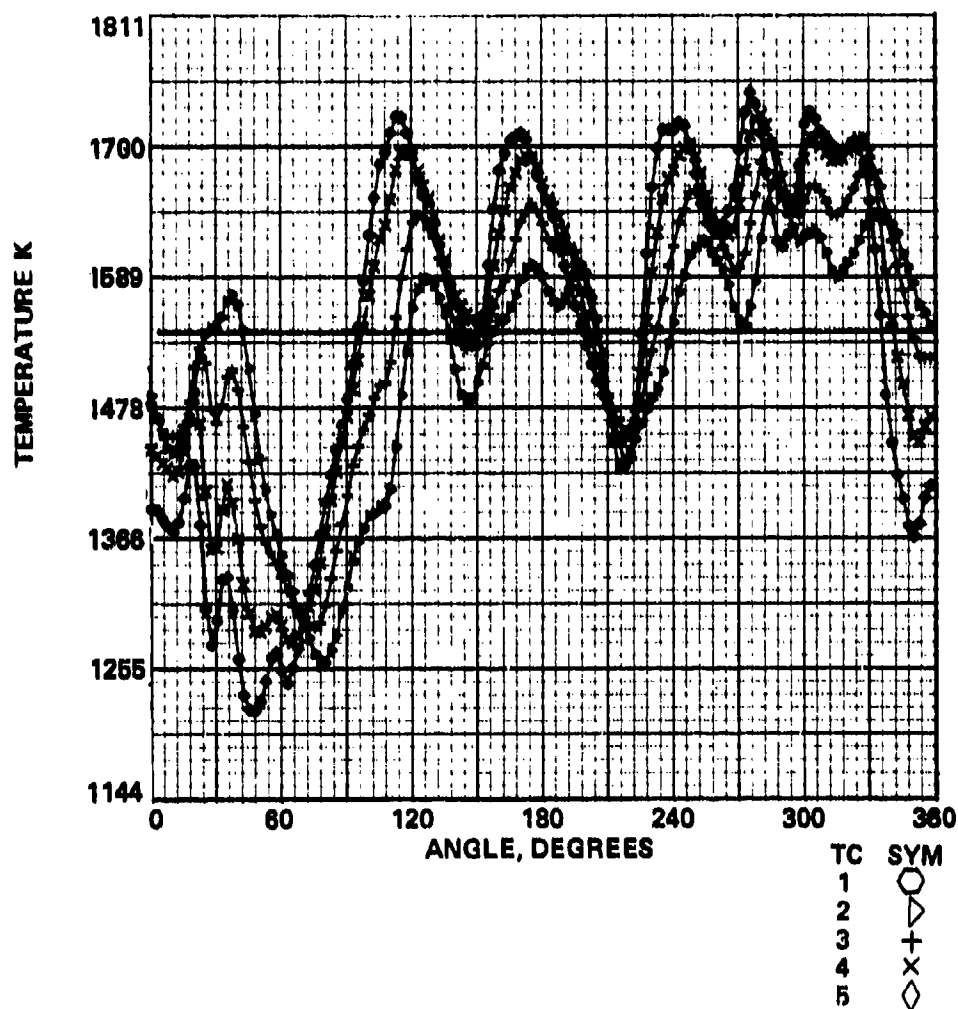
Figure 31.   Concept 1 Exhaust Temperature Scan With
360-Degree Inlet Distortion.

NOTE: Isotherms written on combustor liner are in
degrees F. Convert degrees F to degrees K
as follows:

$$K = (5/9)(F+459.67)$$

Figure 32. Concept I Liner Wall-Temperature Characteristics
with 360-Degree Inlet Distortion.

4. Liner Durability Tests

To test liner durability, 600 4-minute cycles simulating transient temperature effects, were conducted. Each cycle consisted of 2 minutes of steady-state operation at the sea-level maximum power test condition, a step change (less than 1 second) in fuel flow to the sea-level taxi-idle test condition, 2 minutes of steady-state operation at this condition, and finally a step change in fuel flow returning to the original test condition. No parameters, other than fuel flow, were varied; however, the airflow rate was approximately 10 percent higher at the taxi-idle point due to the decrease in momentum pressure loss.

Figures 33 and 34 show the exhaust-temperature scans before and after the test; and as can be seen, no deterioration in pattern factor is evident. Figure 35 shows a typical interior view of the combustor liner and reveals no significant damage. None of the cooling-slot lips exhibited any indication of thermal stress, however, a crack had developed near the middle attachment weld of each dome louver. This was not considered a serious problem as the dome louver design was selected as an economical rig test configuration. For an engine test, the louvers would normally have been inserted from outside through slots with the attachment weld being on the outer dome surface. This would have reduced the stress in the louver because of the cooler environment.

The slight carbon formation, shown in Figure 35, was no more than that usually found after tests of much shorter duration. The fuel nozzles showed no adverse effects except for a slight carbon accumulation on a few of the swirler nuts.

5. Ignition and Blowout Tests

The required goals of ignition and lean blowout limits of the combustion system was accomplished through fuel staging. The

77

WT AVG = 1551   WT TSF = 0.222   ST AVG = 1554   ST TSF = 0.219
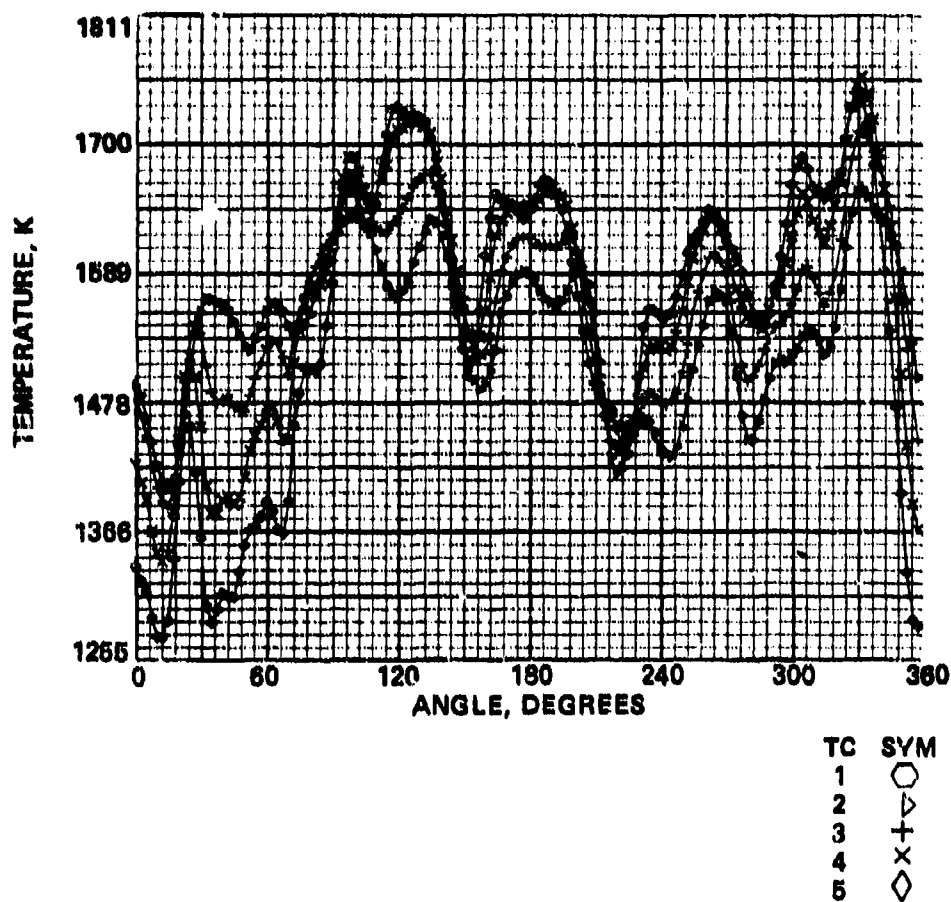
Figure 33.   Concept 1 Exhaust Temperature Scan
Before Thermal Cycle Test.

78

CYCLES, WT AVG = 1534   WT TSF = 0.181   ST AVG = 1536   ST TSF = 0.178
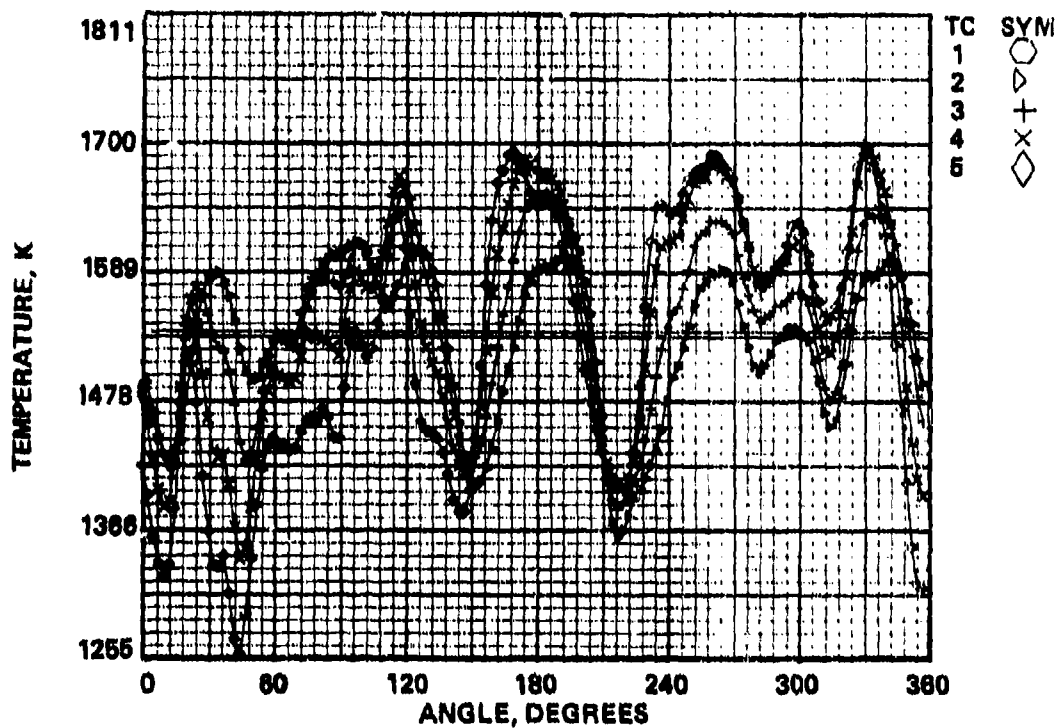
Figure 34.   Concept 1 Exhaust Temperature Scan After
             Thermal Cycle Test.

79
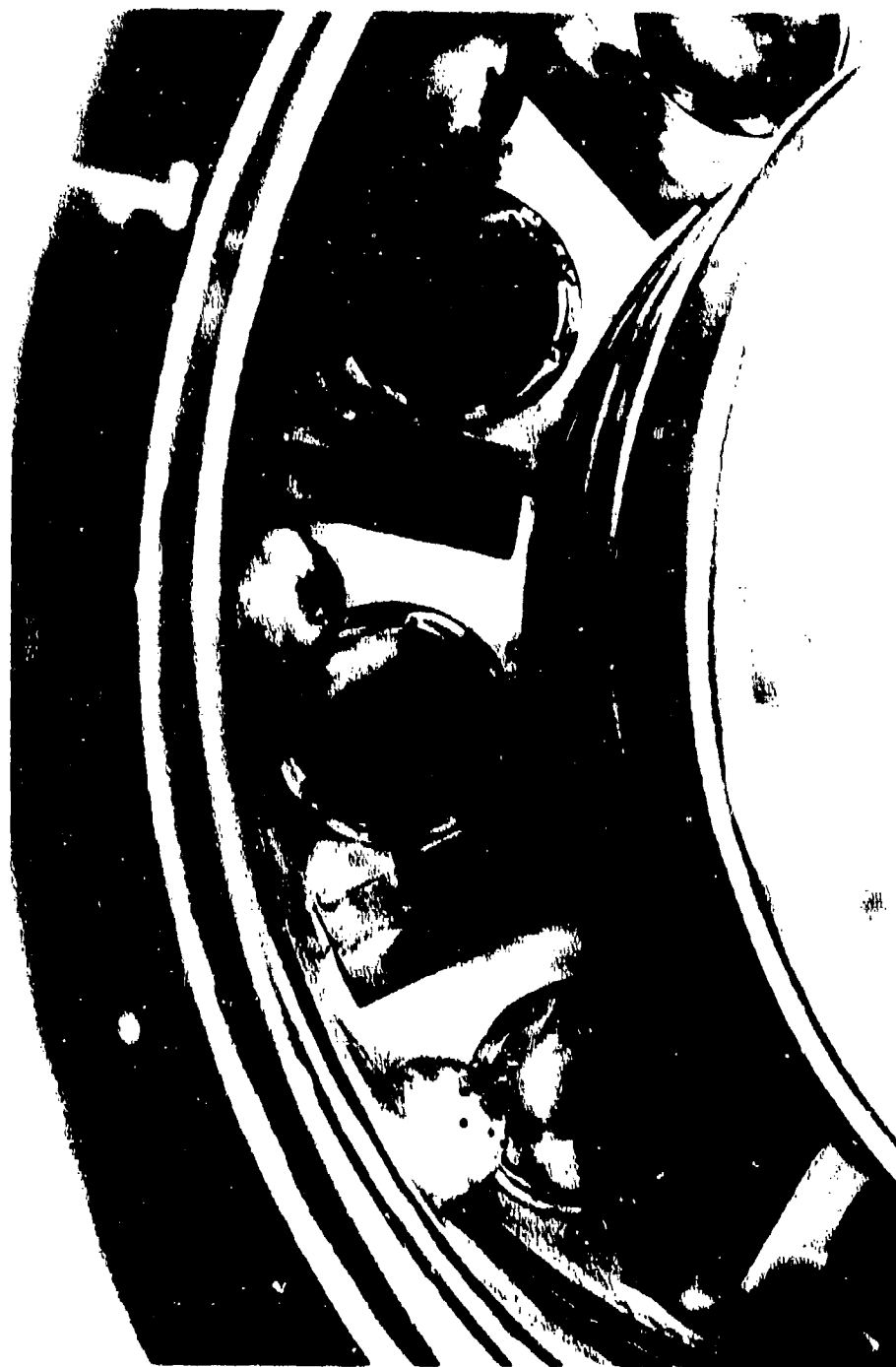
Figure 35.   Concept I Liner After Thermal Cycle Test

80

optimum start (primary) and run (secondary) fuel nozzle configuration was determined to be three primary and seven secondary nozzles.

It was originally intended to determine the lean ignition limits at 20- and 30-percent cranking speed for altitudes from sea level to 6096 meters. However, the testing was terminated after the first three test points, shown in Table 7, exhibited high light-off fuel/air ratios.

TABLE 7. LIGHT-OFF FUEL/AIR RATIOS
WITH 138 kPa AIR ASSIST.

Cranking Speed, %	Altitude, M	
	Sea Level	1,524
20	0.031	0.034
30	0.029	---

These results were particularly surprising, considering the liner displayed quite acceptable blow-out limits (fuel/air ratio of 0.00307) at sea-level idle with 34.5 kPa air assist.

It was felt that this behavior would not have resulted if the ignitor was located in the optimum position. Since hardware modification was prohibitively expensive, it was decided to determine the blow-out fuel/air ratio at the same test conditions that were originally intended for the ignition tests. From these data, the light-off characteristics of the combustor with an optimum ignitor location could be inferred.

Figures 36 and 37 show the blow-out fuel/air ratio for various light-off cranking speeds, altitudes, and air-assist pressures. The performance deterioration at 138 kPa air-assist resulted from the increased airflow, which leaned the fuel/air mixture in the vicinity of the fuel nozzle, while providing

81
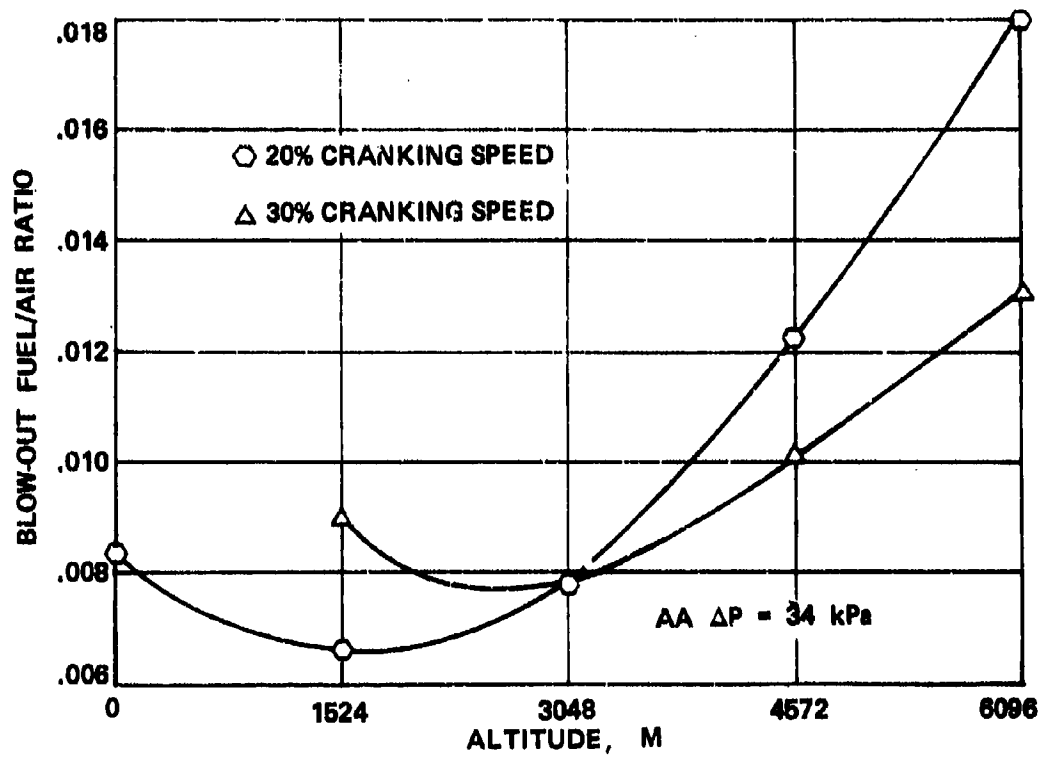
Figure 36. Concept I Lean Stability
            At Light-Off Conditions.

82
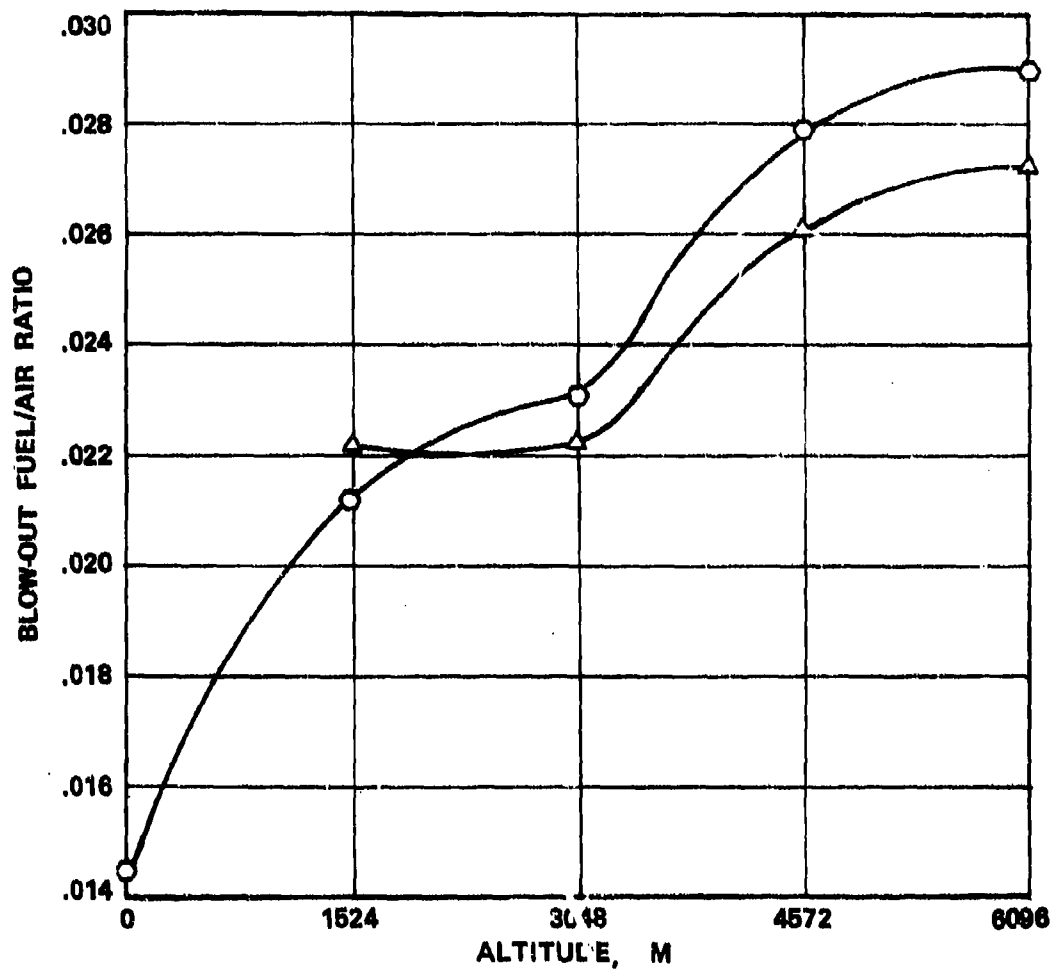
Figure 37. Concept I Lean Stability at Light-Off Conditions.

83

practially no improvement in Sauter mean diameter. AiResearch combustors typically produce light-off fuel/air ratios from two to three times the corresponding blow-out value. This would indicate (based on Figure 36) that had the ignitor been positioned in the optimum location, the light-off fuel/air ratio below 3048 meters would have been approximately 0.02 rather than the 0.03 measured.

6. Acoustic Emission

Acoustic measurements were taken on Concept I at idle and maximum power conditions for various altitudes. The sound pressure level of the combustor was monitored using an "infinite-tube" acoustic probe. This type of probe determines the sound pressure level accurately for frequencies less than 1000 hz.

The acoustic data for Concept I was taken at sea-level idle, 3048 meters idle, 6096 meters idle, sea-level 100-percent power, and 3048 meters 100-percent power, and are shown in Figures 38 through 47. Figures 38, 40, 42, 44, and 46 show the 1/3-octave sound pressure level with combustion. Figures 39, 41, 43, 45, and 47 show the 1/3-octave sound pressure level without combustion; i.e., the same combustor airflow, inlet temperature, and pressure as in Figures 38, 40, 42, 44, and 46, respectively, but with no fuel flow. Figures 39, 41, 43, 45, and 47 show the noise present in the combustion rig due to noncombustion processes, such as noise generated by airflow through valves in the piping system. Therefore, the difference between the sound pressure levels, shown in the two series of figures, is due to the combustion process. The sound pressure level increase, due to combustion, varied by approximately 9 db in the frequency range between 25 and 1000 Hz at the sea-level idle condition, 9 to 10 db in the 25 to 1000 Hz range at the 3048 meter idle condition, 6 to 10 db in the 25 to 1000 Hz range at the 6096 meter idle condition, 5 to 12 db in the 25 to 1000 Hz range at the sea-level 100-percent power condition, and 7 to 14 db in the 25 to 1000 Hz range at the

TEST CONDITIONS: WITH COMBUSTION
TEMPERATURE: INLET 450 K, EXHAUST 956 K
SIMULATED POWER LEVEL: IDLE
ALTITUDE: SEA-LEVEL
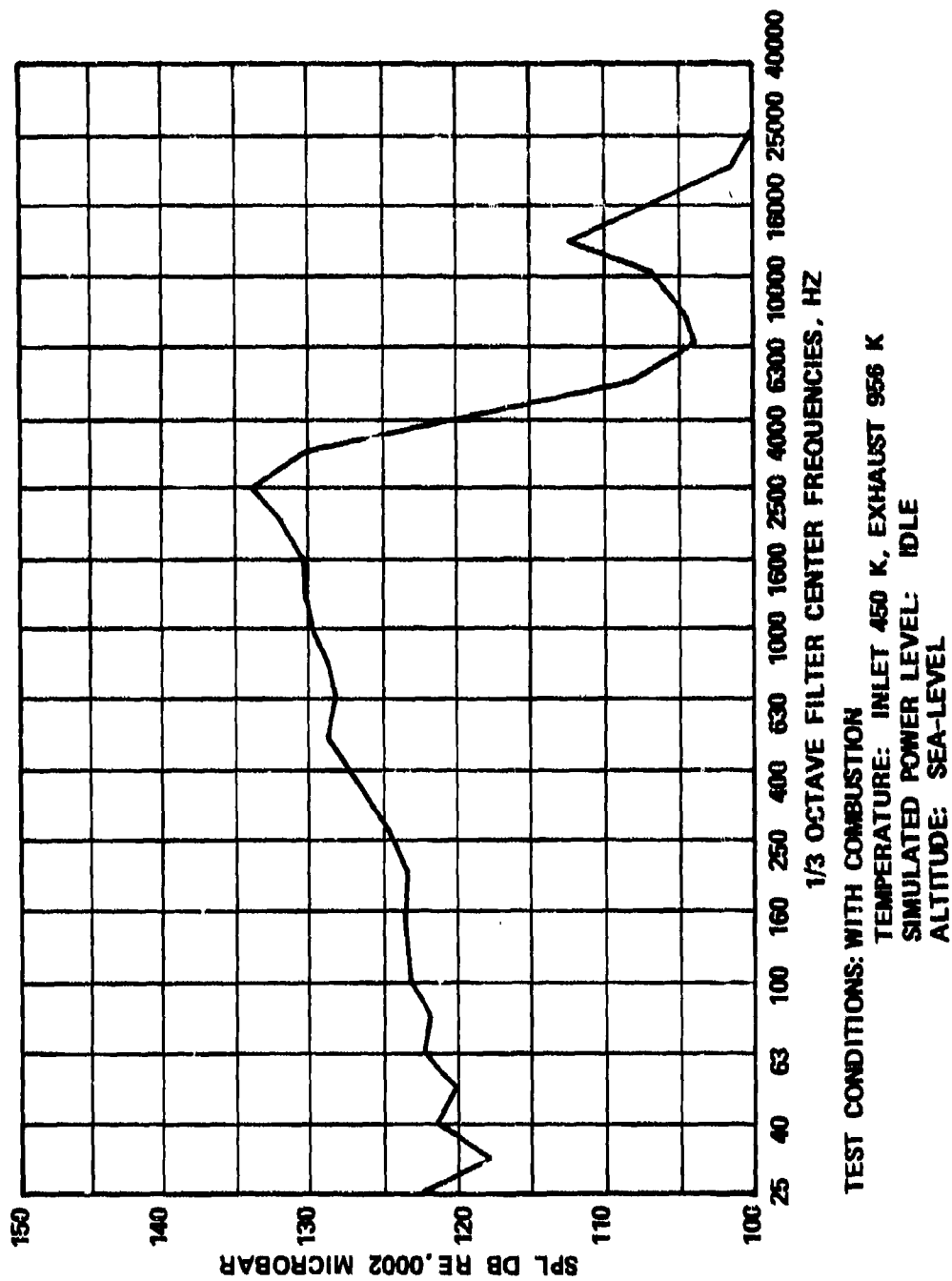
Figure 38. Combustor Sound Pressure Level with Combustion at Sea-Level Idle.
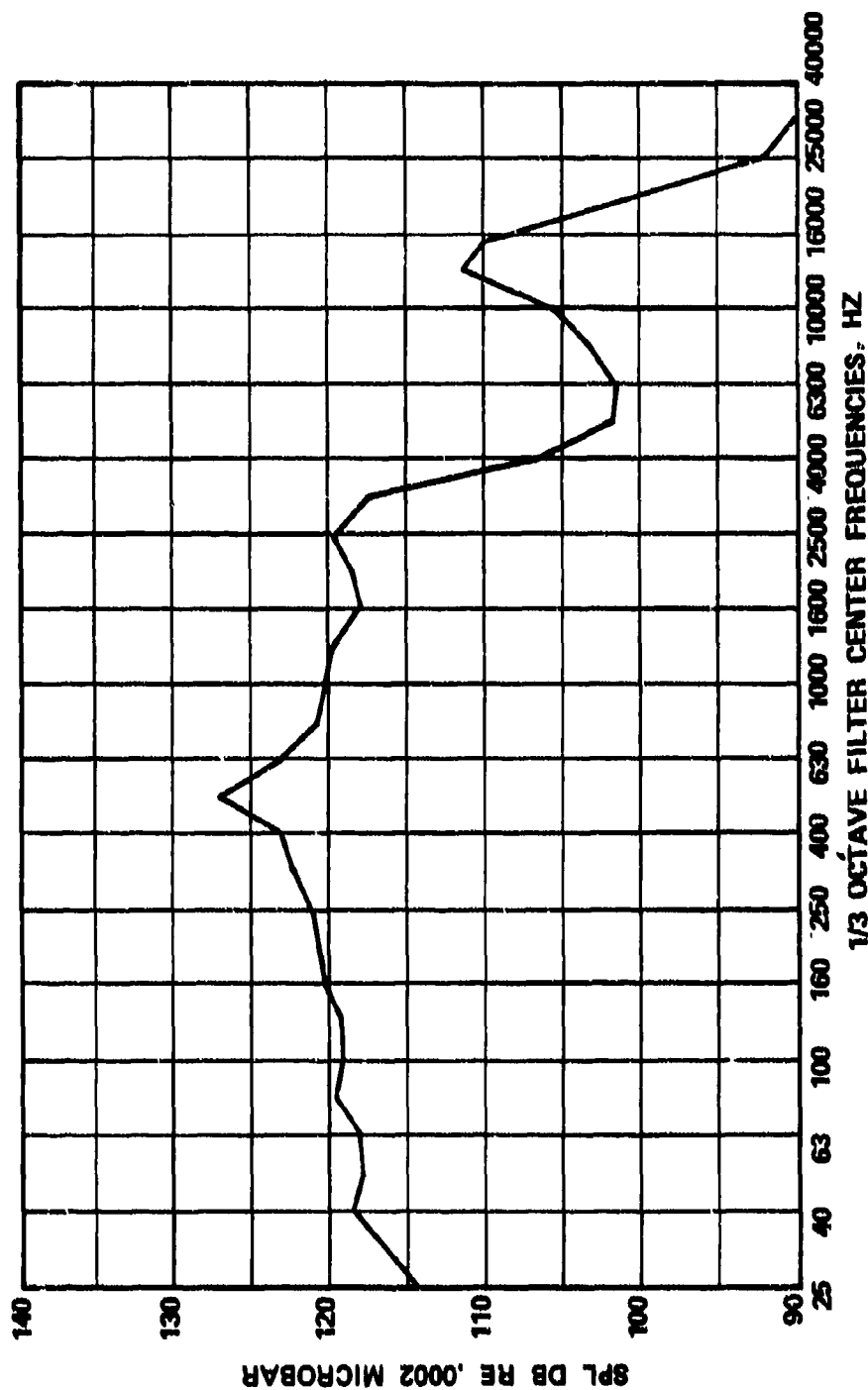
TEST CONDITIONS: WITHOUT COMBUSTION
TEMPERATURE: INLET 450 K
SIMULATED POWER LEVEL: IDLE
ALTITUDE: SEA-LEVEL

Figure 39. Combustor Sound Pressure Level without Combustion at Sea-Level Idle.
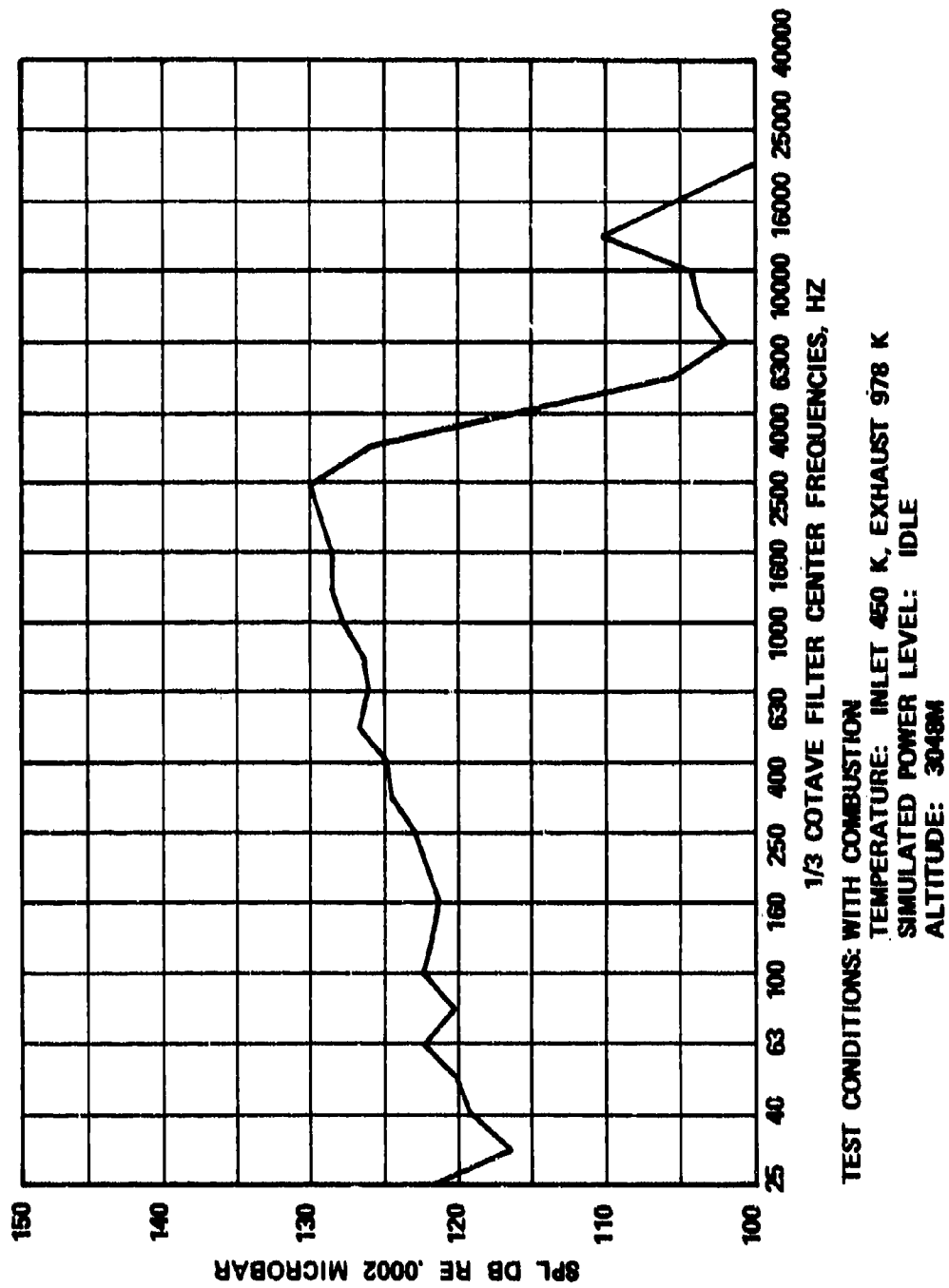
Figure 40. Combustor Sound Pressure Level with Combustion at 3048 Meters Idle.

87
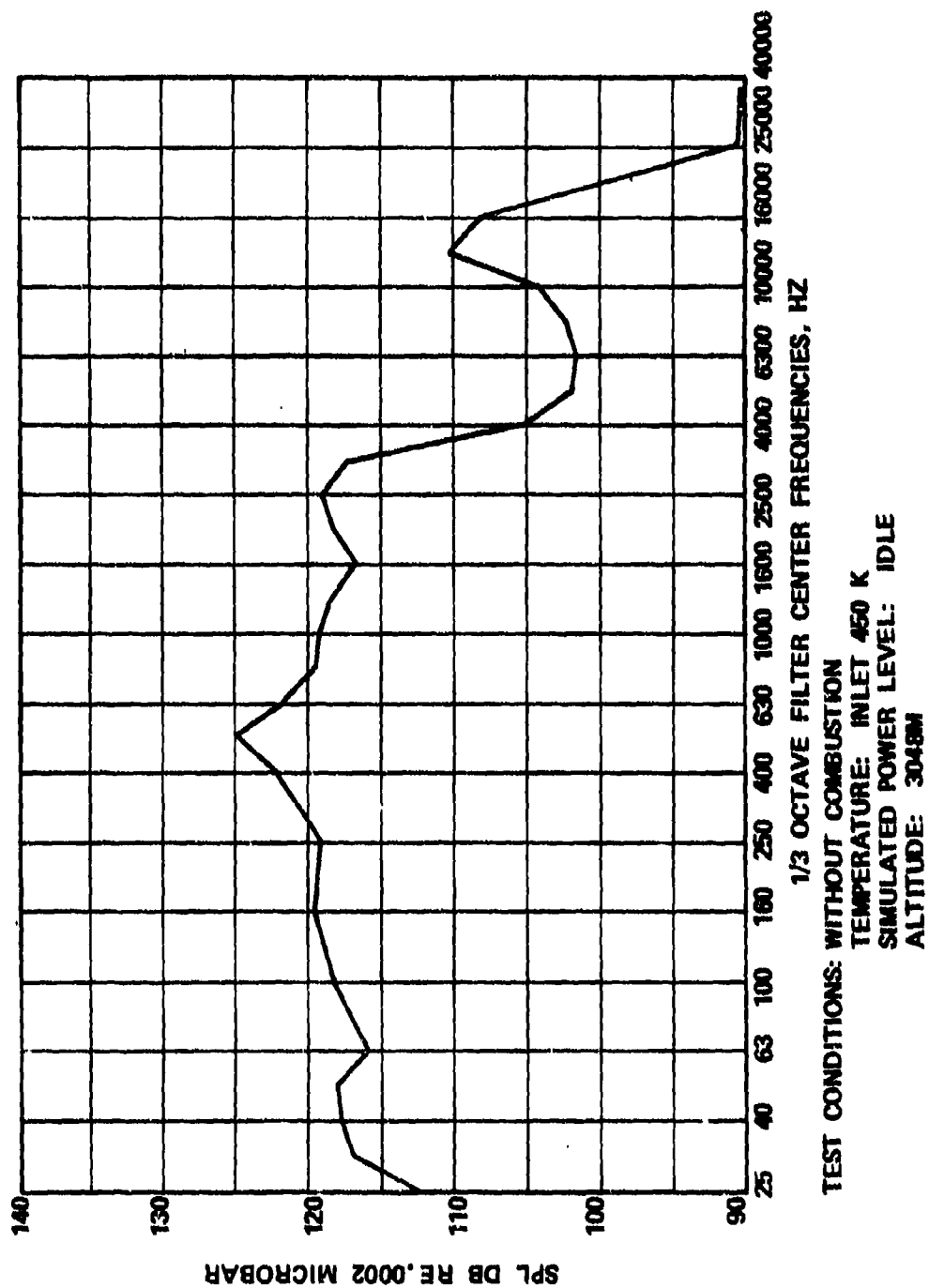
Figure 41. Combustor Sound Pressure Level without Combustion at 3048 Meters Idle.

88

1/3 OCTAVE FILTER CENTER FREQUENCIES, HZ
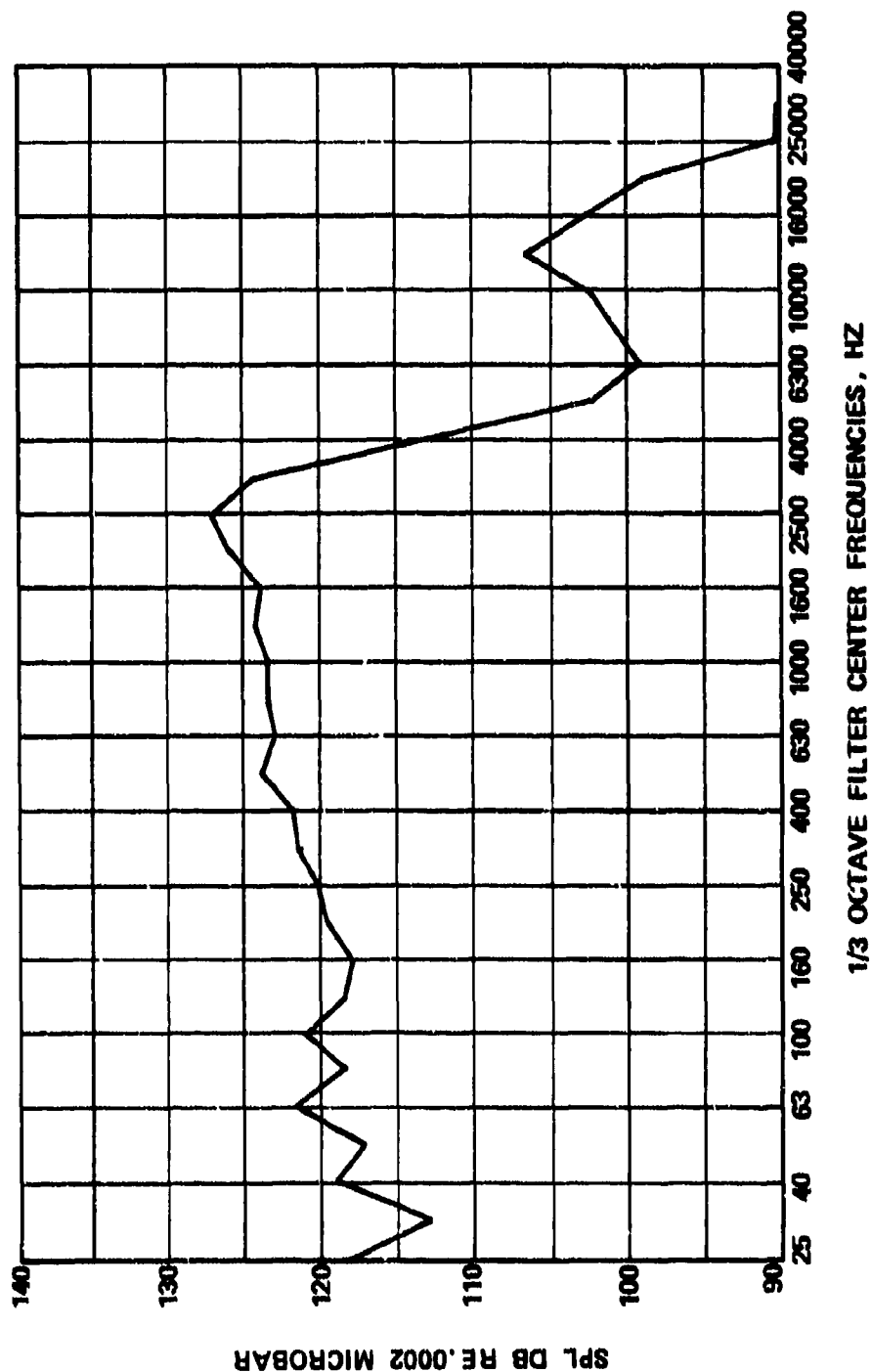
TEST CONDITIONS: WITH COMBUSTION
TEMPERATURE: INLET 429 K, EXHAUST 1005 K
SIMULATED POWER LEVEL: IDLE
ALTITUDE: 6096M

Figure 42. Combustor Sound Pressure Level with Combustion at 6096 Meters Idle.

TEST CONDITIONS: **WITHOUT COMBUSTION**
                   TEMPERATURE: INLET 436 K
                   SIMULATED POWER LEVEL: IDLE
                   ALTITUDE: 6096M
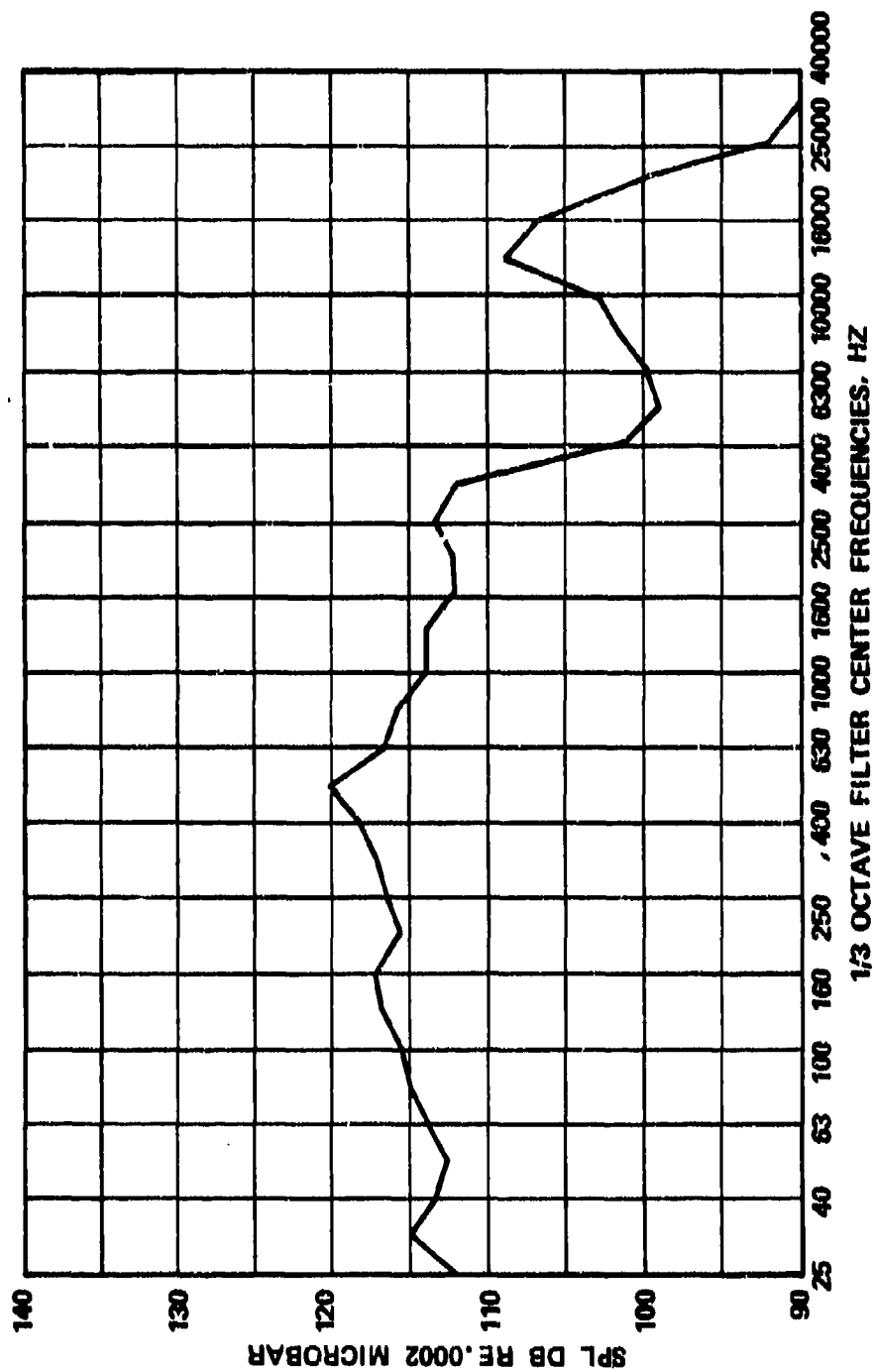
Figure 43. Combustor Sound Pressure Level without Combustion at 6096 Meters Idle.

90
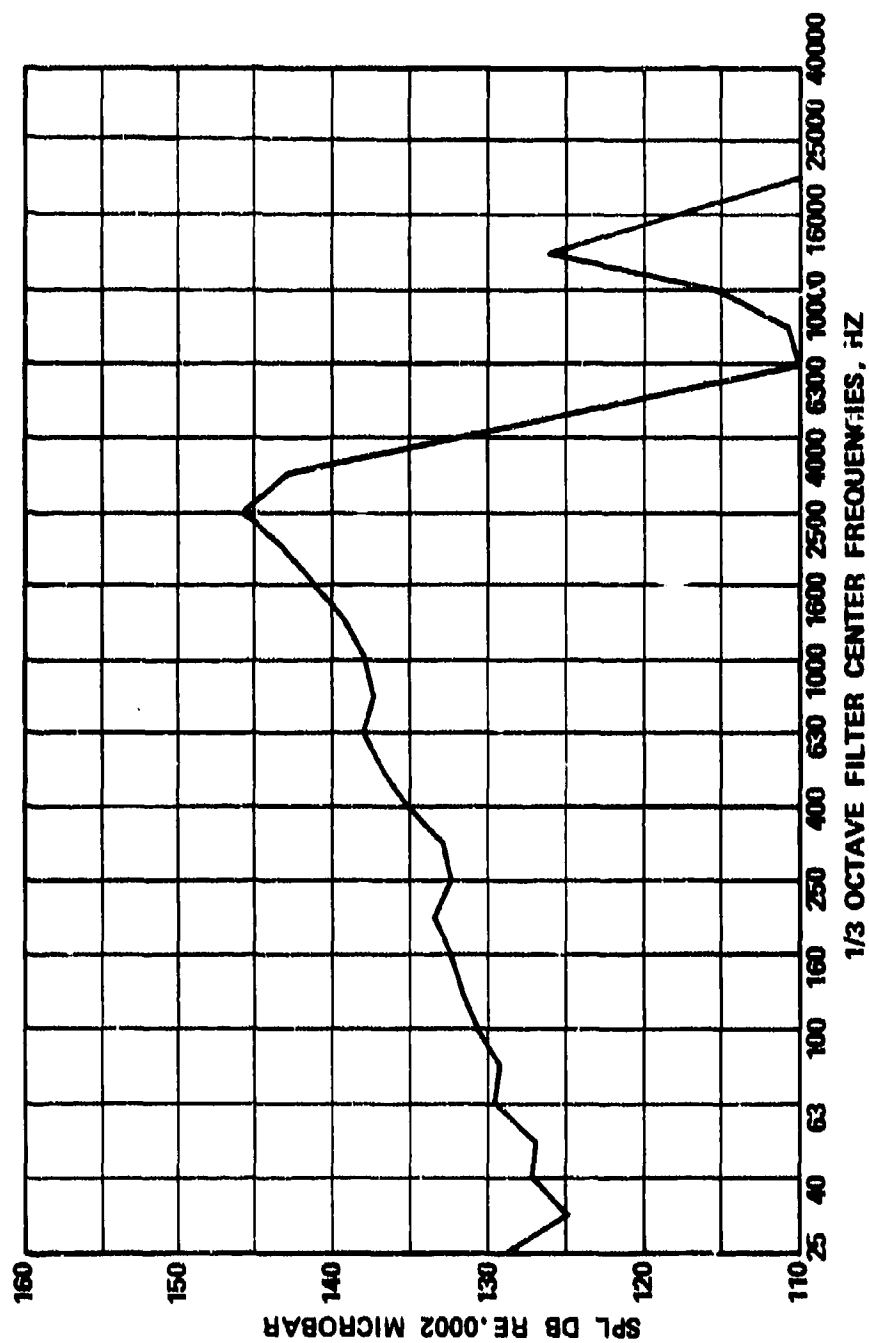
TEST CONDITIONS: WITH COMBUSTION
TEMPERATURE: INLET 623 K, EXHAUST 1533 K
SIMULATED POWER LEVEL: MAXIMUM
ALTITUDE: SEA-LEVEL

Figure 44. Combustor Sound Pressure Level with Combustion at Sea-Level.
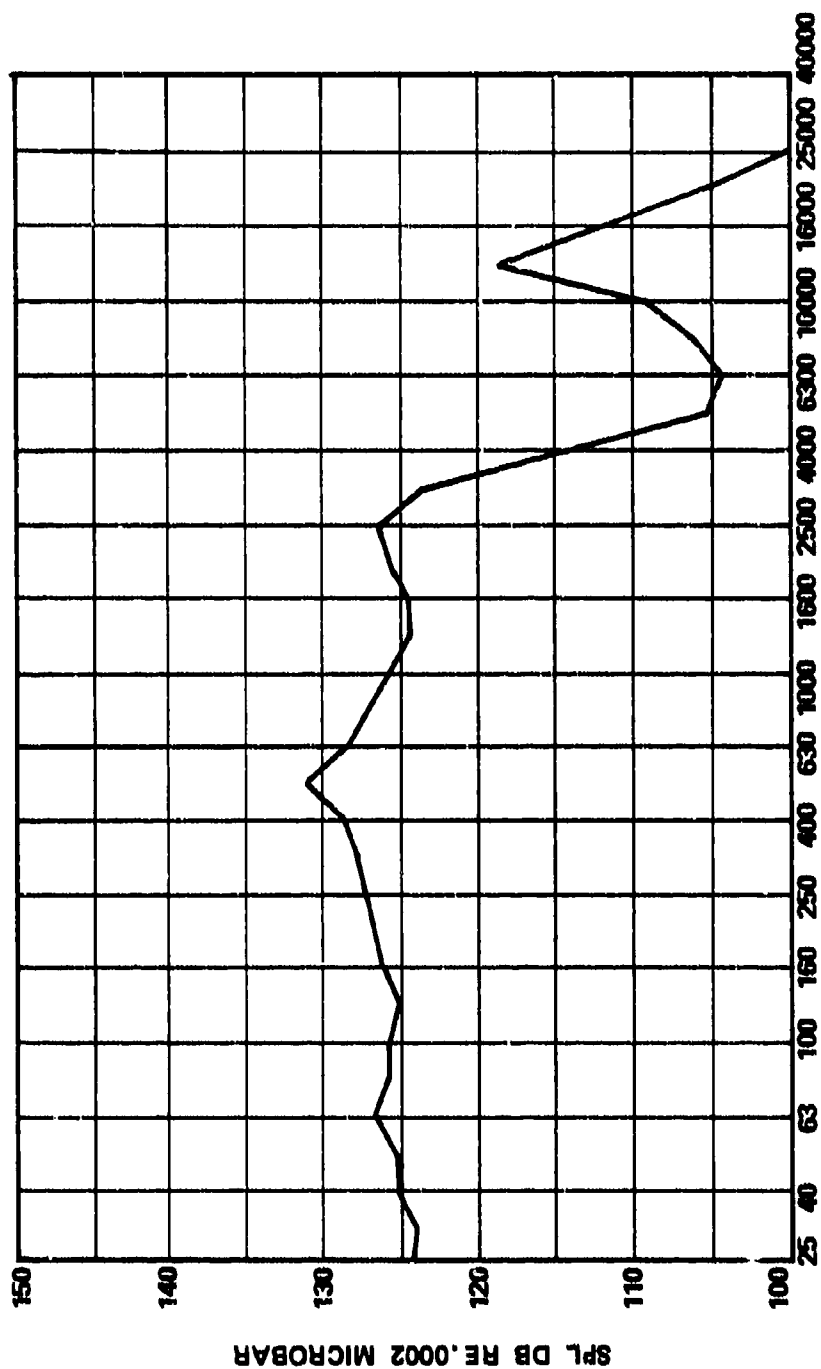
TEST CONDITIONS:

1/3 OCTAVE FILTER CENTER FREQUENCIES, HZ
WITHOUT COMBUSTION
TEMPERATURE: INLET 619 K
SIMULATED POWER LEVEL: MAXIMUM
ALTITUDE: SEA-LEVEL

Figure 45. Combustor Sound Pressure Level without Combustion at Sea Level and Maximum Power.
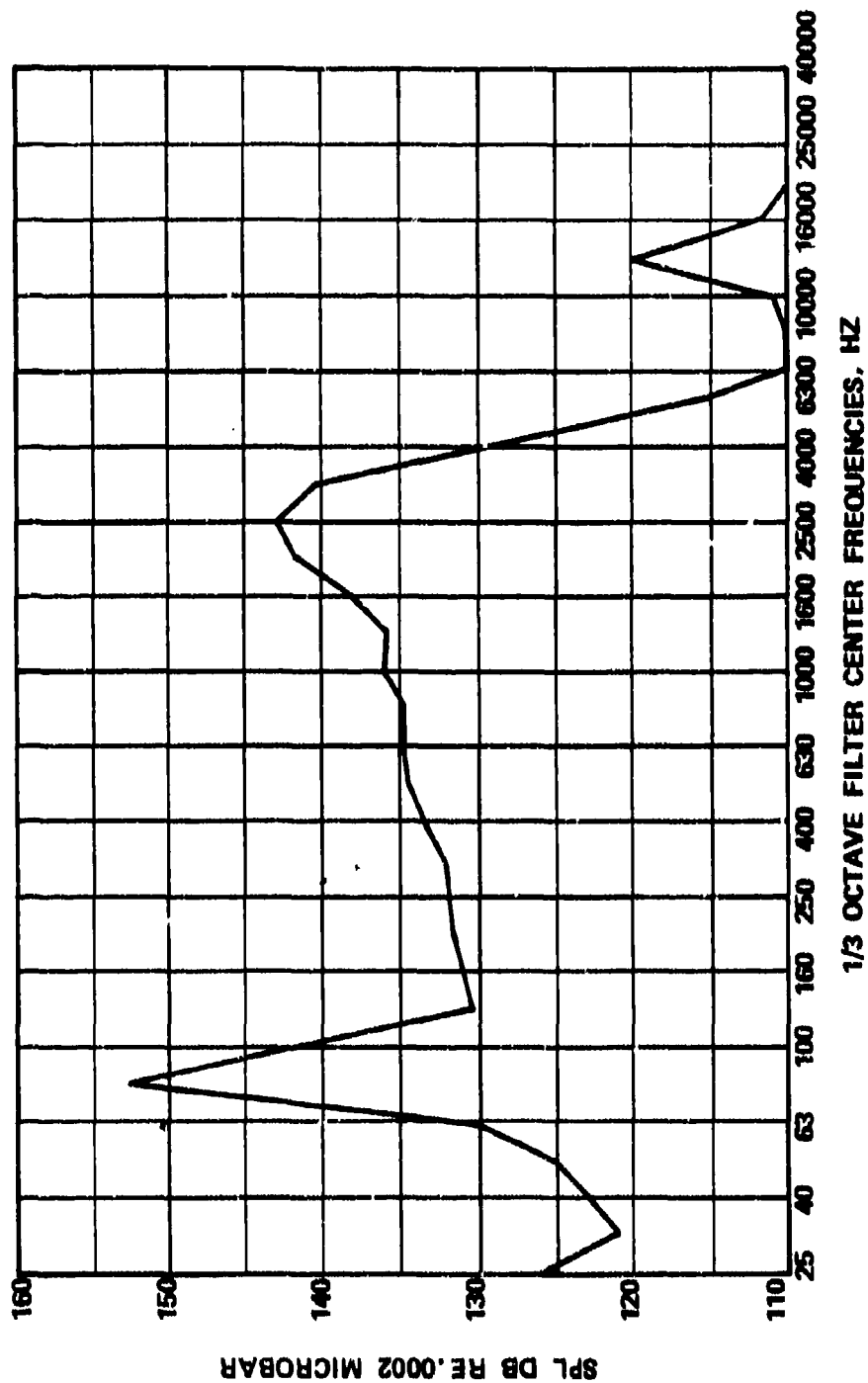
Figure 46. Combustor Sound Pressure Level with Combustion at 3048 Meters Maximum Power.
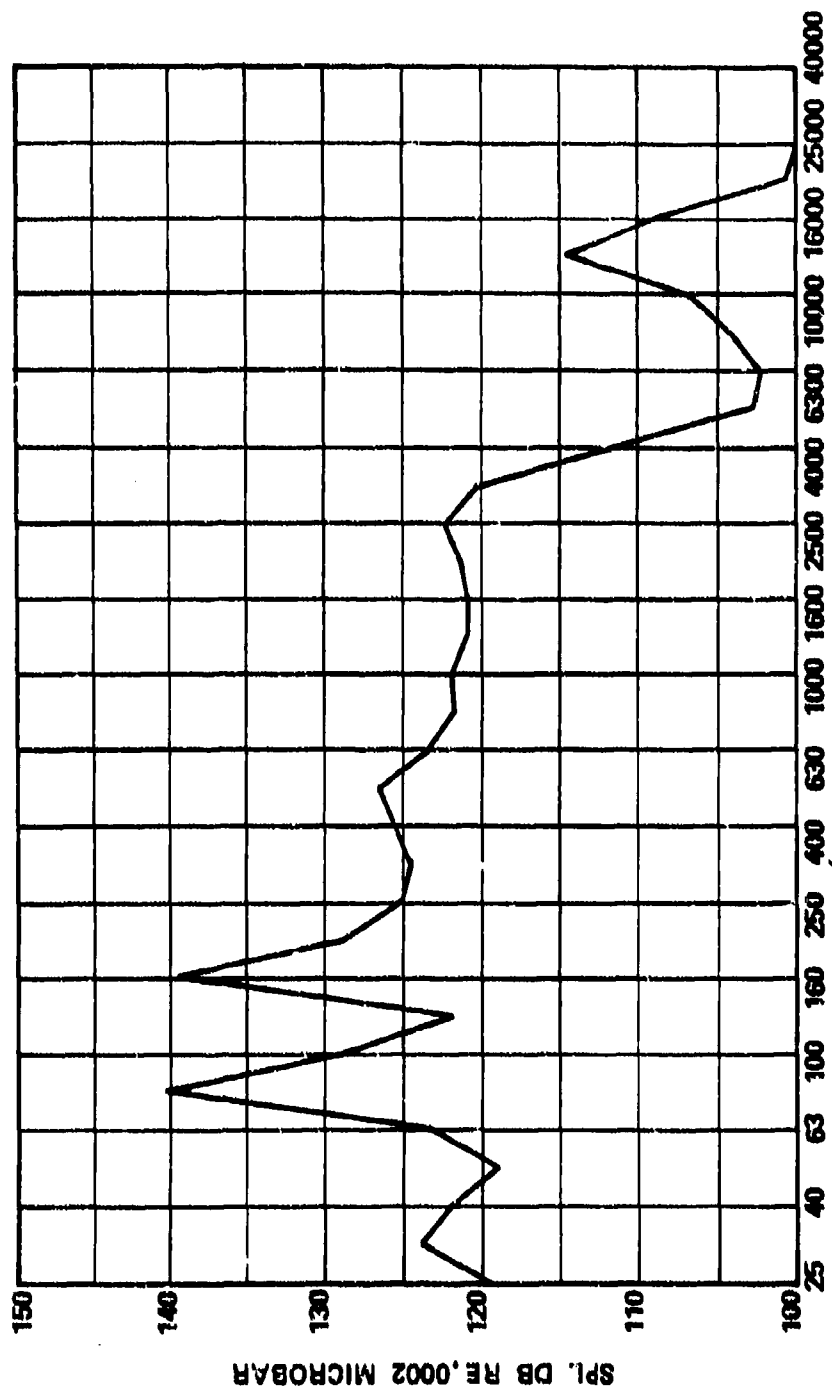
93

Figure 47. Combustor Sound Pressure Level without Combustion at 3048 Meters Maximum Power.

3048 meter 100-percent power condition. These values are all within limits normally expected for the combustion process.

C.   Concept II Testing

The rig test vehicle utilized in testing Concept II was the same as that described for Concept I. The instrumentation, both inlet and discharge, was the same for both concepts. The operating conditions for Concept II are tabulated in Table 2 of the Concept I data. The fuel nozzles were interchangeable.

1.   Preliminary Testing

The Concept II hardware was assembled with fuel nozzle immersion of 1.80 cm and a fuel nozzle back angle of 25 degrees. The preliminary testing was conducted with a basic fuel nozzle set (scalloped shrouds) with a spray-included angle (α) of 45 degrees. Air flow distribution around the basic Concept II combustor annulus, as predicted by the annulus flow model, is given in Figure 48. The measured isothermal total pressure drop is shown in Figure 49. A typical exhaust temperature scan at taxi-idle is shown in Figure 50, with the corresponding radial profile shown in Figure 51. The peak of the radial temperature profile is around 30 percent of the channel height, the circumferential pattern factor was 0.210, with a radial pattern factor of 0.036.

Included in the preliminary testing was the optimization of the fuel nozzle immersion and back angle. The optimum nozzle immersion was found to be nominal, as was predicted for a 90-degree spray. Increasing the back angle from 25 degrees to 50 degrees did not significantly change the exhaust-temperature quality as shown in Figure 52. Since the spray-included angle of the basic nozzle was 45 degrees as opposed to the desired 90 degrees, rig tests were conducted to evaluate the effect of nozzle air-assist on the pattern factor, wall temperatures, liner
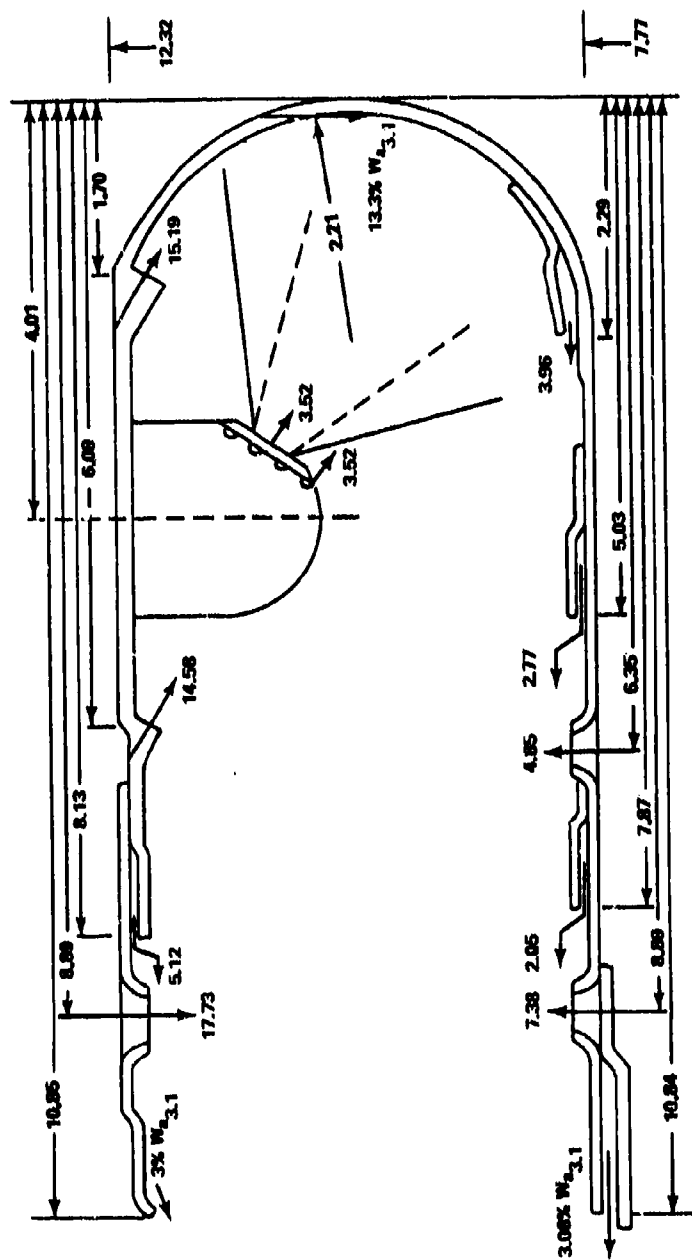
LINER COOLING AIR = 19.96% $w_{a_{3.1}}$

ALL DIMENSIONS IN CM.

Figure 48. Airflow Distribution Around Concept II Liner.
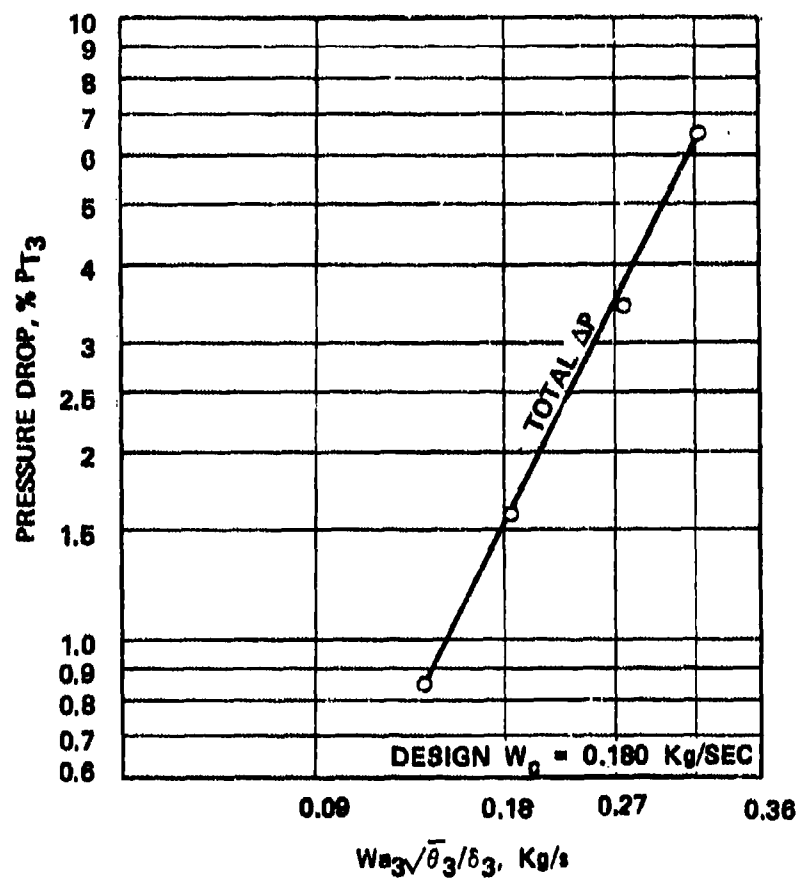
Figure 49. Measured Isothermal Total Pressure Drop of Concept II

97

WT AVG = 980 WT TSF = 0.26 ST AVG = 982, ST TSF = 0.121
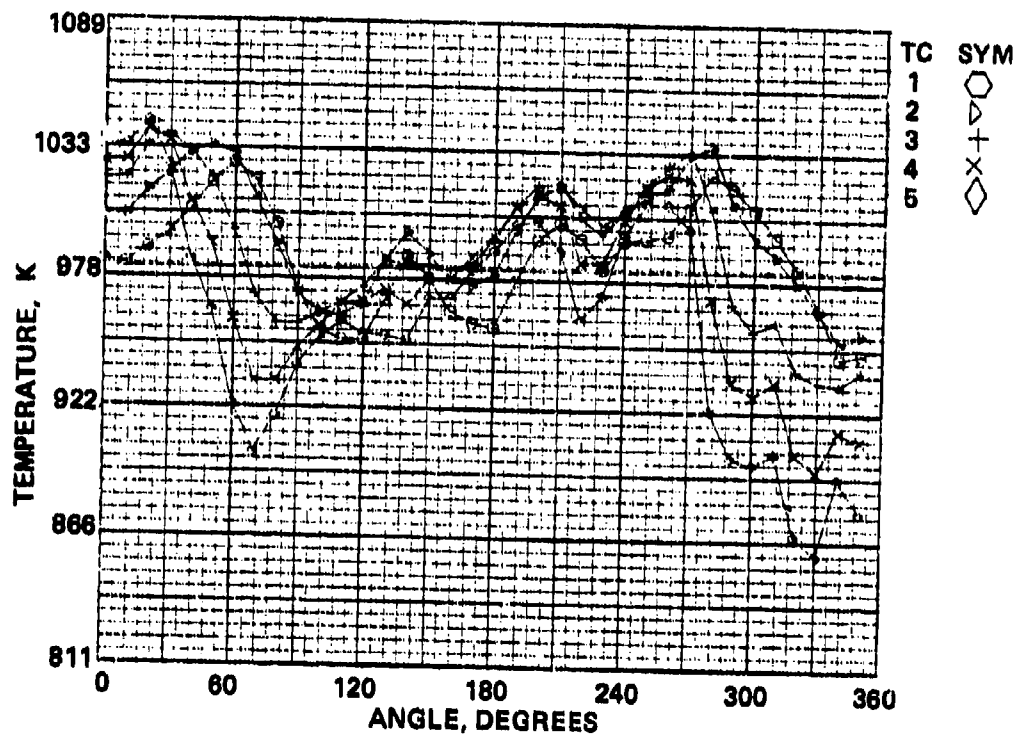
Figure 50. Exhaust Temperature Scan of Concept II at Taxi-Idle with Nozzle Back-Angle = 25°, Nozzle Immersion Depth = 1.81 cm, and Air-Assist Δp = 552 kPa
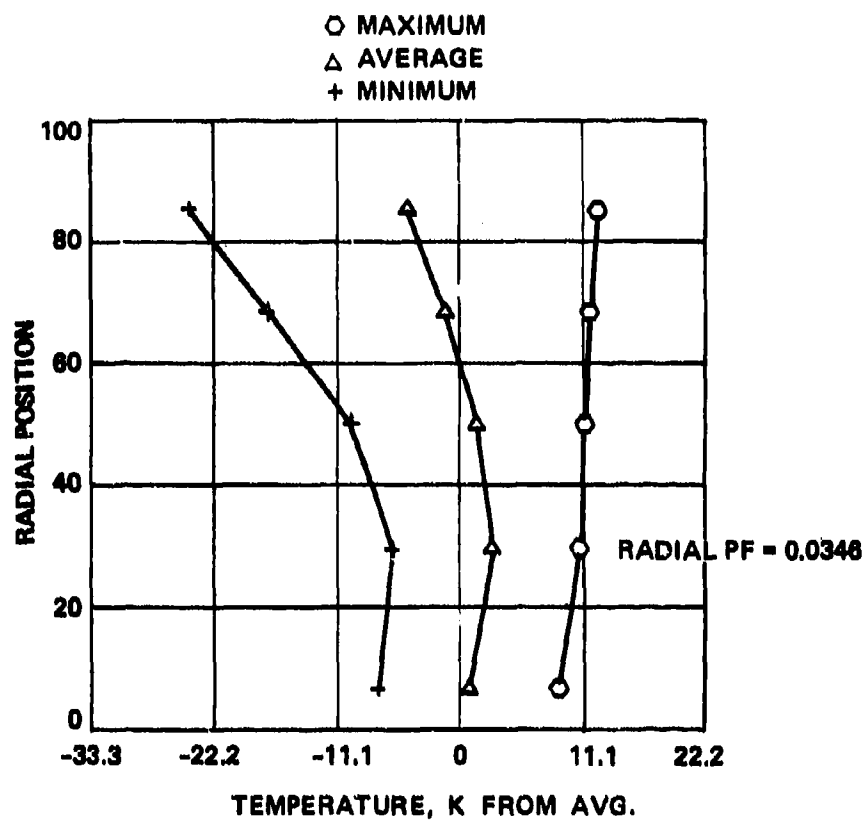
Figure 51. Radial Temperature Profile of Concept II at Taxi-Idle
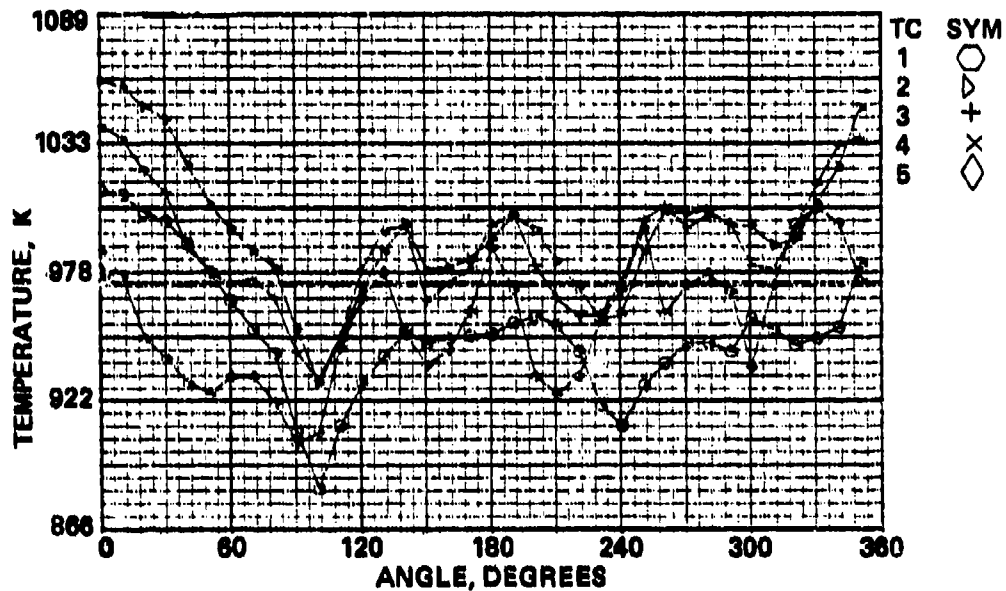
Figure 52.   Exhaust Temperature Scan of Concept II at Taxi-Idle
with Nozzle Back-Angle = 50°, Nozzle Immersion
Depth = 1.81 cm, and AA ΔP = 552 kPa.

carbon formation, and gaseous emissions. In general, increasing air-assist ΔP improved the pattern factor at all of the power points tested with different back angles.

Figure 53 shows Concept II liner wall temperature levels and characteristics as obtained with OG-6 Thermindex temperature paint. The dome area exhibited excessively high temperature levels and gradients. Increasing the fuel nozzle back angle to 50 degrees (Figure 54) improved wall temperature gradients, but the dome air jets appeared to be ineffective in providing a cooling film for the dome. In addition, on the O.D. primary panel it was assumed that the twenty 6-degree sections spaced between the primary slots would not create a significant structural durability problem as the air from the neighboring slots would be able to provide an effective cooling film due to the combustor inlet swirl. However, from the thermal paint photographs (Figure 53), the internal combustor flow field does not appear to have sufficient swirl to provide a protective film for the uncooled sections. Since the 3-D combustor flow analysis was conducted with continuous primary slots and with the dome air entering radially, the observed hot spots (Figures 53 and 54) were not predicted by the model.

The gaseous emission characteristics of Concept II Basic Configuration with 50 degree back-angle fuel nozzles, as averaged from 36 scans of 10-second intervals, are summarized in Figures 55 through 57. The taxi-idle CO emission index decreased from 38.6 g/Kg fuel at air-assist (AA) ΔP of 275.8 kPa to 24.9 at 689.5 kPa as shown in Figure 55. The corresponding HC emission indices were 32.1 and 11.5, respectively, (Figure 56). The variation of idle gaseous emissions with fuel/air ratio is shown in Figure 57 with 413.7 kPa air-assist air pressure drop. The combustion efficiency increased from 89-percent at a f/a equal to 0.01 to 98.2 percent at the idle design point where the f/a equals 0.014. This efficiency level is slightly above the design goal of 98

NOTE: Isotherms written on combustor liner are in
        degrees F.   Convert degrees F to degrees K
        as follows: $K = (5/9)(F+459.67)$

Figure 53.   Concept II Liner Wall Temperature Characteristics at
             Sea Level 55-Percent Power Point. $P_{T3} = 765$ kPa
             $T_3 = 586$ K, $T_4 = 1288$ K, $\Delta P/P_t$ 2.2%, and Nozzle
             Back-angle = 25°.
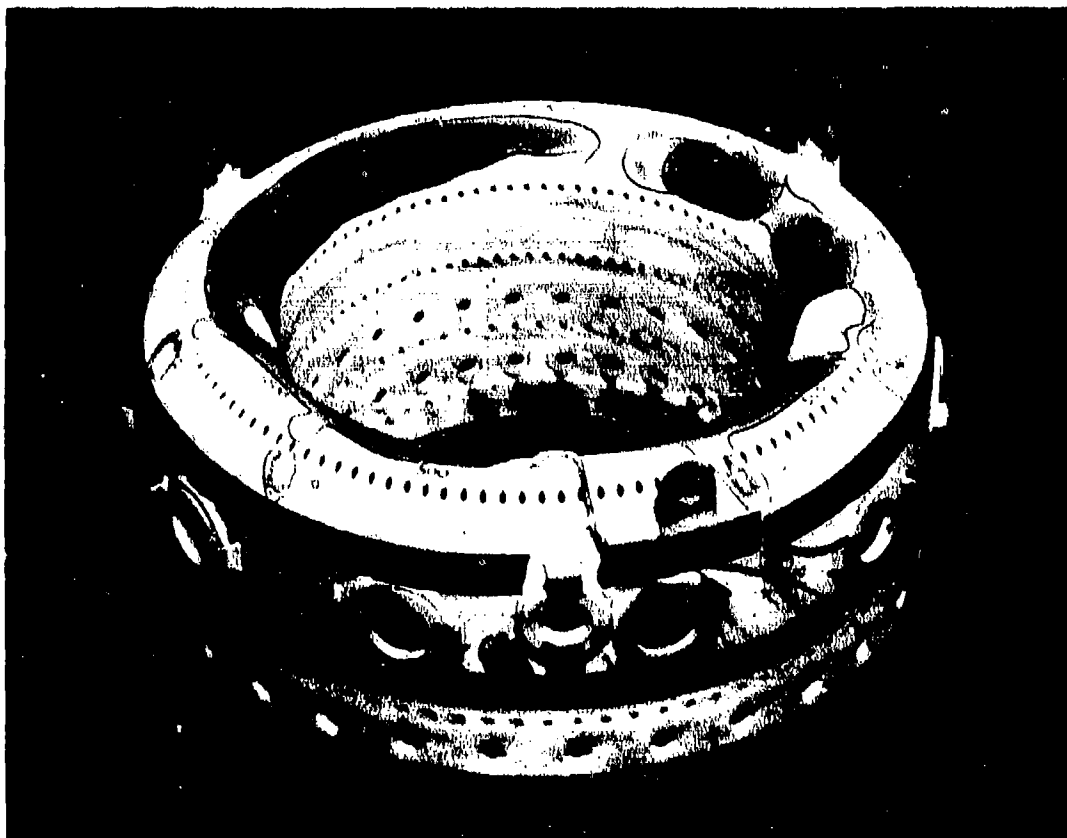
NOTE: Isotherms written on combustor liner are in degrees
F. Convert degrees F to degrees K as follows:

$$K = (5/9)(F+459.67)$$

Figure 54. Concept II Liner Wall Temperature Characteristics at
Sea-Level 55-Percent Power Point, $P_{T3} = 765$ kPa
$T_3 = 585$ K, $T_4 = 1318$ K, $\Delta P/P_t = 2.1\%$ and Nozzle
Back-angle $= 50°$.

103
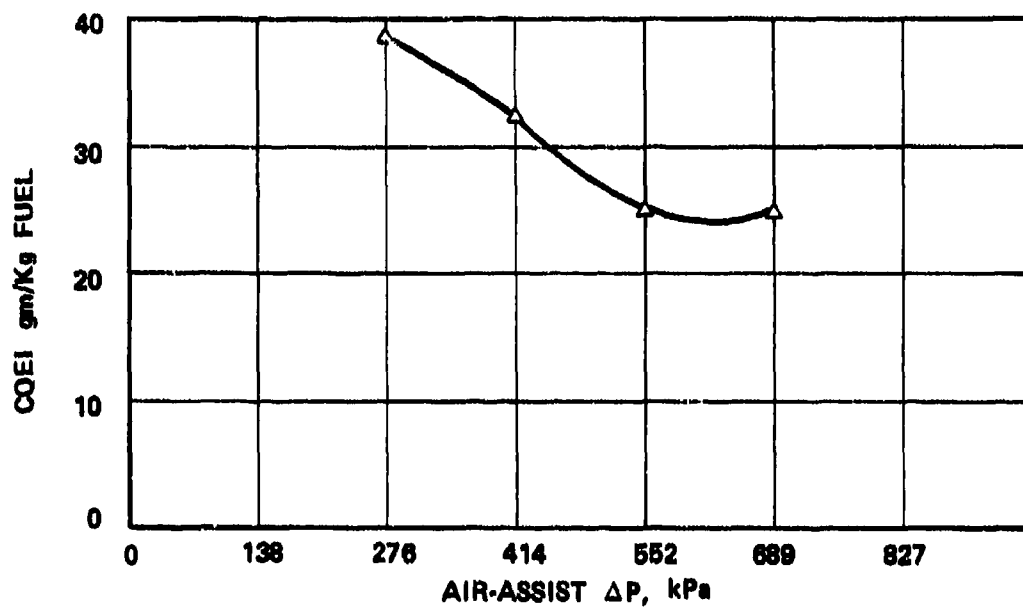
Figure 55.   CO Emission Index Versus Air-Assist Air-Pressure
Drop of Concept II at Taxi-Idle with Scalloped
Shrouds (α=45°) and Nozzle Back-angle (β)=50°.
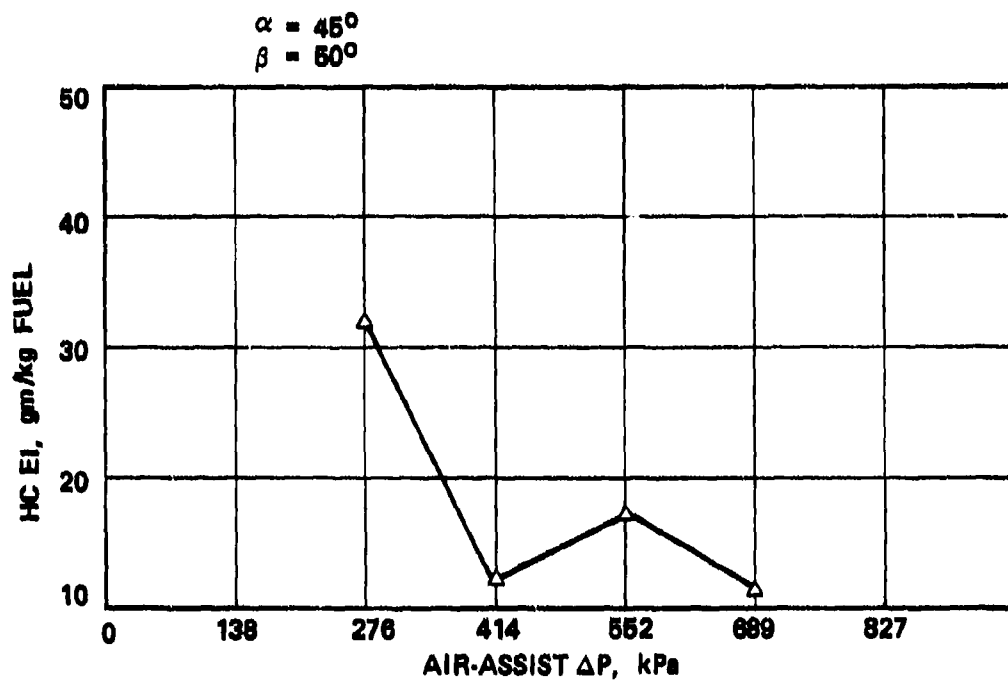
Figure 56.   HC Emission Index Versus Air-Assist
            Air-Pressure Drop of Concept II at
            Taxi-Idle.

105
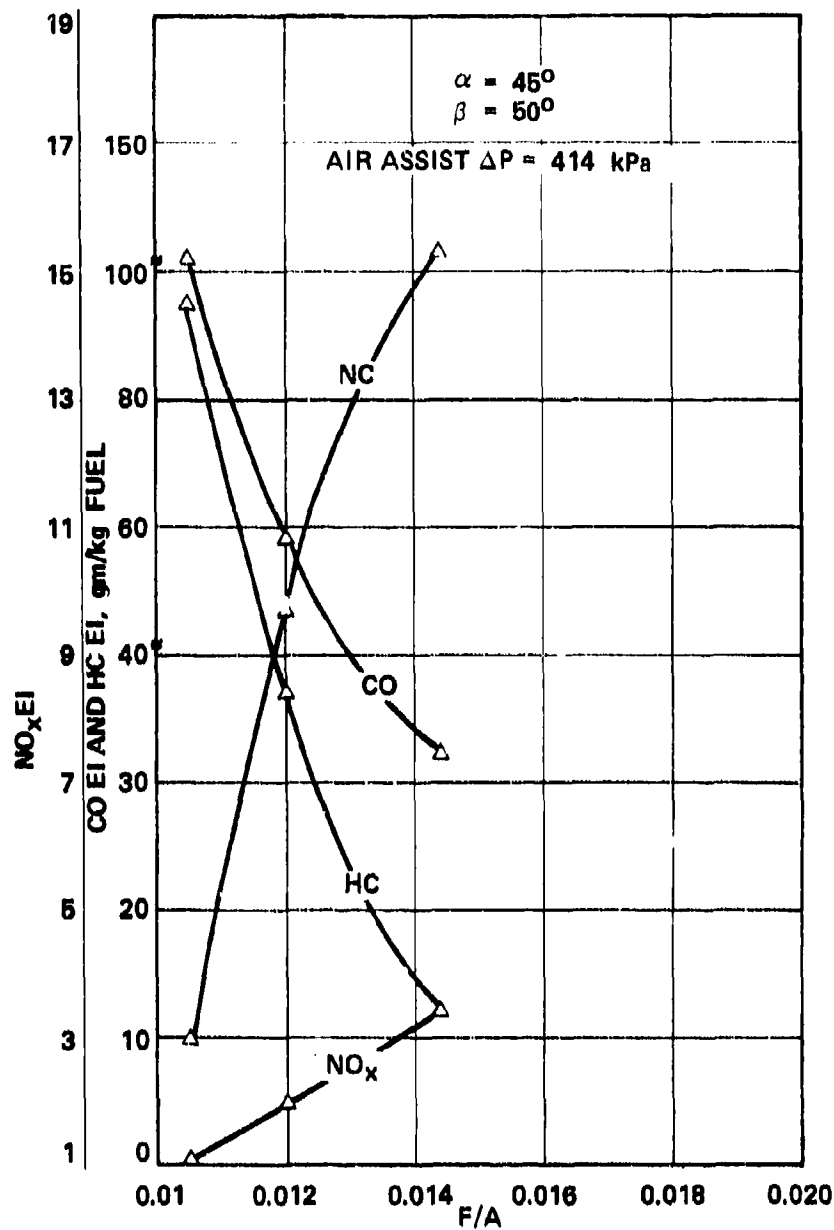
Figure 57.   Concept II Taxi-Idle Gaseous Emissions and
Combustion Efficiency Versus Fuel/Air Ratio.

106

percent. The measured combustion efficiency of the baseline design, at the 55-percent power point, was 99.9 percent, and the corresponding smoke number was zero.

The preliminary testing indicated that Concept II would probably be considered a successful candidate if the liner wall temperature levels and gradients could be brought down to the design objective of 1144 K and 210K/cm. Concept II also exhibited poor lean blowout characteristics, which was attributed to a weak recirculation zone and a nozzle cone angle of 45 degrees with resulting higher degree of nozzle-to-nozzle communication. The latter observation was made by comparing the exhaust temperature scan made with the 10-nozzle configuration versus T_4 profiles measured when only five fuel nozzles were flowing with the fuel-flow per nozzle remaining the same in both cases.

2. Combustor Modifications

Based upon Concept II preliminary data analysis and 3-D predictions, it was decided to modify the basic combustor (P/N 3551512). The modified combustor has 30 equally spaced 0.475-cm-diameter primary holes placed 3.86 cm from the combustor dome to change the internal flow field. In order to alleviate the liner cooling problem, as shown in Figure 58, a number of hardware changes were undertaken. The high temperature regions between the 20 slots on the O.D. primary panel, as described in the previous section, necessitated cooling of these areas. The slots near the dome were cooled by placing nine discrete cooling bands between the slots as shown in Figure 59. In addition, coarse-transpiration cooling holes were placed upstream of the igniter grommet. The area between the ten slots downstream on the O.D. panel were not cooled to determine if moving the I.D. primary orifices would terminate the reaction upstream and alleviate the liner temperature in this area. A directing skirt was placed under the tangential jets in the dome to sweep the dome with the
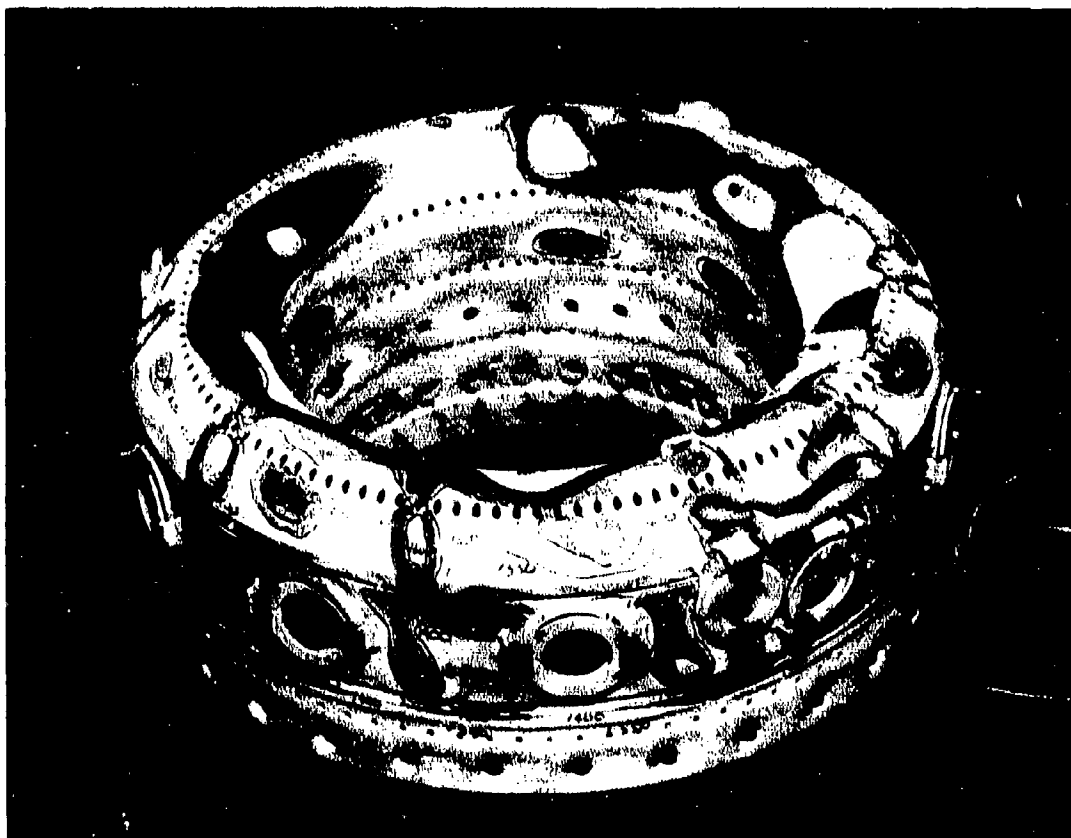
107

NOTE: Isotherms written on combustor liner are in degrees F.
Convert degrees F to degrees K as follows:
$$K = (5/9)(F+459.67)$$

Figure 58. Concept II Liner Wall Temperature Characteristics
at Sea-Level, 75-Percent Power Point, β = 50 Degrees.
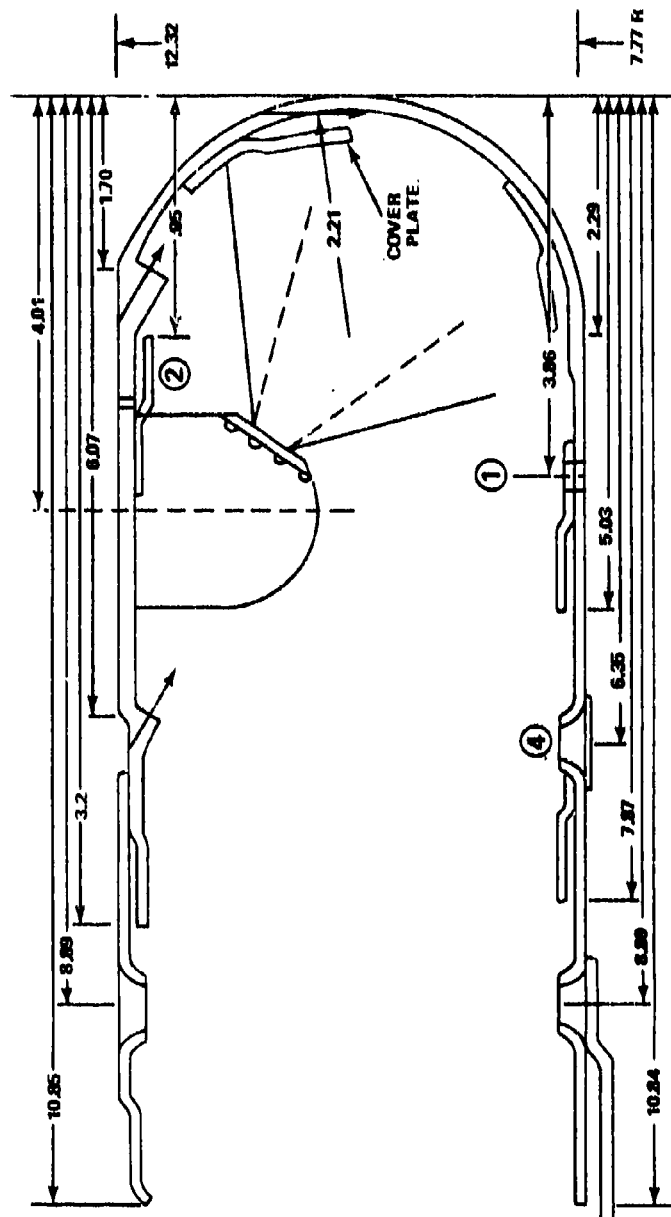
MODIFICATIONS FROM CONCEPT II (DRAWING NO. 3551512)

① ADDITION OF ID PRIMARY HOLES (30 – 0.475 CM DIA) EQUALLY SPACED INLINE WITH EXISTING ID PRIMARY HOLES MARKED ④

② 9 ISOLATED COOLING BANDS WITH EACH HAVING 5 – 0.173 CM HOLES

③ COARSE - TRANSPIRATION COOLING HOLES (32 – 0.05 CM DIA HOLES) PLACED UPSTREAM OF IGNITER GROMMET

④ BLOCK OFF - EXISTING ID PRIMARY HOLES MARKED

DIMENSIONS IN CM

Figure 59.   Concept II -3 Combustor

air, as was originally intended. In order to better understand the Concept II combustor flow field, the above proposed hardware changes were accomplished in two intermediate steps, as depicted in Figures 60 and 61. In the -1 combustor, the air-flow rate through the two rows of I.D. primary orifices marked 1 and 4 is equal to that through the I.D. primary holes of the -3 configuration. On the other hand, the airflow rate through the I.D. primary for the -2 configuration (Figure 61) is equal to that of the basic configuration, as shown in Figure 48. The -4 combustor (Figure 62) employs a coarse-transpiration cooling scheme between the ten slots downstream of the fuel nozzles.

Figure 63 shows the wall-temperature characteristics of the -1 combustor at the sea-level, 75-percent power point with the original shrouds and the nozzle back angle equal to 45 degrees. A significant improvement was obtained compared to the baseline (Figure 58). Further improvements in wall-temperature levels and gradients were achieved by decreasing the back angle to 25 degrees, as was originally desired (Figure 64).

The next test was conducted with the cooled unscalloped fuel nozzle shrouds which gave a cone angle (α) equal to 90 degrees. The wall-temperature results of this modification, which was intended to improve lean stability by increasing the spray cone angle to the design value, are shown in Figure 65. In a further attempt to improve lean stability, the combustor was modified to a -2 configuration in which the second row of 30 I.D. primary orifices were blocked. No adverse effects were noted in wall temperatures, as shown in Figure 66.

An acceptable exhaust-temperature quality was obtained with the -1 combustor and cooled unscalloped fuel nozzle shrouds with zero air-assist, as shown in Figure 67. Unlike the original shrouds, the nozzle air-assist with cooled unscalloped shrouds deteriorated the circumferential pattern factor, as typically
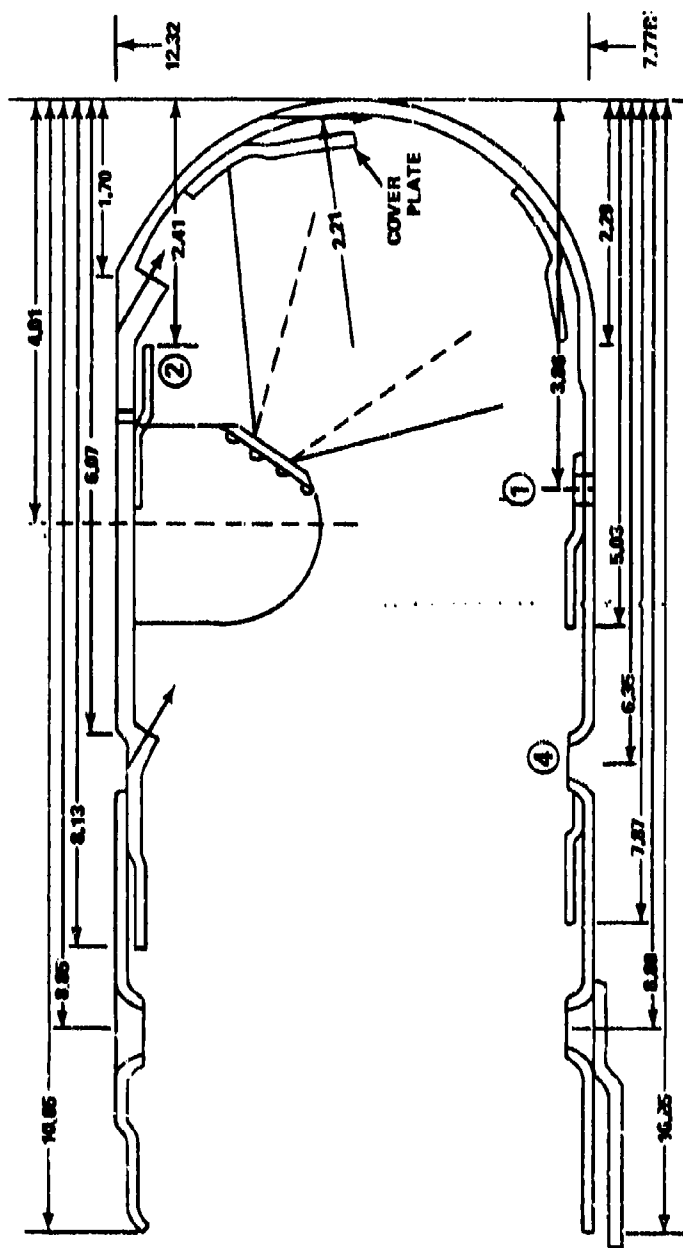
MODIFICATIONS FROM CONCEPT II (DRAWING NO. 3651512)

① ADDITION OF ID PRIMARY HOLES (30 – 0.33 CM DIA) EQUALLY SPACED INLINE EXISTING ID PRIMARY HOLES MARKED ④

② 9 ISOLATED COOLING BANDS WITH EACH HAVING 5 – 0.173 CM HOLES

③ COARSE-TRANSPIRATION COOLING HOLES (32 – 0.05 CM DIA HOLES) PLACED UPSTREAM OF IGNITER GROMMET

DIMENSIONS IN CM

Figure 60. Concept II –1 Combustor.
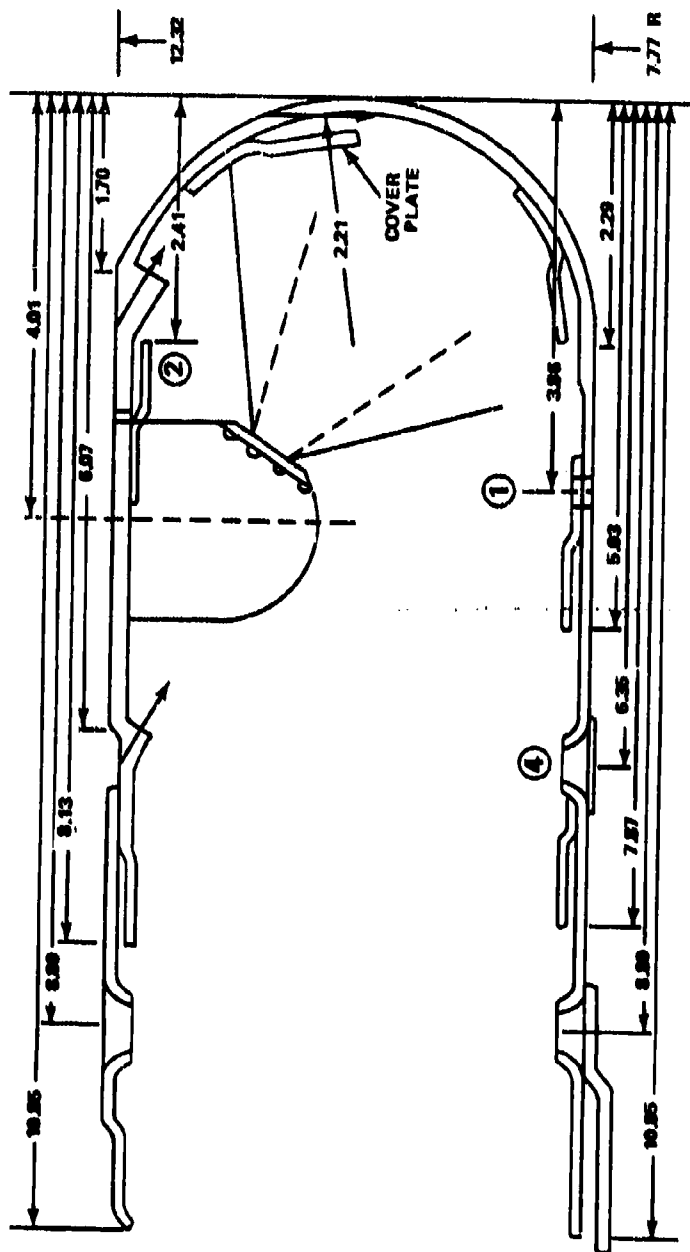
MODIFICATIONS FROM CONCEPT II (DRAWING NO. 3551512)

① ADDITION OF ID PRIMARY HOLES (30 — 0.33 CM DIA) EQUALLY SPACED INLINE WITH
   EXISTING ID PRIMARY HOLES MARKED ④

② 9 ISOLATED COOLING BANDS WITH EACH HAVING 5 — 0.173 CM HOLES

③ COARSE-TRANSPIRATION COOLING HOLES (32 — 0.05 CM DIA HOLES) PLACED UPSTREAM OF
   IGNITER GROMMET

④ BLOCK OFF EXISTING ID PRIMARY HOLES

DIMENSIONS IN CM

Figure 61. Concept II -2 Combustor.

112
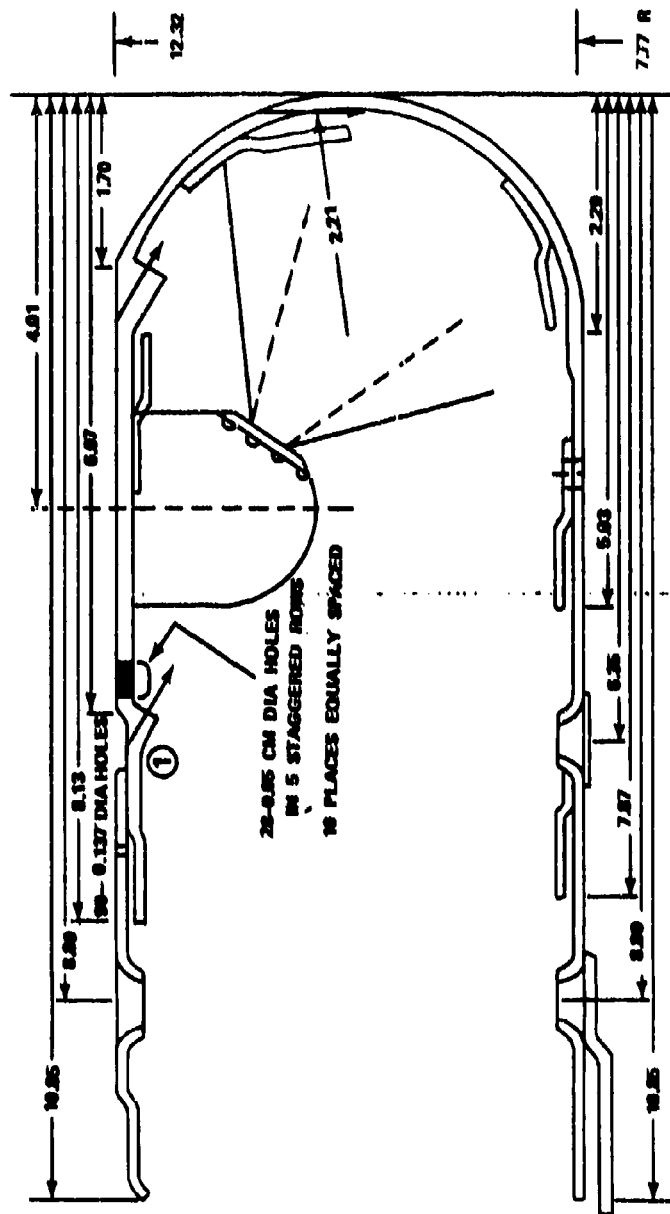
MODIFICATIONS FROM CONCEPT II - 3 CONFIGURATION

- ADDITION OF 90 – 0.137 CM DIA HOLES STAGGERED WITH EXISTING COOLING ORIFICES
- LOCAL COOLING OF REGIONS IN BETWEEN EXISTING 10 SLOTS DOWNSTREAM OF NOZZLES BY COARSE TRANSPIRATIONS COOLING

DIMENSIONS IN CM

Figure 62. Concept II, -4 Combustor.

113

NOTE: Isotherms written on combustor liner are in
degrees F. Convert degrees F to degrees K
as follows:

$$K = (5/9)(F+459.67)$$

Figure 63. Concept II -1 Liner Wall Temperature
Characteristics at Sea-Level, 75-Percent
Power Point, P_{T3} = 883 kPa, and β = 45 Degrees,
α = 45 Degrees.

114

NOTE: Isotherms written on combustor liner are in
        degrees F.   Conver: degrees F to degrees K
        as follows:
$$K = (5/9)(F+459.67)$$

Figure 64.   Concept II -1 Liner Wall Temperature Characteristics at
             Sea-Level, 75-Percent Power Point.   AA Δ P = 827 kPa, and
             β = 25 Degrees, α = 45 Degrees.

115

NOTE: Isotherms written on combustor liner are in degrees F. Convert degrees F to degrees K as follows:

$$K = (5/9)(F+459.67)$$

Figure 65. Concept II -1 Liner Wall Temperature Characteristics at Sea-Level, 75-Percent Power Point, with Cooled Unscalloped Nozzle Shrouds and β = 25 Degrees, α = 90 Degrees.

NOTE: Isotherms written on combustor liner are in degrees F. Convert degrees F to degrees K as follows:

$$K = (5/9)(F+459.67)$$

Figure 66. Concept II -2 Combustor Wall Temperature at 75-Percent Power Point with Cooled Unscalloped Nozzle Shrouds and $\beta = 25$ Degrees, $\alpha = 90$ Degrees.

117
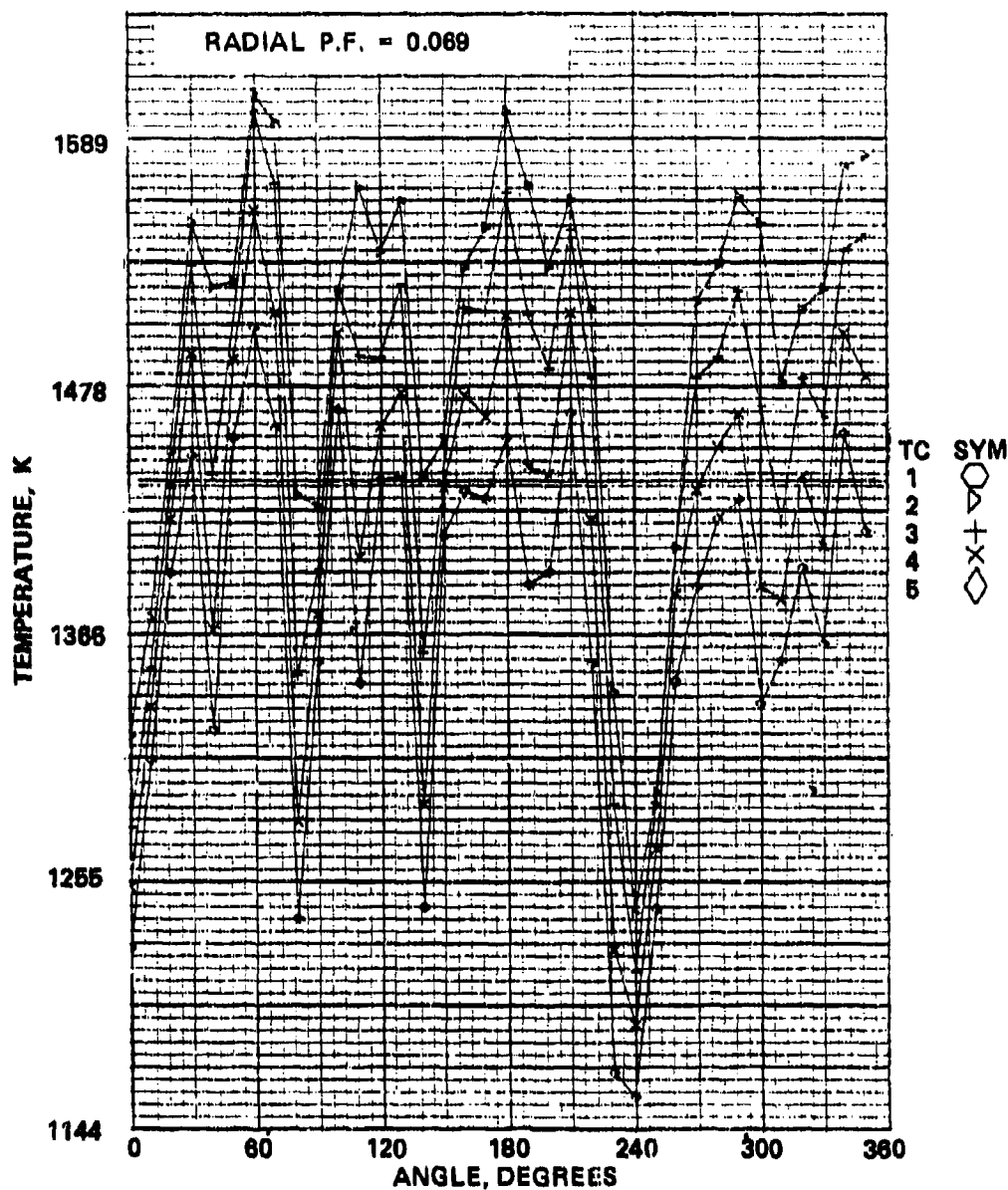
Figure 67. Exhaust-Temperature Scan of Concept II -1 Combustor
at Sea-Level, 75-Percent Power Point with Cooled
Unscalloped Nozzle Shrouds (α =90°) and Air-Assist
ΔP = 0.

shown in Figure 68. The -2 combustor configuration exhibited a slightly higher circumferential pattern factor (Figure 69) as compared to the -1 combustor (Figure 67).

The Concept II -2 combustor was then modified to the -3 configuration (Figure 59) which exhibited a circumferential pattern factor of 0.240 (Figure 70) at the sea-level, 75-percent power point.

The final configuration (-4 combustor) was produced by incorporating a coarse-transpiration cooling scheme between the ten slots downstream of the fuel nozzles.

3. Performance Mapping

Full performance data was recorded for the Concept II final configuration from taxi-idle to 100 percent power for altitudes from sea-level to 6096 meters. The measured circumferential pattern factors from the sea-level to 6096 meter altitude, maximum power points, as shown in Figures 71 through 75, varied between 0.21 and 0.26 when compared to the program goals of 0.23. Similarly, the wall-temperature characteristics were within the design goals, as shown in Figure 76.

Continuous scan data was taken on Concept II, by the same method as described for Concept I. Table 8 summarizes the data. As for Concept I, the percent error between 36 and 144 scans is acceptable.

4. Gaseous Emissions

The gaseous emissions at the sea-level idle conditions and the 6096-meter altitude 10-percent power condition, as a function of fuel/air ratio and air-assist pressure drop, are shown in

119

WT AVG = 1429. WT TSF = 0.323 ST AVG = 1426. ST TSF = 0.327
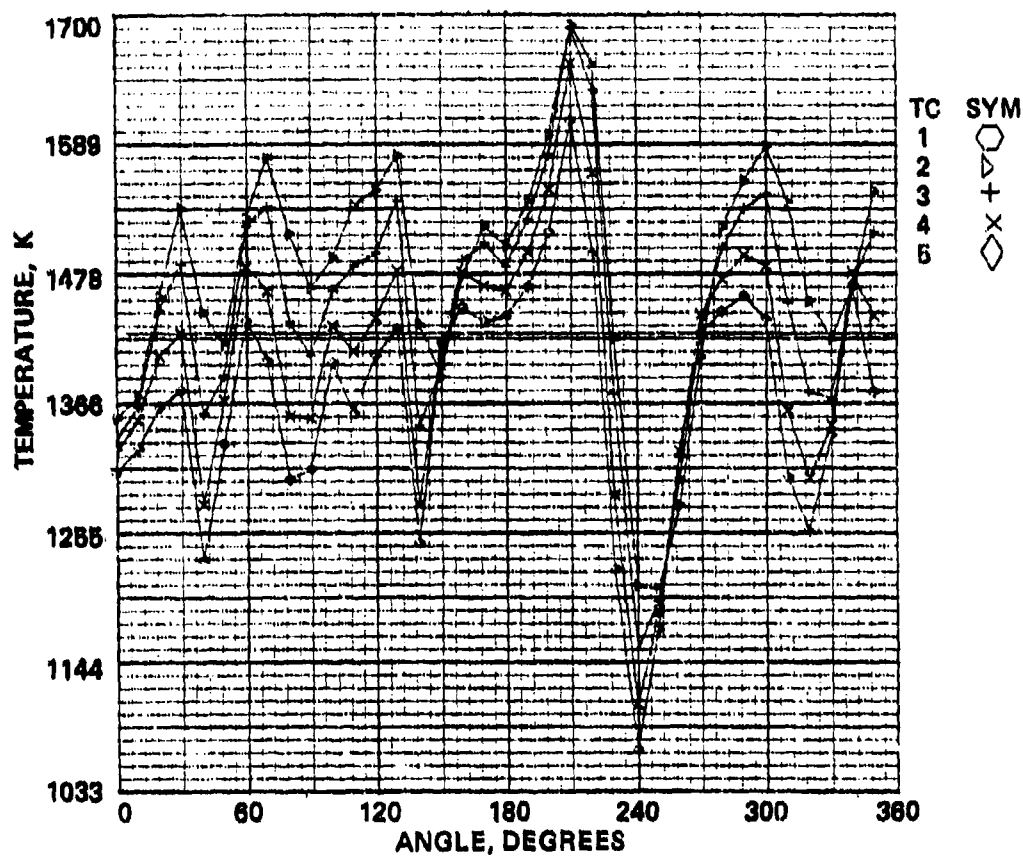
RADIAL P.F. = 0.061

Figure 68. Exhaust-Temperature Scan of Concept II -1 Combustor
at Sea-Level, 75-Percent Power Point with
Cooled Unscalloped Shrouds (α=90°) and Air Assist
ΔP = 414 kPa.

120

WT AVG = 1433.   WT TSF = 0.263   ST AVG = 1429.   ST TSF = 0.270

RADIAL P.F. = 0.071
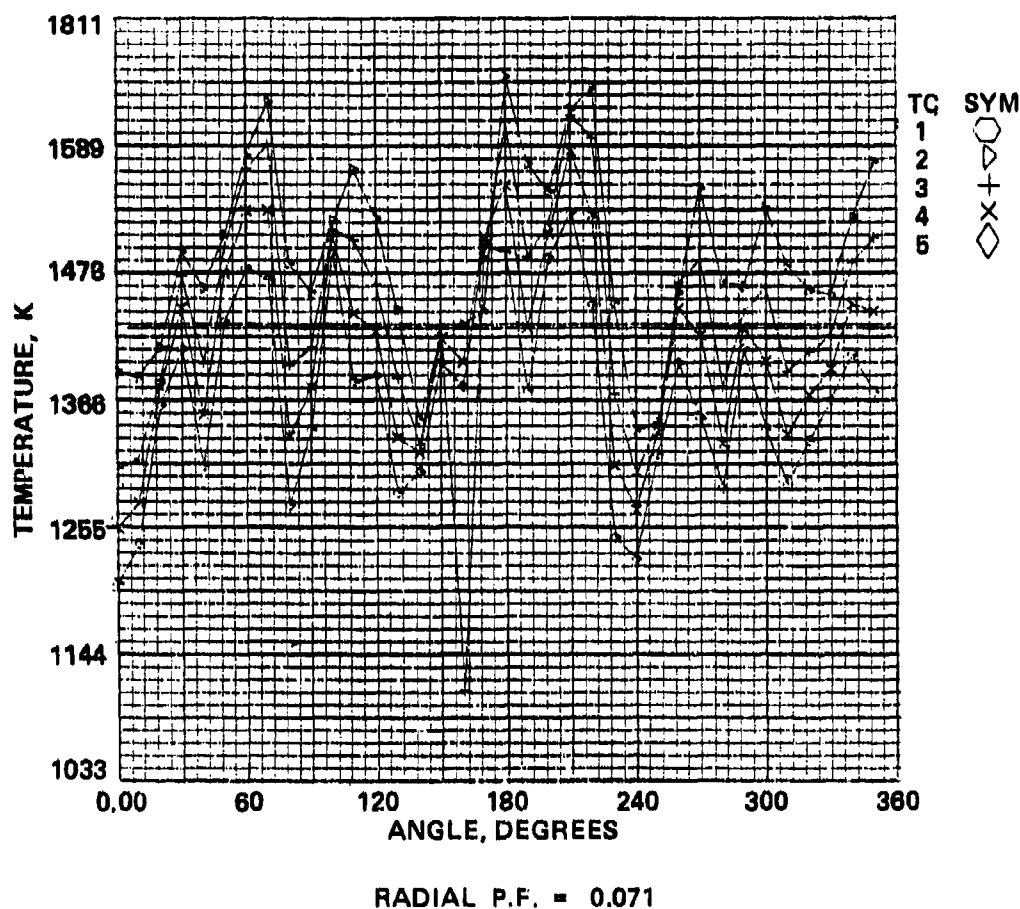
Figure 69.   Exhaust-Temperature Scan of Concept II
             -2 Combustor at Sea-Level 75-Percent Power Point
             with Cooled Unscalloped Shrouds (α=90°) and Air-
             Assist ΔP = 0.

121
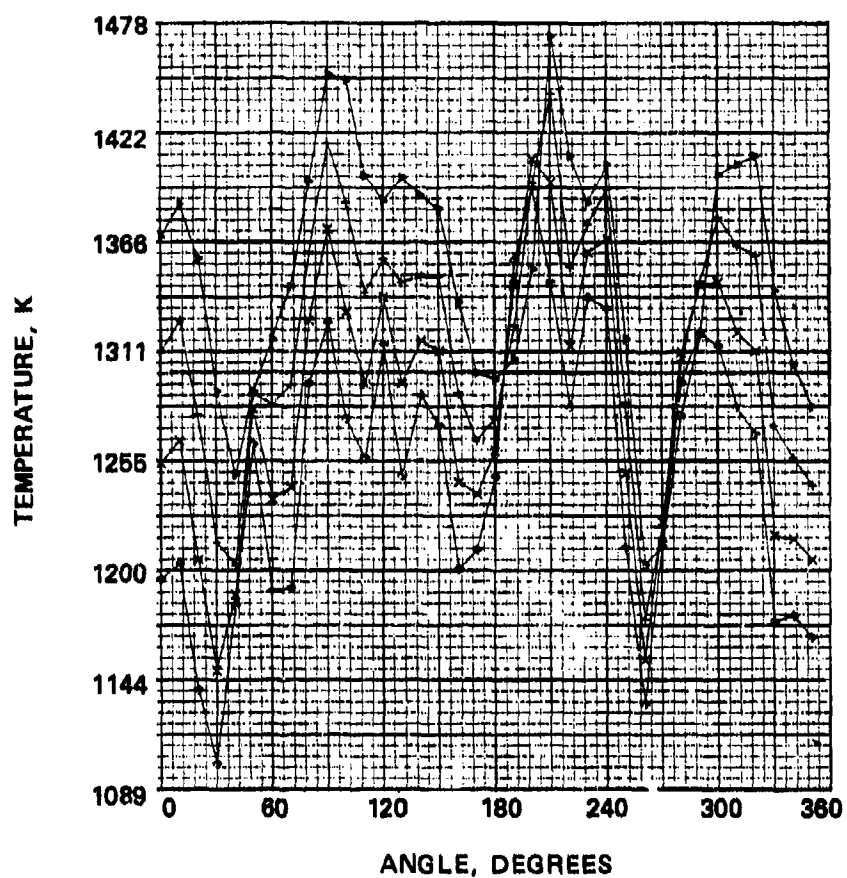
Figure 70. Concept II -3 Combustor Exhaust
Temperature Scan, $\beta = 25$ Degrees,
$\alpha = 90$ Degrees.

WT AVG = 1528.   WT TSF = 0.222   ST AVG = 1526.   ST TSF = 0.225
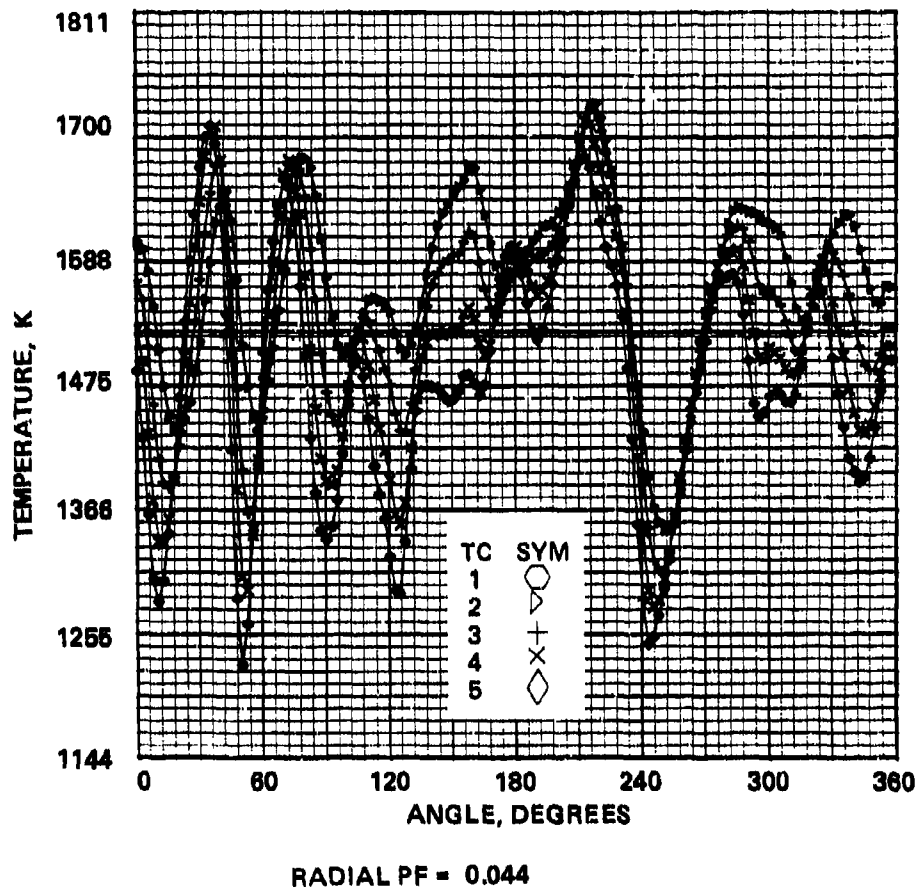
Figure 71.   Concept II -4 Exhaust Temperature Scan at
Sea-Level Maximum Power Point.

123

WT AVG = 1534.   WT TSF = 0.256   ST AVG = 1532.   ST TSF = 0.258
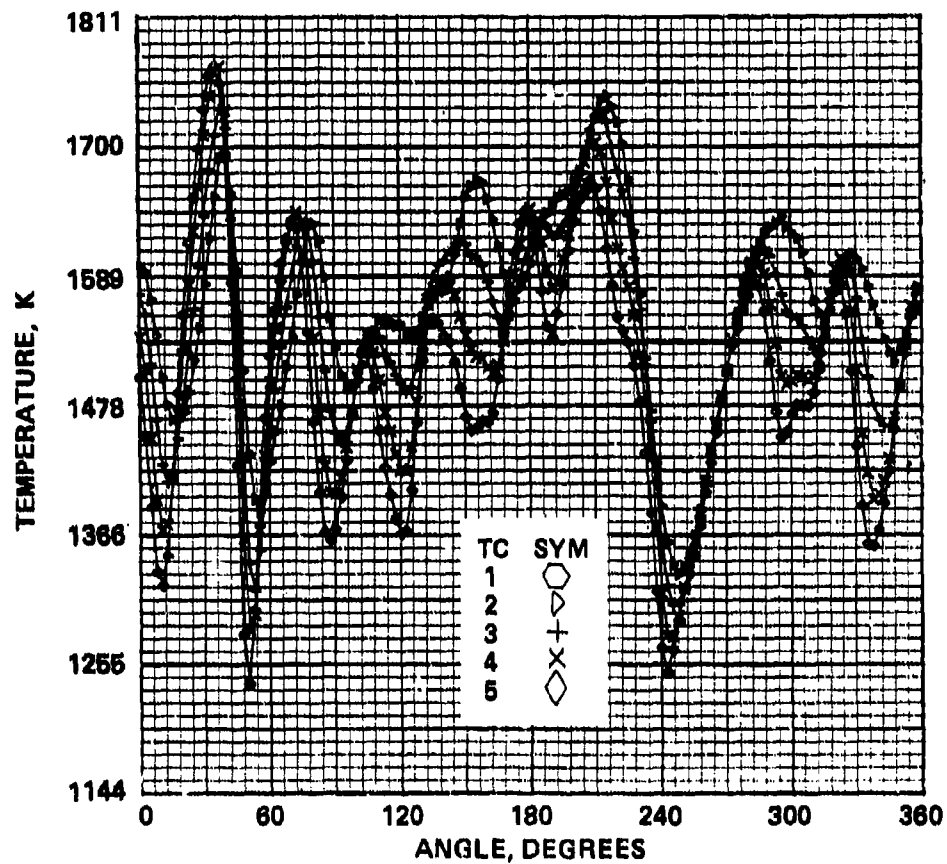
RADIAL PF = 0.0326

Figure 72.   Concept II -4 Exhaust Temperature Scan at
1524 M Altitude Maximum Power Point.

124

Figure 73.   Concept II -4 Exhaust Temperature Scan at 3048 Meter Altitude Maximum Power Point.

WT AVG = 1515. WT TSF = 0.211   ST AVG = 1514. ST TSF = 0.212
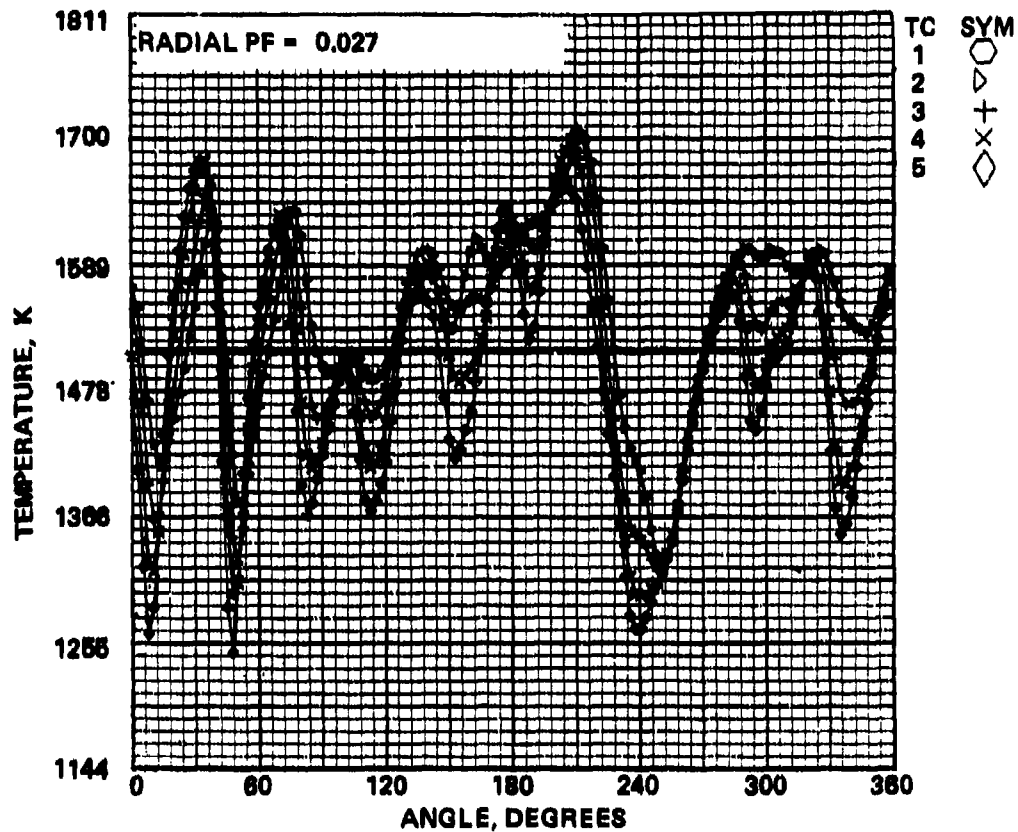
Figure 74.   Concept II -4 Exhaust Temperature Scan at
              4572 Meter Altitude Maximum Power Point.

126

WT AVG = 1532. WT TSF = 0.224   ST AVG = 1531.   ST TSF = 0.225
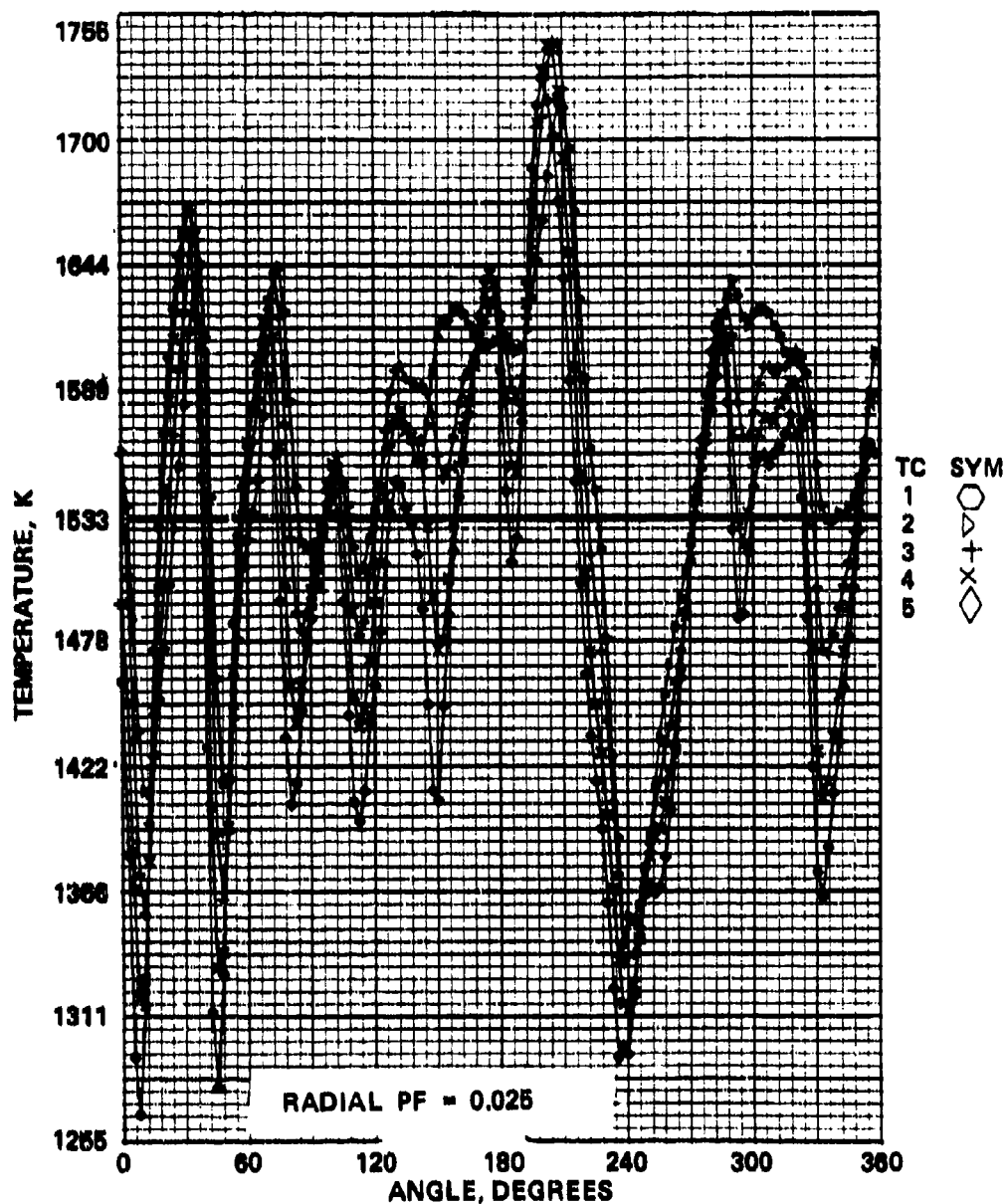
Figure 75.   Concept II -4 Exhaust Temperature Scan at
6096 Meter Altitude Maximum Power Point.

127

NOTE: Isotherms written on combustor liner are in
degrees F.   Convert degrees F to degrees K
as follows:

$$K = (5/9)(F+459.67)$$

Figure 76.   Concept II -4 Liner Wall Temperature Character-
istics at Sea-Level Maximum Power Point.

TABLE 8. EFFECT OF NUMBER OF CIRCUMFERENTIAL SCANS ON AVERAGE T_4 AND PF, CONCEPT I.

	Pattern Factor With					Average T_4 (K) With				
	144	72	48	36	24 Scans	144	72	48	36	24 Scans
SL maximum power	0.243	0.240	0.240	0.240	0.240	1564	1565	1565	1565	1565
1524 m altitude maximum power	0.223	0.223	0.223	0.225	0.226	1560	1559	1560	1559	1557
3048 m altitude maximum power	0.228	0.229	0.225	0.214	0.214	1551	1551	1550	1550	1550
4572 m altitude maximum power	0.267	0.267	0.268	0.268	0.268	1541	1541	1540	1540	1540
6096 m altitude maximum power	0.215	0.217	0.204	0.172	0.175	1538	1536	1537	1536	1533
SL 55-percent power	0.194	0.195	0.182	0.180	0.181	1345	1345	1345	1345	1344
1524 m altitude 54-percent power	0.189	0.189	0.186	0.182	0.187	1310	1309	1309	1309	1307
3048 m altitude 56-percent power	0.188	0.180	0.183	0.168	0.169	1298	1297	1297	1297	1296
4572 m altitude 59-percent power	0.237	0.235	0.237	0.236	0.219	1294	1294	1294	1293	1292
6096 m altitude 61-percent power	0.292	0.293	0.289	0.294	0.284	1334	1333	1333	1333	1331
SL 6-percent power	0.348	0.346	0.343	0.343	0.345	945	945	9	945	945
1524 m altitude 5-percent power	0.342	0.338	0.342	0.331	0.332	931	931	931	931	931
3048 m altitude 6-percent power	0.343	0.343	0.336	0.343	0.309	944	944	943	944	943
4572 m altitude 8-percent power	0.335	0.334	0.334	0.334	0.333	964	964	964	964	965
6096 m altitude 10-percent power	0.352	0.351	0.351	0.351	0.351	950	950	950	950	950

Figures 77 through 81. Definition of the data symbols is presented in Table 9. The effect of nozzle back angle on idle efficiency with the fuel/air ratio is quite small as shown in Figure 77. The combustor was relatively insensitive to the angle variation between 12 and 25 degrees. A slight gain in combustion efficiency was obtained with JP-4 fuel (Figure 78) compared with Jet-A (Figure 77). In both cases, the idle combustion efficiency exceeded the program goal of 98 percent. Similarly, the performance at the 6096 meter altitude 10-percent power point was quite acceptable as depicted in Figure 79.

The CO levels as a function of air-assist pressure drop are shown in Figure 80. The basic combustor configuration with the scalloped fuel nozzle shrouds ($\alpha = 45°$) produced higher levels of CO as well as unburned hydrocarbons (Figure 81) and displayed poor blowout characteristics as summarized in Table 10. Figure 82 shows the NO_x emission index versus fuel/air ratio characteristics of Concept II at the sea-level 75-percent power point. The highest NO_x value was produced by the -1 combustor configuration with the scalloped fuel nozzle shrouds (as indicated by ∇) and the nozzle back angle equal to 45 degrees. Decreasing the fuel nozzle back angle to 25 degrees resulted in approximately a 20 percent reduction in NO_x without increasing the lean blowout fuel/air ratio (Table 10). Increasing the nozzle spray cone angle, i.e., using the cooled unscalloped fuel nozzle shrouds, brought some reduction in the NO_x level as expected. Increasing the primary zone fuel/air ratio (the -2 combustor configuration) resulted in increased NO_x output. The -3 combustor, which had the same primary zone airflow split as the -1 combustor configuration but with larger ID primary orifices and·smaller primary zone residence time produced the lowest NO_x levels. Increasing the air-assist pressure drop to 414 kPa caused a slight increase in NO_x emissions, indicating diffusion controlled stoichiometric or slightly lean combustion.

130
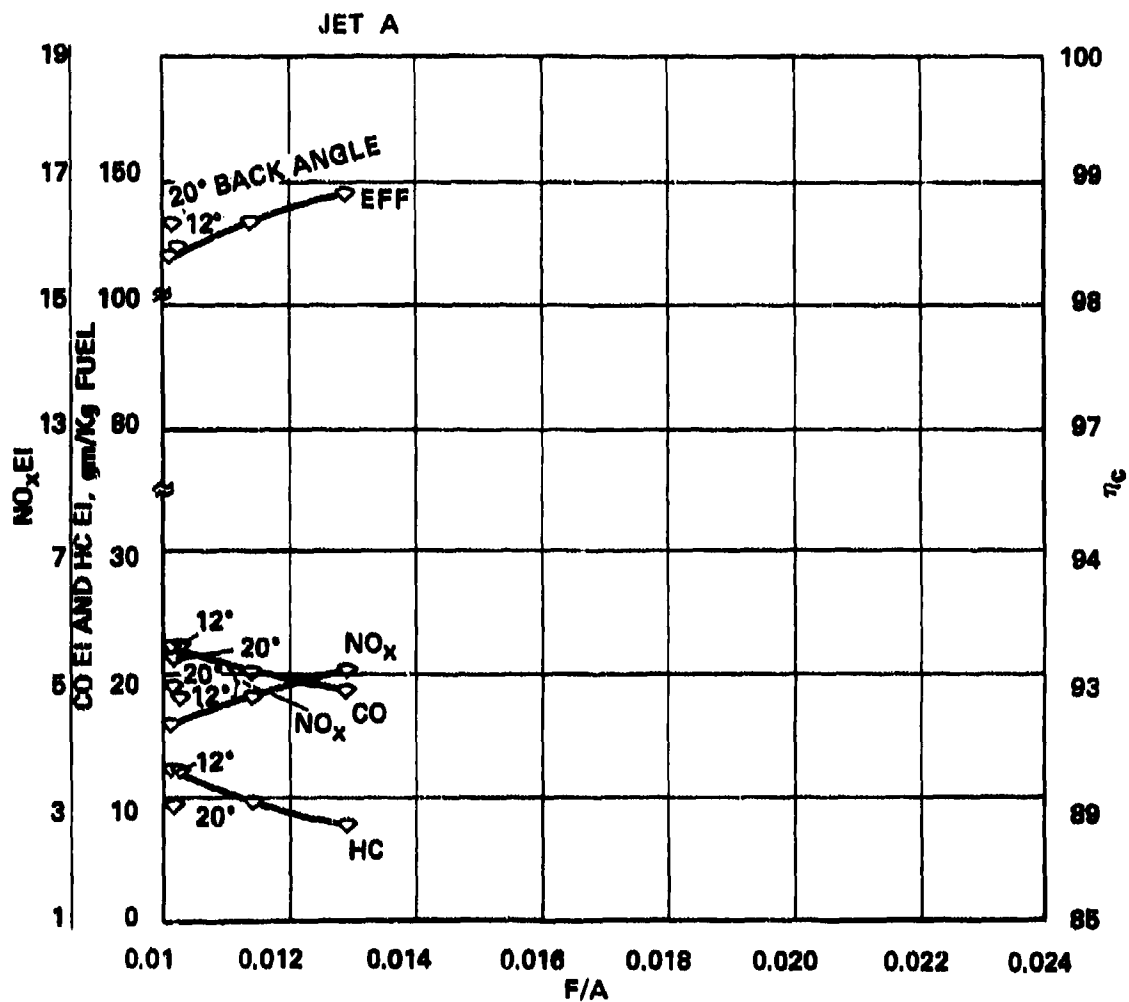
Figure 77. Effect of Nozzle Back-Angle and Fuel/Air Ratio on Concept II - 3 Combustor Gaseous Emissions at Sea-Level, Taxi-Idle with the Cooled Unscalloped Fuel Nozzle Shrouds ($\alpha = 90°$) - Air-Assist$\Delta P = 414$ kPa.

131
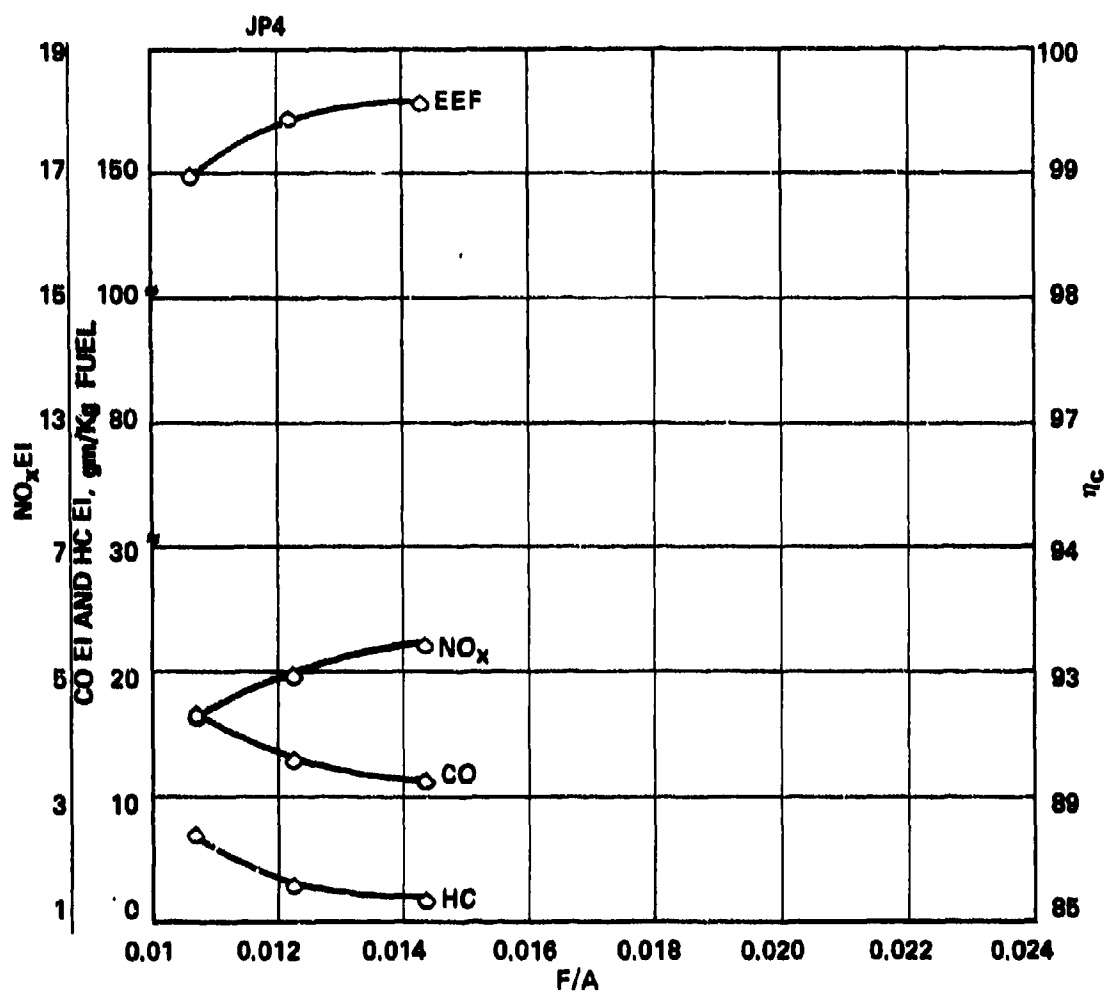
Figure 78. Concept II -4 Combustor Gaseous Emissions Versus
Fuel/Air Ratio at Sea-Level, Taxi-Idle with JP-4
Fuel – Air-Assist $\Delta P = 414$ kPa
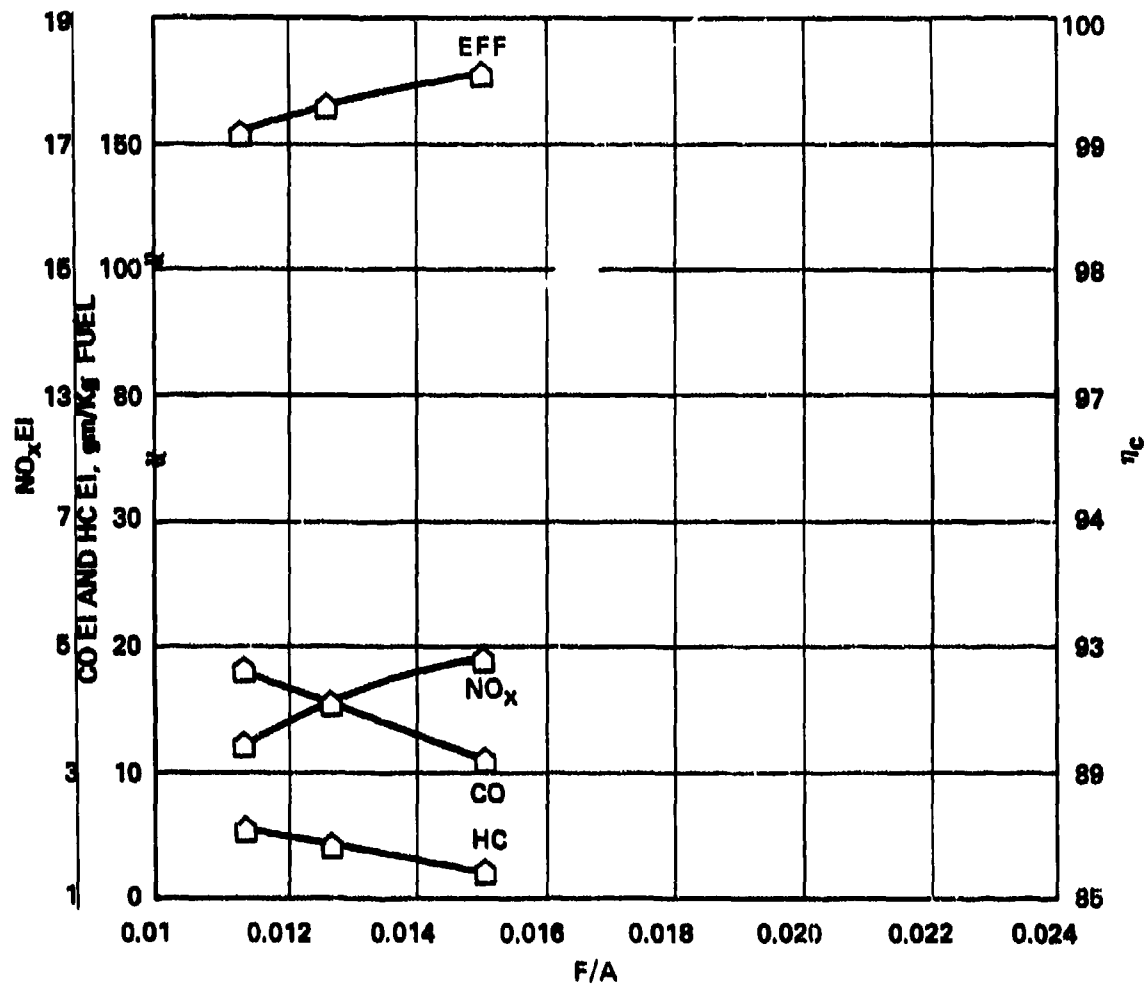
Figure 79. Concept II -4 Gaseous Emissions Versus Fuel/Air
Ratio at 6096 Meter Altitude 10-Percent Power
Point with JP-4 Fuel - Air-Assist ΔP = 414 kPa.

133
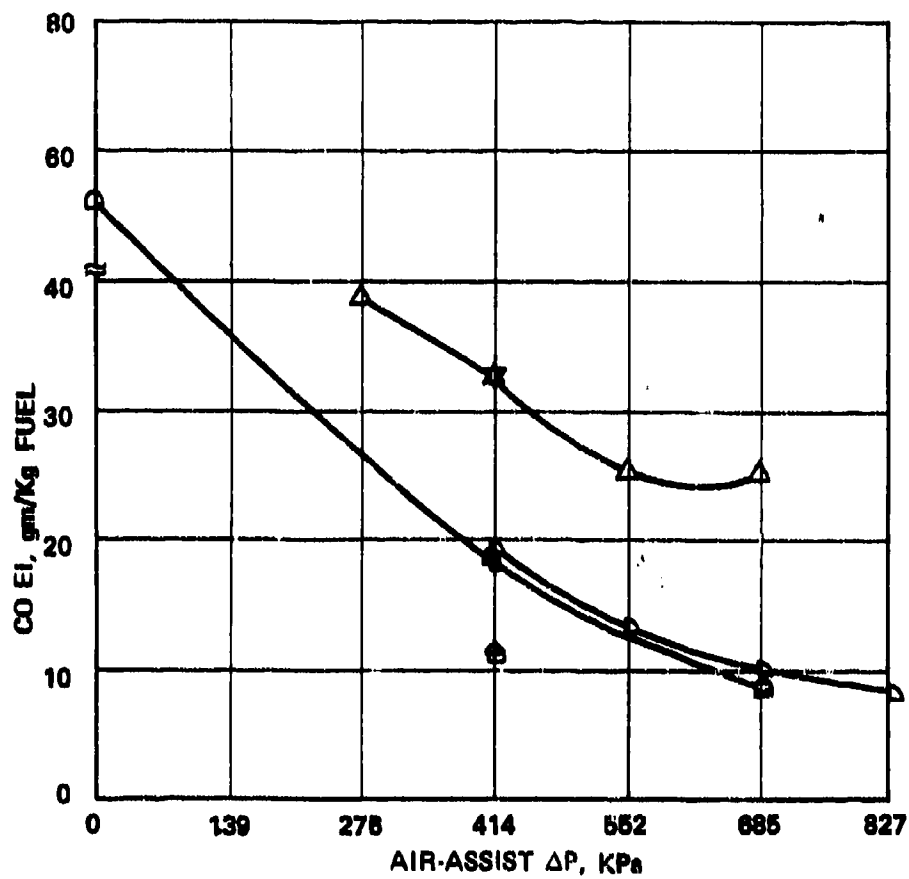
Figure 80. CO Emission Index Versus Air-Assist Pressure Drop of Concept II at Sea-Level, Taxi-Idle, and 6096 Meter Altitude 10-Percent Power Point.

134
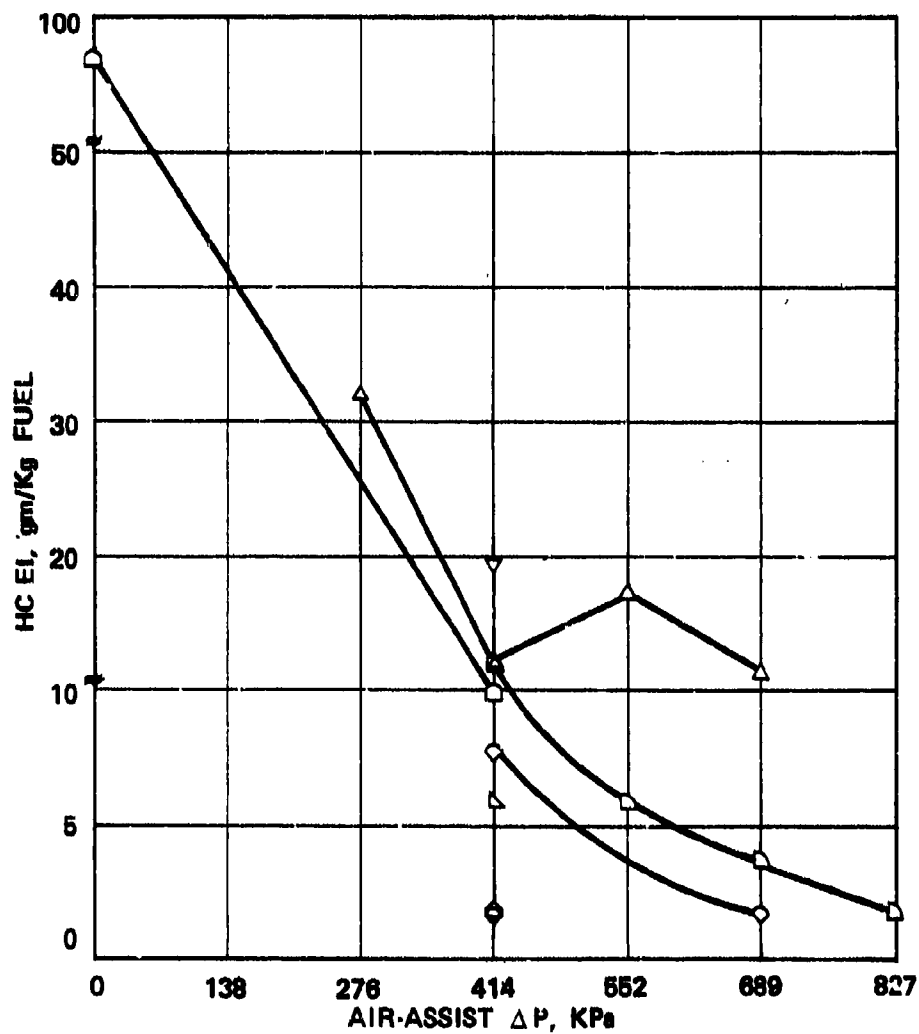
Figure 81.   Unburned Hydrocarbons Emission Index Versus Air-
Assist Pressure Drop of Concept II at Sea-Level,
Taxi-Idle, and 6096 Meter Altitude 10-Percent
Power Point.

135

TABLE 9. DESCRIPTION OF CONCEPT II EXPERIMENTAL DATA SYMBOLS FOR FIGURES 77 THROUGH 84.

Symbol	Nozzle Back Angle (Degrees)	Nozzle Immersion (cm)	Combustor P/N	Nozzle Shroud Configuration	Fuel	Description
◁	50	1.80	Basic	Scalloped	Jet-A	
▷	45	1.80	-1	Scalloped	Jet-A	
◿	25	1.30	-1	Scalloped	Jet-A	Tested Up to Sea-Level 75% Power Point
◖	25	1.80	-1	Cooled Unscalloped	Jet-A	
◗	25	1.80	-2	Cooled Unscalloped	Jet-A	
◇	25	1.80	-3	Cooled Unscalloped	Jet-A	
◇	25	1.80	-4	Cooled Unscalloped	JP-4	Tested Sea-Level Maximum Power
△	25	1.80	-4	Cooled Unscalloped	JP-4	6096 m Altitude Performance
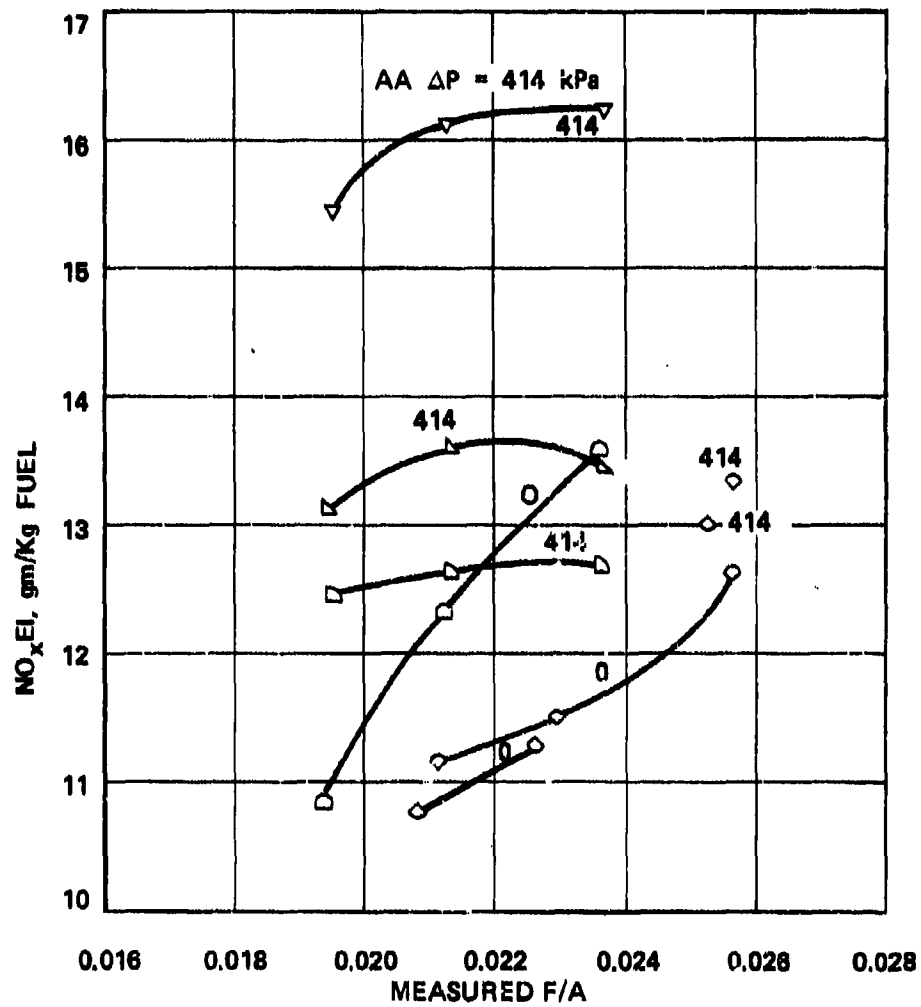
Figure 82.   NO$_x$ Emission Index Versus Fuel/Air Ratio of
              Concept II at Sea-Level 75-Percent Power Point.

137

TABLE 13. CONCEPT II LEAN-BLOWOUT FUEL/AIR RATIO.

Symbol	Nozzle Back Angle (Degrees)	Nozzle Immersion (cm)	LBO F/A at SL Idle With 5 Nozzles	LBO F/A at SL Idle With 10 Nozzles	LBO F/A at 6096 m Alt 10% Power 5 Nozzles	LBO F/A at 6096 m Alt 10% Power 10 Nozzles	Air-Assist ΔP kPa	Comments
△	50	1.80	-	0.01035	-	-	413.7	Basic Combustor
▽	45	1.80	0.0075	0.0102	0	0	0	-1 Combustor
◭	25	1.80	-	0.00989	-	-	413.7	-1 Combustor
			-	0.00762	-	-	172.4	
◭	25	1.80	-	0.00707	-	-	172.4	-1 Combustor
			-	0.00968	-	-	0	Cooled Unscalloped Shrouds
◖	25	1.80	0.00530	0.6053	-	-	172.4	
							413.7	
			0.00643	-	-	-	0	
◖	25	1.80	-	0.00623	-	-	413/7	-2 Combustor
◇	25	1.80	-	0.00597	-	-	413.7	-3 Combustor
◈	25	1.80	0.00686'	-	-	-	413.7	-4 Combustor, JP-4
△	25	1.80	0.00482	-	-	0.0062	0	
			-	-	-	-	0	

138

Figure 83 depicts the NO_x emission index of the -4 combustor configuration at the sea-level maximum power point, which produced 15 g of NO_x per kg of fuel. The NO_x characteristics at the 6096 meter altitude 61-percent and maximum power conditions are shown in Figure 84. Since the variation of NO_x with fuel/air ratio is quite small, the combustion can be assumed to be mostly diffusion controlled. The blowout fuel/air ratio of the -4 combustor configuration with 5 nozzles at the sea-level idle point was 0.00482 (Table 10) and is considered to be satisfactory.

5. Acoustic Emissions

Acoustic measurements were completed for Concept II at various altitudes and power levels. The sound pressure level at the exhaust of the Concept II combustor was monitored in the combustion test rig using the same "infinite-tube" type acoustic probe as was used in Concept I testing, and previously described.

Acoustic data taken at sea-level idle, 3048 meters idle, 6096 meters idle, and sea-level 100-percent power is shown in Figures 85 through 92. Figures 85, 87, 89, and 91 show the 1/3-octave sound pressure level with combustion. Figures 86, 88, 90 and 92 show the sound pressure level without combustion; i.e., the same combustor through-flow, inlet temperature, and pressure as in Figures 85, 87, 89, and 91, respectively, but with no fuel flow. Figures 86, 88, 90, and 92 show the noise present in the combustion rig due to noncombustion processes, such as noise generated by flow through valves and bends in the piping system.

Thus, the differences between the sound pressure level shown in Figures 85, 86, 87 and 88, etc., are due to the combustion process. The sound pressure level increase, due to the combustion process, varied from approximately 6 to 13 dB in the frequency range between 25 and 1000 Hz for sea-level idle, as shown by comparing Figures 85 and 86. Similar results were obtained
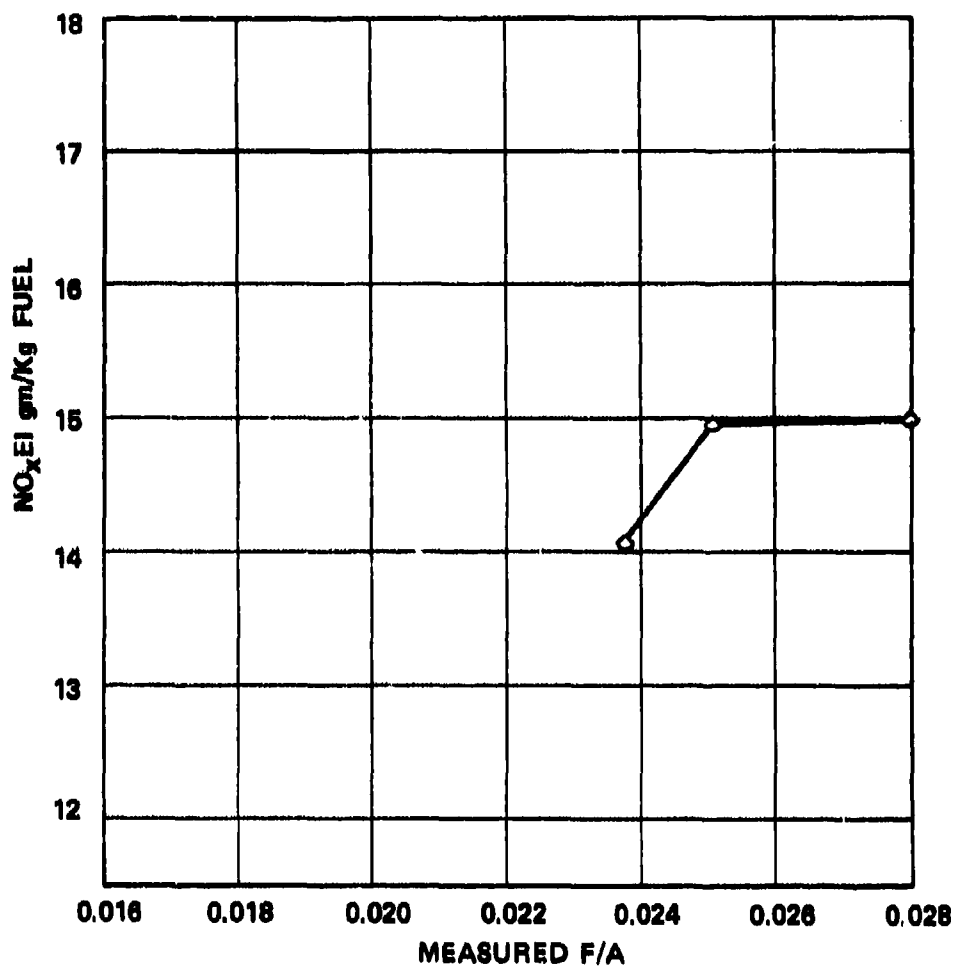
Figure 83. NO$_x$ Emission Index Versus Fuel/Air Ratio of Concept II at Sea-Level Maximum Power Point with JP-4 Fuel.
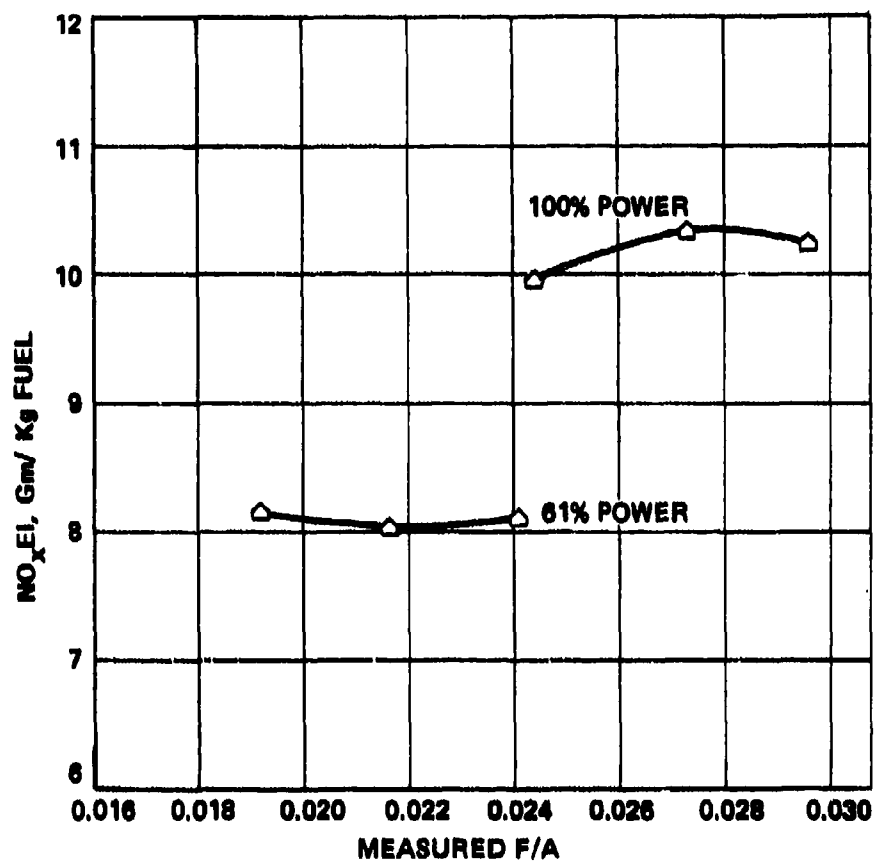
Figure 84.   NO$_x$ Emission Index Versus Fuel/Air Ratio of Concept II at 6096 Meter Altitude Maximum Power and 61-Percent Power Points with JP-4.

141

1/3 OCTAVE FILTER CENTER FREQUENCIES, HZ
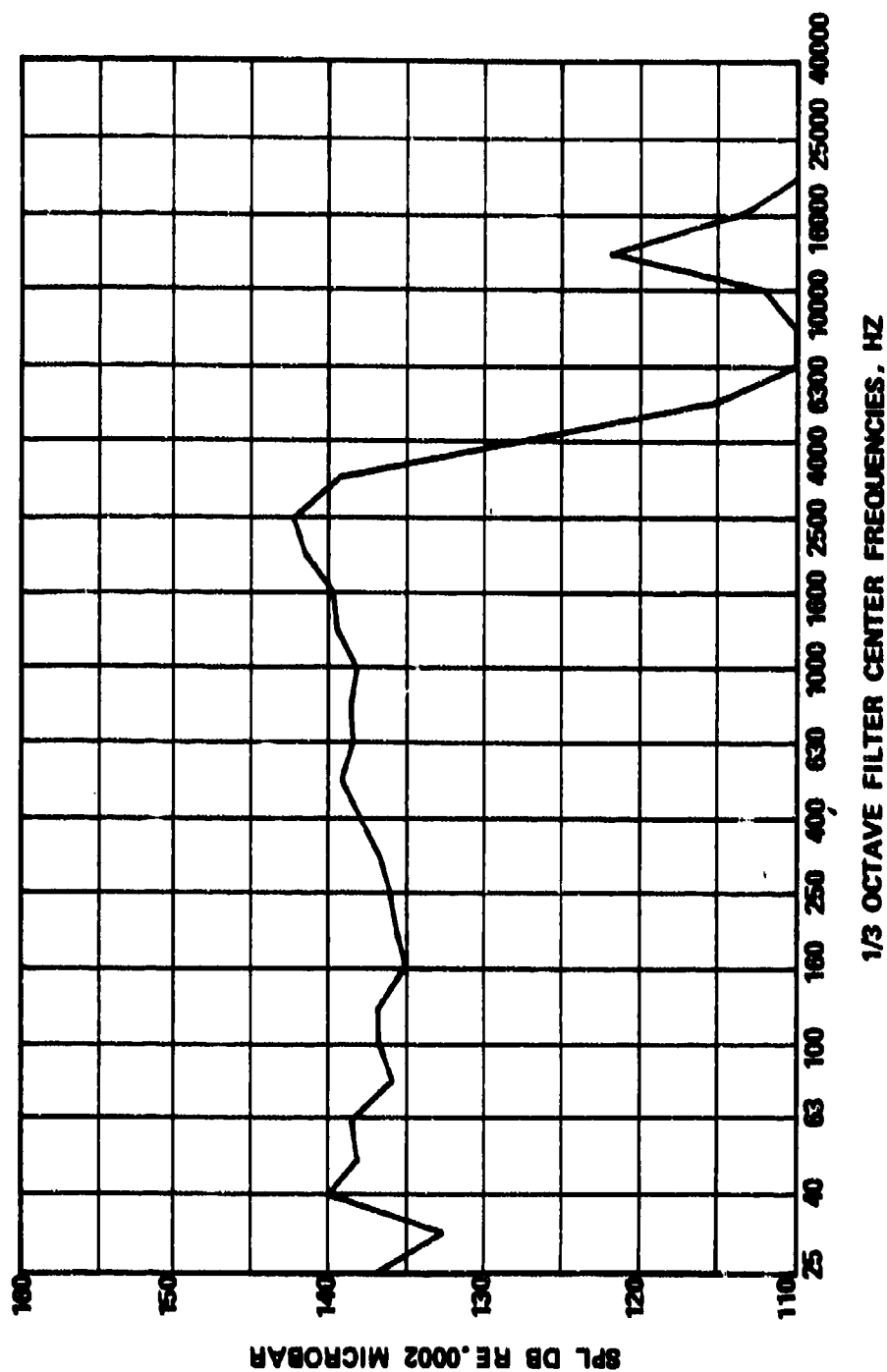
TEST CONDITIONS: WITH COMBUSTION
    TEMPERATURE: INLET 452 K; EXHAUST TEMPERATURE 956 K
    SIMULATED POWER LEVEL: IDLE
    ALTITUDE: SEA LEVEL

Figure 85.   Combustor Sound Pressure Level with Combustion at Sea-Level Idle.
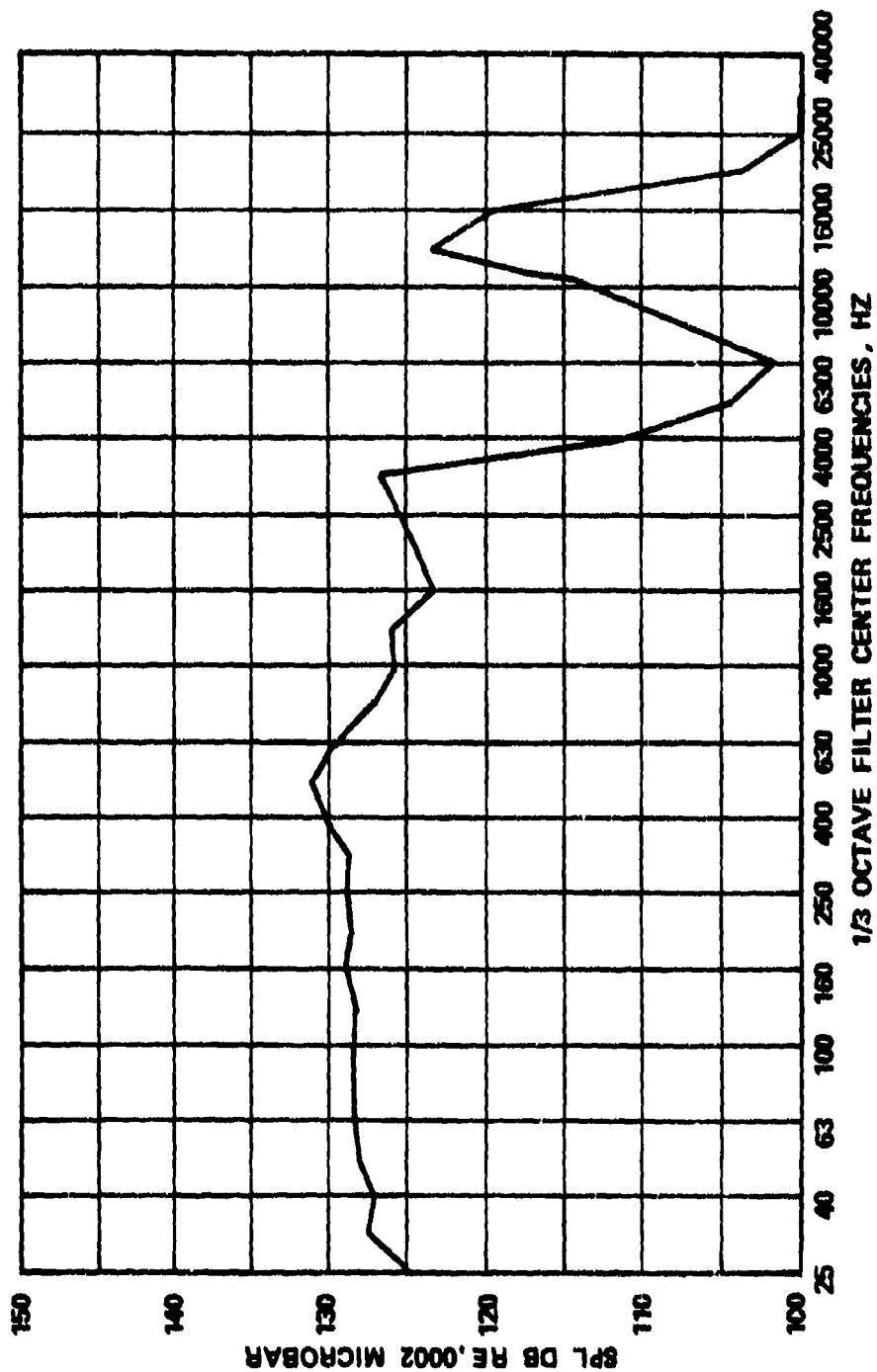
142

Figure 86. Combustor Sound Pressure Level without Combustion at Sea-Level Idle.

143

Figure 87. Combustor Sound Pressure Level with Combustion at 3048 Meters Idle
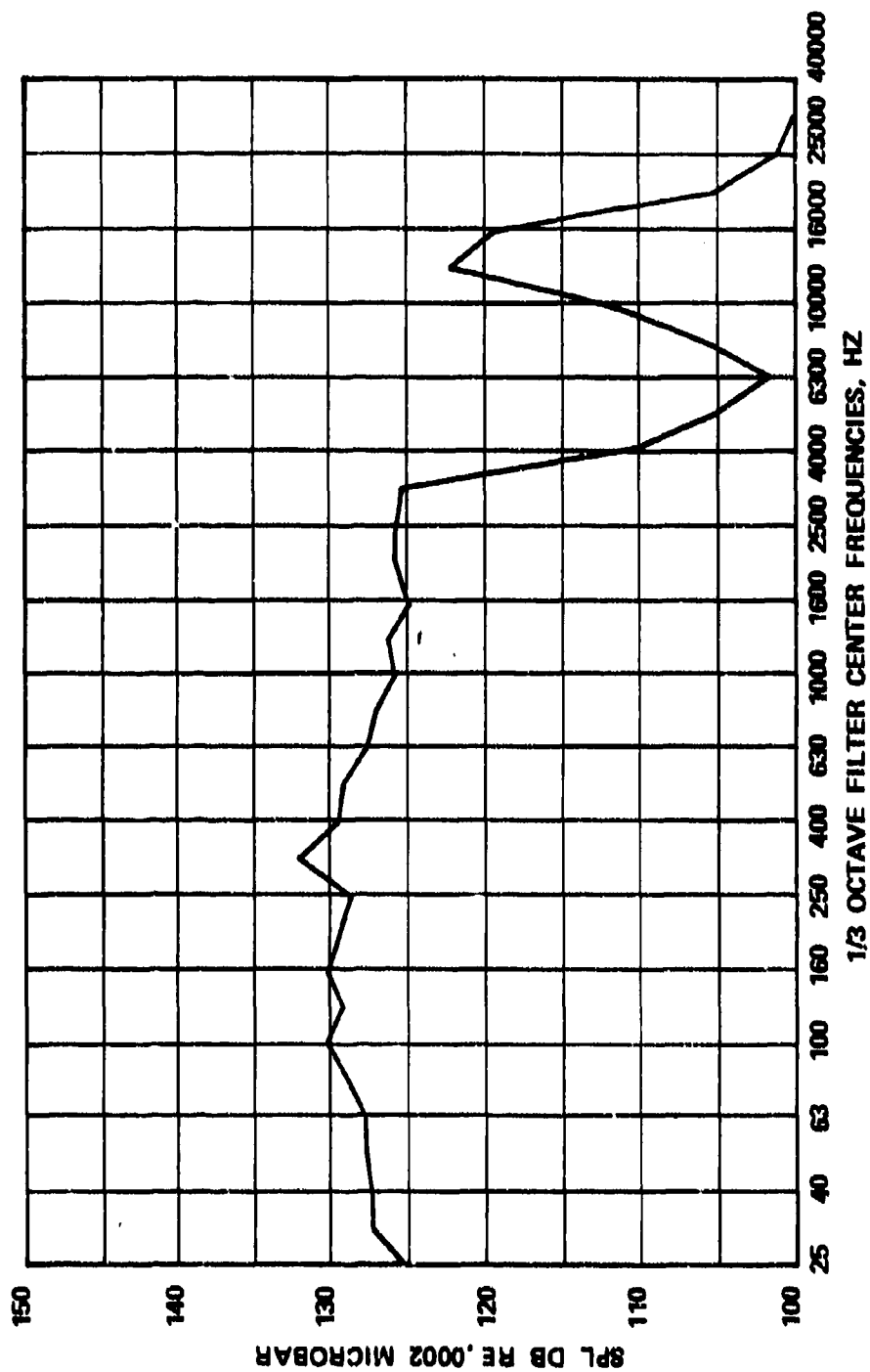
144

Figure 88.   Combustor Sound Pressure Level without Combustion at 3048 Meters   Idle.

145
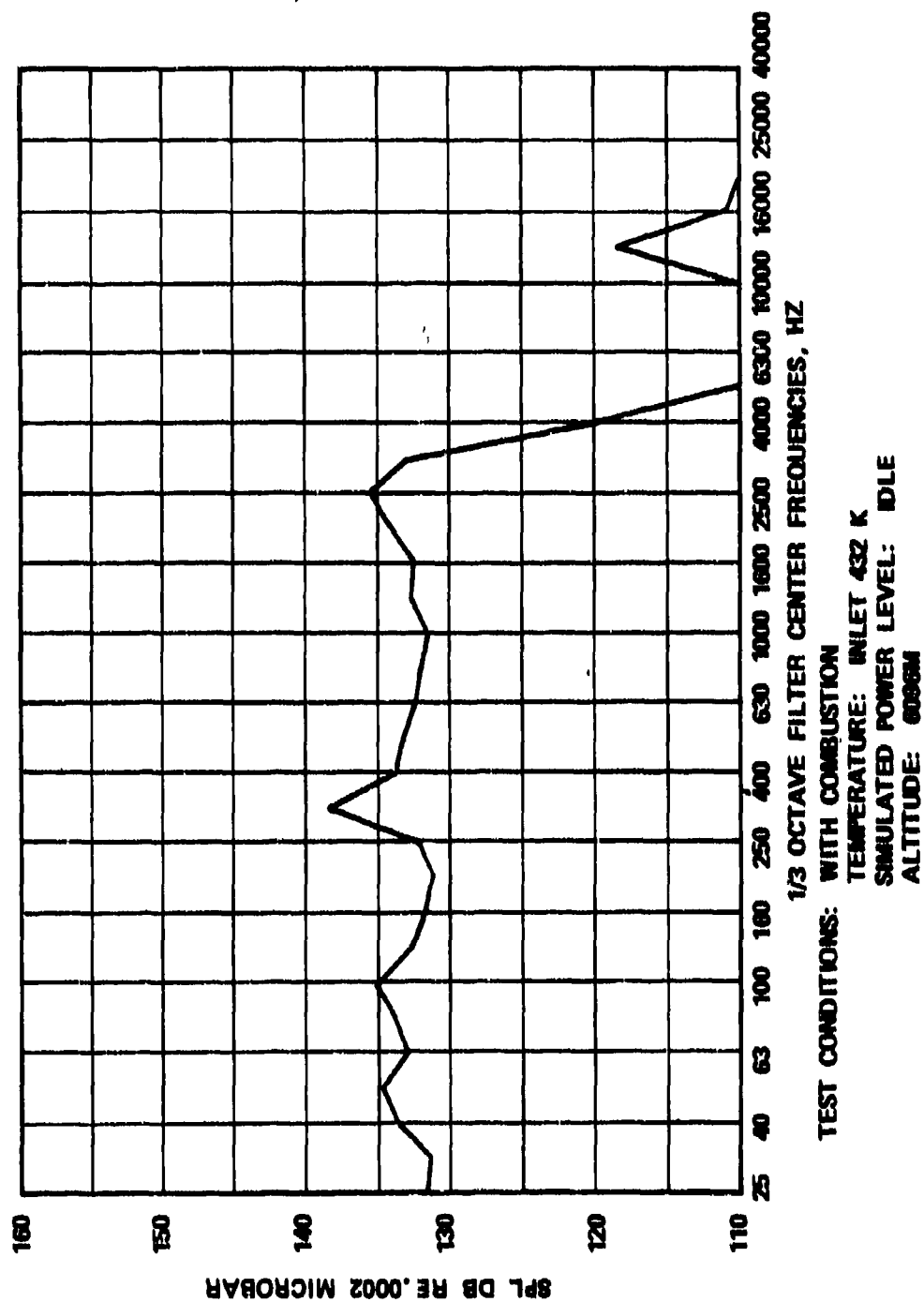
Figure 89. Combustor Sound Pressure Level with Combustion at 6096 Meters Idle.

146

1/3 OCTAVE FILTER CENTER FREQUENCIES, HZ

TEST CONDITIONS: WITH COMBUSTION
TEMPERATURE: INLET 432 K
SIMULATED POWER LEVEL: IDLE
ALTITUDE: 6096M
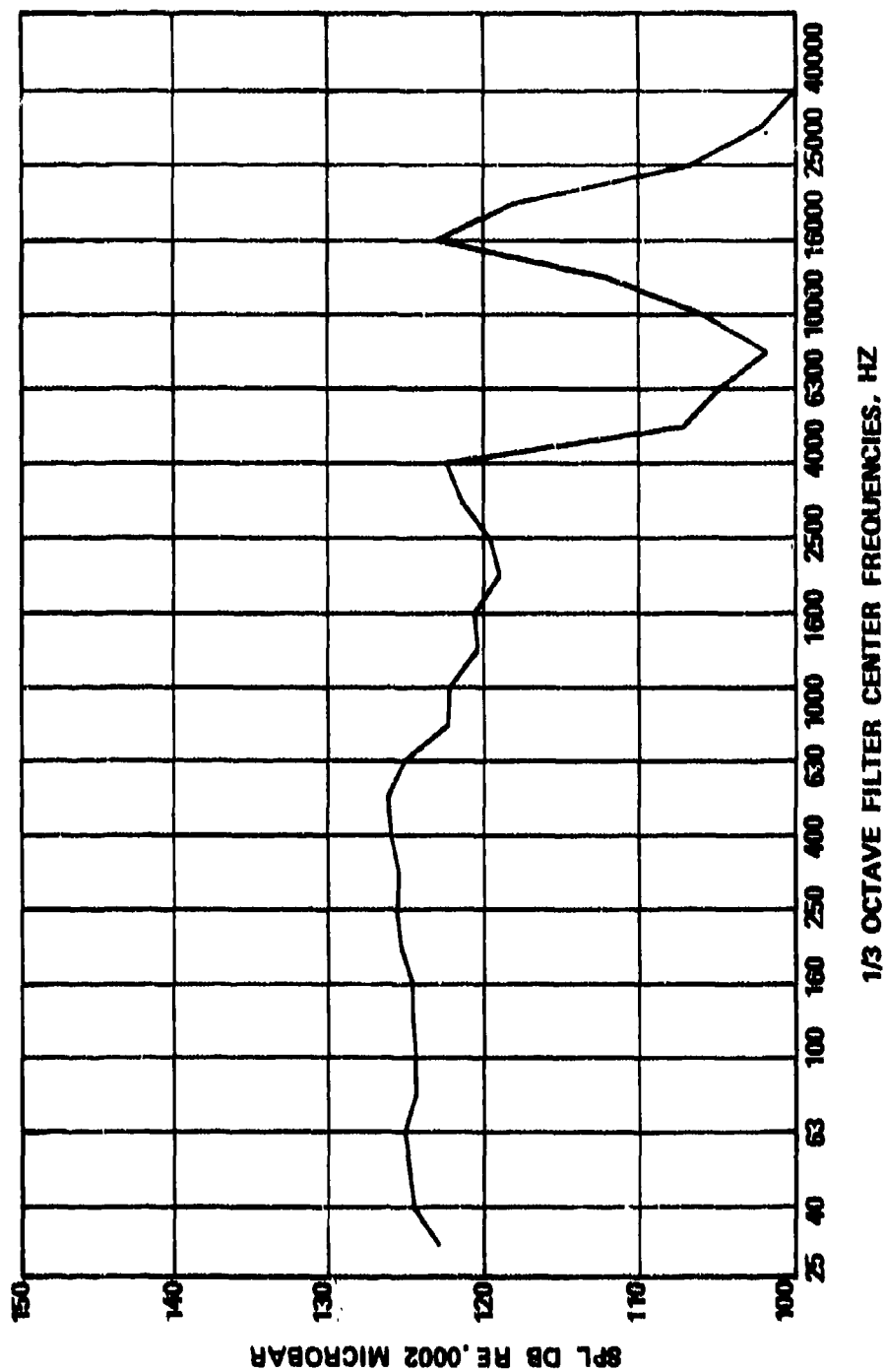
Figure 90. Combustor Sound Pressure Level without Combustion at 6096 Meters Idle.
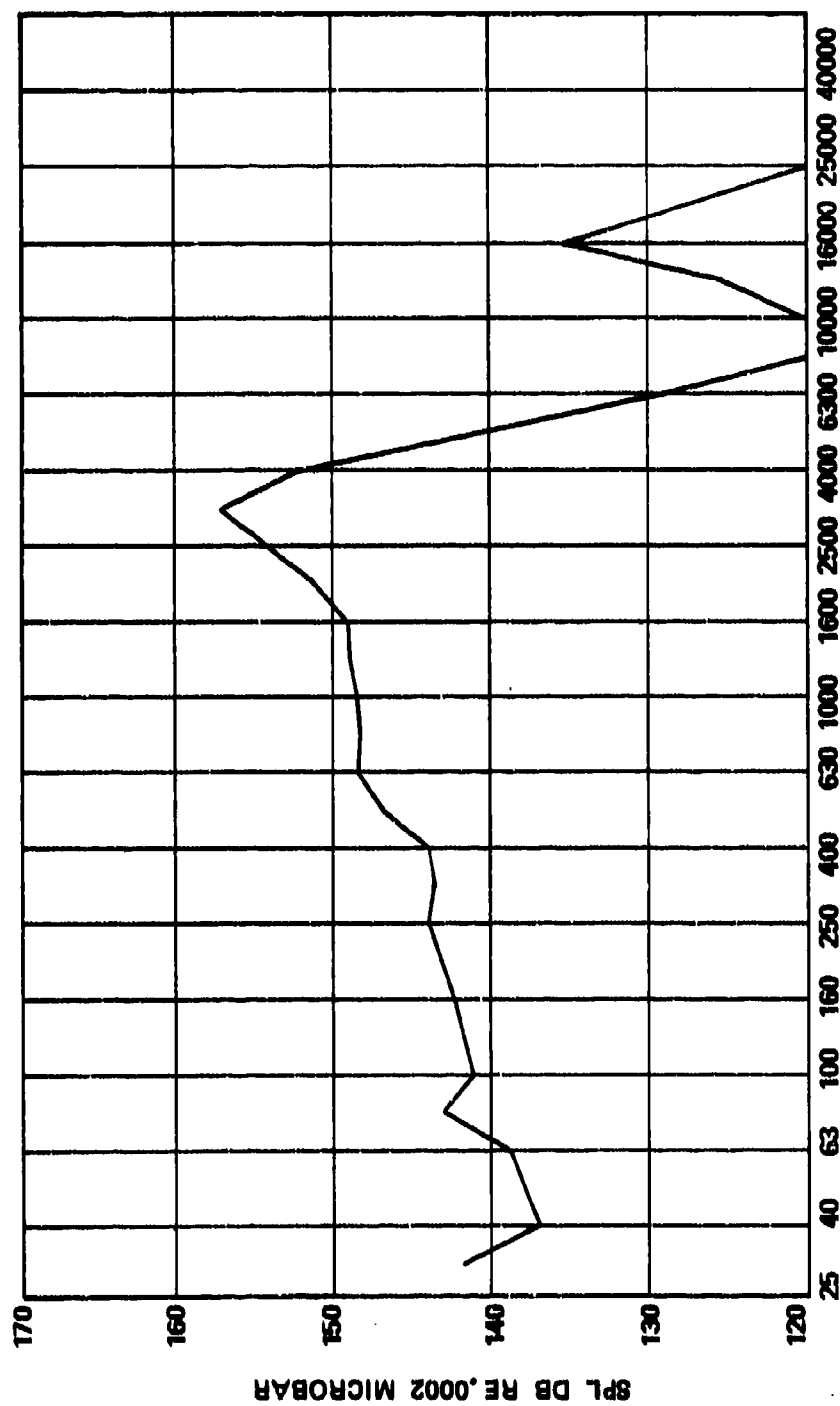
147

1/3 OCTAVE FILTER CENTER FREQUENCIES, HZ

TEST CONDITIONS: WITH COMBUSTION
TEMPERATURE: INLET 626 K, EXHAUST 1533 K
SIMULATED POWER LEVEL: 100
ALTITUDE: SEA LEVEL

Figure 91. Combustor Sound Pressure Level with Combustion 100 at Sea Level.

148

1/3 OCTAVE FILTER CENTER FREQUENCIES, HZ
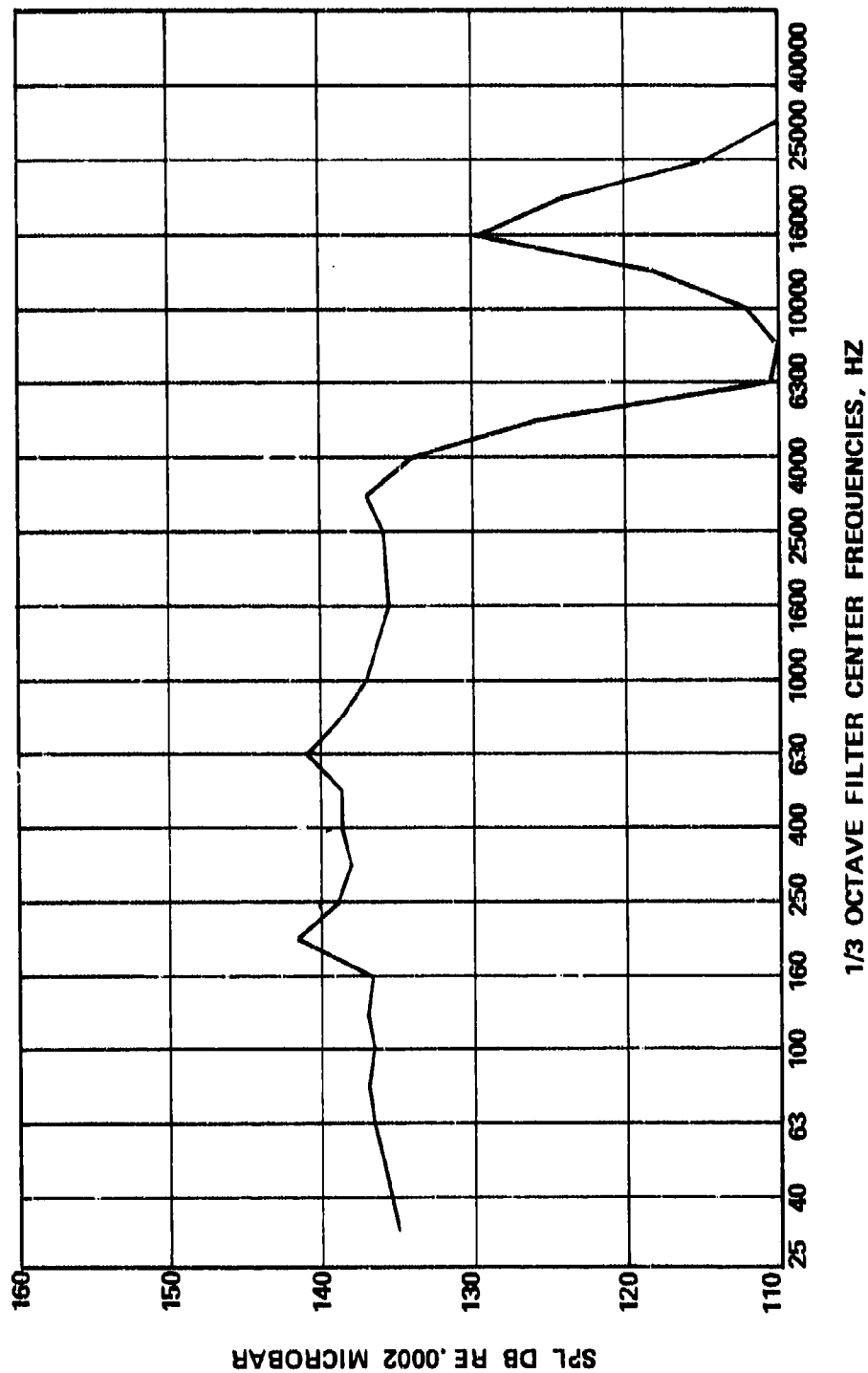
TEST CONDITIONS: WITHOUT COMBUSTION
TEMPERATURE: INLET 620 K
SIMULATED POWER LEVEL: 100
ALTITUDE: SEA LEVEL

Figure 92. Combustor Sound Pressure Level without Combustion 100 at Sea Level.

149

for the 3048 meters and 6096 meters idle conditions. For sea-level 100-percent power, the sound pressure level increased, due to the combustion process, varying from approximately 2 to 13 dB in the frequency range between 25 and 1000 Hz, as shown by comparing Figures 91 and 92.

6. Liner Wall Temperature Characteristics

The Concept II combustor was tested at sea-level, hot day, max-power conditions, i.e., T_3 = 642 K, P_{t3} = 886 kPa, W_{a3} = 1.07 kg/sec. The results are shown in Figures 93 and 94. The measured circumferential pattern factor was 0.165 at an average discharge temperature of 1551 K (Figure 93). Wall temperature levels, as indicated by OG6 Thermindex temperature sensitive paint, indicated maximum temperatures of 1144 K for the O.D. panel, and 1116 K for the I.D. (Figure 94), which meet the design goals.

D. Nozzle Spray Characteristics.

One of the airblast fuel nozzles, Figure 8, procured from the fuel nozzle vendor, was tested on a fuel spray rig. The spray quality was studied as a function of combustor liner (air box) pressure drop, air-assist air-pressure drop, and fuel-flow rate. Figures 95 through 99 show the results with the scalloped shrouds. The increasing air box pressure drop improved atomization, as shown qualitatively in Figures 95 through 97. The corresponding change in the spray-cone angle was quite small. The effect of air-assist pressure drop on the spray quality was quite pronounced, as shown in Figures 98 and 99.

The mean droplet size of the nozzle was measured on the rig using a light-scattering technique. The results are presented in Figures 100 and 101. The droplet size measurements were done with water as the working fluid. The corresponding SMD with
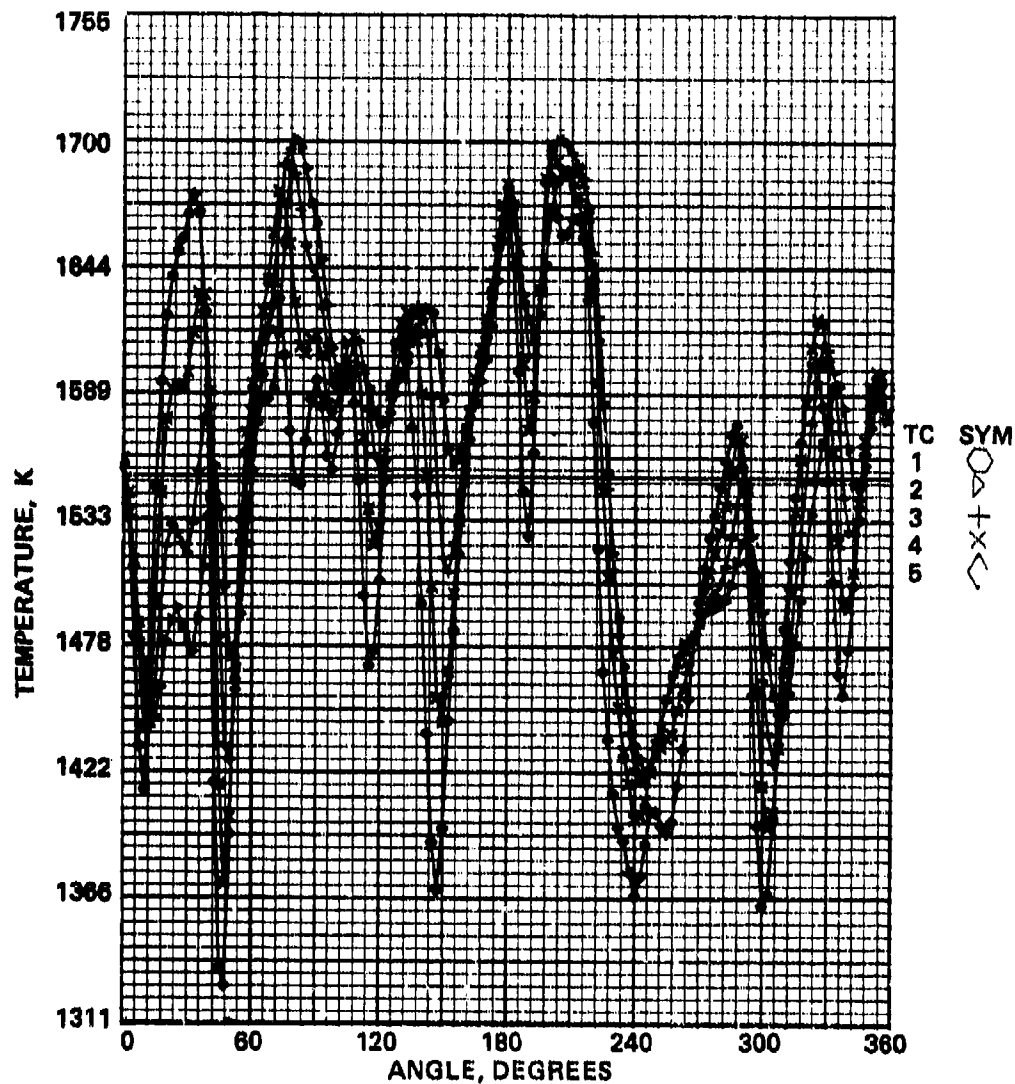
Figure 93.   Concept 2 Exhaust Temperature Scan at Sea-Level,
Hot-Day, Max-Power Point.

NOTE: Isotherms written on combustor liner are
in degrees F. Convert degrees F to
degrees K as follows:

$$K = (5/9)(F+459.67)$$

Figure 94. Concept II Liner Wall Temperature Characteristics
at Sea-Level, Hot-Day, Max-Power Point.

Figure 95. Spray Quality of Air-Assist - Airblast Nozzle at 31.8 cm H_2O Airbox Pressure Drop (ΔP) and 12.2 Kg/hr Fuel Flow Rate (W_F).
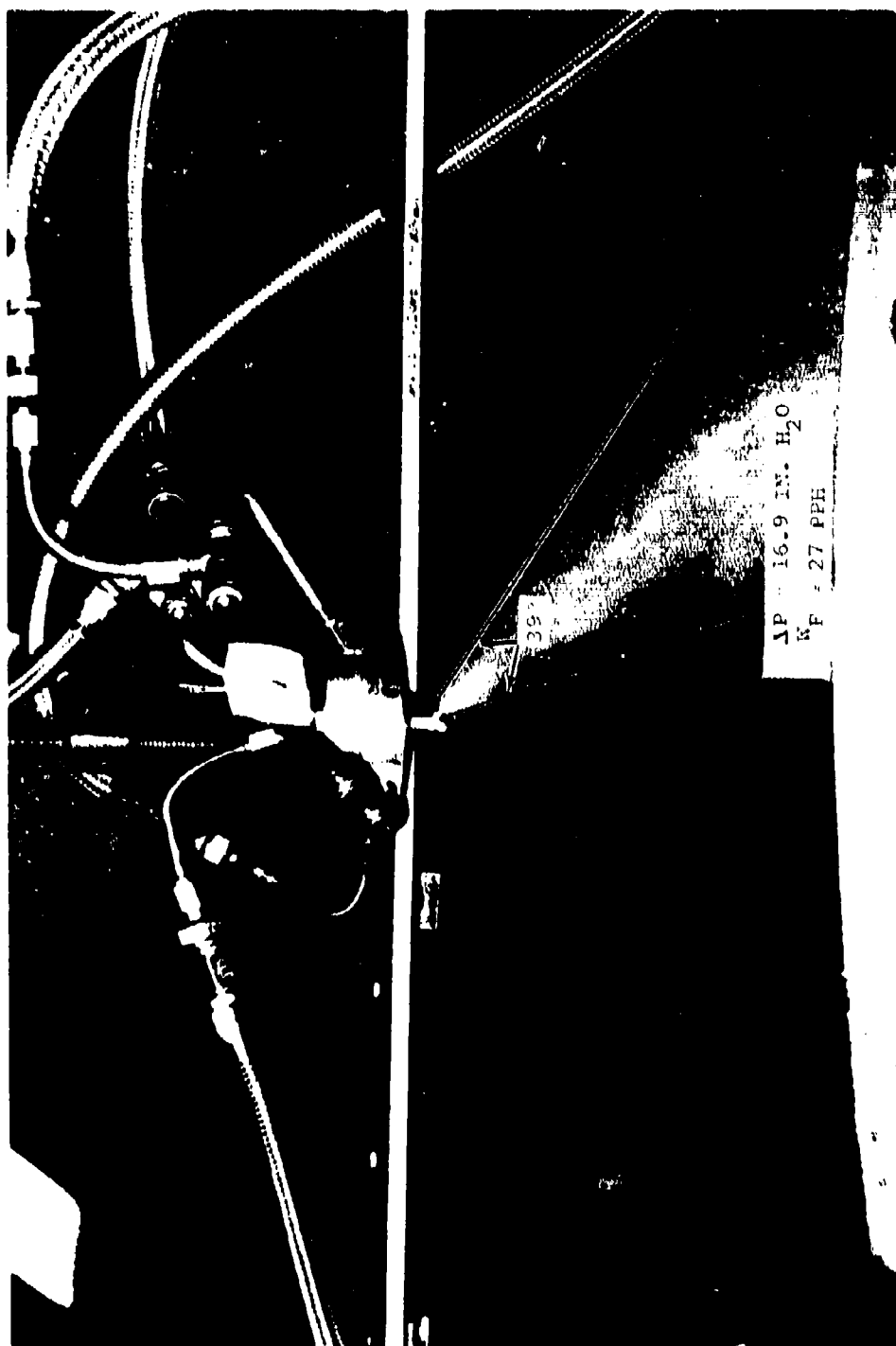
Figure 96. Spray Quality of Air-Assist – Airblast Nozzle at 42.9 cm
H_2O Airbox Pressure Drop (ΔP), and 12.2 Kg/hr Fuel Flow
Rate (W_F).

154
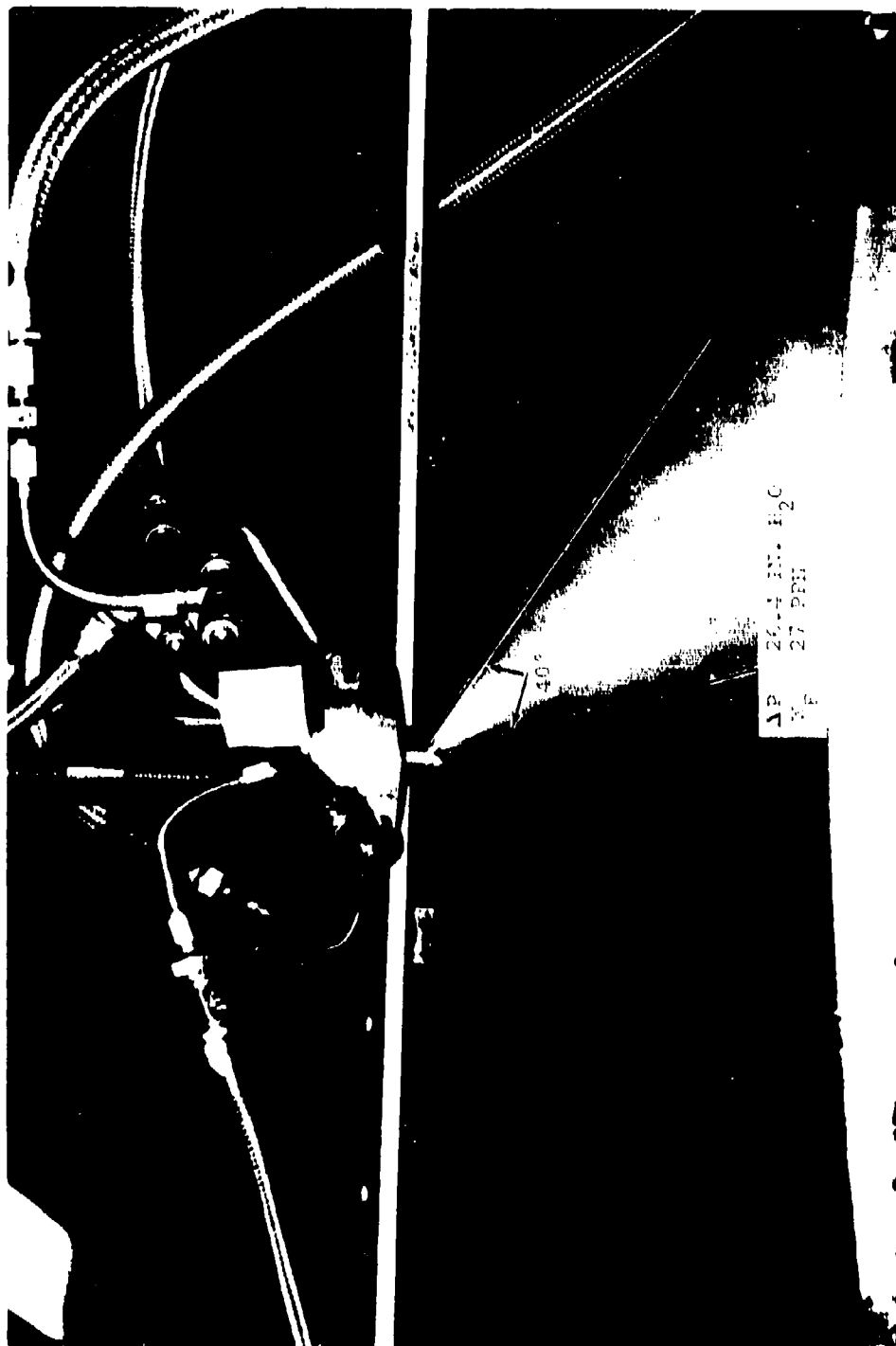
Figure 97. Spray Quality of Air-Assist - Airblast Nozzle at 67.7 cm.
H_2O Airbox Pressure Drop (ΔP) and 12.2 Kg/hr fuel flow
Rate (W_F).
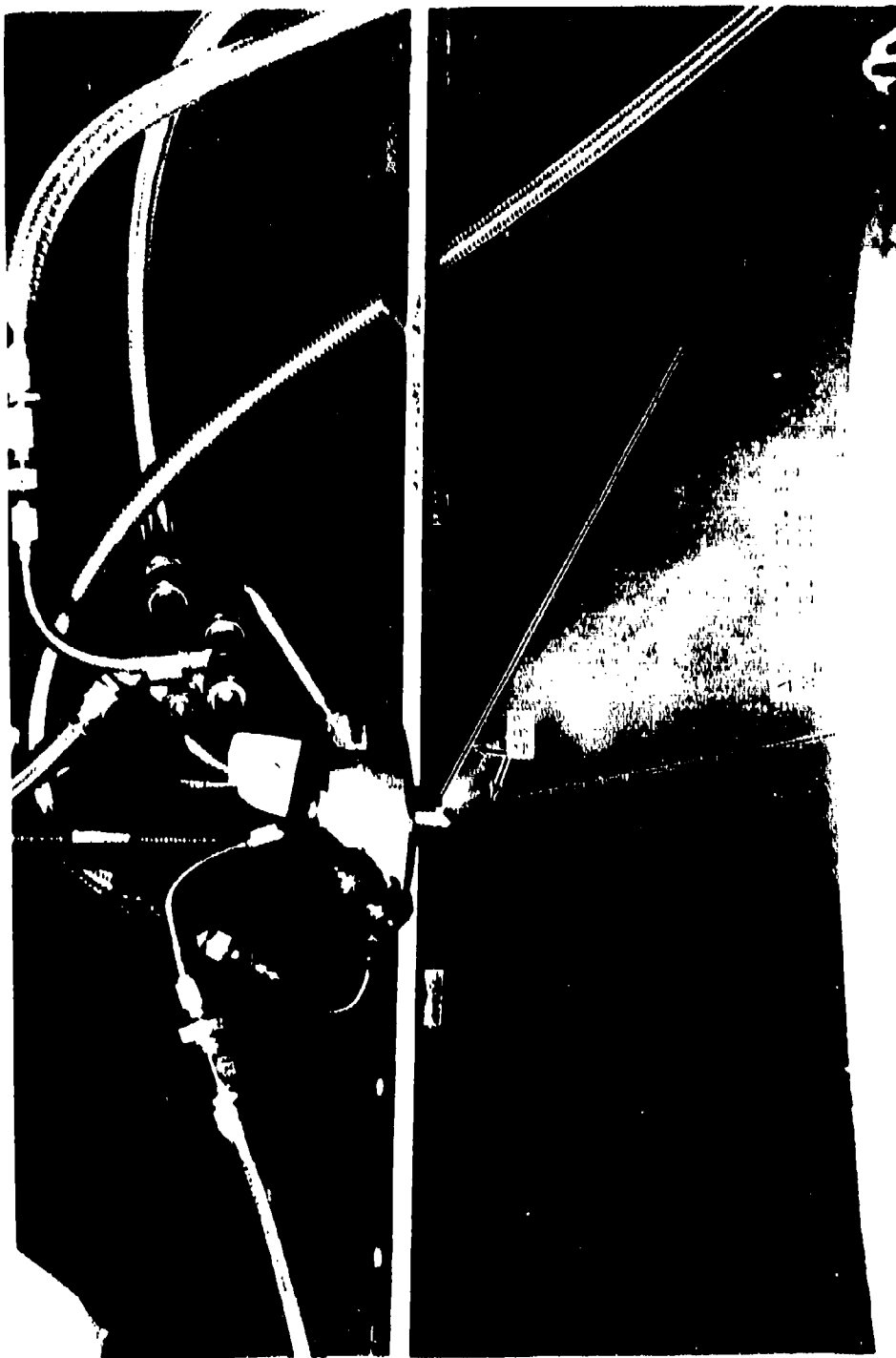
Figure 98. Spray Quality of Air-Assist - Airblast Nozzle at 30.2 cm H_2O Airbox Pressure Drop (ΔP) and 5.8 Kg/hr Fuel Flow Rate (W_F).
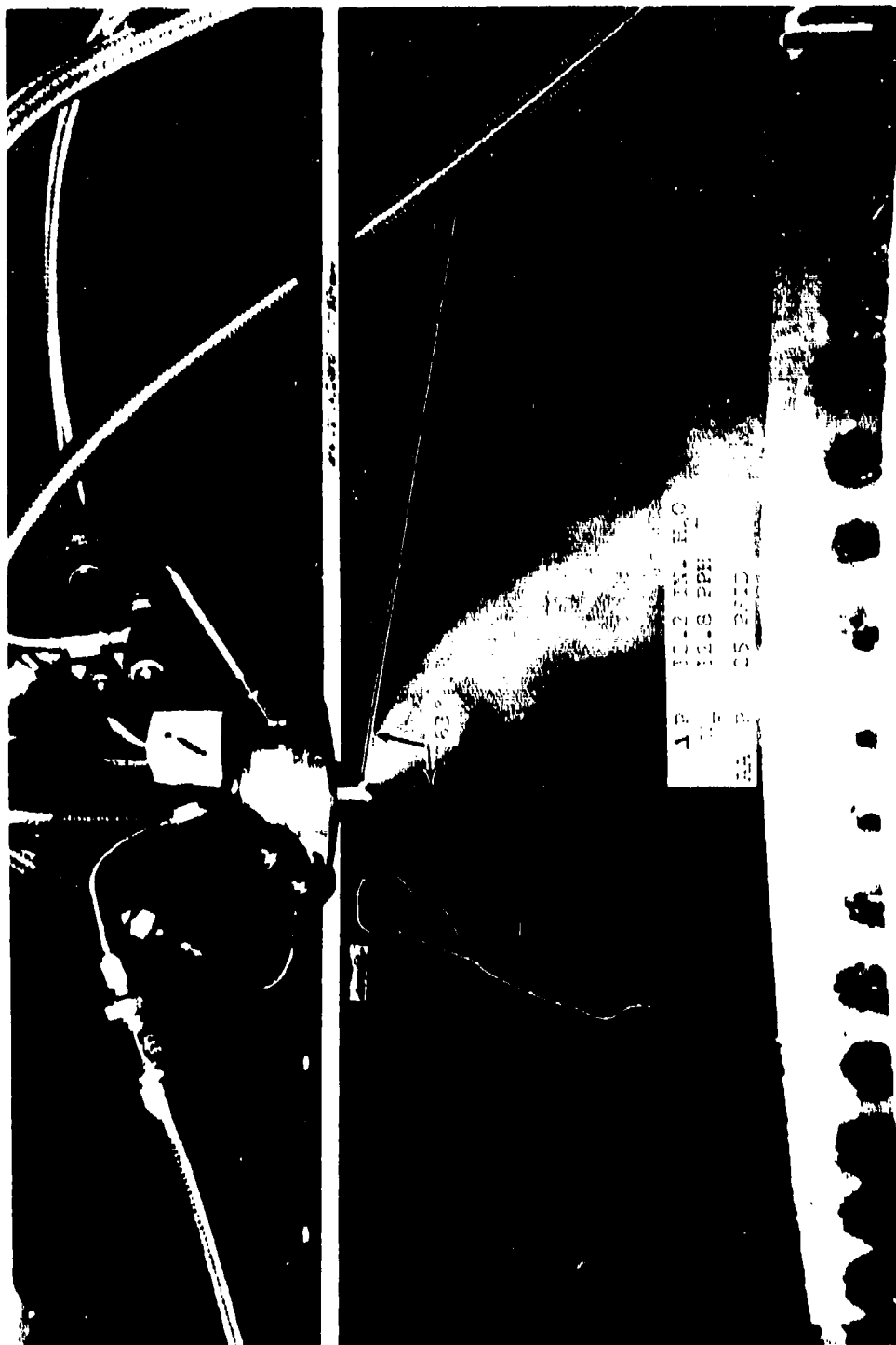
Figure 99. Spray Quality of Air-Assist - Airblast Nozzle at 31.0 cm. H_2O Airbox Pressure Drop (ΔP) 5.8 Kg/hr Fuel Flow Rate ($\dot{W}_F$) and AA ΔP = 172 kPa.
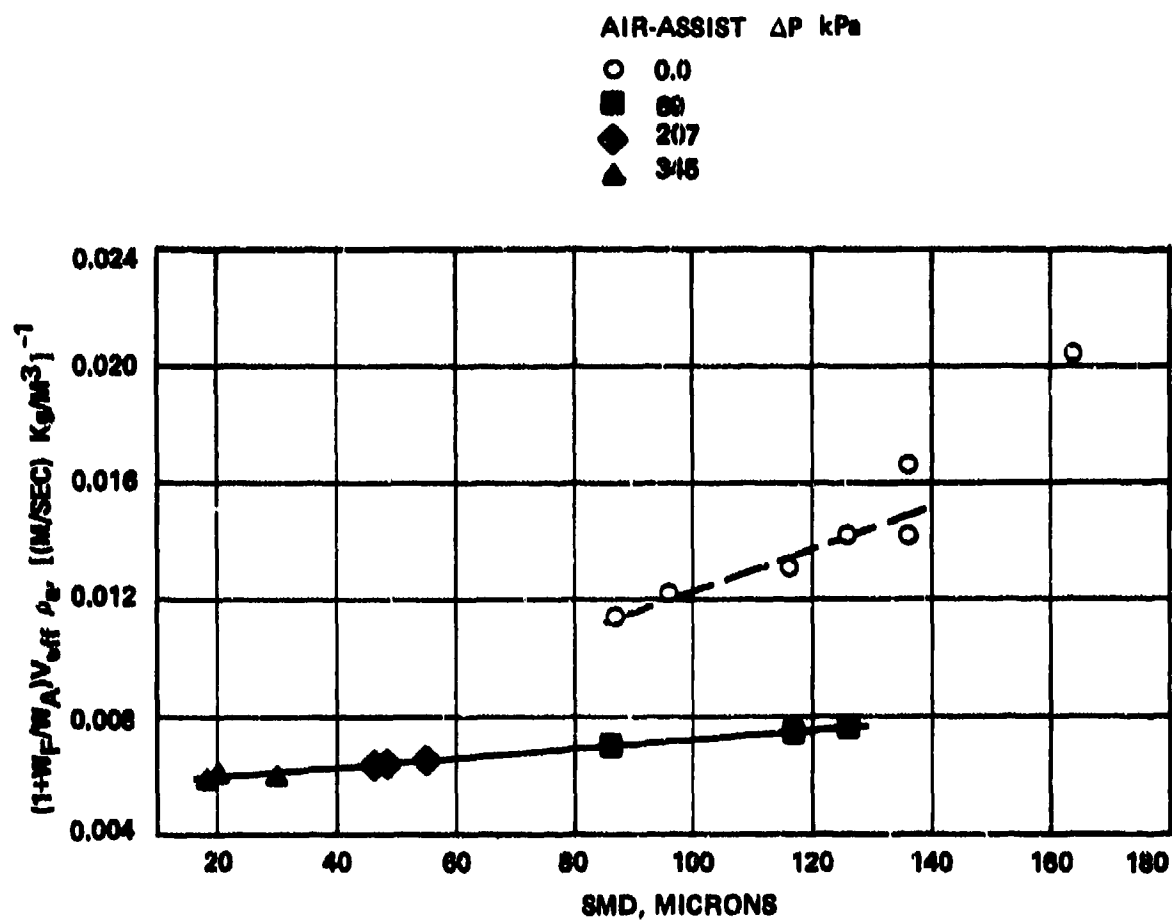
Figure 100. SMD Characteristics of Airblast Nozzle.
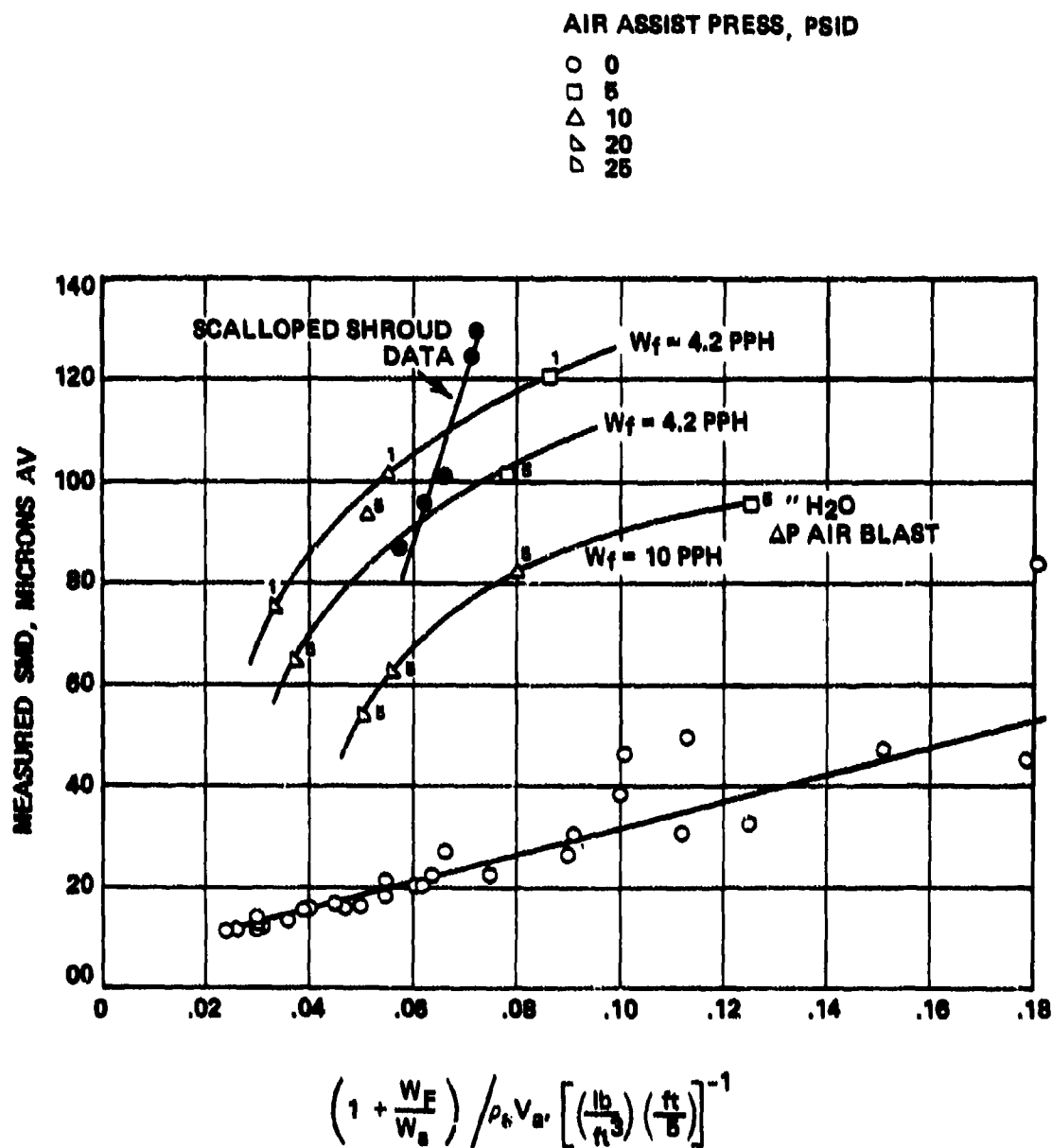
Figure 101. Measured SMD Data of Airblast Nozzle with Different Linear ΔP and Air-Assist ΔP.

159

Jet-A fuel was estimated by using a correction factor suggested by Prof. Lefebvre:

$$\frac{(SMD)_{Jet-A}}{(SMD)_{water}} = \frac{(\sigma\rho)^{1/2}_{Jet-A}}{(\sigma\rho)^{1/2}_{water}} = 0.51$$

where: σ and ρ denote liquid surface tension and density, respectively.

Close inspection of the scalloped nozzle showed that the shroud air was exiting the nozzle without any swirl component which resulted in a much higher SMD. Also, the spray cone inclusive angle of 45° was less than desired. The cooled unscalloped nozzle shrouds were found to have a spray cone angle of 90°.

A fuel contamination test was conducted with the fuel injection system in order to determine its tolerance to contaminated fuel. The fuel manifold and nozzles were run for 20 hours with contaminated JP-4 fuel in accordance with MIL-E-8593A, Table X with filtration to 10 microns. Figure 102 gives the contaminates and amounts that were used. After operating at 109 kg/hr, which corresponds to engine operation at 90 percent sea-level, static, standard-day conditions, for 20 hours one nozzle was plugged, another nozzle was 63 percent low on fuel flow, and a third nozzle was 88 percent low on flow. The other seven nozzles were within 6 percent spread.

160

TABLE X. FUEL CONTAMINANTS PER MIL-L-8593A

Contaminant	Particle Size	Quantity
FERROSO-FERRIC Iron oxide [Fe_3O_4, (Black Color), Magnetite]	0-5 microns	3.70 mg/litre
FERRIC Iron oxide (Fe_2O_3 Hematite)	0-5 microns	3.83 mg/litre
FERRIC Iron oxide (Fe_2O_3, Hematite)	5-10 microns	0.396 mg/litre
Crushed Quartz	1000-1500 microns	0.0661 mg/litre
Crushed Quartz	420-1000 microns	0.463 mg/litre
Crushed Quartz	300- 420 microns	0.264 mg/litre
Crushed Quartz	150- 300 microns	0.264 mg/litre
Prepared dirt conforming to A.C. Spark Plug Co. Part No. 1543637 (coarse Arizona road dust)	Mixture as follows: 05- microns (12 percent) 5-10 microns (12 percent) 10-20 microns (14 percent) 20-40 microns (23 percent) 40-80 microns (30 percent) 80-200 microns (9 percent)	2.11 mg/litre
Cotton linters	Below 7 staple (U.S. Department of Agriculture Grading Standards SRA - AMS 180 and 251)	0.0264 mg/litre
Crude naphthenic acid		0.03 percent by volume
Salt water prepared by dissolving salt volume entrained in distilled water or other water containing not more than 200 parts per million of total solids.	4 parts by weight of NaCl 96 parts by weight of H_2O	0.01 percent by

Figure 102. Fuel Contaminants Table from MIL-E-8593A.

V. MODEL PREDICTIONS

The combustor analytical models, described in Section I, were mainly used for refining empirically designed combustion systems before making detail drawings. It was expected that the basic combustor geometries would be closer to meeting the design objectives compared to the initial empirically designed combustor configurations. The models were also utilized during the course of combustor development testing, such as for Concept II described in Section IV.C. Since a large number of computer runs were made before arriving at the most promising configuration, it is difficult to present all of the model predictions. Instead, the model predictions are given in Sections V.A and V.B of the final combustor geometries for each concept. The predictions are qualitatively compared with the test results where possible.

A. Concept I Predictions.

The basic Concept I configuration achieved or exceeded the program performance goals, as described in Section IV.B. Predictions of this configuration are presented in the following paragraphs.

The annulus flow model was used to compute the pressure drop and the airflow distribution around the liner, including jet velocity and efflux angles. The computed airflow distribution was previously presented in Figure 3. The predicted isothermal pressure drop was 1.9 percent compared to a measured pressure drop of 2.5 percent. The fuel insertion model, along with the measured data on the spray mean droplet size and inclusive cone angle, was used to compute initial spray conditions. The 3-D Combustor Performance Model was used to predict the internal flow-field at the sea-level standard day as well as hot-day maximum power conditions. The transition mixing model was used to predict mixing of the hot gases within the combustor transition

162

liner. Finally, the wall cooling model was used to predict the liner wall temperature levels.

1. <u>3-D Combustor Performance Model Prediction</u>.

A combustor sector of 36 degrees with the swirler centerline located at $\theta = 18$ degrees was analyzed by the 3-D program. A combustor length of 12.6 cm was divided into 30 x-nodes, whereas the combustor channel height of 4.4 cm was covered by 19 y-nodes. The circumferential sector of 36 degrees was uniformly divided by 13 θ-nodes. The radius of the inner liner wall was 7.85 cm. The two O.D. primary jets were located at x = 3.2 cm and $\theta = 18$ and 30 degrees, respectively. The six impinging intermediate jets were at x = 5.1 cm and $\theta = 6$, 18, and 30 degrees, respectively. Similarly, the six impinging dilution jets were at x = 7.6 cm and $\theta = 6$, 18, and 30 degrees, respectively. The three O.D. cooling slot lips were at x = 1.4, 4.3 and 6.6 cm, respectively. Similarly, the four I.D. cooling slots were located at x = 1.4, 4.3, 6.6 and 9.8 cm, respectively. The nozzle swirler center was at the mid-channel height with x = 0 and $\theta = 18$ degrees. The nozzle shroud was located at x = 2.7 cm, whereas the spray exited at x = 1.90 cm and y = 2.92 cm from the inner liner wall and $\theta = 9$ degrees compared to the swirler center being at $\theta = 18$ degrees, i.e., 9 degrees downstream from the spray origin along the direction of combustor inlet swirl. The spray initial cone angle was 90 degrees with the center of the spray making a back angle of 25 degrees and a down angle of 35 degrees. A back angle of 90 degrees means the spray is directly facing the dome; whereas with a 90-degree down angle, the fuel is being injected into the combustor along the radial direction toward the I.D. wall. A total of 20 rays emanated from the nozzles spaced equally across 2π radians with an initial droplet velocity of 61.4 meters per second. Each of these rays consisted of five droplet sizes with an estimated SMD of 30 microns. Consequently, the spray was simulated by a set of 100 droplets. The trajectory

163

of each of these droplets was computed based upon force balance and the evaporation/combustion rate. The momentum and energy transfer from the droplets to the gas phase was taken into account.

Figure 103 presents predicted fuel/air ratio profiles, expressed in terms of the equivalence ratio, of Concept I at the sea-level, standard-day, maximum power condition. The results are for three r-θ planes upstream of the spray origin. At a plane 0.38 cm downstream from the dome there are two nearly stoichiometric fuel regions. A small region exists near the I.D. liner wall at around θ = 12 degrees, whereas the nozzle spray originated at θ = 9 degrees. On the other hand, all of the 36-degree sector adjacent to the outer liner wall has an equivalence ratio between 0.8 and 1.0. This area is therefore expected to exhibit high wall temperatures unless properly cooled. The liner wall discoloration, after a number of performance tests, indicated that these areas were quite hot, although below the allowable level of 1144 K. At x = 1.09 cm, i.e., 0.81 cm upstream from the spray origin, the stoichiometric region near the I.D. wall has grown slightly. This region is leaned out at x = 1.91 cm due to a cooling film exiting at x = 1.4 cm. Therefore, it can be said that in order to minimize the hot spot on the I.D. wall the cooling slot preferably should be located at x less than 1.09 cm.

The high fuel/air ratio region near the O.D. wall at x = 0.38 cm has been reduced at x = 1.09 cm because of the spreading of the air from the dome swirlers and the tangential louvers. At this plane there are three separate stoichiometric fuel pockets. Two of these are located at the mid-channel, at around θ = 10 and 30 degrees, respectively. The third is near the I.D. wall as discussed above. At x = 1.91 cm, the plane where the spray originates, a 1.3-equivalence-ratio region extends across the 36-degree sector indicating good nozzle-to-nozzle communication. The stoichiometric region is located away from both liner walls, thereby resulting in acceptable wall-temperature control.

164
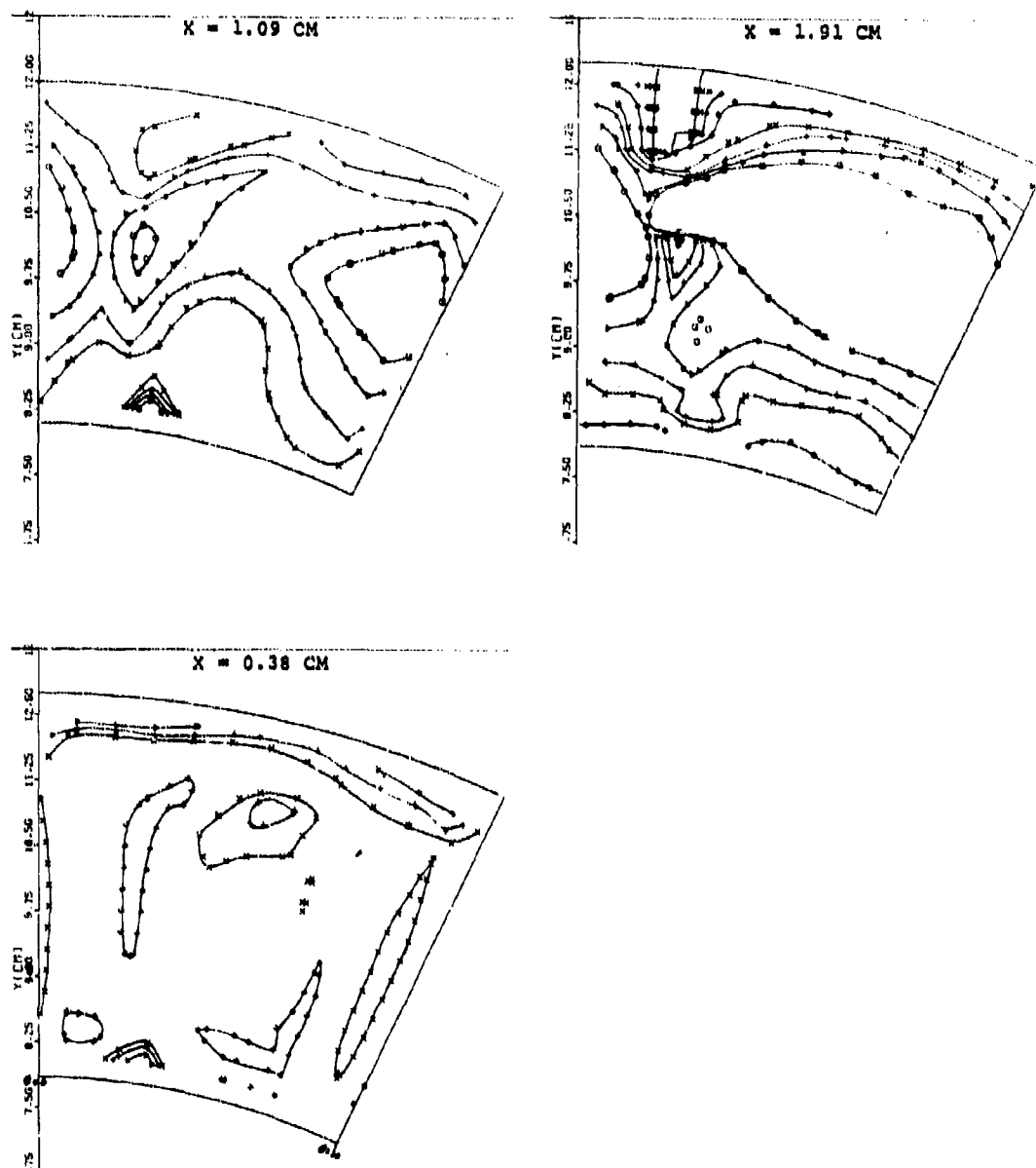
Figure 103. Predicted Fuel/Air Ratio Profiles in the Primary Zone of Concept I Upstream of the Spray Origin.

Figure 104 shows predicted fuel/air ratio profiles for four r-θ planes starting downstream from the spray origin and extending up to the plane of the dilution orifices. At x = 2.67 cm, the combustor has a maximum flow area with an equivalence ratio greater than unity. However, the peak temperature region is largest at x = 3.18 cm. Consequently, maximum radiation loading should be expected around x = 3 cm, with attendant maximum wall-temperature levels. This was confirmed by a thermal paint run. The two primary jets on the O.D. lower wall located at x = 3.18 cm divide the 1.3-equivalence ratio region that existed at x = 2.67 cm into two separate pockets as shown. The 0.8 equivalence-ratio locus is closer to the I.D. wall compared to the O.D. wall indicating that the former would be at higher temperature levels than the latter. In addition, the entire inner wall at x = 3.17 cm would be uniformly hot and only the region of the O.D. wall between the primary jets would be hot, as subsequently confirmed experimentally.

The penetration of the six opposing intermediate jets at x = 5.08 cm is quite small, as intended, so as to keep fuel off the liner walls. A small stoichiometric region exists in between the intermediate jets located at θ = 18 and 30 degrees, respectively. The penetration of the six opposed dilution jets at x = 7.6 cm is more pronounced compared to intermediate jets. A small region of 0.8 equilvance ratio exists at this plane.

Figure 105 presents predicted fuel/air ratios for the three x-y planes along θ = 9, 18, and 30 degrees, respectively. The spray origin and the two primary jets are located in these planes. Notice the axial locations of both I.D. and O.D. cooling slots, as shown by symbols ∧ and ∨, respectively. Five of the twenty spray rays are shown by broken lines. At θ = 9 degrees there exists a relatively small stoichiometric region, which grows as θ increases to 30 degrees. The I.D. wall primary panel has a maximum fuel/air ratio of 0.6 around θ = 18 degrees. The

166
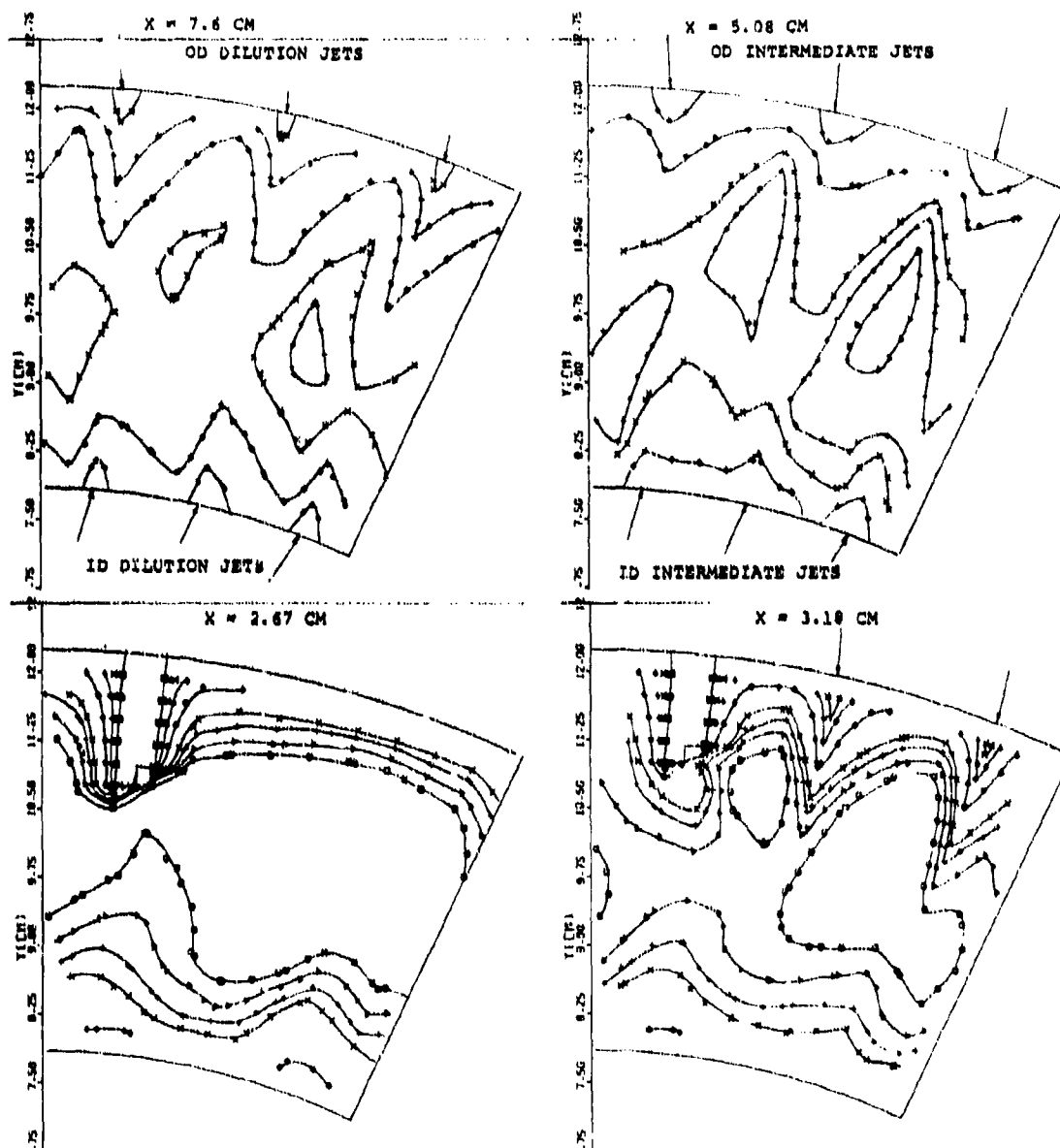
Figure 104. Predicted Fuel/Air Ratio Profiles in the Primary and Intermediate Zones of Concept I Downstream from the Spray Origin.

167
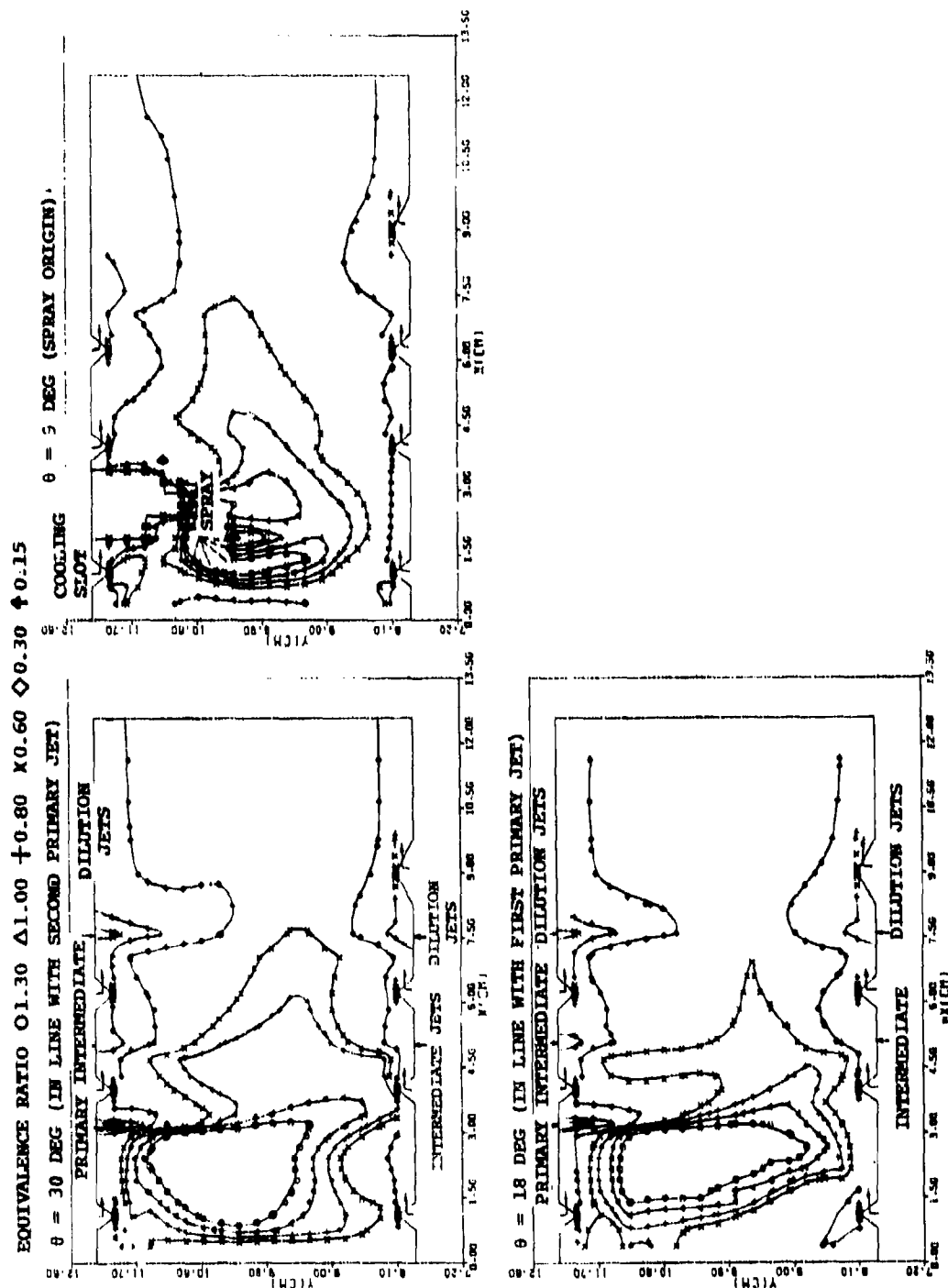
Figure 105. Predicted Fuel/Air Ratio Profiles Along Different X-Y Planes of Concept I.

168

168

first primary jet (θ = 18 degrees) penetration is more than that of the second primary jet due in part to a low-pressure region created by the fuel nozzle shroud. The stoichiometric fuel region extends only slightly downstream of the primary orifices, indicating that the combustor would exhibit good exhaust patterns with distorted combustor inlet flow, as experimentally observed and reported in Section IV.B.

Figure 106 shows predicted profiles of unburned fuel for the same three X-Y planes as presented for the fuel/air ratio in Figure 105. By comparing these two figures, the amount of fuel burned and also the approximate levels of combustion efficiency can be estimated. At θ = 9 degrees there is a small pocket of 0.08 fuel mass fraction that grows until θ = 18 degrees. It is this region that would perhaps produce carbon particles. At approximately the middle of the intermediate zone, the amount of unburned fuel mass fraction is 0.00001. The computed combustion efficiency levels at the planes of intermediate and dilution-orifices are 98.0 and 99.9 percent, respectively.

Figure 107 presents prediction profiles of CO mass fraction for the three X-Y planes. A small region of peak CO mass fraction value of 0.02 or approximately 20,000 PPM exists at θ = 9 degrees. There are, however, a number of CO pockets with approximately 10,000 PPM concentration scattered throughout the primary zone. The CO level increases to a maximum around the primary orifices followed by a decay period. The average mass flux of CO across the planes of intermediate and dilution orifices were 1000 and 10 PPM, respectively.

Predicted isothermal contour plots are shown in Figure 108. The area under the 2300K isothermal curve increases from the θ = 9-degree plane to θ = 30-degree plane. The hottest temperature region is closer to the I.D. wall compared to the O.D. wall except for a small region adjacent to the O.D. wall and the dome. Notice a small cooler region next to the nozzle shroud created by

169
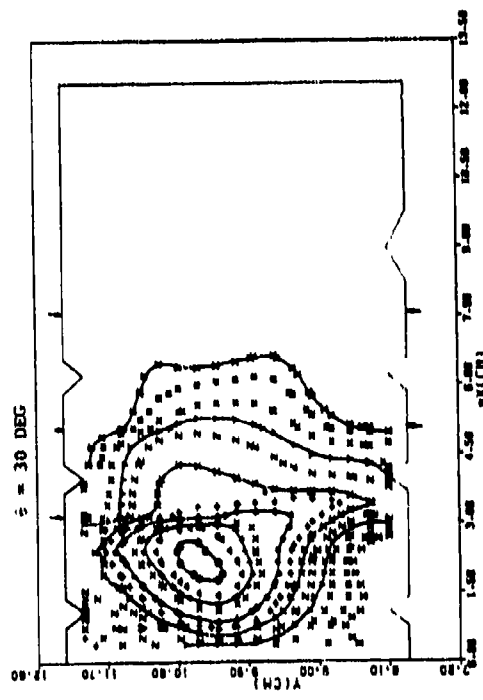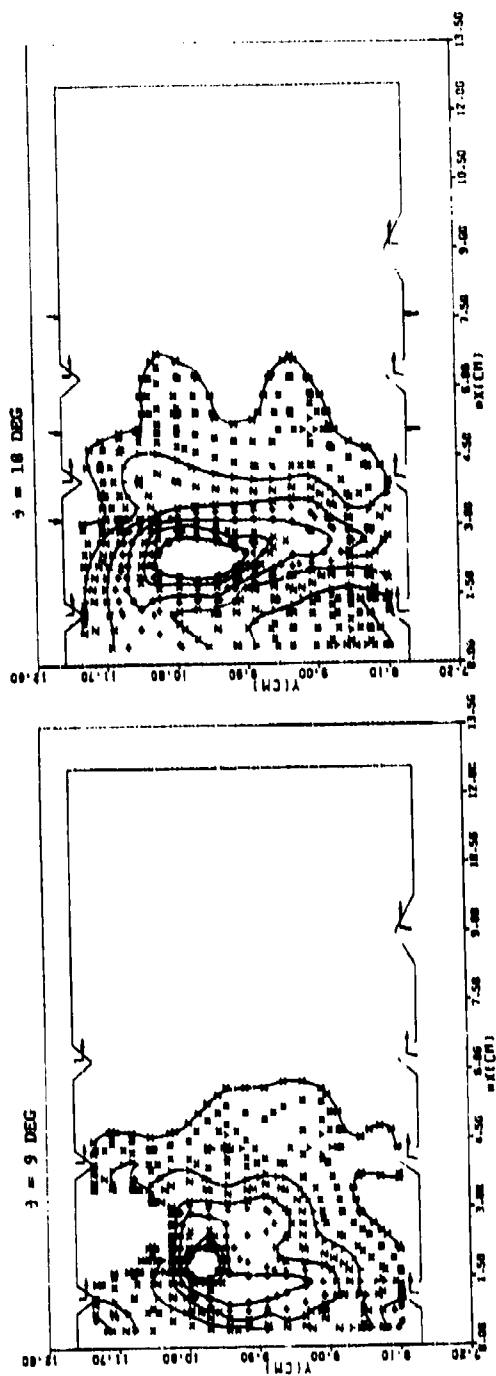
Figure 106. Predicted Unburned Fuel Mass Fraction Profiles Along Different X-Y Planes of Concept I.
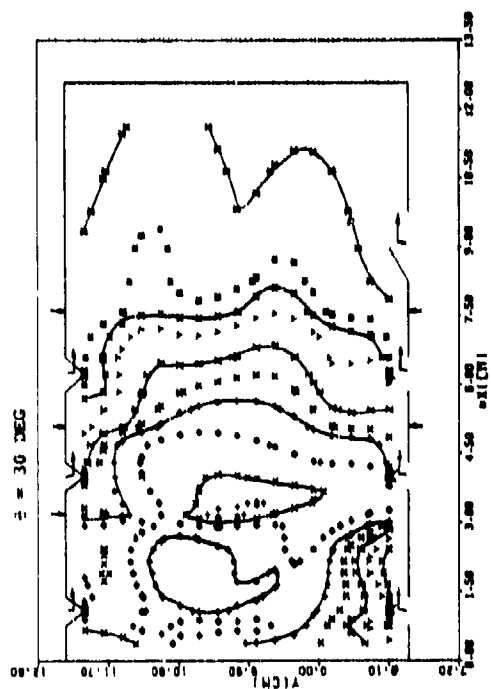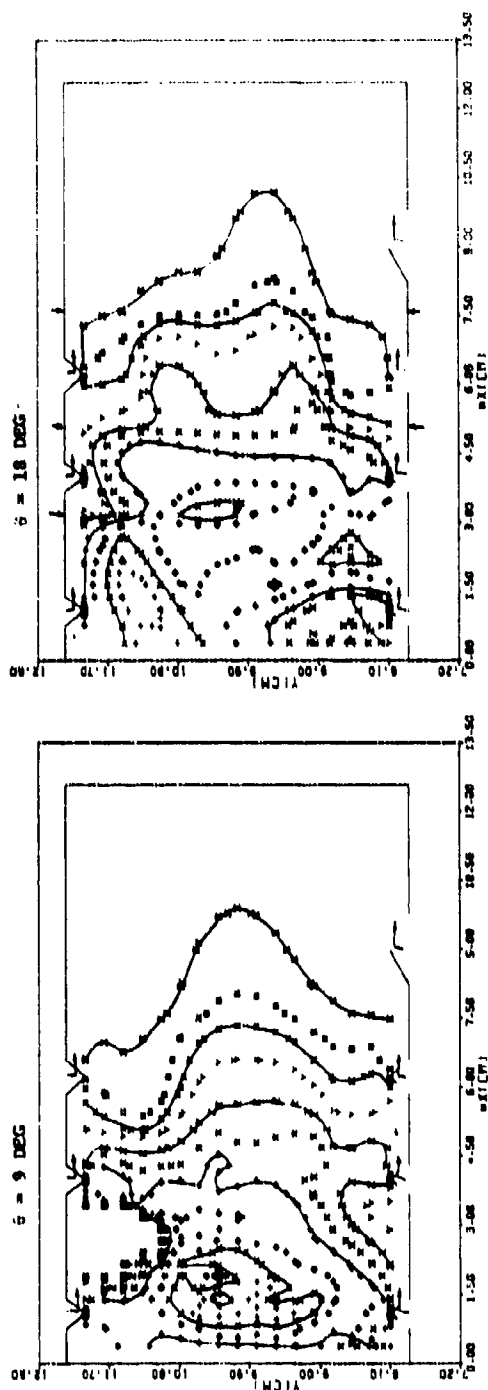
Figure 107. Predicted CO Mass Fraction Profiles Along Different X-Y Planes of Concept I
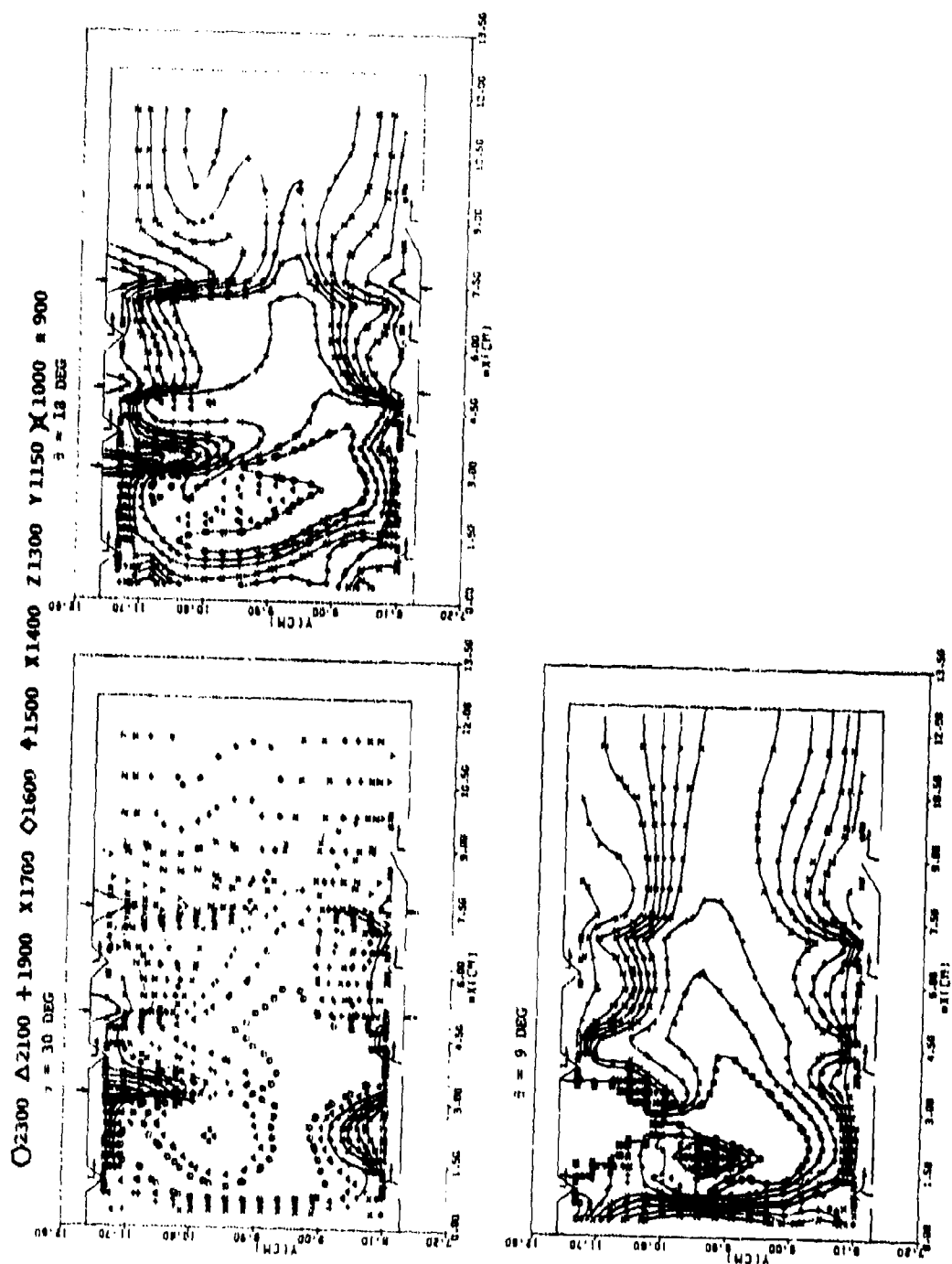
Figure 108. Predicted Isothermal Lines (K) Along Different X-Y Planes of Concept I.

shroud air and the fuel spray. The mixing of the cooler film air with the combustor hot gases can be inferred by following isothermal lines emanating from the cooling slot lip. Similarly, the bending of the isothermal lines by radial jets may be observed. The penetration of the primary jet and subsequent tendency of the hot gases to get close to both the I.D. and O.D. liner walls was successfully thwarted by intermediate jets. If the intermediate jets were too big so as to cause entrainment of hot gases in their wakes, such as shown for the primary jet, there would have existed a hot temperature region downstream from the intermediate orifices. Large dilution orifices entrain the hot gases as shown.

The location and volume of the recirculation zone is important from a combustion efficiency and lean blowout standpoint. Figure 109 shows predicted reverse-flow regions predicted for the three X-Y planes along θ = 12, 18, and 24 degrees, respectively. It may be recalled that the spray originates at θ = 9 degrees. Since the spray travels along the tangential direction with a 25-degree back angle and toward the dome with a 35-degree down angle, the reverse flow region should be located in such a way as to provide the needed ignition source without excessive fuel (impingement of the dome). If the nozzle is well immersed into the region of reverse-flow causing droplets to recirculate back toward the nozzle tip, an undesirable carbon fouling problem may result. In the case of Concept I, the reverse-flow region at θ = 12 degrees is small enough to create carboning of the nozzle tip. The maximum size of the bubble is at θ = 24 degrees, i.e., 15 degrees downstream from the nozzle tip. If the droplets produced by the nozzle are too small to travel up to θ = 24 degrees, the combustor lean stability might deteriorate. It was demonstrated during testing that increasing the external air-assist with an attendant improvement in fuel spray SMD increased the lean blowout fuel/air ratio.
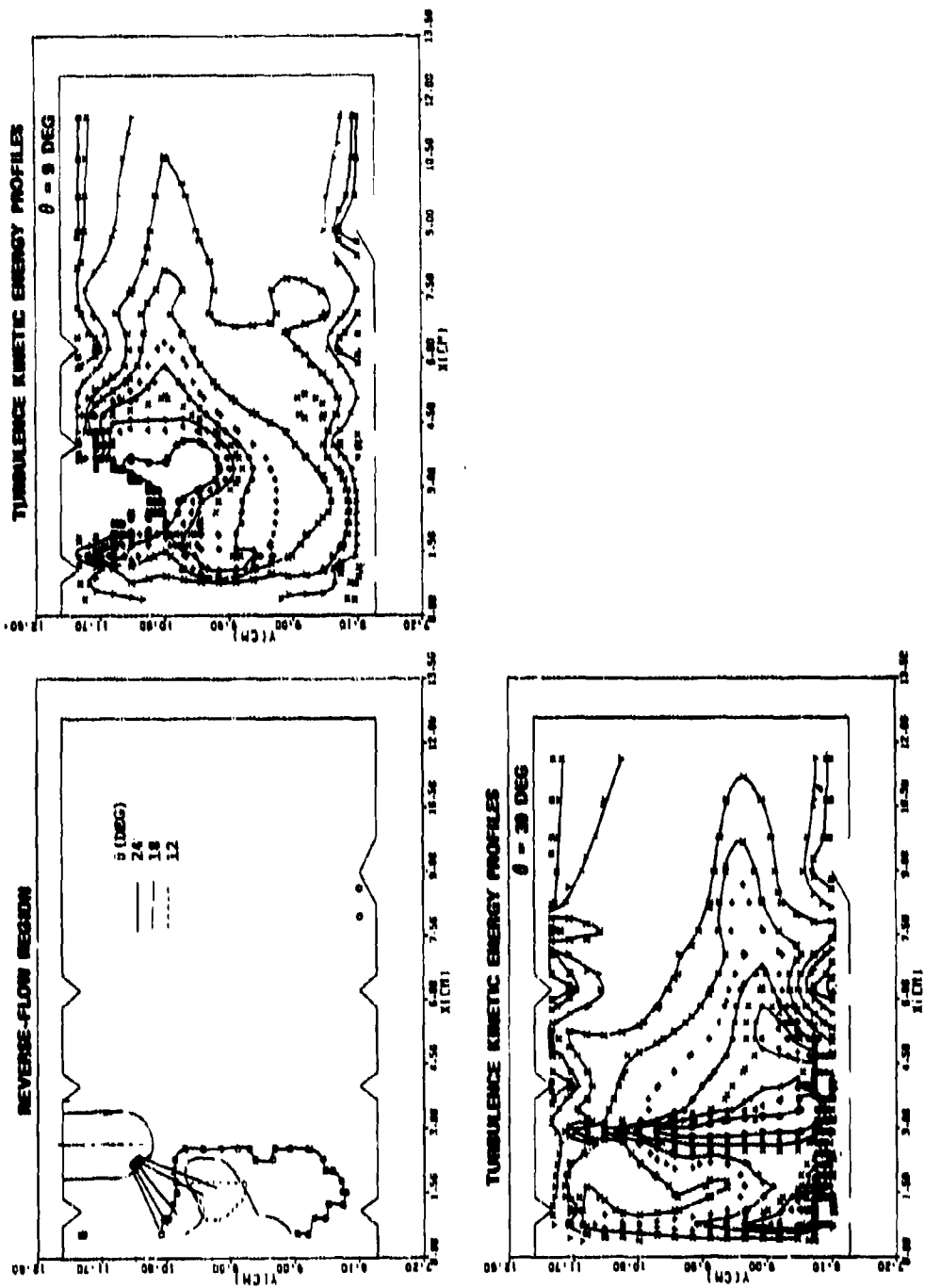
Figure 109. Predicted Reverse-Flow Region and Turbulence Kinetic Energy Profiles for Different X-Y Planes of Concept I.

174

The turbulence kinetic energy (k) profiles, as well as length scales, greatly influence the overall combustion rate. Figure 109 also presents typical turbulence kinetic energy profiles for the two X-Y planes in line with θ = 9 and 30 degrees, i.e., in the planes of the spray origin and where maximum fuel/air ratio and associated hot streaks exist, as shown previously in Figures 105 and 108, respectively. To maximize the reactivity, it is desirable to have the maximum fuel region coincide around the region of maximum k. At θ = 9 degrees, the combustor has low fuel/air regions, as well as a small region of high turbulence. However, at θ = 30 degrees, where a large fuel rich pocket exists, the maximum turbulence region coincides with it. This results in high combustion intensity inferred from the unburned fuel-mass concentration profiles of Figure 106.

A majority of the rig performance tests were conducted with the Concept I liner coated with OG-6 Thermindex thermal paint to determine liner wall temperature levels and gradients. These tests usually required running a number of different conditions over the engine cycle. In order to evaluate the wall temperature characteristics at a very critical point, a single test point was located corresponding to the sea-level, hot-day, static, maximum power condition. Consequently, a 3-D computer run was made for this condition. The predicted results were similar to those of the standard-day condition, as presented in Figures 103 through 109. Figure 110 shows the predicted isothermal plots for the hot-day run and may be compared with Figure 108 for a standard-day, maximum power condition. A slight difference in regard to the size and location of the peak temperature region may be noted. Otherwise, the profiles appear to be similar.

The combustion intensity is determined, for the most part, by spray evaporation, mixing, and reaction rate. At high power points, the first two are not usually rate determining processes. The reaction rate, in turbulent flows, is controlled by chemical

175
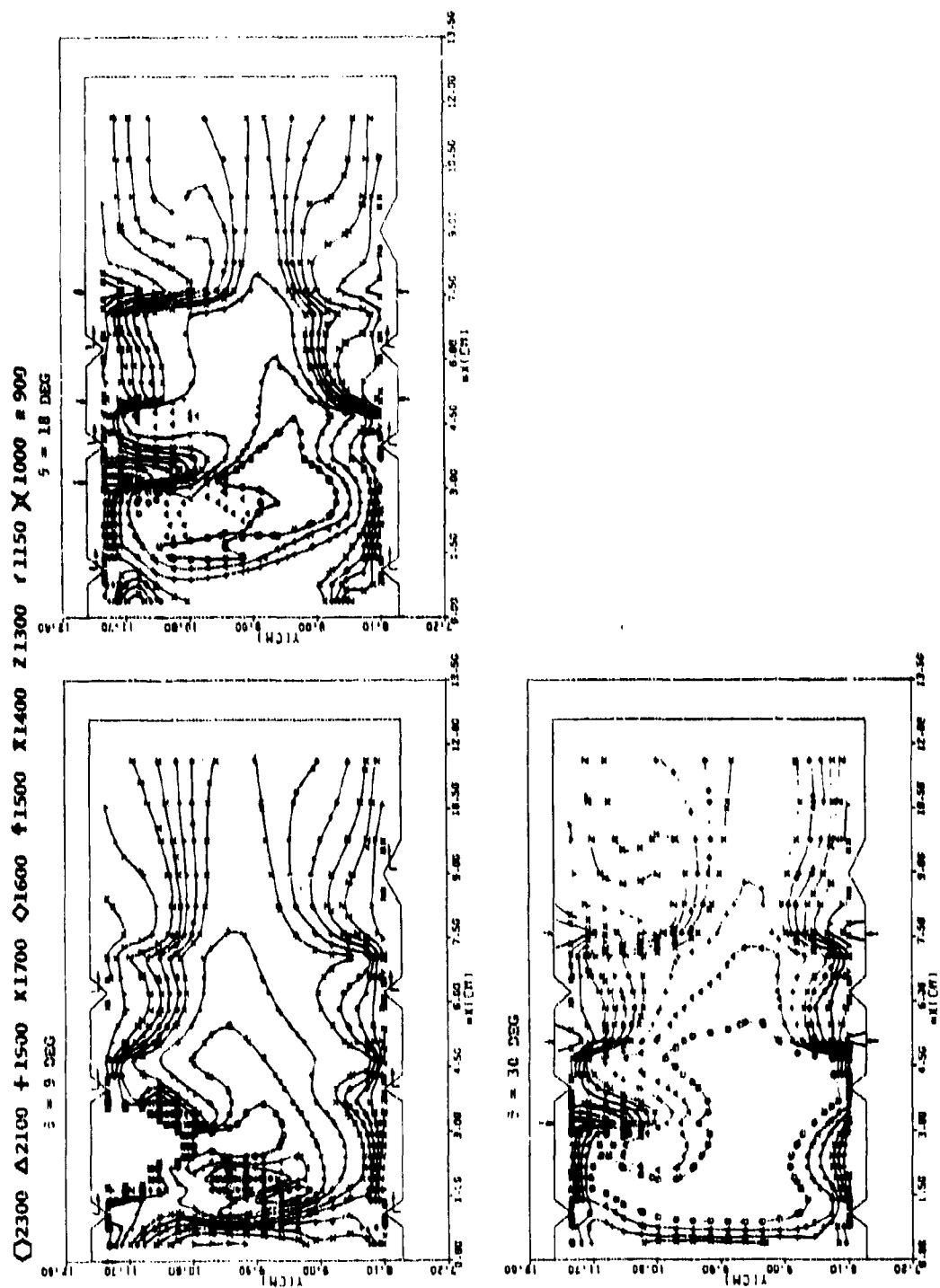
Figure 110. Predicted Isothermal Plots of Concept I at Sea-Level, Hot-Day Maximum Power Point.

kinetics, turbulence, and scale. A rather simple model is used in present calculations in that the rate is the minimum of the Arrhenius expression and the products $M_{fu} \frac{\epsilon}{K}$ and $\frac{M_{ox}\epsilon}{i\,k}$, where M_{fu}, M_{ox}, i, k, and ϵ are mass fractions of unburned fuel and oxygen, stoichiometric oxygen-to-fuel ratio, turbulence kinetic energy and dissipation rate, respectively. Depending upon the concentrations of M_{fu}, M_{ox}, $(M_{fu})^{1/2} \times M_{ox}$, ϵ/k and gas temperature, the reaction rate in different parts of the combustor is controlled by chemical kinetics and the availability of oxygen and fuel. Such regions for Concept I at the sea-level, standard day, maximum power point are shown in Figure 111. The results are shown for the X-Y plane along $\theta = 0$ degrees. There is a small region close to the dome and around the mid-channel that is controlled by kinetics. Around this region the overall fuel oxidation rate is determined by the availability of oxygen, i.e., this region is fuel rich. The reaction rate in the rest of the combustor is controlled by the fuel mass fraction.

2.   Transition Mixing Model Predictions

The 2-D transition mixing model was used to predict the mixing rates of the combustor gases while passing through the combustor transition liner. A total of eleven Z-Y planes, corresponding to $\theta = 3$, 6, 9, 12, 15, 18, 21, 24, 27, 30, and 33 degrees were analyzed. It may be recalled that the spray origin, the swirler center, and the two primary jets lie along $\theta = 9$, 18, 18, and 30 degrees, respectively. Since the transition mixing model is a parabolic program, it requires specification of the initial boundary conditions. The 3-D model predictions for the station X = 9.78 cm from the combustor dome were taken as the initial conditions for the transition mixing model. It may be recalled that the dilution orifices are located at X = 7.6 cm, which means that the inlet for the transition mixing model is 3.18 cm downstream from the dilution orifices.

177
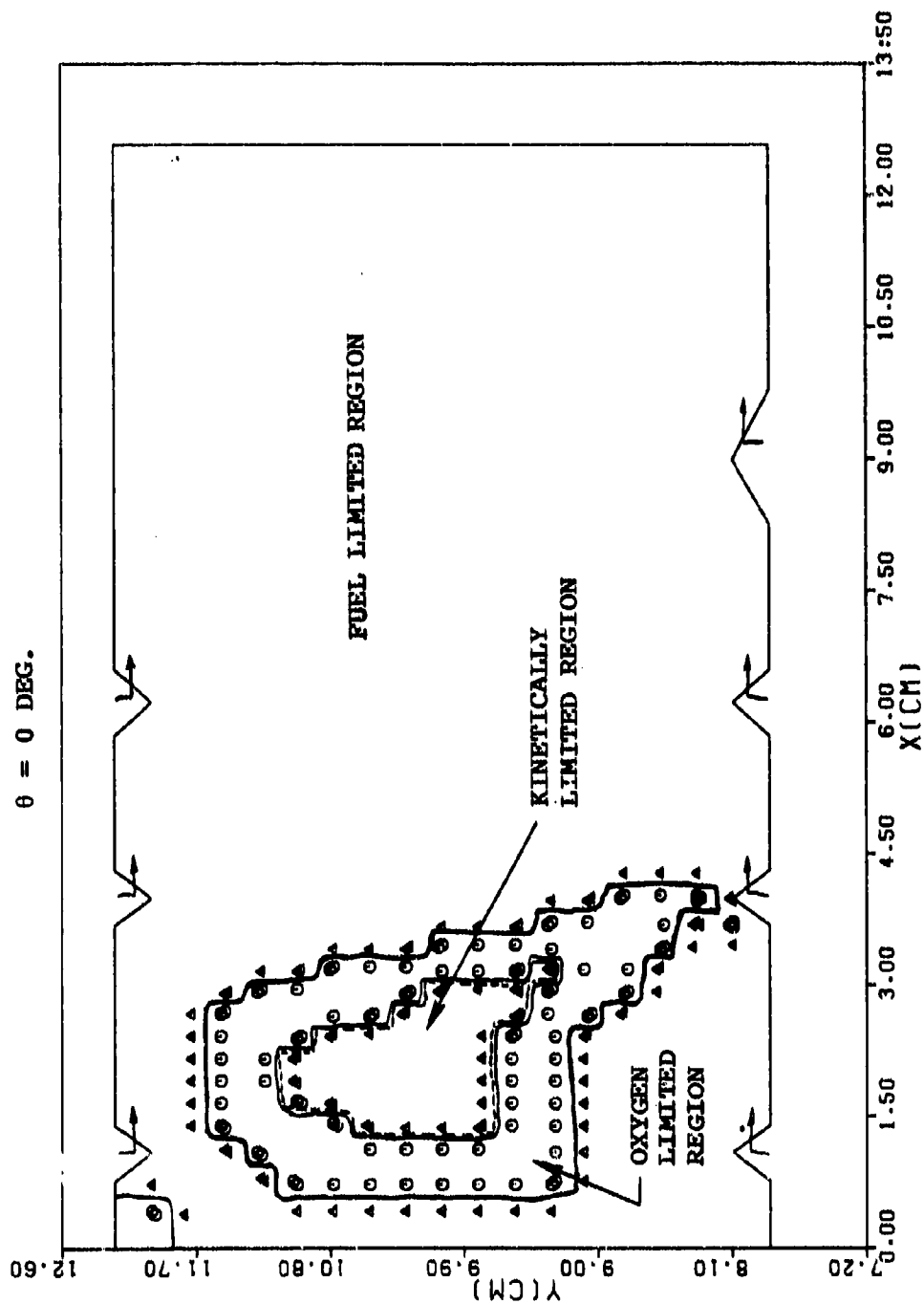
Figure 111. Predicted Concentrations of Fuel and Oxygen for Concept I at the Sea-Level Standard Day, Maximum Power Point.

178

Figure 112 presents a schematic of the combustor transition liner that was used with both the Concept I and Concept II combustor liners. The transition liner geometry was defined by 19 discrete points on the outer as well as inner transition liner walls. Here X_E and X_I denote distance along the external and internal liner walls, respectively. The radial position of any point P is given by

$$R = R_I + Y \cos \alpha$$

where R_I, Y and α are radius of the inner wall, normal distance from the inner wall, and the angle from the radial direction, respectively. It may be noticed that the gas particle that was initially close to the combustor outer wall ends up close to the stator hub after transversing through the combustor transition liner. Thirty-three nodes were used for the Y-direction. Approximately 200 steps were taken to cover the length of the transition liner.

Figure 113 presents predicted combustor exit (stator inlet) temperature profiles of Concept I at conditions corresponding to the sea-level, hot-day maximum power condition for the four Z-Y planes. Also shown are the corresponding transition liner inlet profiles predicted by the 3-D Combustor Performance Model. The radial profiles are presented in terms of the normalized channel height. For the inlet plane the radii of the inner and outer walls are 7.85 and 12.32 cm, respectively, with a corresponding channel height of 4.47 cm and a flow area of 283 cm^2. On the other hand, the transition liner, exit radii, channel height, and flow area are 2.79 cm, 4.83 cm, 2.03 cm, and 48.6 cm^2, respectively. The ratio of the transition liner inlet-to-outlet flow area is 5.82 with attendant flow acceleration from the inlet to the outlet. Consequently, the model predicted a slightly lower level of turbulence at the liner exit plane compared to the inlet. The mixing rate is also expected to decrease in the

179
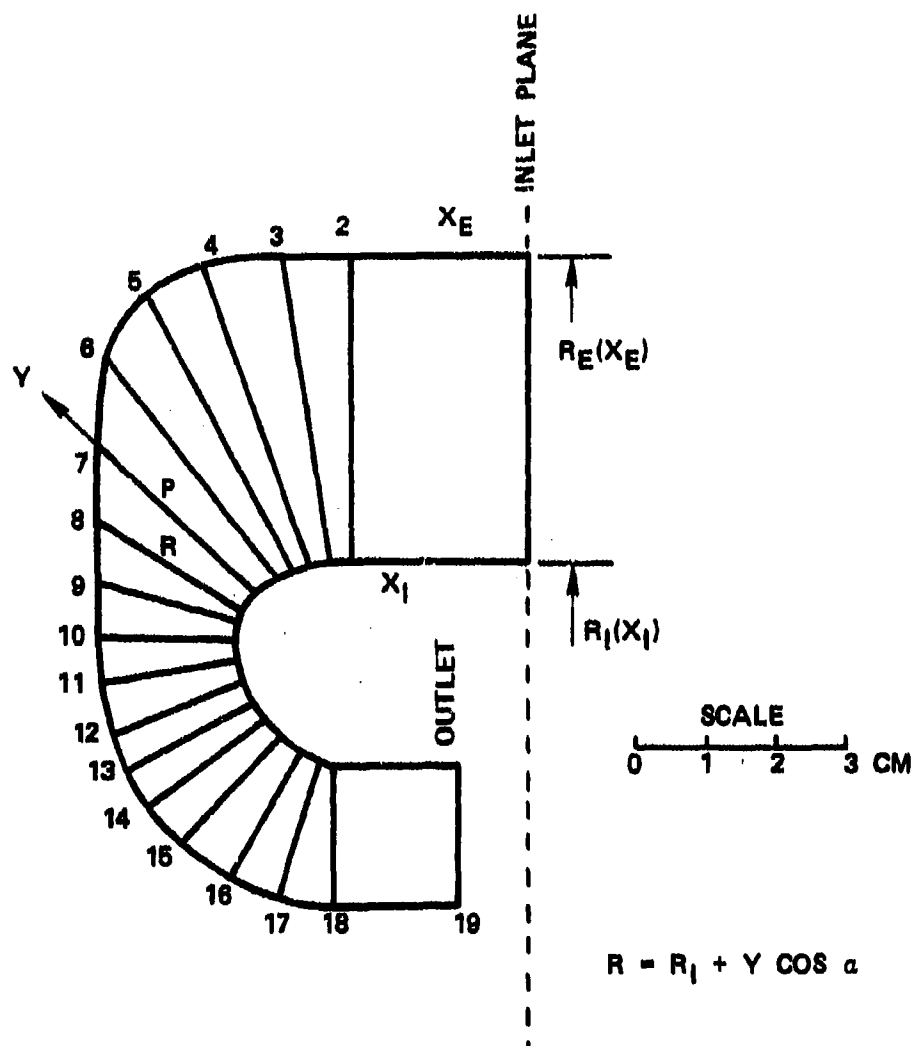
Figure 112.   Concept I and Concept II Combustor
              Transition Liner.
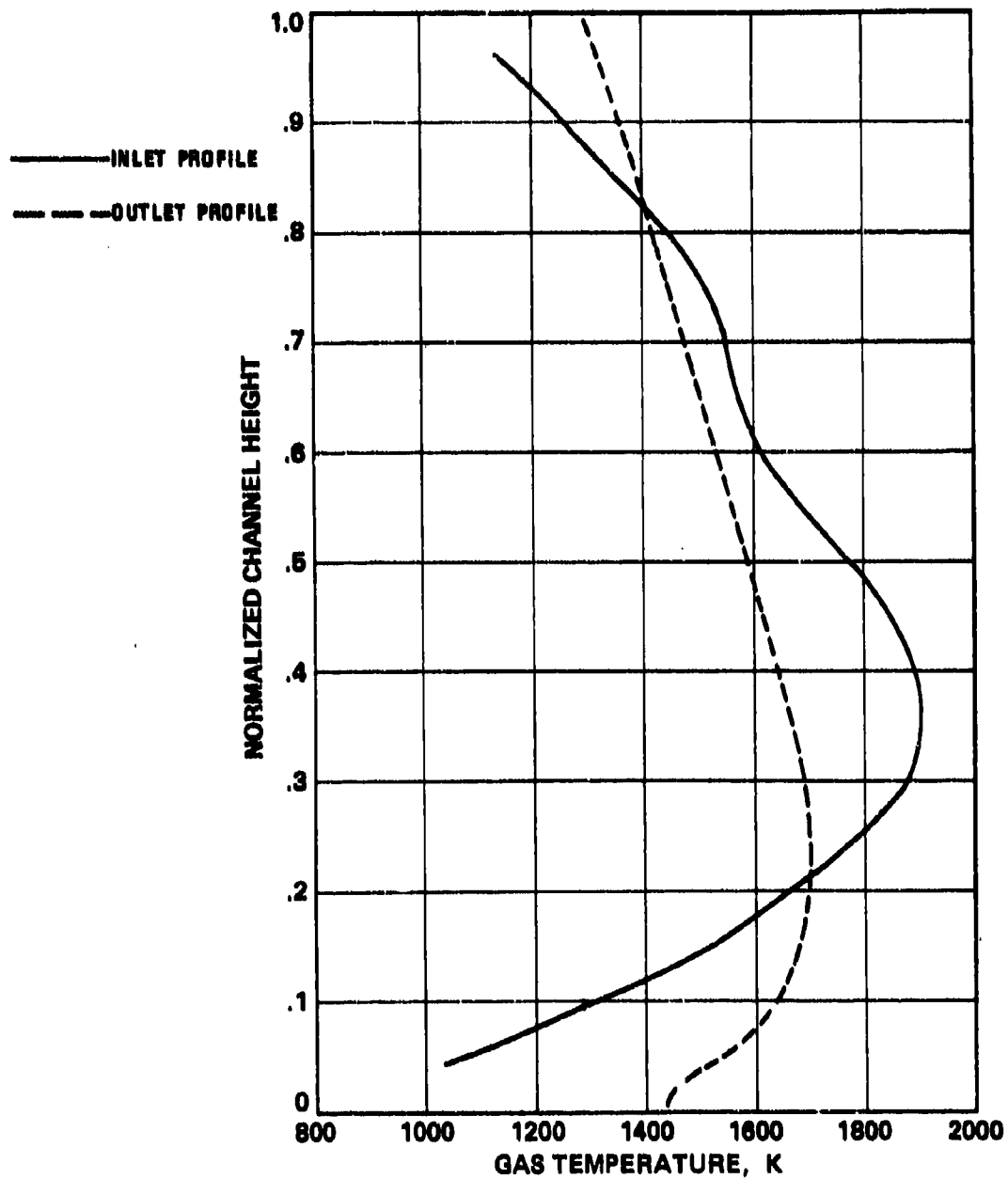
180

Figure 113. Predicted Stator Inlet Temperature Profiles
of Concept I at the Sea-Level, Hot-Day Maximum
Power Point for the Planes θ = 3, 6, 9 and 12
Degrees   (Sheet 1 of 4).

181
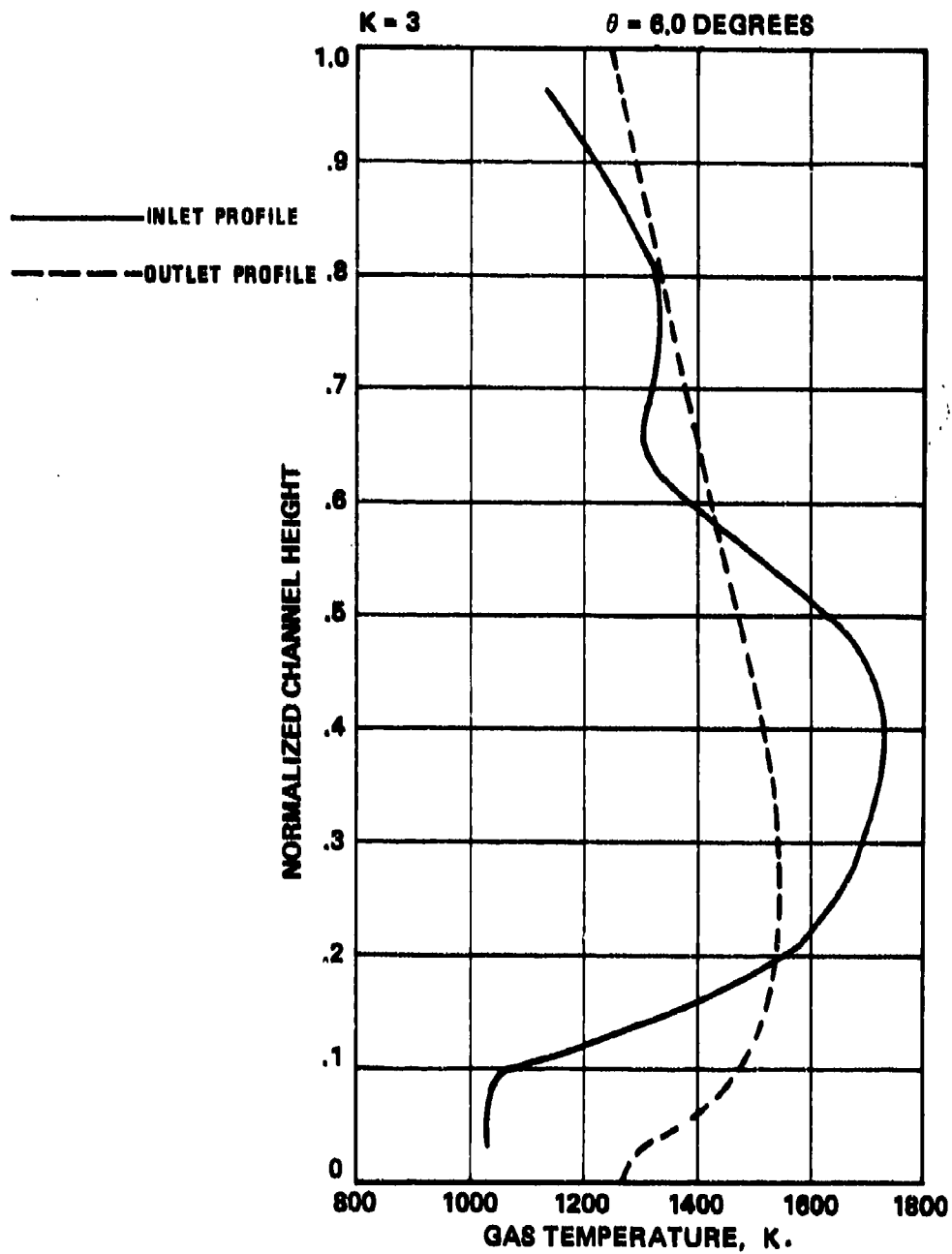
Figure 113.   Predicted Stator Inlet Temperature Profiles
of Concept I at the Sea-Level, Hot-Day Maximum
Power Point for the Planes θ = 3, 6, 9 and 12
Degrees   (Sheet 2 of 4).
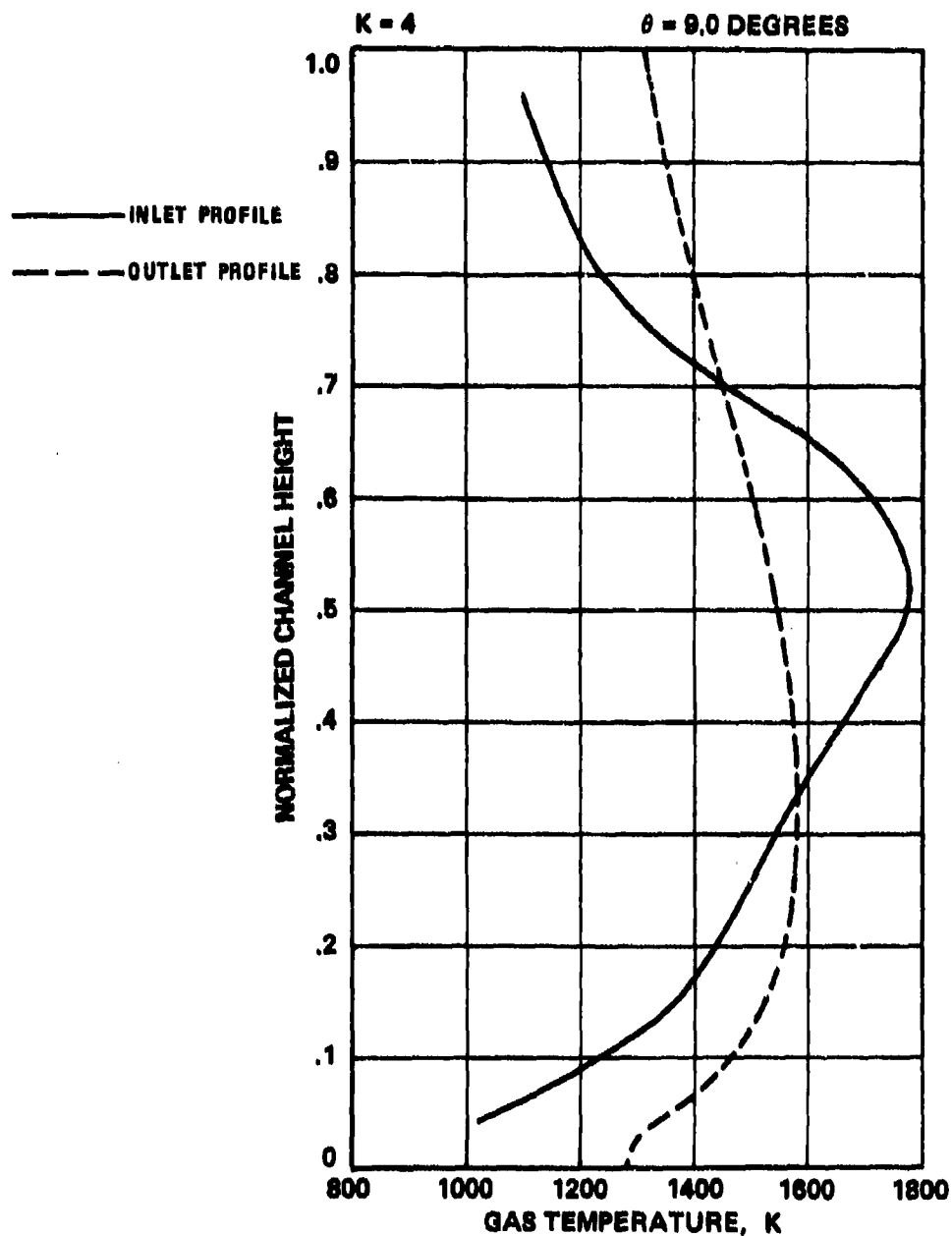
182

Figure 113. Predicted Stator Inlet Temperature Profiles of Concept I at the Sea-Level, Hot-Day Maximum Power Point for the Planes θ = 3, 6, 9 and 12 degrees (Sheet 3 of 4).
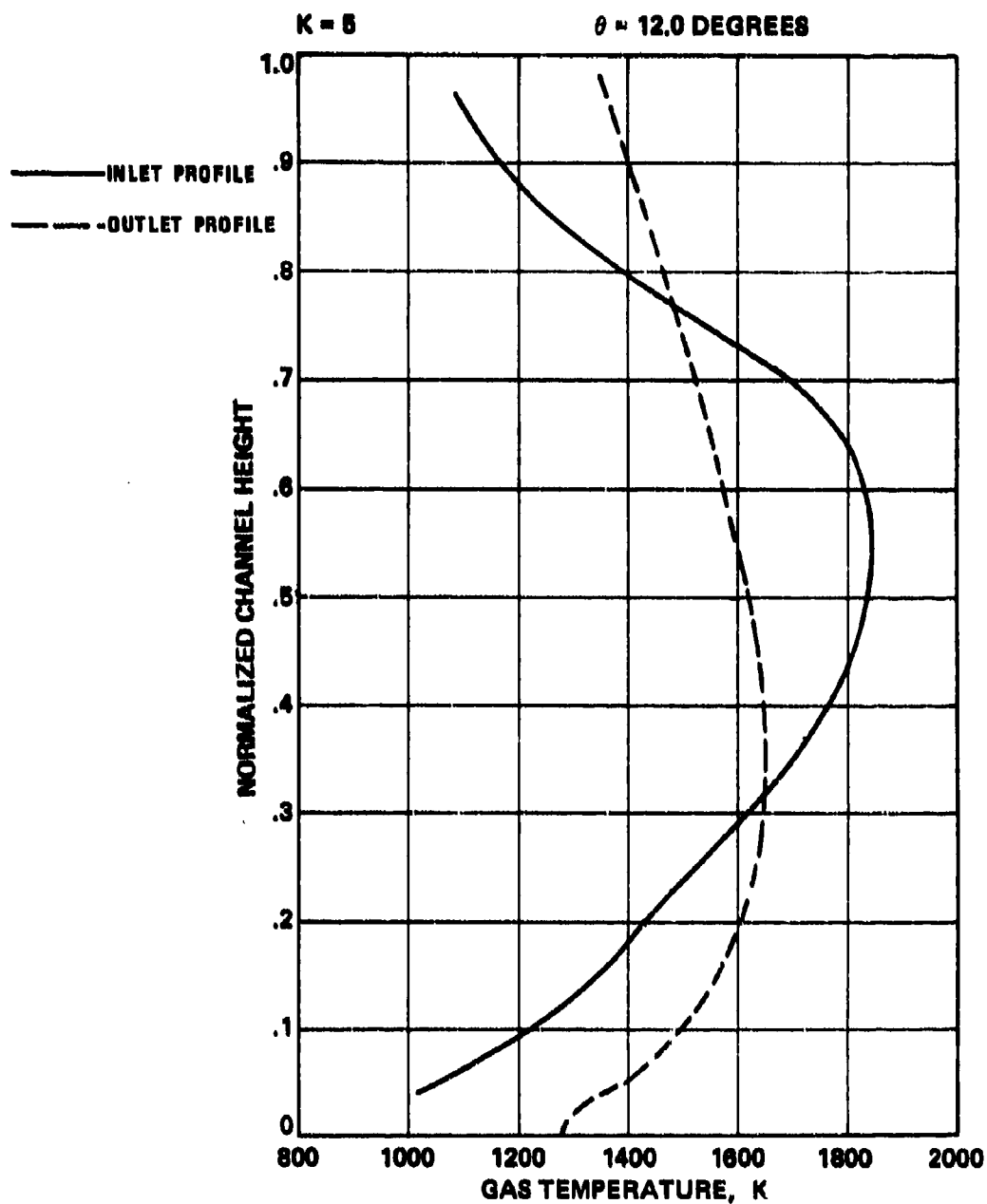
183

Figure 113. Predicted Stator Inlet Temperature Profiles of Concept I at the Sea-Level, Hot-Day Maximum Power Point for the Planes θ = 3, 6, 9 and 12 Degrees (Sheet 4 of 4).

region of accelerating flow. Figure 114 presents peak temperature as a function of distance along the transition liner outer wall to illustrate the mixing rate in the liner. The results are for a plane with the maximum exit temperature peak, i.e., along θ = 24 degrees. From these results, it appears that the rate of mixing of the hot streak is approximately constant over the entire transition liner length of approximately 15 cm.

The predicted exit plane profiles in Figure 113 as well as Figures 115 and 116 are plotted so that a zero normal distance denotes the stator tip and unity corresponds to the hub. The results have been plotted this way so that the radial shift in the peak temperature of the profiles at the liner inlet and outlet could be discerned. For example, as shown in Figure 113, the temperature peak at the inlet for the planes along θ = 3, 6, 9, and 12 degrees were located at 0.35, 0.42, 0.54, and 0.52 channel height from the inner wall, respectively. The corresponding temperature levels were 1900, 1730, 1779 and 1840 K. On the other hand, at the outlet, these peaks shifted to 0.22, 0.26, 0.34, and 0.34 channel height from the stator tip. The corresponding temperature levels are 1695, 1552, 1584 and 1652 K. Consequently, the peak temperature values along these planes reduced by 205, 178, 195, and 188 K, because of the mixing in the transition liner.

Two major deficiencies of the transition mixing model must be pointed out in order to facilitate a proper evaluation of the above results. The model is taken to be locally 2-D, whereby diffusion along the θ direction is assumed to be negligible. The maximum difference between the peaks at the inlet for the region $3 \leq \theta \leq 12°$ is 170 K which is comparable with the average drop of 192 K in the peaks from the inlet to the outlet. Had the mixing along the θ direction been allowed, the hot-streak would have dissipated more than the rate predicted by the 2-D model. A second deficiency in the model is in regard to neglecting the
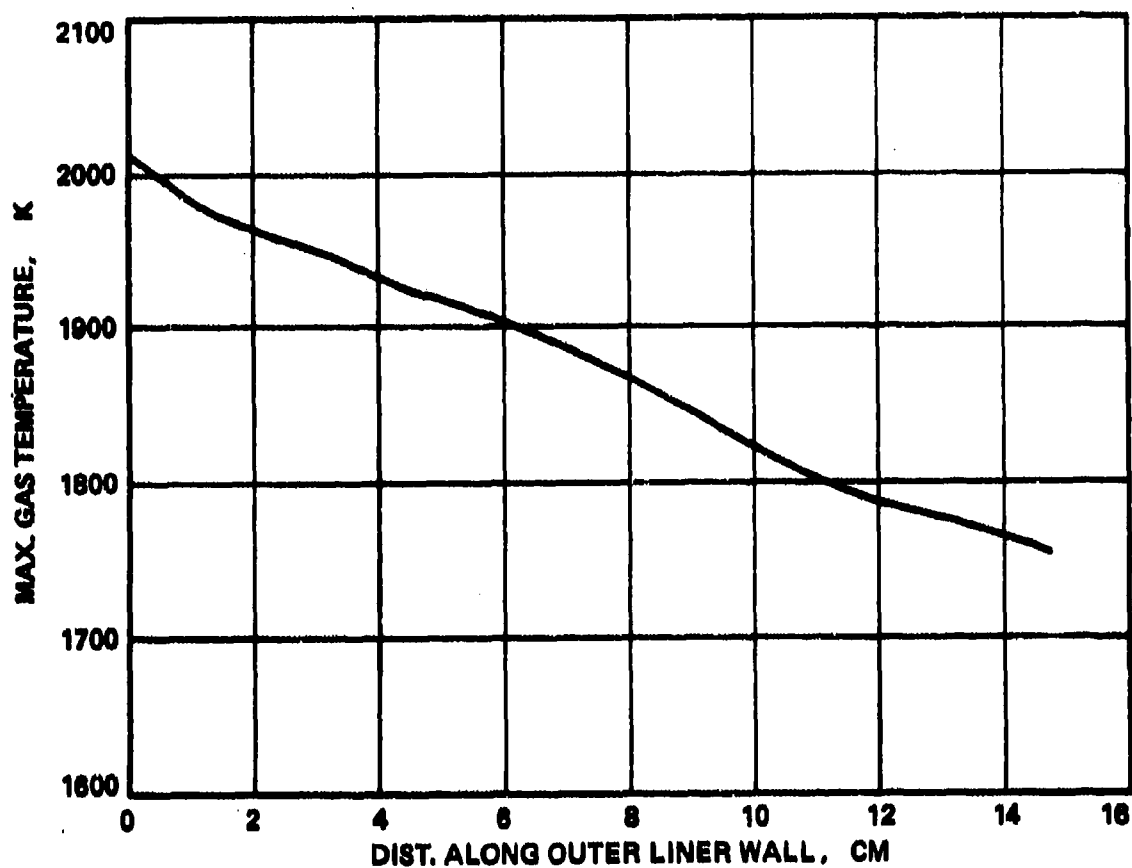
Figure 114. Predicted Mixing Rate in the Transition Liner
as a Function of Distance Along the Outer
Liner Wall for θ = 24 Degrees.
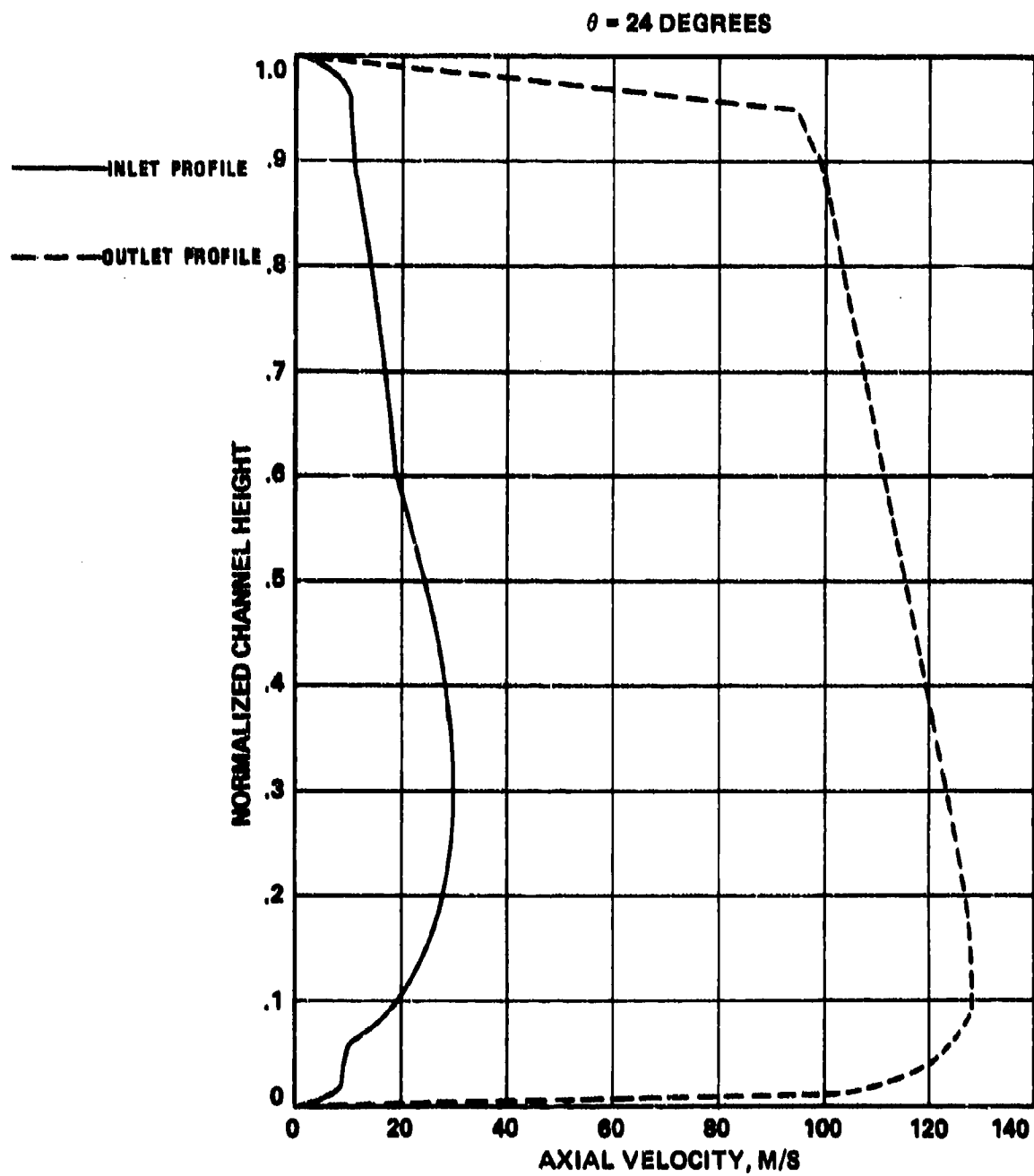
Figure 115. Predicted Combustor Exit Profile of Axial Velocity.
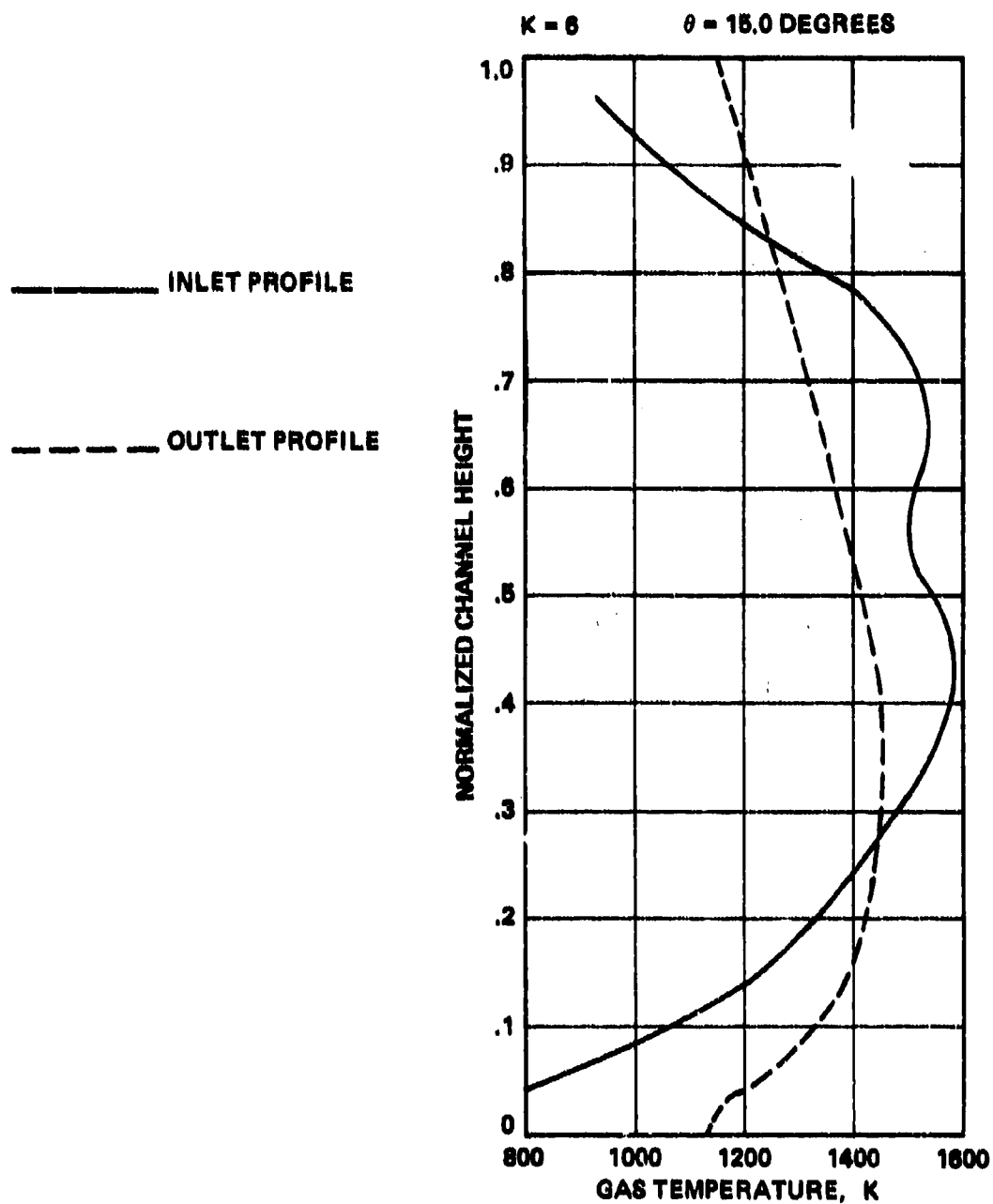
Figure 116. Predicted Stator Inlet Temperature Profiles of
Concept I for the Planes θ = 15, 18, 21 and 24
Degrees (Sheet 1 of 4).
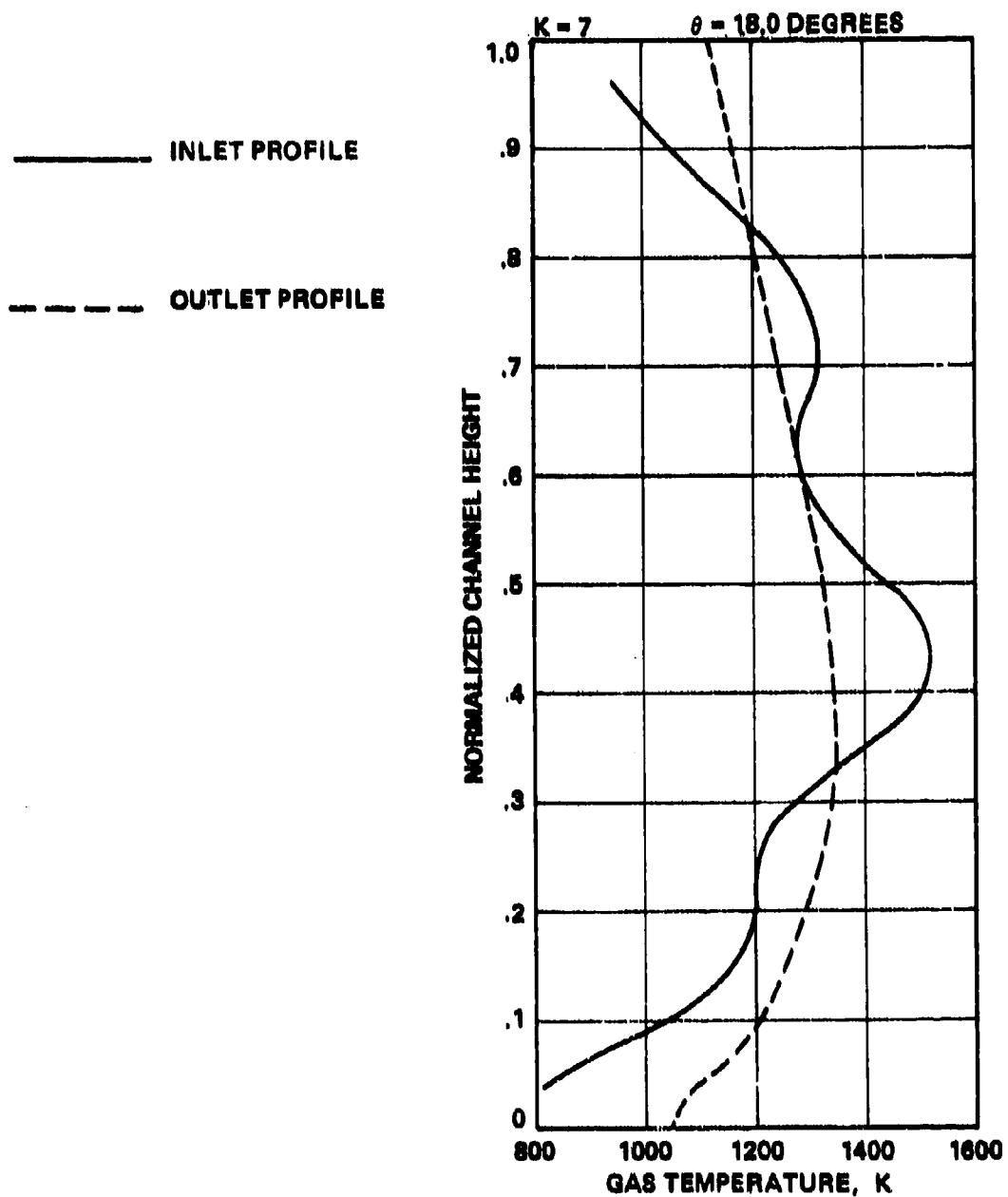
188

Figure 116. Predicted Stator Inlet Temperature Profiles of Concept I for the Planes θ = 15, 18, 21 and 24 Degrees (Sheet 2 of 4).
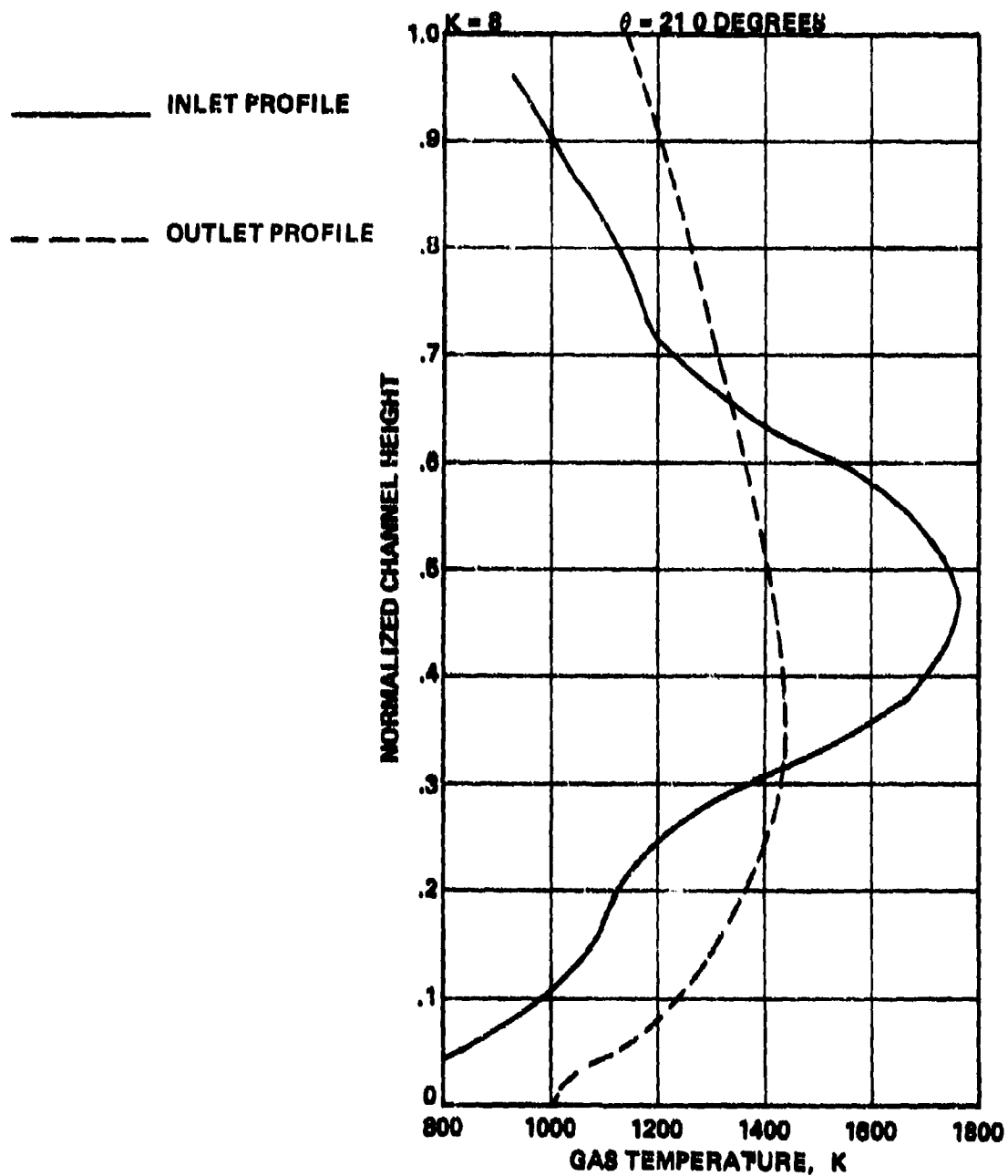
Figure 116. Predicted Stator Inlet Temperature Profiles of
Concept I for the Planes θ = 15, 18, 21 and 24
Degrees (Sheet 3 of 4).
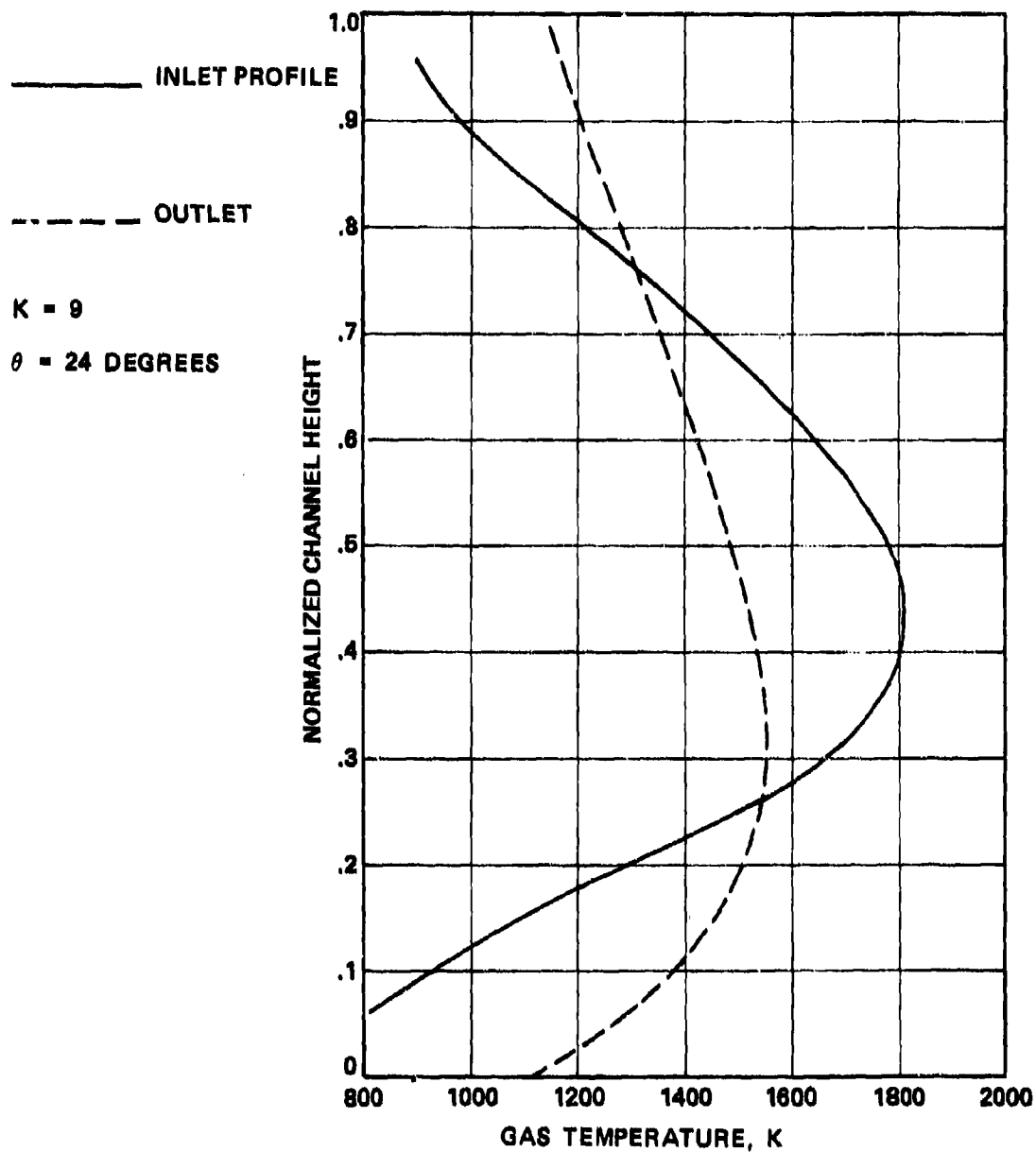
190

Figure 116. Predicted Stator Inlet Temperature Profiles of Conept I for the Planes θ = 15, 18, 21 and 24 Degrees (Sheet 4 of 4).

elliptic effects of pressure due to streamline curvature, although the model allows for a radial variation in pressure. How important elliptic effects are in estimating the mixing rate and the shift in radial profiles remain to be determined. Figure 115 shows predicted axial velocity profiles at the stator inlet for the θ = 24-degree plane. The corresponding transition liner inlet profile is also shown.

Figures 116 and 117 present predictions for the remaining seven exit planes. Note again the radial shift of the peaks. The maximum temperature peak is at the plane inline with θ = 24 degrees, i.e., a 6-degree shift from the center of the combustor dome swirler. This peak is also in line with the plane having a maximum recirculation bubble area, as shown previously in Figure 109. In addition, this hot streak emanated from a combustor sector lying between the primary orifices. The hot day thermal paint run also exhibited a number of hot spots on the liner wall region in between the primary orifices. The predicted circumferential pattern factor of 0.22 compares reasonably well with the measured value of 0.18 but needs to be qualified as discussed below.

The creation of hot streaks in a gas turbine combustor is due to nonuniform airflow distributions around the combustor liner caused in part by compressor discharge profiles of total pressure and velocity. In addition, local flow distortions are created by local obstructions, swirlers, fuel nozzle shrouds, and ignitor bosses, etc., in the flow path, which create local regions of low pressures. The fuel nozzle distribution, along with differing spray characteristics can also result in creating locally nonuniform flow stations. The 3-D calculations are generally performed with periodicity conditions applied for each of the nozzle sectors to minimize the computation effort. It is theoretically possible to analyze a sector comprised of three or more fuel nozzles so that the cyclic·conditions applied to the
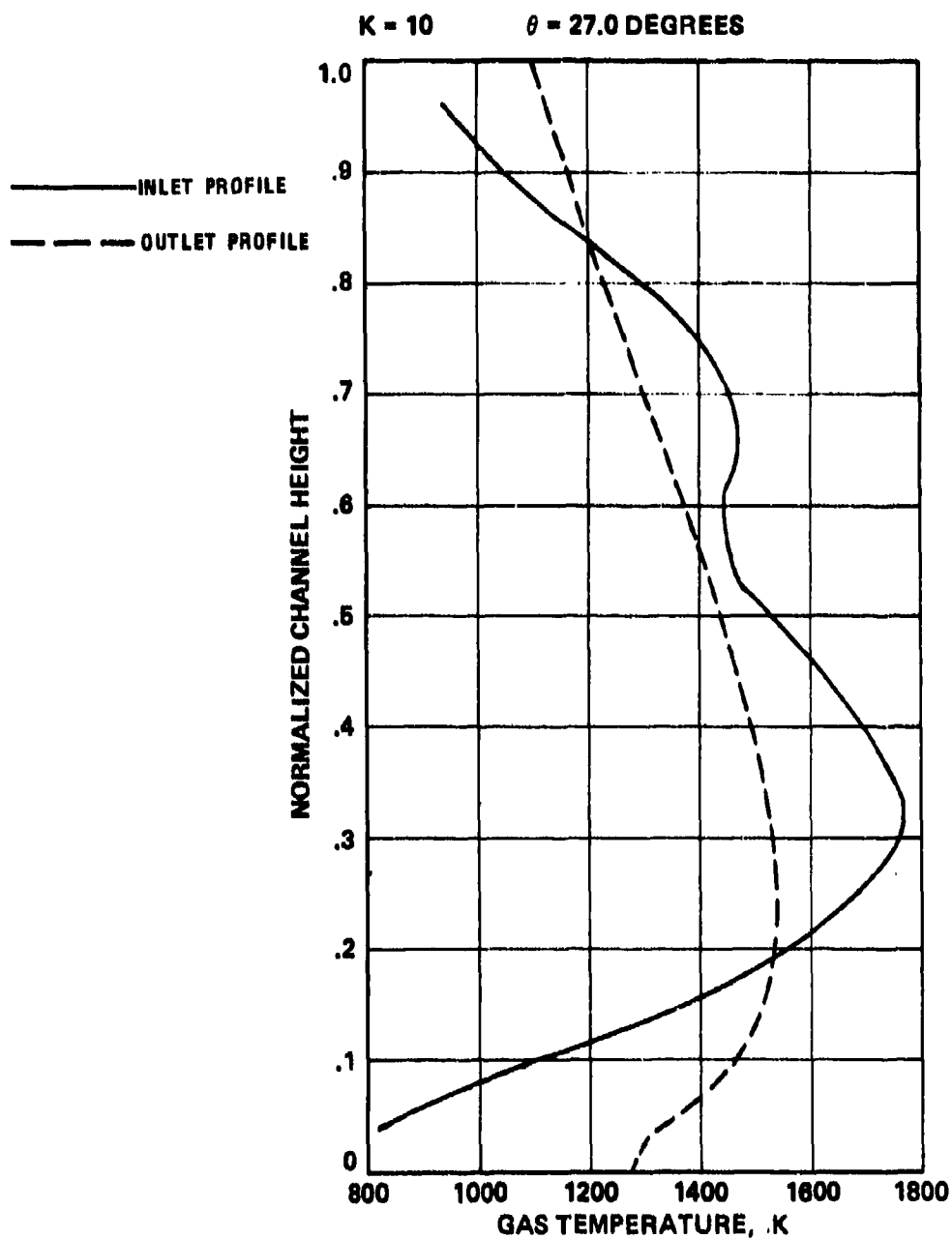
192

Figure 117. Predicted Stator Inlet Temperature Profiles of
             Concept I for the Planes θ = 27, 30 and 33 Degrees
             (Sheet 1 of 3).

K = 11 θ = 30.0 DEGREES
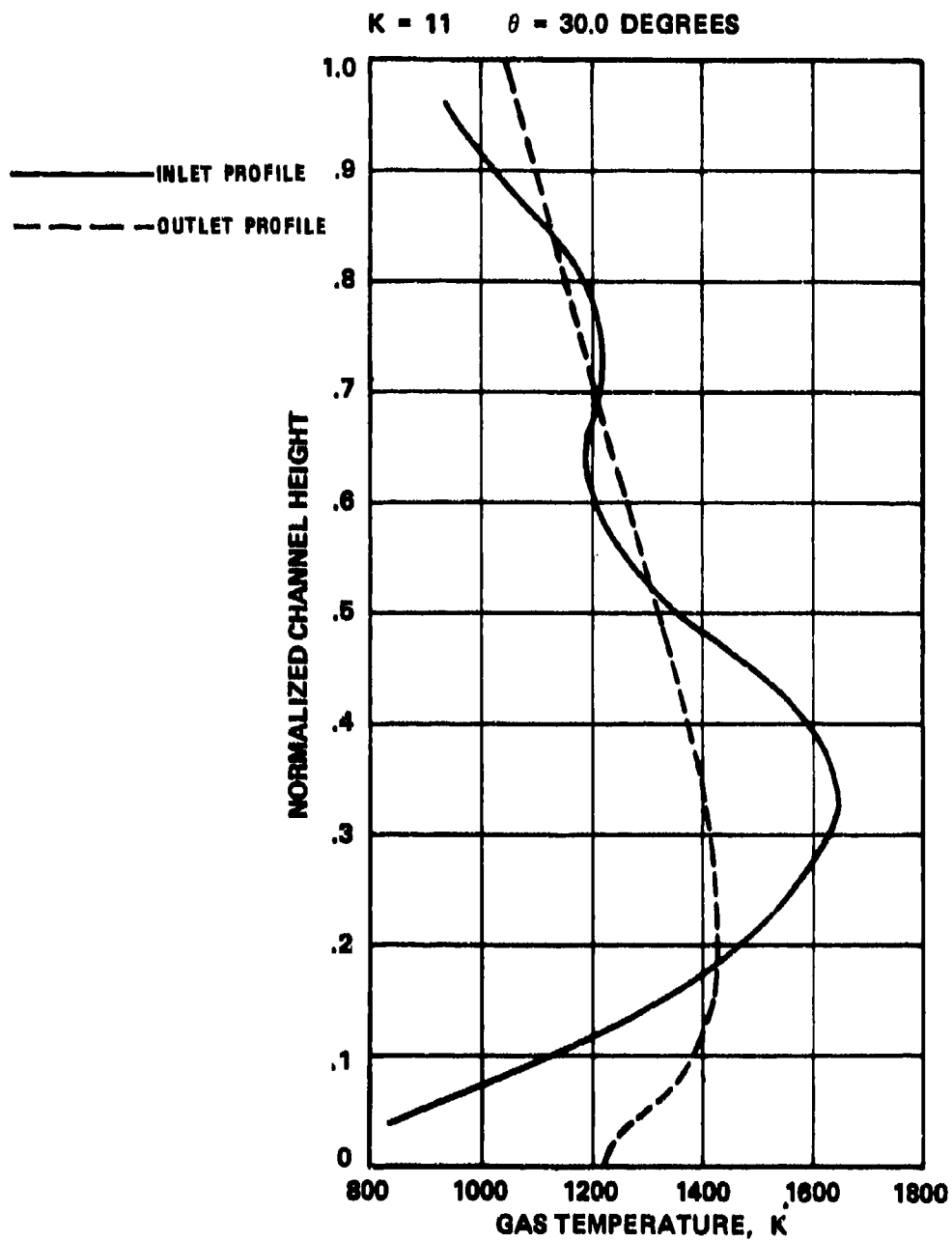
Figure 117. Predicted Stator Inlet Temperature Profiles of Concept I for the Planes θ = 27, 30 and 33 Degrees (Sheet 2 of 3).

Figure 117. Predicted Stator Inlet Temperature Profiles of Concept I for the Planes θ = 27, 30 and 33 Degrees (Sheet 3 of 3).

195
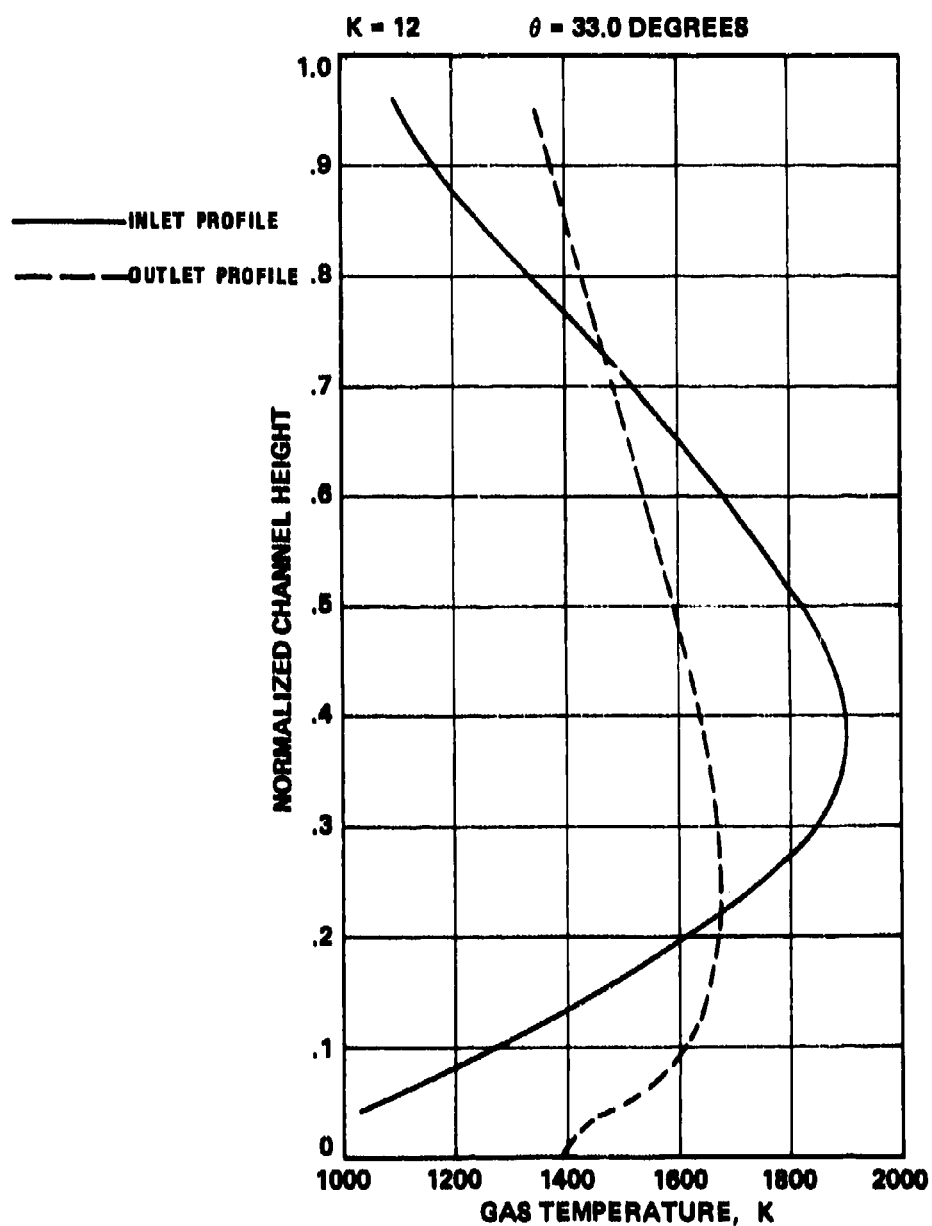
outermost nozzle sections have minimal effect on the predictions of the flow field fed by the middle fuel nozzle.

With such an arrangement one can then impose assumed or estimated nonuniform airflow rates through the various liner orifices, and can analytically predict the changes in the exhaust temperature patterns. Similarly, if one can specify the boundary conditions of the spray in case of its malfunctioning, the effect of nozzle characteristics on exhaust temperature quality can be analytically predicted. Such an exercise might be useful for synthesizing a production problem, but it is of little use for designing new combustion systems because of the lack of suffi- cient information in regard to the boundary conditions. However, the combustor analytical models can be usefully employed for relative performance evaluation of different conceptual designs to identify the most promising concept for undertaking hardware testing.

With a limited understanding of the turbulent reactive flows encountered in turbopropulsion combustors, analytical models became a valuable tool. One must not expect good quantitative correlation with all of the measured combustor performance.

3.   Liner Wall Temperature Predictions

A 2-D liner wall cooling model was used to predict liner wall temperature levels along different X-Y planes. The initial boundary conditions for each of the cooling slot panels were the same as predicted by the 3-D model. The entire combustor channel was analyzed to account for radiation emitted by both the I.D. and O.D. liner walls. Two hundred cross-stream nodes were used, of which 50 were within the cooling slot height. The marching step size was maintained at 0.1S, where S is the slot height.

The slot exit conditions were assumed to be of uniform temperature equal to that of the annulus air. Similarly, uniform values of turbulence kinetic energy of $0.2 \, U_{AVG}^2$ and length scale of 0.02 S were assumed. The velocity profile was assumed to be given by the following expression

$$U = U_{AVG} \left\{ 1 - [2 \, ABS \, (\tfrac{\Delta Y}{S} - 0.5)]^a \right\}/b$$

where

b   =   0.83

a   = $\dfrac{1}{1-b} -1$

ΔY =   Distance from liner wall

U_{AVG} =   Mass-average axial velocity

Figure 118 presents predicted wall temperature levels downstream from the lip of the cooling slot of all three of the outer wall cooling bands. The first cooling band is for the primary panel, the second for the intermediate and the third for the dilution panel. Similar results for the inner liner wall are presented in Figure 119. The predicted results may be compared with the hot-day paint test results shown previously in Figure 26 of Section IV.B.

The following observations may be made in regard to the outer wall temperature predictions. Due to radiation heat loading, the wall temperature immediately downstream of the first cooling slot lip is approximately 769 K compared to the cooling film exit temperature of 648 K. The predictions for this panel are shown for the X-Y planes along θ = 6, 12, and 24 degrees, whereas the primary orifices are along θ = 18 and 30 degrees. Initially there is a difference of approximately 266 K between
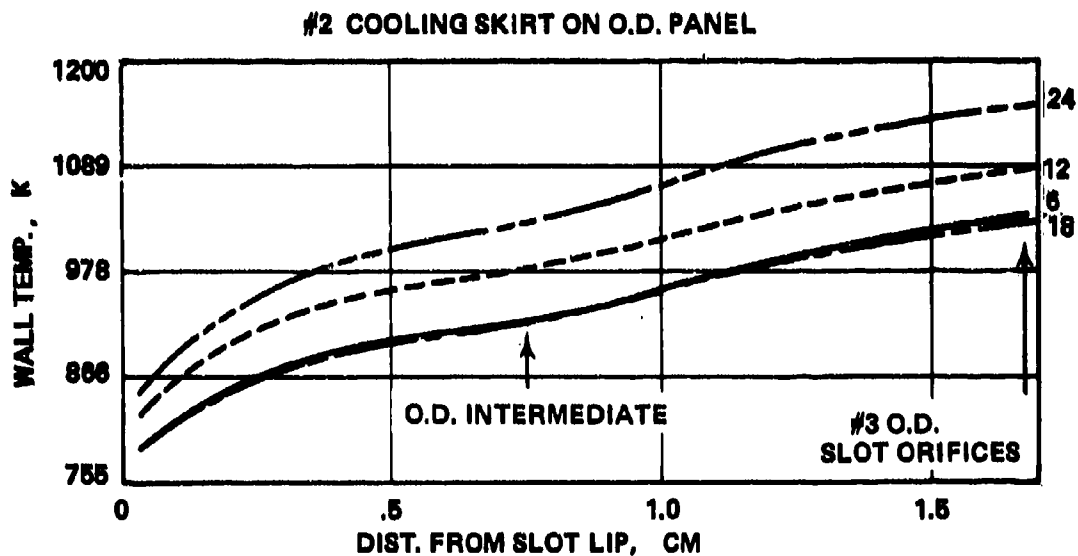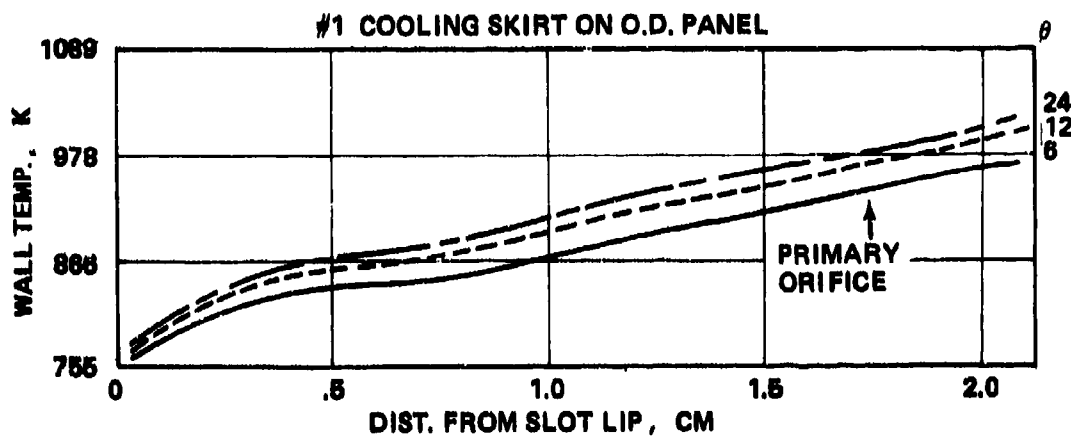
Figure 118.   Predicted Outer Liner Wall Temperature Levels
of Concept I at the Sea-Level, Hot-Day Maximum
Power Point (Sheet 1 of 2).

Figure 118.   Predicted Outer Liner Wall Temperature Levels
of Concept I at the Sea-Level, Hot-Day Maximum
Power Point (Sheet 2 of 2).

199
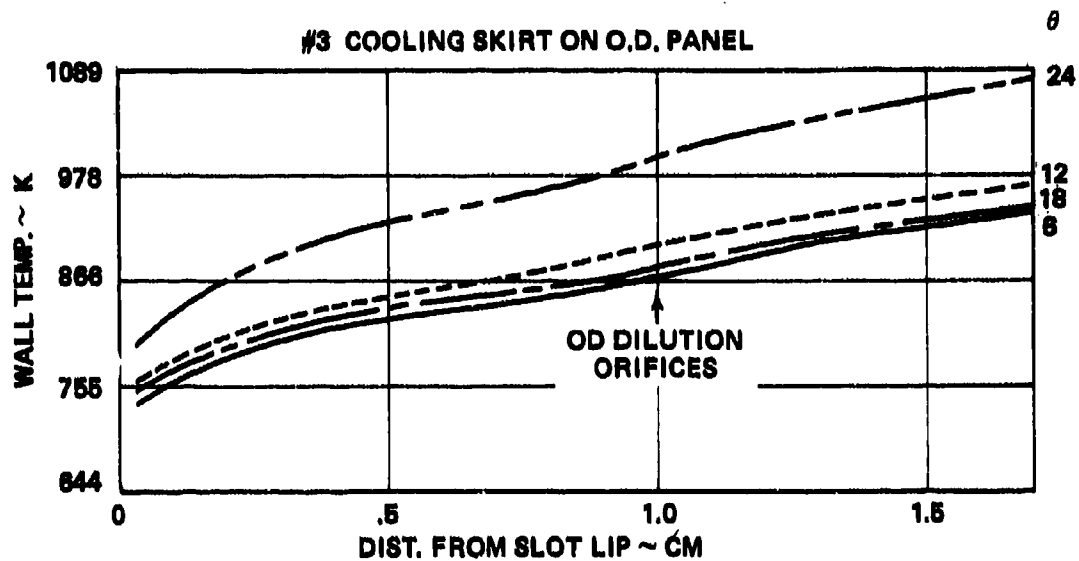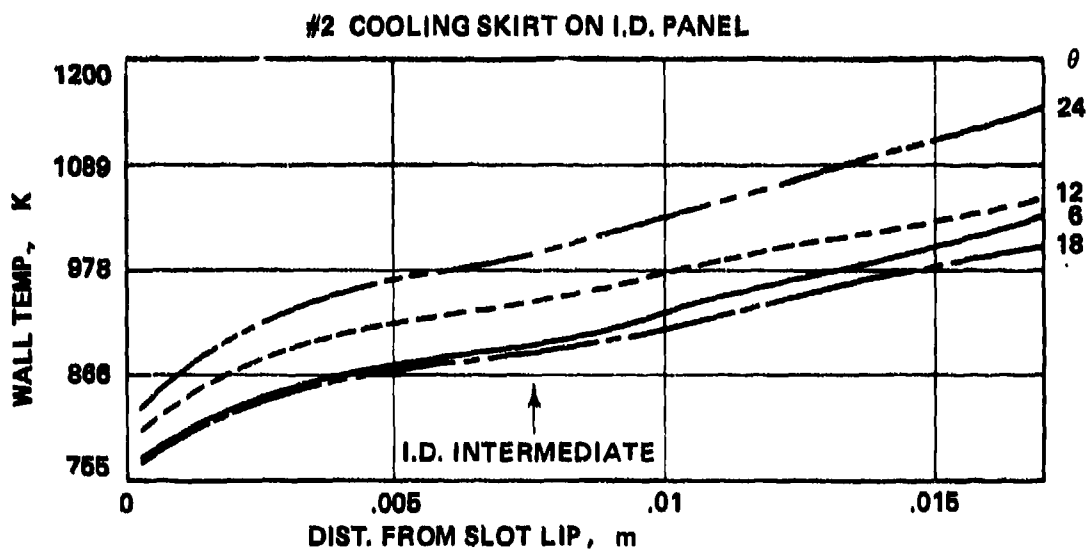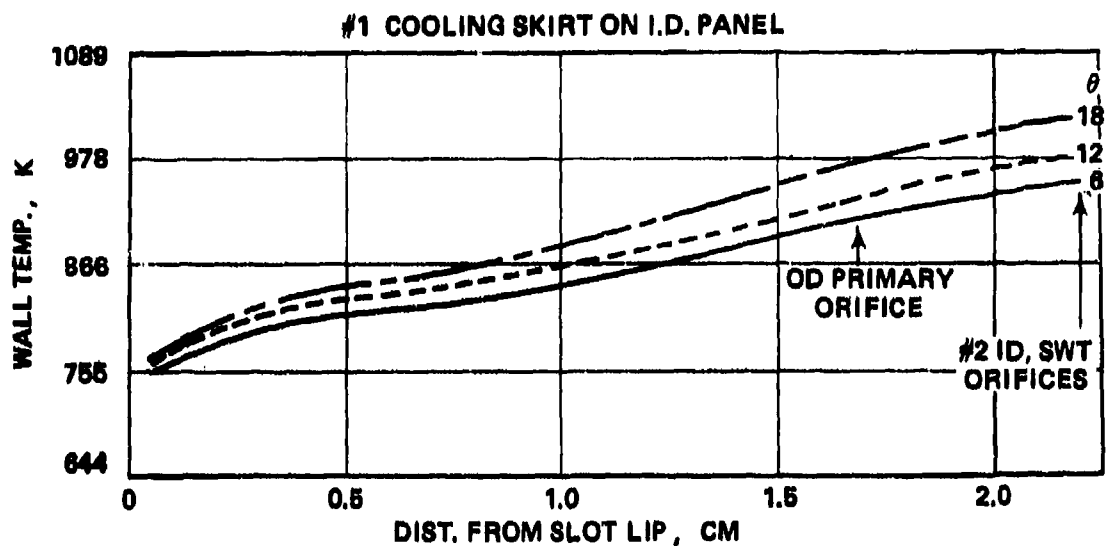
Figure 119.   Predicted Inner Liner Wall Temperature Levels of
Concept I at the Sea-Level, Hot-Day Maximum
Power Point (Sheet 1 of 2).

Figure 119. Predicted Inner Liner Wall Temperature Levels of Concept I at the Sea-Level, Hot-Day Maximum Power Point (Sheet 2 of 2).

201
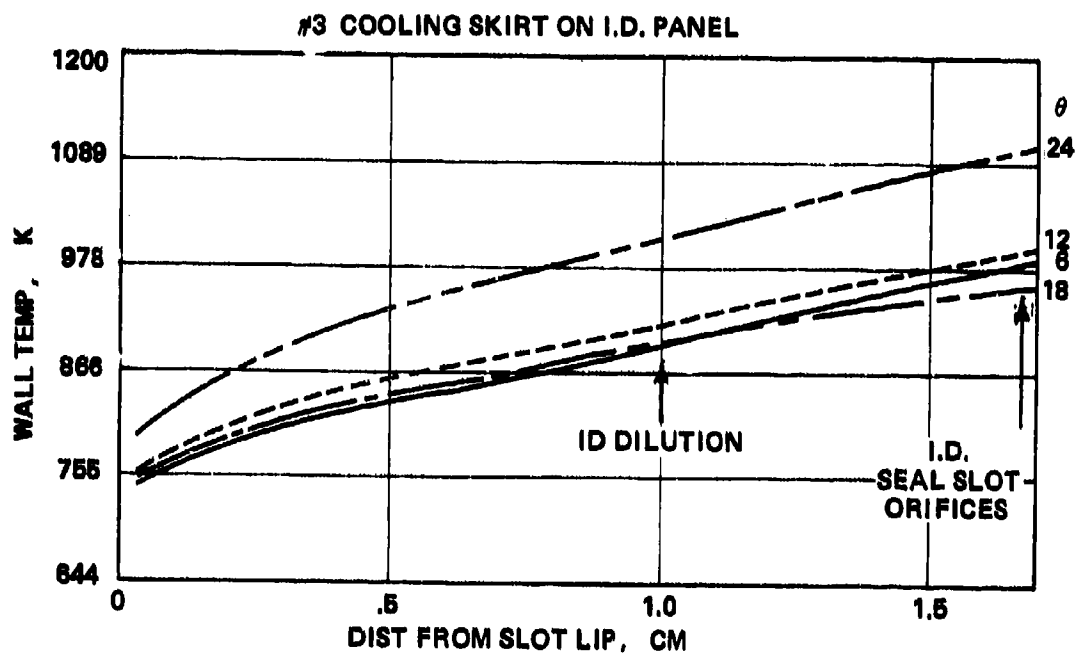
wall temperatures along the three planes calculated. This difference increases to approximately 300 K at 1.15 cm downstream from the lip, beyond which the difference remains relatively constant. The wall temperature levels at X = 1.66 cm, where the primary orifices are located, range from 933 to 972 K, which agree reasonably well with the measured data of 811 to 964 K.

The model predictions for the liner beyond the primary orifices are not accurate because they do not take into account the presence of the radial jets. This error becomes significantly more important for the second cooling slot analysis because the air from the secondary orifices is used to help cool the liner wall, and the 2-D model is not taking that into account. Consequently, the wall temperature keeps increasing downstream from the secondary orifices. For the second panel at the plane of the O.D. intermediate orifices, predicted wall temperature levels of 922·to 1028 K are in fair agreement with measured hot spots of 964 K considering that the next color change of the temperature sensitive paint occurs at 1047 K. Similarly, the predicted wall temperatures at the plane of O.D. dilution orifices are in the range of 872 to 997 K.

It should be noted that the predicted liner hot spots are along θ = 24 degree plane, inline with the hot streak and exist between the primary jets. Figure 119 presents the results for the inner combustor wall. The results are in fairly good agreement with the measurements.

B.   Concept II Predictions.

The Concept II basic configuration, as shown previously in Figure 48, did not meet all program performance goals as explained in Section IV.C. The problem areas were the structural durability of the uncooled regions between the primary slots and the dome jets. Because of the combustor inlet swirl, it

was assumed during the design and analysis phase of this program that the primary slot air would spread out enough to provide satisfactory protection for the uncooled liner wall region between the slots. The 120 orifices were drilled tangent to the dome with the assumption that the jets would sweep the inner dome region and thereby strengthen the reverse-flow region created by the 20 primary slots. Because of a low liner pressure drop, it was not considered desirable to weld a splash plate underneath the dome orifices to help direct the jets along the desired direction. The test sequence indicated that none of the assumptions were correct, thus leading to unacceptable combustor performance. The combustor was therefore modified in accordance with the sequence explained in Section IV.C.

Figure 120 presents a schematic of the modified Concept II combustor configuration. As with Concept I, the annulus loss model was used to compute the pressure drop and airflow distribution around the liner including jet velocity and efflux angles. The predicted isothermal pressure drop was 1.6 percent compared to the measured pressure drop of 1.7 percent. A detailed analysis of the modified Concept II combustor similar to Concept I described previously in Section V.A. was conducted and is described in Sections V.B.1. through V.B.3.

1. 3-D Combustor Performance Model Predictions

A combustor length of 13.69 cm was divided into 30 nonuniformly distributed axial nodes. Similarly, the combustor channel height of 4.4 cm was divided into 19 y-nodes. The 36-degree nozzle sector was uniformly divided into 13 θ-nodes. The nozzle spray originated at x = 3.09 cm from the combustor dome and y = 2.69 cm from the liner inner radius wall, and its circumferential location was at θ = 9.0, the same as Concept I. Therefore, the predicted profiles of Concept II can be easily compared with those of Concept I. There are three I.D. primary orifices per

ROW NUMBERS
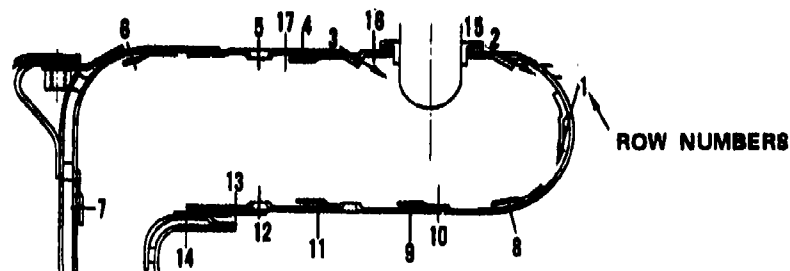
ROW NO.	TYPE OF ORIFICE	NUMBER OF ORIFICES	DIAMETER MM	TOTAL AREA MM2	AIRFLOW % TOTAL
OUTER DIAMETER					
1	DOME	120	2.2	465.5	11.40
2	PRIMARY SLOT	10	64.3 x 0.76	490.0	12.46
3	PRIMARY SLOT	10	64.3 x 0.76	490.0	11.62
4	COOLING	90	1.6	189.7	4.01
5	DILUTION	30	5.2	635.7	13.80
6	COOLING	90	1.2	98.6	1.89
7	COOLING	90	1.2	96.5	1.85
15	LOCAL COOLING	45	1.7	105.4	2.44
16	LOCAL COOLING	280	0.5	56.8	0.95
17	ADDITIONAL COOLING	90	1.4	133.0	2.84
INNER DIAMETER					
8	COOLING	90	1.9	246.4	3.61
9	COOLING	90	1.5	166.9	2.87
10	PRIMARY	30	4.7	523.1	9.70
11	COOLING	60	1.6	118.8	2.04
12	DILUTION	30	3.8	344.3	7.34
13	COOLING	60	1.1	54.9	1.20
14	COOLING	60	1.1	60.2	1.31

Figure 120. A Schematic of the Concept II -4 Configuration.

nozzle located at x = 3.63 cm and θ = 6, 18 and 30-degrees, respectively.

The first primary slot, indicated as Row No. 2 in Figure 120, is located at x = 1.72 cm, whereas the second primary slot is at x = 6.31 cm. Both of these slots plus cooling air from Rows 15 and 16 of Figure 120 are assumed to span the whole sector of 36 degrees with air injected uniformly with a 30 degree angle from the O.D. liner wall. Six opposing dilution jets are located at x = 8.86 cm and θ = 6, 18 and 30-degrees, respectively. The O.D. cooling slot lip is located at x = 5.47 cm. On the other hand, the I.D. liner cooling bands are at x = 2.48, 5.09, 7.84 and 11.9 cm, respectively.

Figure 121 presents predicted fuel/air ratio profiles in the primary zone of Concept II upstream of the spray origin for the conditions corresponding to the sea-level static, standard day maximum power condition. At x = 1.71 cm where the first primary slot is located, a 0.3-equivalence ratio region is predicted to exist adjacent to the combustor outer wall, whereas near the inner radius wall the equivalence ratio is ~1.3. The low fuel/air ratio value near the O.D. wall is due to the presence of the primary slots. Due to the air from the dome, the fuel/air ratio near the I.D. wall is reduced to approximately 0.04 at x = 2.1 cm, i.e., approximately 1.0 cm upstream from the spray origin. At this station there exists a stoichiometric region stretched diagonally and close to the liner outer wall. The combustor liner outer wall region of $18° < \theta \le 36°$ is expected to be hotter than the other half sector that lies closer to the fuel nozzle. It was this region that initially contained a 6-degree-wide uncooled portion of the combustor. Consequently, there were hot spots in this area as shown previously in Figure 58 of the baseline configuration. It should also be noted that even with the modified combustor, the results shown in Figure 63 substantiate the prediction in regard to the region further from the nozzle in

205
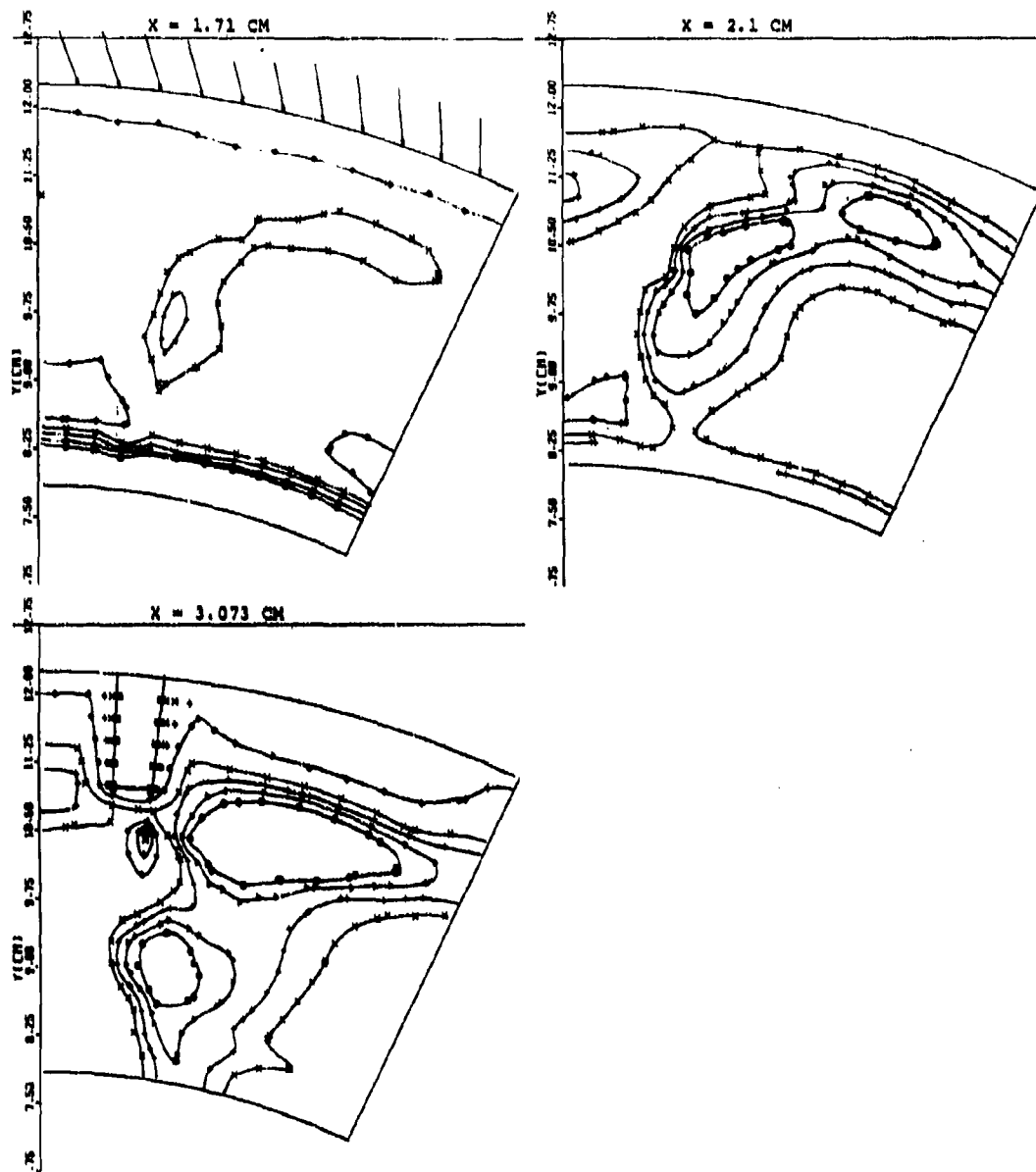
Figure 121. Predicted Fuel/Air Ratio Profiles in the Primary
           Zone of Concept II Upstream of the Spray Origin.

the direction of swirl getting hotter than the region close to the nozzle. At x = 3.07 cm, where the spray originates, two 1.3-equivalence-ratio pockets are predicted to exist. The shape, size, and orientation of these pockets is quite different from that of Concept I, previously shown in Figure 103. In both combustors there is a small region adjacent to the liner I.D. wall where the fuel/air ratio is higher than 0.04.

Figure 122 shows the predicted fuel/air ratio distribution for the primary and intermediate zones downstream from the spray origin. The size of the fuel-rich zone is largest at x = 3.6 cm where the primary orifices are located. However, the size of the pocket is quite small compared to that of Concept I previously shown in Figure 104 at x = 2.67 cm. It should be noted that these planes of Concept I and Concept II are located 0.76 cm and 0.56 cm, respectively, downstream from the spray origin. The reader should also observe the difference between Concept I and Concept II in regard to the primary jet penetration, which is deeper in the case of Concept I. The profiles of Concept II at x = 6.31 cm, the second primary slot plane, indicate that the outer wall should have less wall temperature problems than the inner wall. The measured small hot spots of 866 K on the outer wall were around the previously uncooled area that was later protected by a full-coverage cooling scheme. These small radial orifices could not be simulated exactly by the 3-D model. On the other hand the I.D. liner wall exhibited hot spots in the region between the primary and secondary orifices and approximately in the plane of the fuel nozzle. The location of these hot spots is approximately in line with the fuel impingement predicted to occur at x = 3.07 cm, shown previously in Figure 121. It can therefore be hypothesized that the ten discrete hot spots observed on the I.D. liner wall might have been caused by fuel impingement.

207
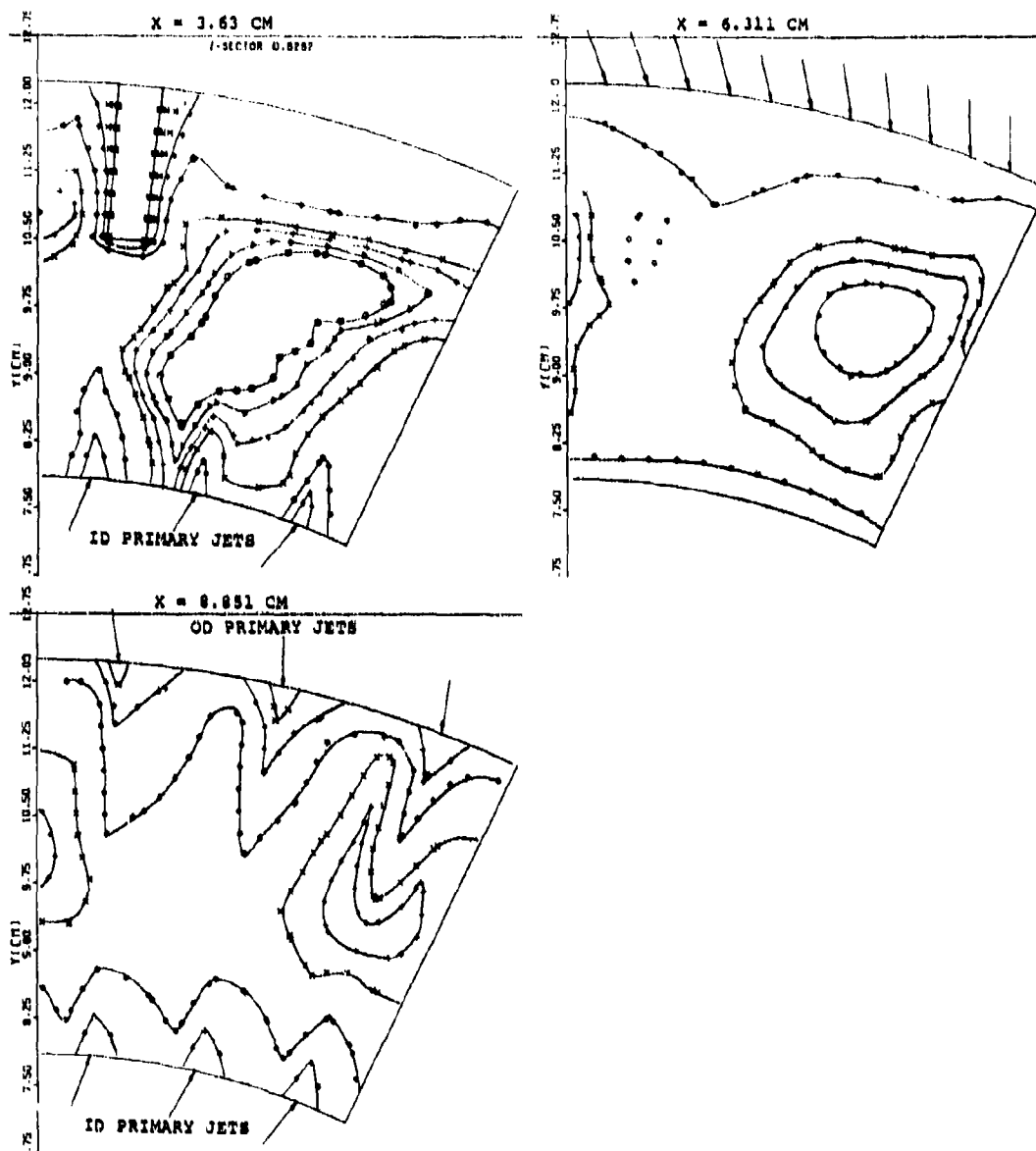
Figure 122. Predicted Fuel/Air Ratio Profiles in the Primary
and Intermediate Zone of Concept II Downstream
from the Spray Origin.

208

The predicted fuel/air ratio profiles of the $r-\theta$ plane of the dilution orifices at $x = 7.6$ cm for Concept I and at $x = 8.85$ cm for Concept II show the following. The penetration of the dilution jets, defined by the 1.0-equivalence-ratio line, appear to be approximately equal for both concepts even though they had different amounts of dilution air. A total of 13.65-percent combustor air was used for dilution in Concept I compared to 21.14-percent for Concept II. The size of the maximum equivalence ratio pocket of 0.8 was comparable for both combustors.

Figure 123 shows predicted fuel/air ratio profiles for the three x-y planes lying in line with the spray origin, and the second and third primary jets, respectively. The results are presented for the same planes as previously shown for Concept I in Figure 72 to facilitate a direct comparison between internal profiles of both combustors. Five of the 20 rays that have been used to simulate the spray are shown in the figures by broken lines. If the spray had been simulated by a single centerline spray with five or more droplet sizes, it would not have been possible to predict in the case of Concept II a fuel-rich region slightly upstream of the dome orifices which are located at $y = 10.05$ cm. Without the splash plate, as in the case of the Concept II baseline configuration, the dome jets would help in holding off a flame in this location with an attendant hot spot as observed in Figure 58. However, with the splash plate the jets would be directed along the dome surface without causing any hot spots, as was in the case of the modified Concept II thermal paint test shown in Figure 94.

The size and orientation of the 1.3-equivalence-ratio pockets is quite different for the three planes shown in Figure 123. The two pockets near the dome and upstream of the first I.D. cooling slot do not change much between these planes. However, the third fuel-rich pocket extends mostly along the radial direction for the plane $\theta = 9$ and 18 degrees. Its size

209
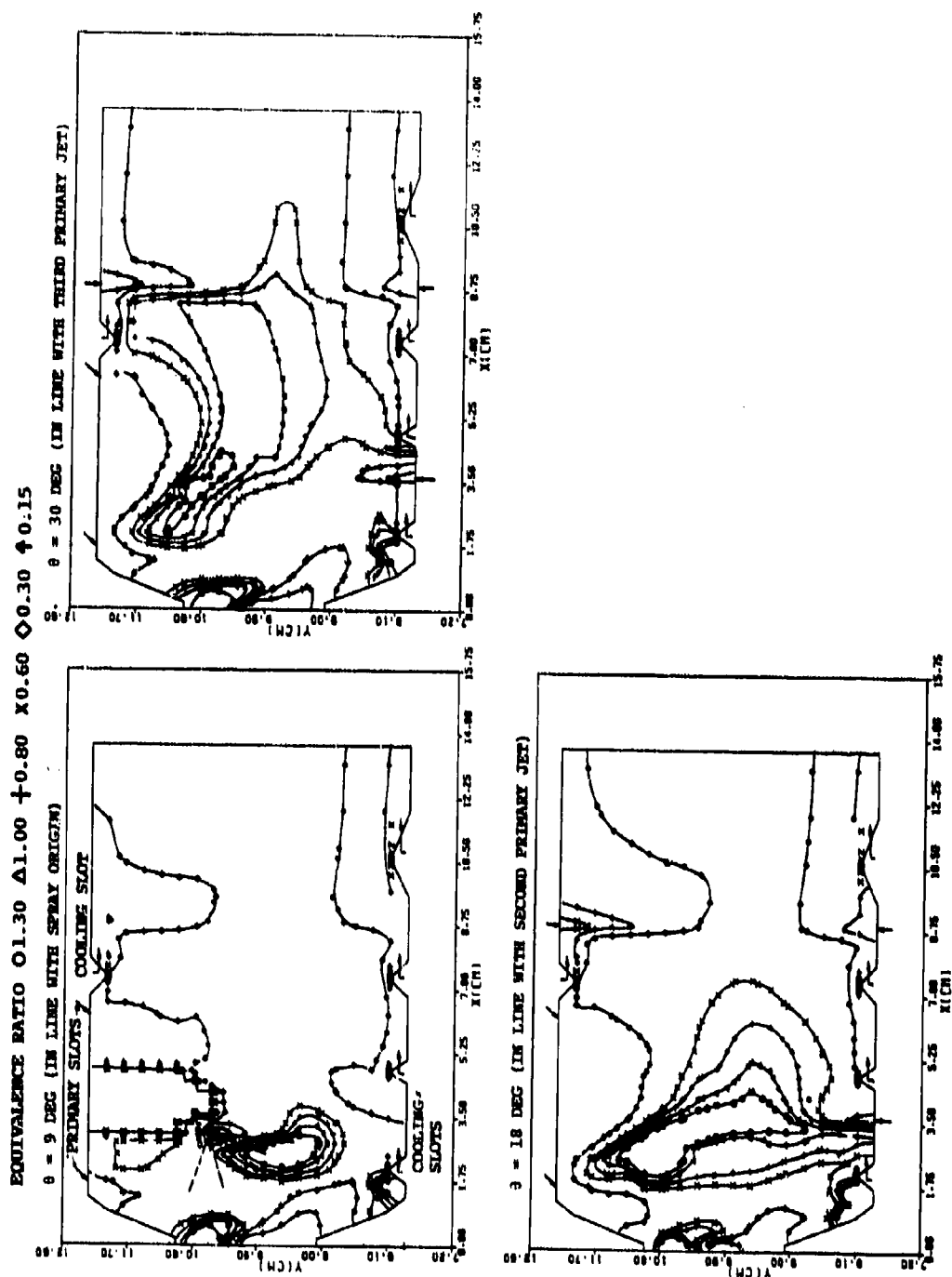
Figure 123. Predicted Fuel/Air Ratio Profiles Along Different X-y Planes of Concept II.

210

reaches a maximum at $\theta = 18$ degrees. It might have been better for the plane $\theta = 18$ degrees to move the I.D. primary jet slightly upstream to align with the stoichiometric isoline. However, the axial location of the third primary jet appears to be appropriate. The size and orientation of the fuel-rich pocket for the $\theta = 30$-degree plane is smaller and is mostly along the axial direction. From predicted profiles of Concept II it therefore appears that there might be a I.D. liner hot spot in line with the second jet, as was observed experimentally.

Although Concept II had smaller predicted fuel-rich pockets compared to Concept I, the former gave a smoke number of 85 compared to approximately a zero smoke number of the latter. A possible explanation may be due to different predicted levels of turbulence intensity and scale that will be discussed later.

Figure 124 presents predicted profiles of unburned fuel of Concept II and may be compared with the corresponding results of Concept I shown previously in Figure 106. At $\theta = 9$ degrees, the maximum unburned fuel/air ratio of Concept II is 0.068 compared to 0.087 in Concept I. In Concept II the pocket is located further away from the dome and the O.D. liner wall. At $\theta = 18°$, both combustors have comparable fuel-rich regions at approximately the same locations. But for the $\theta = 30$-degree plane Concept II again has a significantly lower fuel-rich pocket. Another main difference between Concept I and Concept II is in regard to the combustor length required to oxidize the fuel to less than 0.0001 mass fraction, Concept II requires slightly more length.

Predicted profiles of CO mass fraction are shown in Figure 125 that may be compared with Concept I results presented previously in Figure 107. Both concepts produce comparable levels of peak CO. Notice high reactivity near the second primary jet of Concept II which would be expected to create a hot gas region immediately behind the jet leading to a possible liner

211
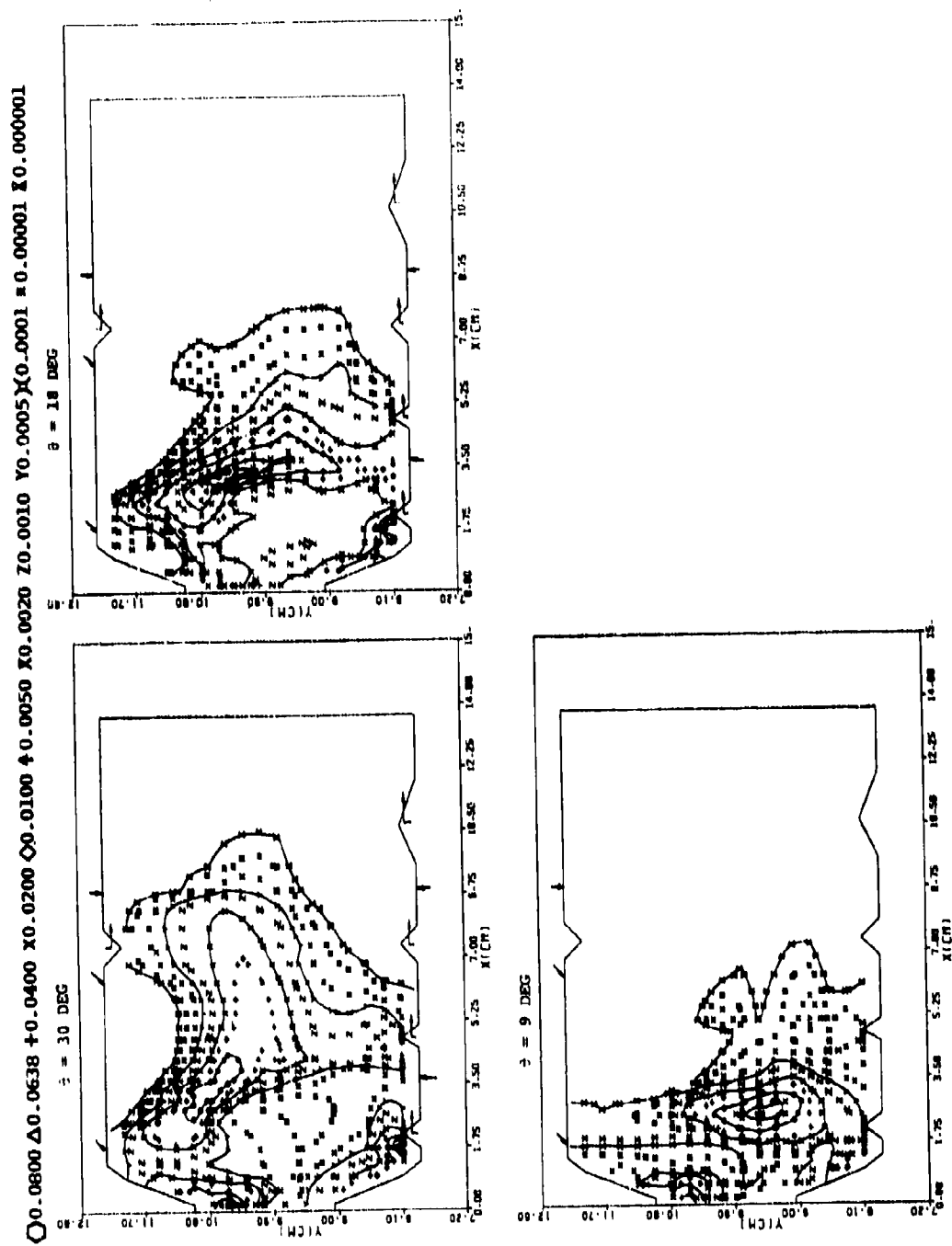
Figure 124. Predicted Profiles of Unburned Fuel Mass Fraction of Concept II.
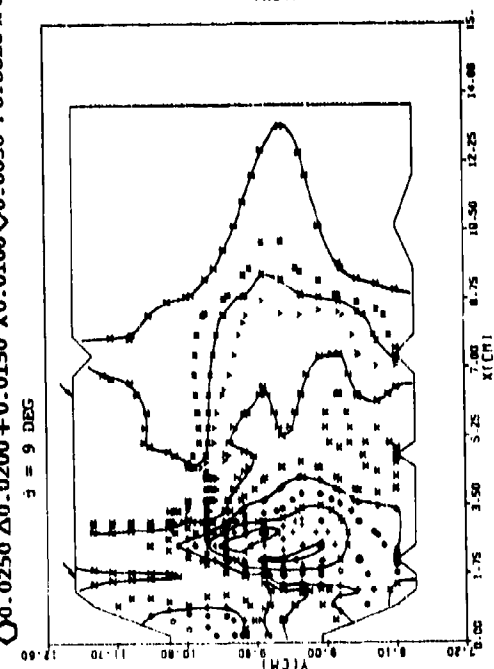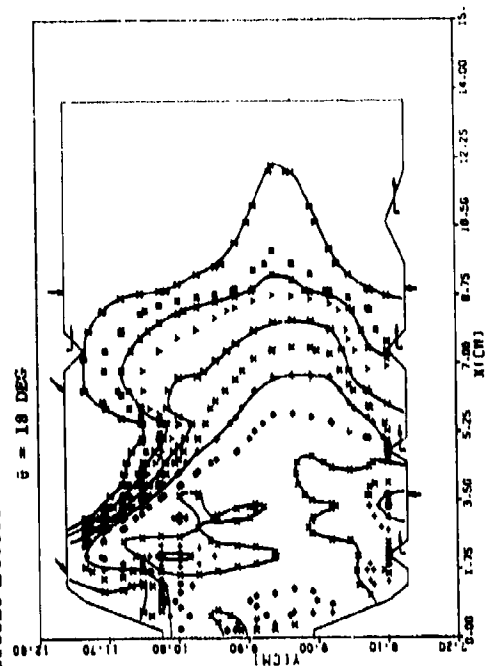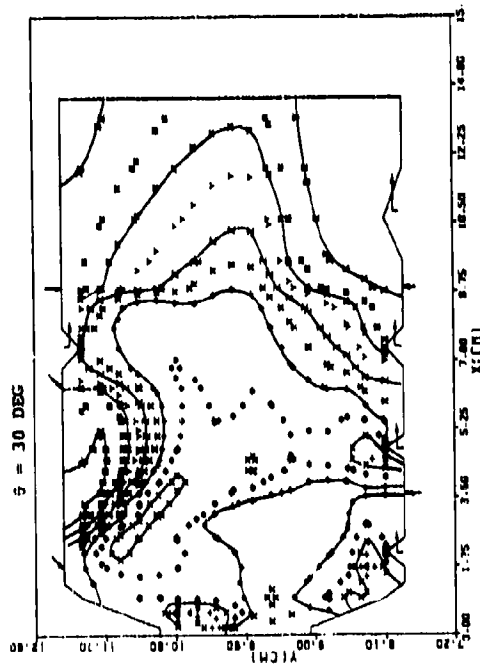
Figure 125. Predicted Profiles of CO Mass Fraction for Concept 'I.

hot spot. Because of a less-than-desirable field resolution possible in the region adjacent to the second primary jet, the model cannot predict the wake created by the jet, and consequently a hot spot is not predicted. However, with experience the combustion engineer is expected to predict liner cooling problems for this area.

Figure 126 presents predicted internal temperature profiles of Concept II and may be compared with Figure 108 of Concept I. Notice a significant difference exists in the profiles of both combustors. The maximum temperature regions of Concept II are smaller than those of Concept I. The gas temperatures adjacent to the O.D. dilution panel of Concept II in line with the nozzle are higher than other cross sections leading to a possibility of this section having hot spots, such as was shown in Figure 94. The maximum temperature regions were well contained for the x-y-planes in line with $\theta = 9$ and 18 degrees. However, for the $\theta = 30°$ plane, the 2300 K streak extends up to the dilution orifice. It is this hot streak that would cause an increase in the pattern factor of Concept II. However, when a hot streak such as this exists close to the boundary of the sector where cyclic boundary conditions are applied, the numerical error becomes quite large, causing a concern in the validity of the predictions.

As in Concept I, Concept II was also evaluated at the sea-level, hot-day, maximum power conditon. For Concept I, the results for the hot-day condition were similar to those of the standard-day. Figure 127 predicted isothermal lines for the hot-day run and may be compared with the standard-day predictions presented in Figure 126. From these figures it can be inferred that the isothermal plots are approximately similar for both runs.
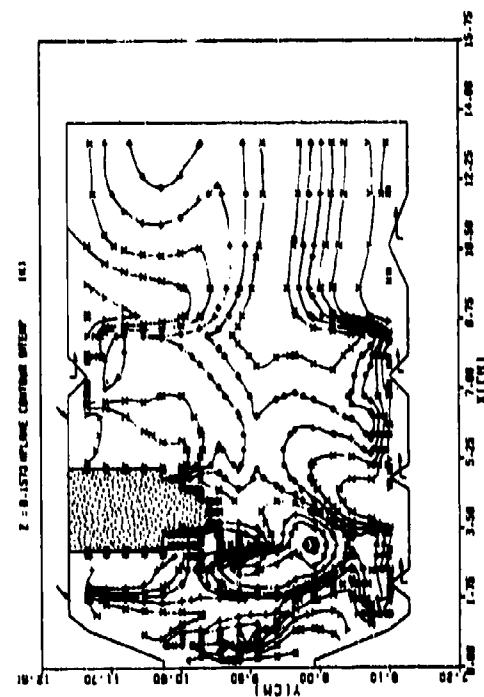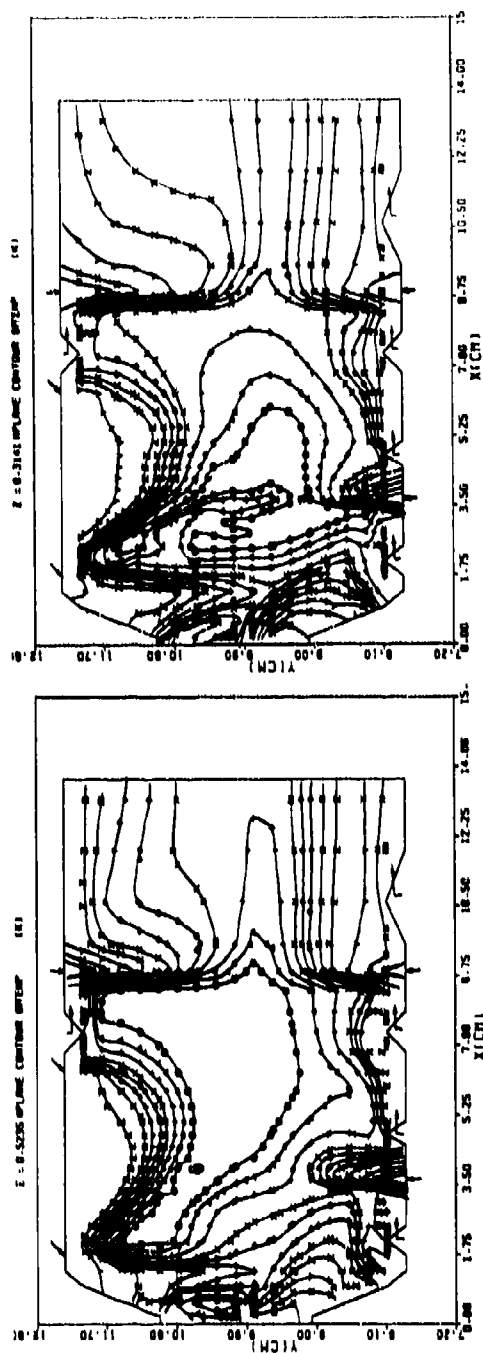
Figure 126. Predicted Isothermal Plots of Concept II.

215
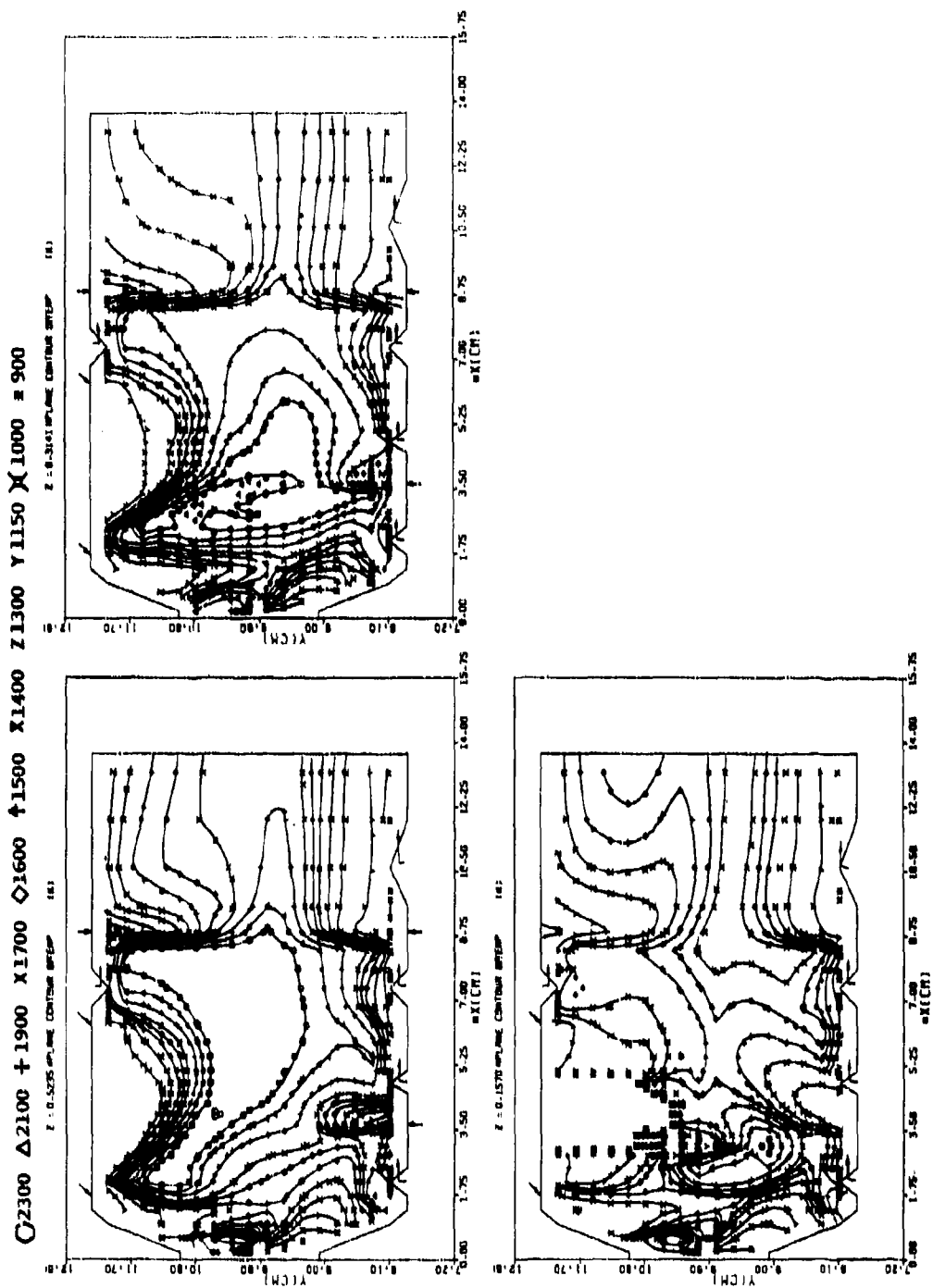
Figure 127. Predicted Isothermal Plots of Concept II at the Sea-Level, Hot-Day Maximum Power Point.

A major difference between Concept I and Concept II internal flowfield exists in regard to the reverse-flow region, turbulence intensity, and scale. Figure 128 shows the predicted reverse-flow region and k-profiles for Concept II compared to Concept I results presented previously in Figure 109. In Concept II the reverse-flow region exists near the O.D. liner wall as it was induced by the primary slots at $x = 1.72$ and 6.31 cm, respectively, and dome orifices at $y = 10.05$ cm. There is a slight variation in the size of the reverse-flow region for the x-y plane in-line with the second primary jet at $\theta = 18$ degrees and in other planes of $\theta = 3$ and 33 degrees. The upper half of the nozzle spray shown by rays 1 and 2 is within the region of supposedly high turbulence intensity because the primary slot reverse-flow is turning toward a positive axial velocity flow. Predicted maximum turbulence kinetic energy profiles approximately coincide with this region. Therefore, it appears that the spray is located close to an optimum place in that the spray should coincide with regions of maximum shear so that an enhanced reaction rate is possible. The maximum turbulence kinetic energy level in Concept II is of the order of 75 $(m/s)^2$ compared to 175 $(m/s)^2$ of Concept I.

Predicted regions of combustion controlled by chemical kinetics, and availability of fuel and oxygen are shown in Figure 129. The regions may be compared with those of Concept I presented previously in Figure 111. For Concept II the model predicted no regions controlled by kinetics. There were three separate regions where the reaction rate is controlled by oxygen. The results for the planes in line with $\theta = 0$ degree shown by dotted lines, are quite different for the $\theta = 18$-degree plane. The fuel oxidation rate in the remainder of the combustor is controlled by the fuel mass fraction.
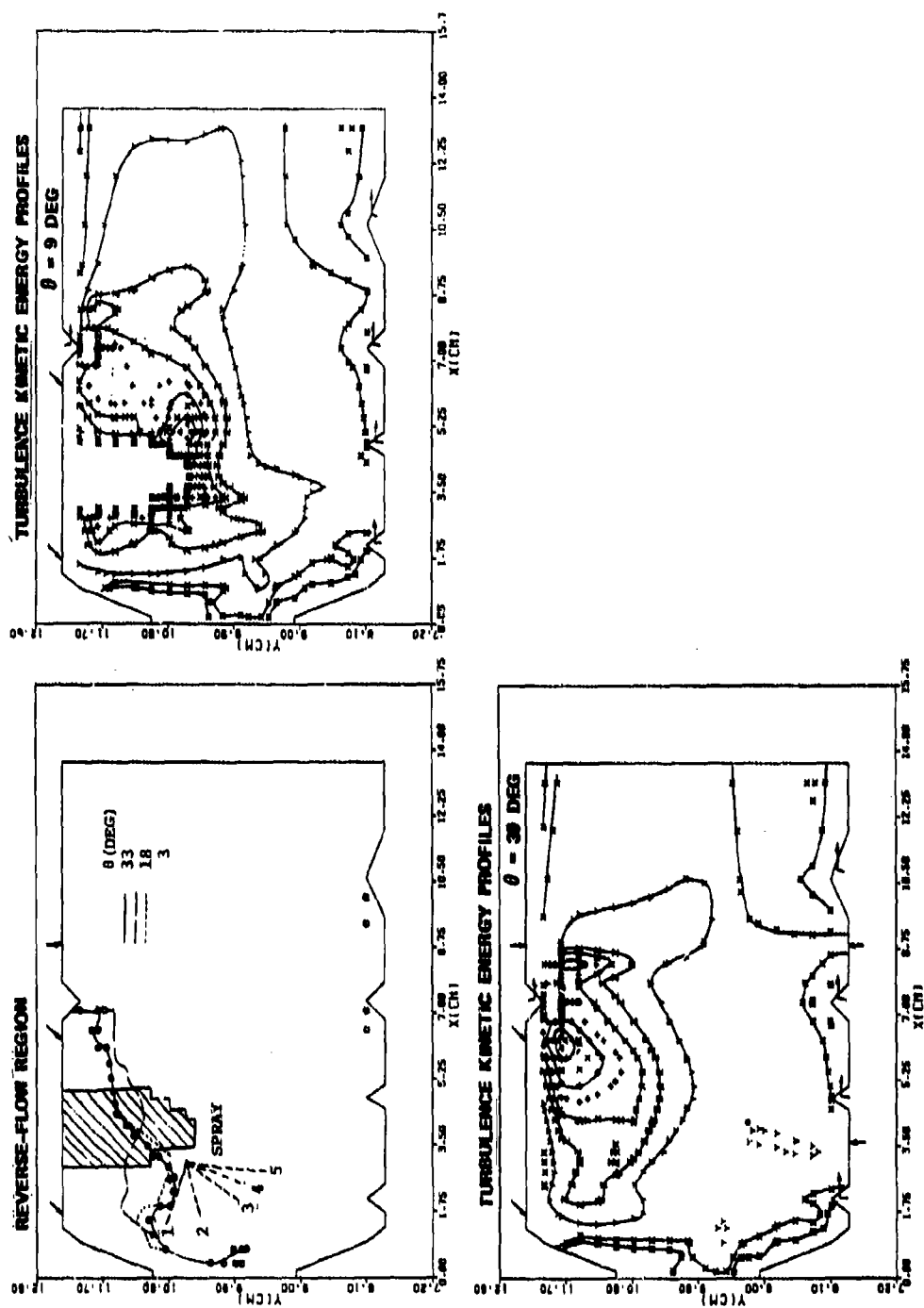
Figure 128. Predicted Reverse-Flow Regions and Turbulence Kinetic Energy Profiles of Concept II at Sea-Level, Standard-Day Maximum Power Point.

218
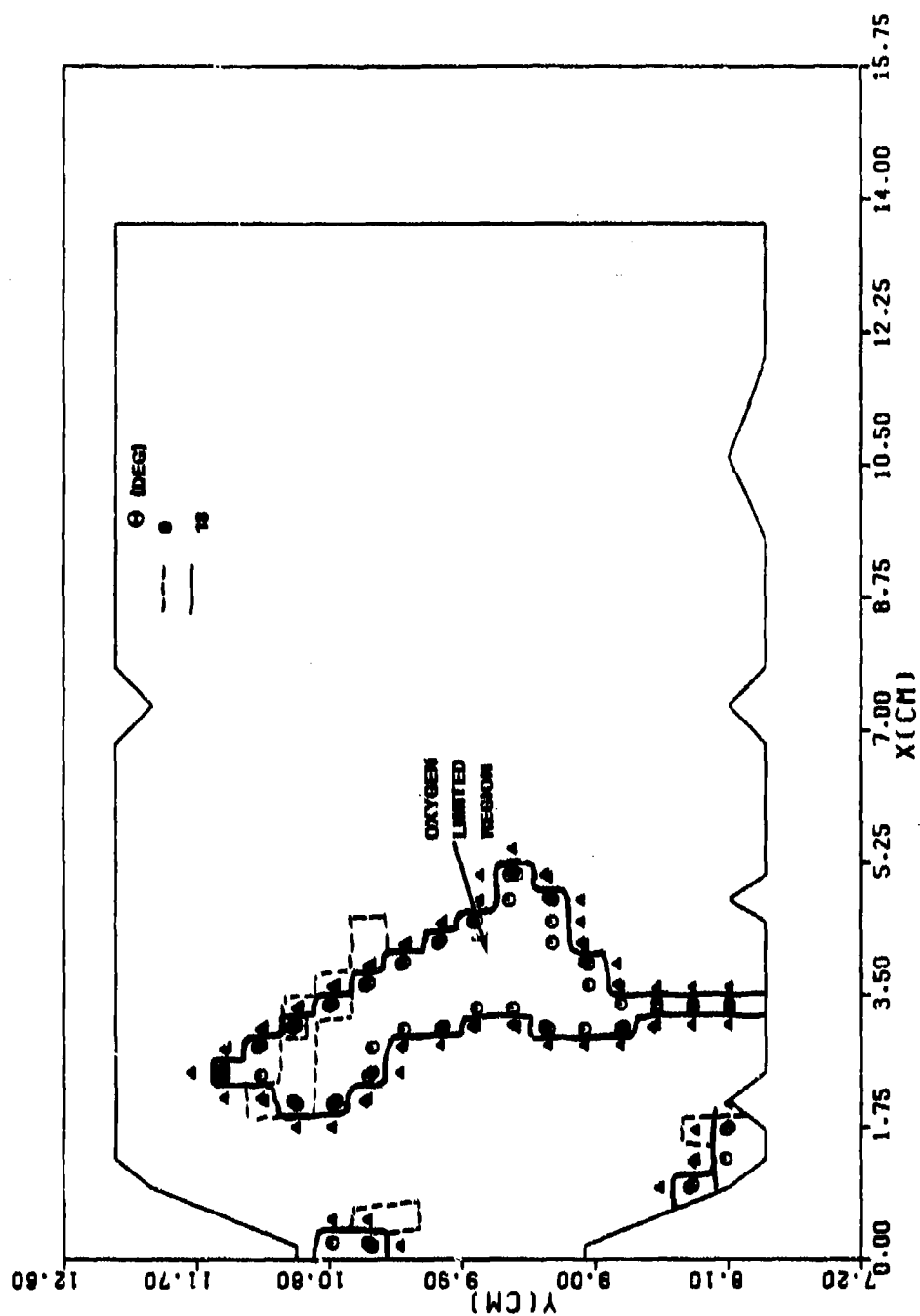
Figure 129. Predicted Regions of Concept II Controlled by Availability of Fuel and Oxygen at the Sea-Level, Standard-Day Maximum Power Point.

219

2. Transition Liner Mixing Prediction.

As in Concept I, the 2-D combustor transition mixing model was used to compute the mixing rate in the transition liner. Figure 130 shows predicted stator inlet temperature profiles for the plane corresponding to $\theta = 6$, 9 and 12 degrees, respectively. It may be recalled that the spray is at $\theta = 9$ degrees, whereas the three primary orifices are at $\theta = 6$, 18 and 30 degrees, respectively. As in the Concept I discussion, the mixing of the profiles and their radial shift while passing through the transition liner may be noted. The corresponding results for the planes along $\theta = 15$, 18 and 21 degrees are presented in Figure 131. Note the difference between the profiles in line with the first primary jet ($\theta = 6$ degrees) and the second primary jets at $\theta = 18$ degrees, and how much different the local pattern factors are. The transition inlet temperature profiles are also quite different for these planes. The predicted local pattern factors for the region between $\theta = 6$ through 24 degrees are comparable with the measurable value of 0.16.

However, for the region between $\theta = 27$ through 33 degrees, the predicted results, shown in Figure 132, are quite high as compared to the data. The mixing rate in the transition liner is low in the case of Concept II, as shown in Figure 133, for Concept II versus Concept I results shown previously in Figure 114. There are two possible explanations for this discrepancy. The turbulence kinetic energy and dissipation profiles at the transition liner inlet were such that the turbulent viscosity of Concept II was lower than Concept I by an order of magnitude. This, in turn, reduced the mixing rate in the transition liner. The effect of the transition liner inlet kinetic energy profile on the mixing rate was investigated. One such calculation is presented in Figure 132 for the plane along $\theta = 33$ degrees. Increasing inlet k profiles by a factor of ten reduced the local circumferential pattern factor from 0.5 to 0.35. A
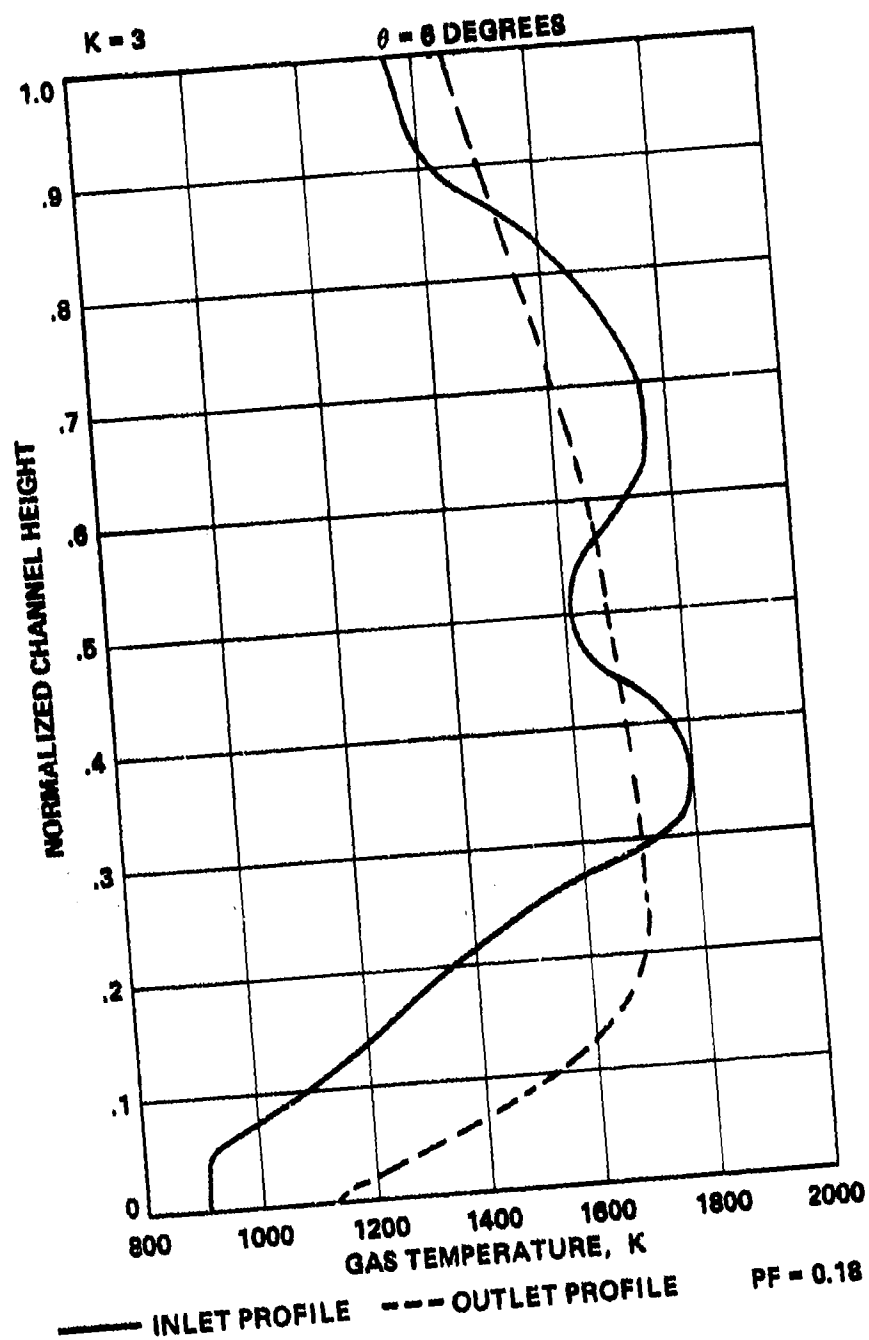
220

Figure 130. Predicted Stator Inlet (Burner Exhaust) Temperature Profiles Along θ = 6, 9 and 12 Degrees for Concept II at Sea-Level, Hot-Day Maximum Power Point (Sheet 1 of 3).
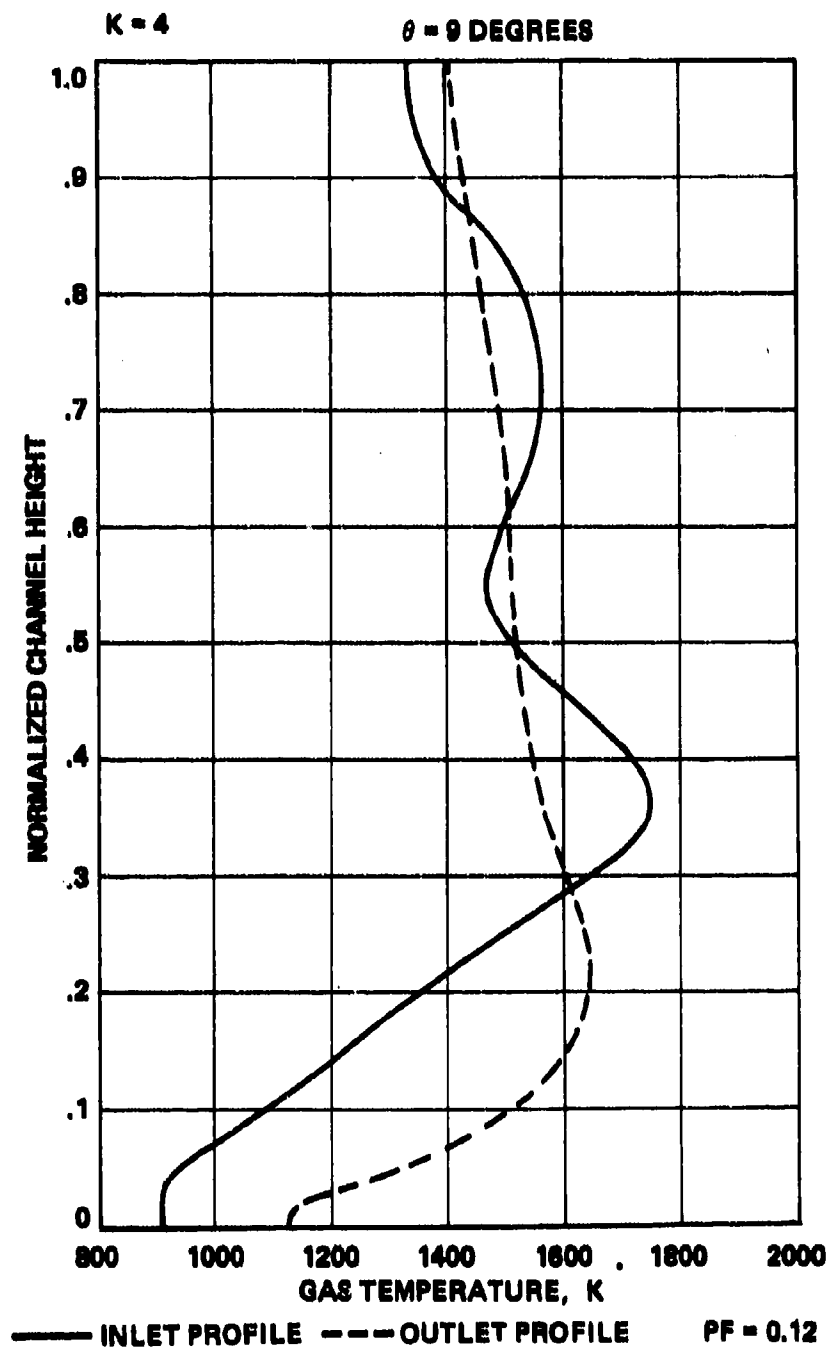
Figure 130. Predicted Stator Inlet (Burner Exhaust)
Temperature Profiles Along θ = 6, 9 and 12
Degrees for Concept II at Sea-Level, Hot-
Day Maximum Power Point (Sheet 2 of 3).
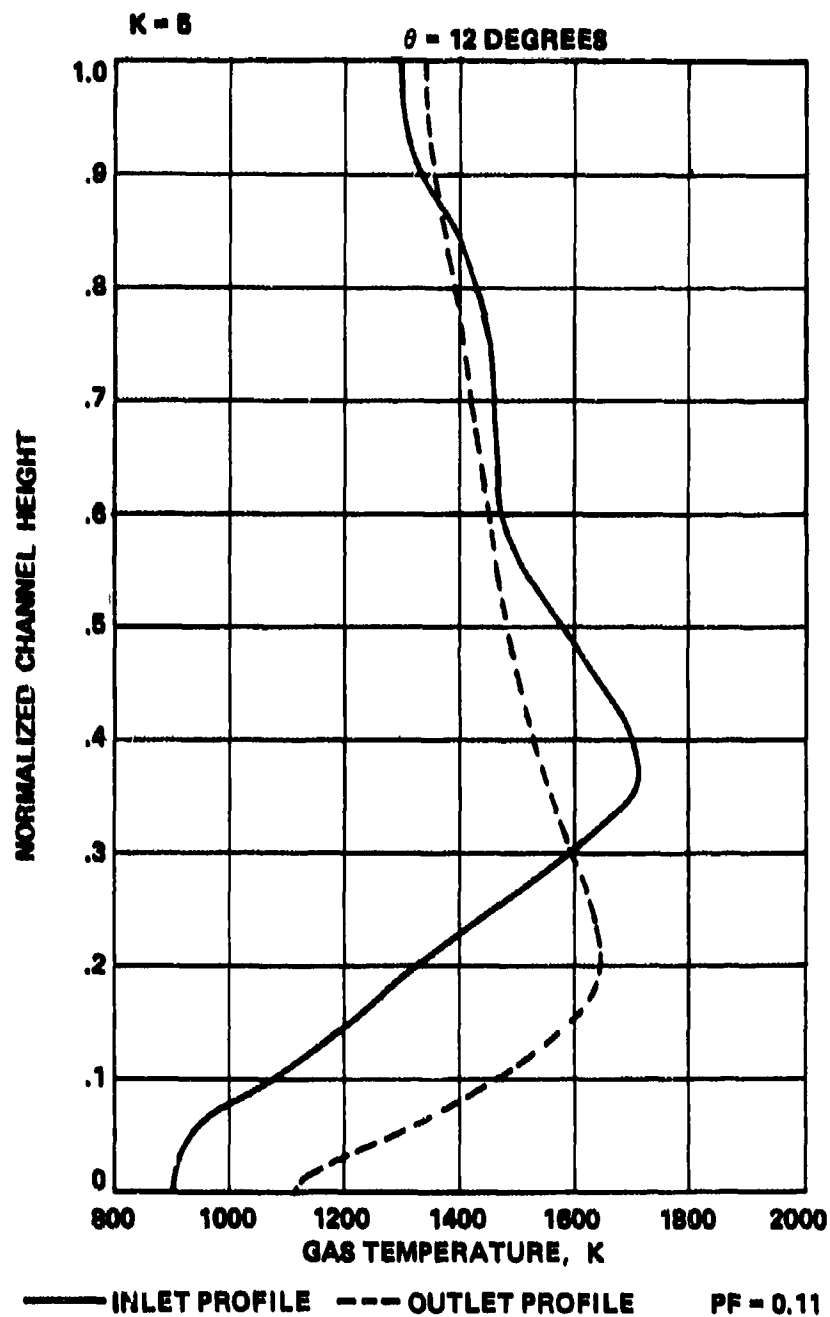
Figure 130. Predicted Stator Inlet (Burner Exhaust)
Temperature Profiles Along θ = 6, 9 and 12
Degrees for Concept II at Sea-Level, Hot-
Day Maximum Power Point (Sheet 3 of 3).

Figure 131. Predicted Stator Inlet Temperature Profiles Along θ = 15, 18 and 21 Degrees (Sheet 1 of 3).

K = 7   θ = 18 DEGREES
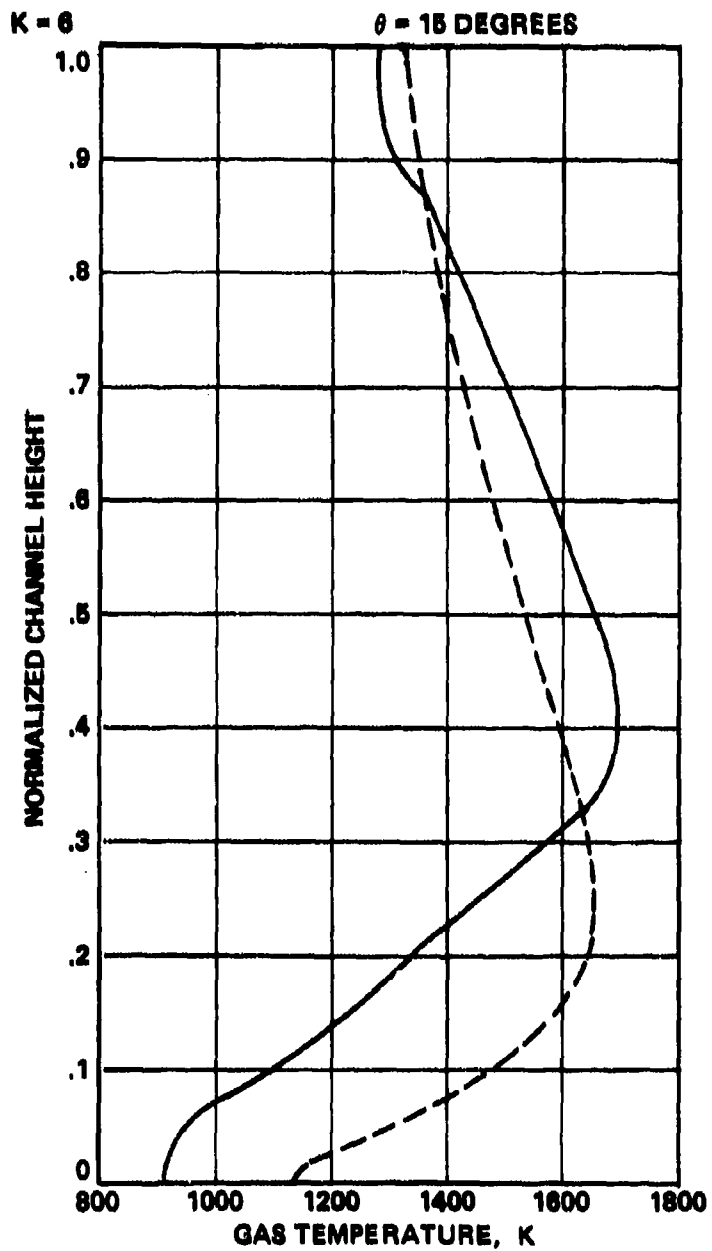
—— INLET PROFILE   — — — OUTLET PROFILE   PF = 0.01

Figure 131. Predicted Stator Inlet Temperature Profiles Along
θ = 15, 18 and 21 Degrees (Sheet 2 of 3).

225

Figure 131. Predicted Stator Inlet Temperature Profiles Along θ = 15, 18 and 21 Degress (Sheet 3 of 3).

Figure 132.   Predicted Stator Inlet Temperature Profiles Along
θ = 27, 30 and 33 Degrees (Sheet 1 of 3).

227
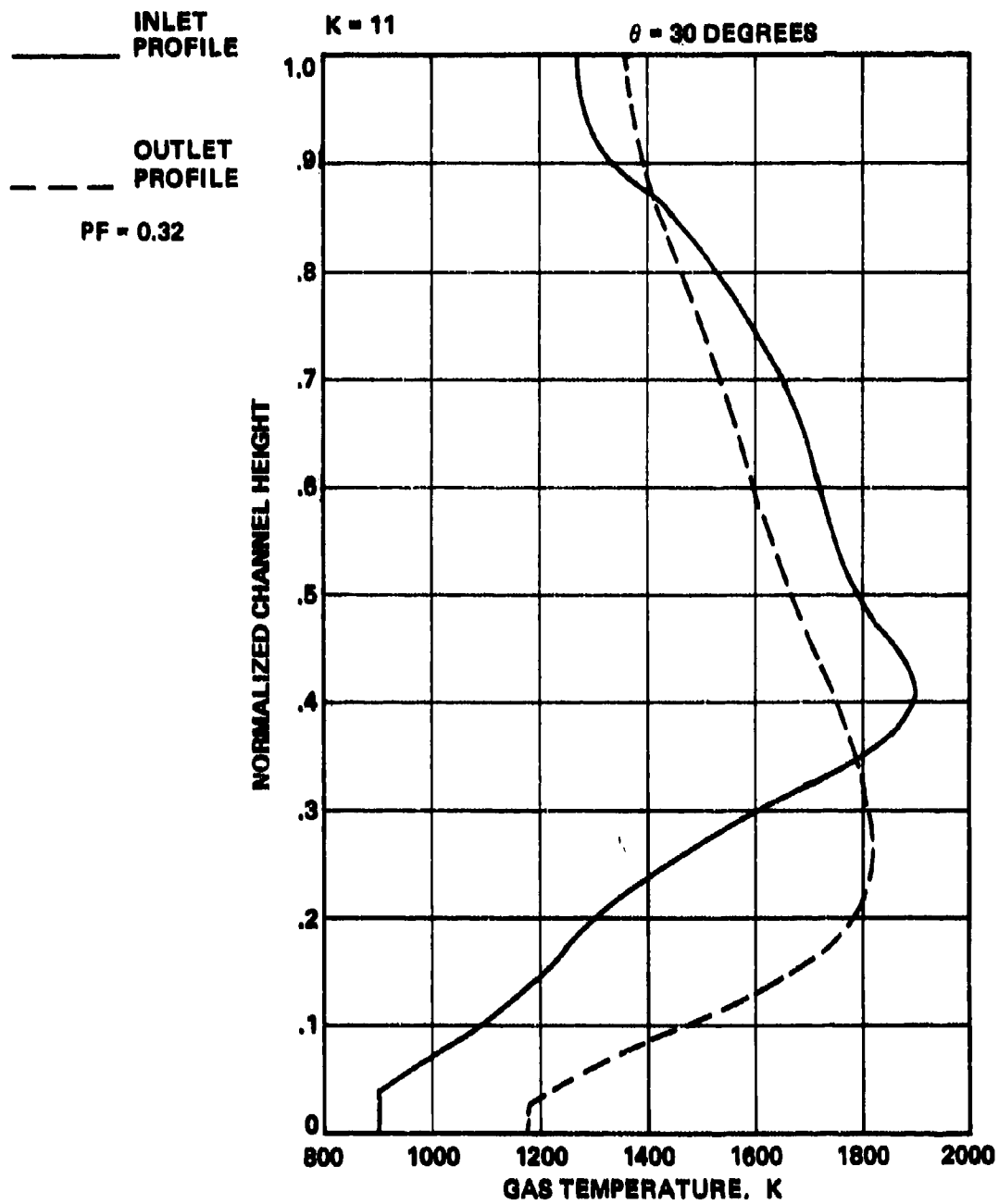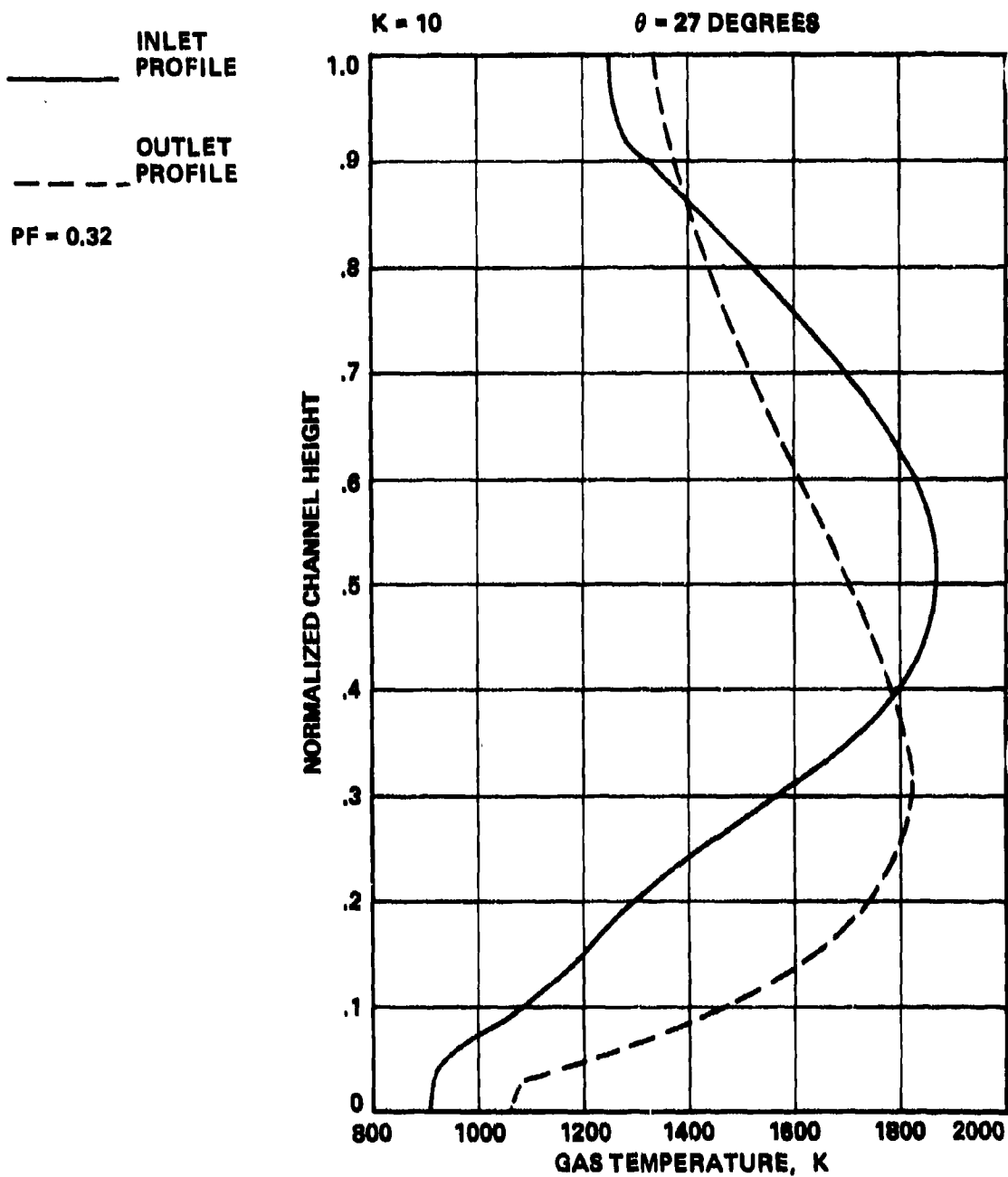
Figure 132. Predicted Stator Inlet Temperature Profiles Along
θ = 27, 30 and 33 Degrees (Sheet 2 of 3).

Figure 132. Predicted Stator Inlet Temperature Profiles Along θ = 27, 30 and 33 Degrees (Sheet 3 of 3).

229
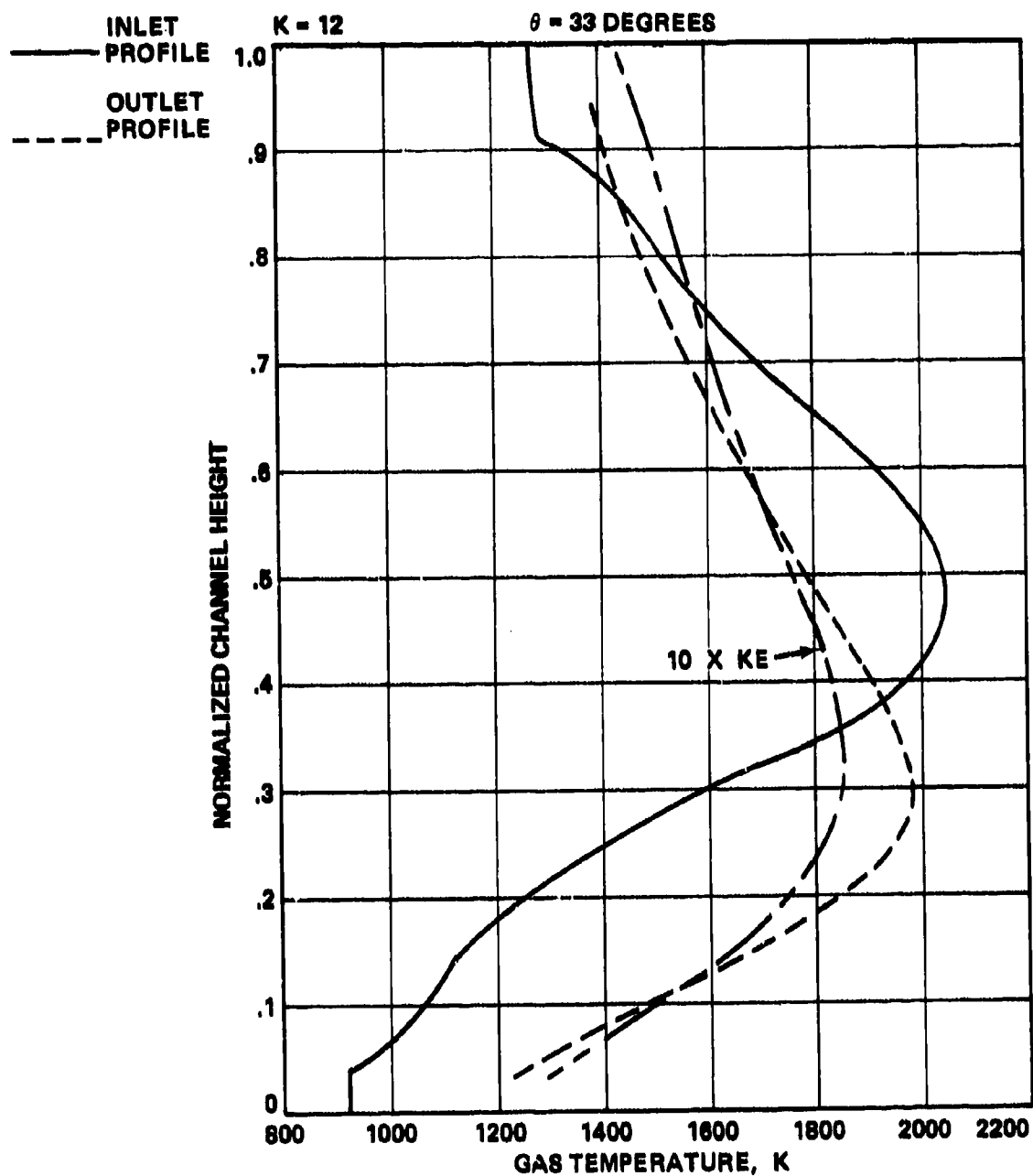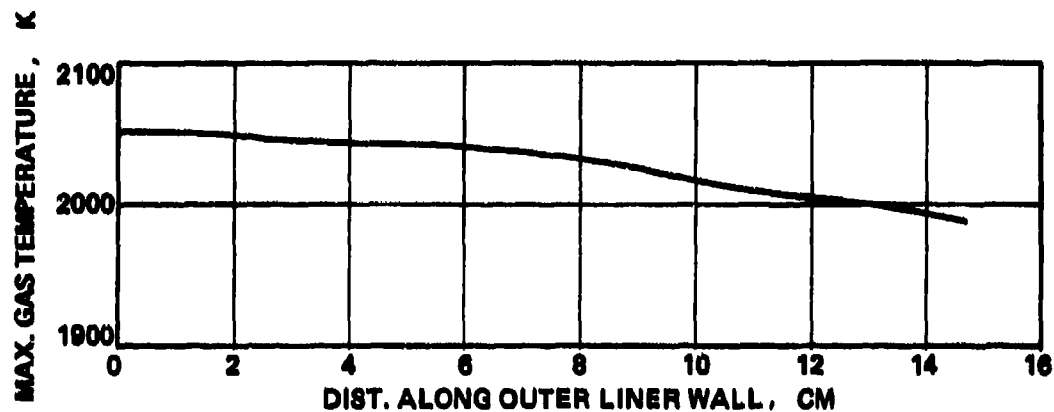
Figure 133.   Predicted Mixing Rate in the Transition Liner
              of Concept II as a Function of Distance Along
              the Outer Liner Wall for θ = 33 Degrees.

second possible explanation is that it is well known that false diffusion inaccuracies are maximum at the boundaries of the domain of the calculation. So it is quite possible that the peak value of the temperature at $\theta = 33$ degrees predicted by a more accurate numerical scheme might have been lower than predicted by the 3-D combustor performance model. Nevertheless, numerically predicted results indicated that the pattern factor of Concept II should be higher than that of Concept I as was observed experimentally.

3. **Liner Wall Temperature Predictions.**

As in Concept I, the 2-D wall cooling model was used to predict liner wall temperature levels at the sea-level, hot-day maximum power condition. All technical discussion pertaining to initial/boundary conditions presented in Section V.A.3 for Concept I liner wall temperature predictions is applicable to Concept I.

Figure 134 presents predicted liner wall temperature levels of the I.D. liner wall for the panels protected by the cooling film from slots numbered 1, 2 and 3, where the first cooling slot is closest to the dome and No. 3 is upstream of the I.D. dilution orifice. At the plane of the I.D. primary orifices predicted wall temperatures range from 866 K for $\theta = 30°$ to 972 K for $\theta = 12$ degrees compared to 866 K indicated by the thermal paint run of Figure 94. For the second panel the maximum temperature is 1078 K at $\theta = 18$ through 30 degrees. On the other hand for $\theta = 12$ degrees, the wall temperature increases from 686 K to 814 K. Therefore, the model predicts a variation of 814 K to 1078 K in wall temperature. The measured data indicate a variation of 866 K to 1116 K. For the third panel the predicted results for the x-y planes along $\theta = 12$ and 18 degrees are in good agreement with the measured data. However, the model predictions for $\theta = 30$ and 33 degrees are high due to a high predicted hot gas streak for

231
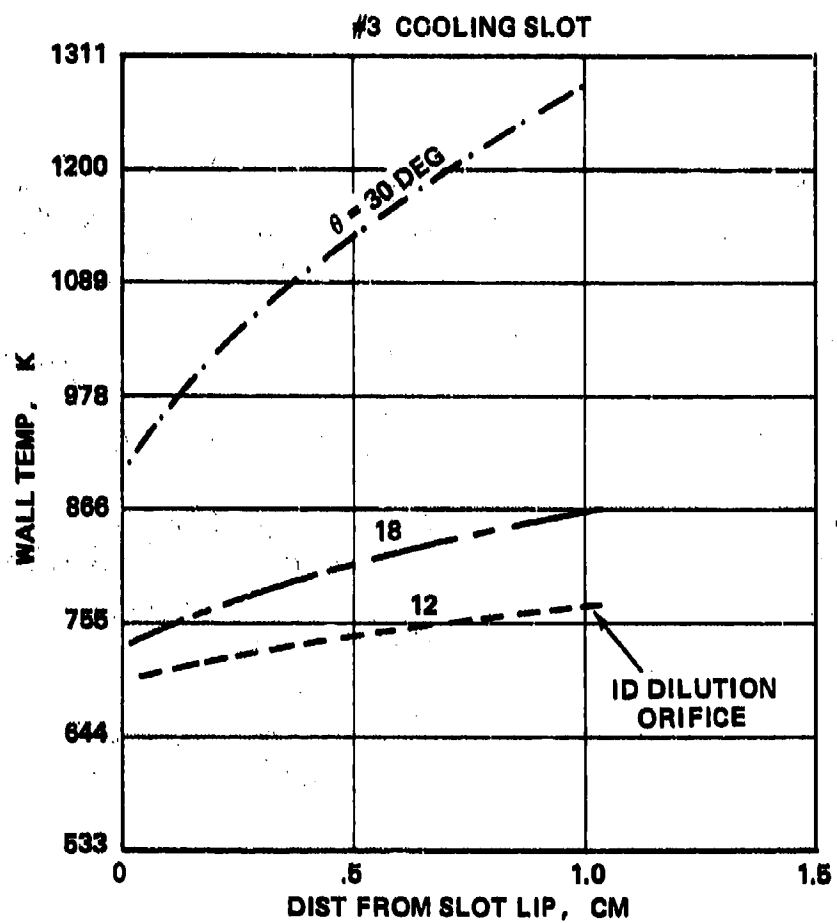
Figure 134. Predicted ID Liner Wall Temperatures of Concept II at the Sea-Level, Hot-Day Maximum Power Point.

this sector as explained in Section V.B.2. Similar behavior is predicted for the outer liner wall upstream of the dilution orifices, as shown in Figure 135. The prediction for the x-y planes in line with θ = 9 and 18 degrees are in good agreement with the data.
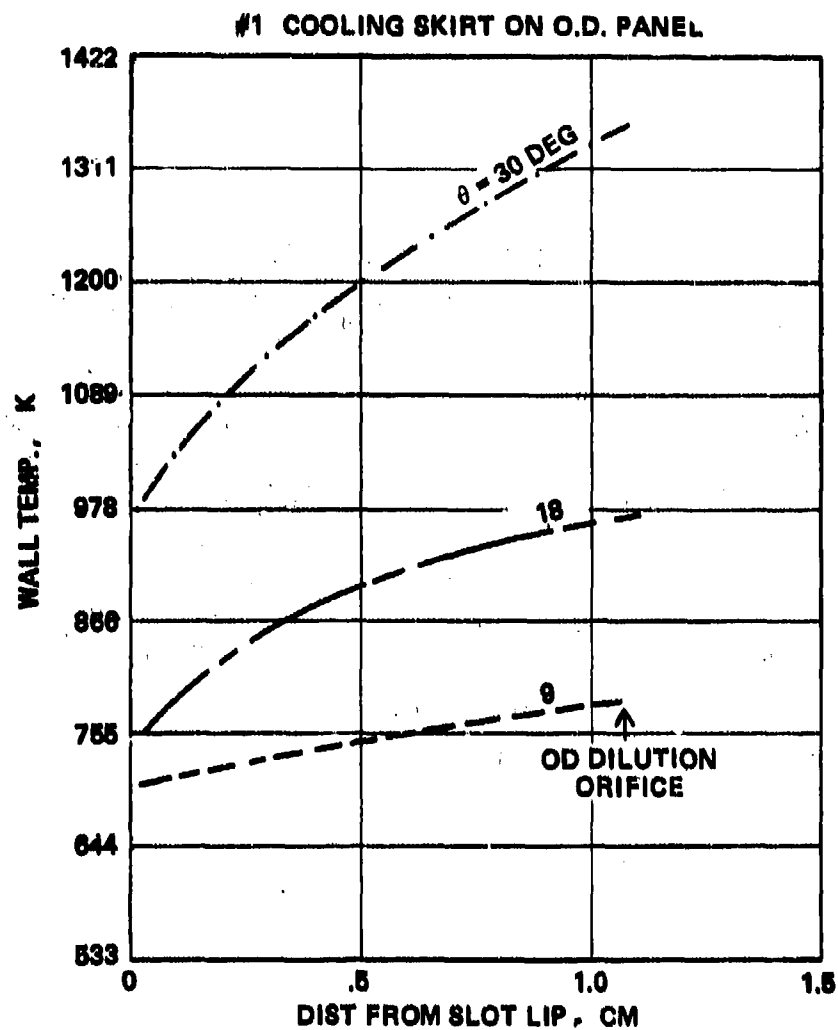
Figure 135. Predicted OD Liner Wall Temperature of Concept II Outer Dilution Panel.

VI. CONCLUSIONS

The following six combustor analytical models that were formulated and validated through element tests in Task I were utilized in conjunction with empirical design procedures to design, fabricate and develop two annular reverse flow combustor concepts in Tasks II and III.

- Annulus flow model
- 3-D combustor performance model
- Wall cooling model
- Transition mixing model
- 2-D emissions model
- Fuel insertion model

The models were not only used as aids in determining the optimum design for each of the two concepts but also were used to make predictions of combustor performance. The success of the input provided by the models to the design/development process was proven by the fact that the two concepts, which were significantly different in design, met all the performance goals in much less time and hence cost less than the traditional empirical process. Concept 1 required no design modifications from the baseline and Concept 2 required only one modification to meet all of the program goals. Both concepts were thoroughly evaluated for performance with Concept I undergoing complete performance mapping in cyclic durability evaluation. The model predictions were in good agreement with the measured and derived test data taken for each concept.

Based upon the test results obtained in Task II and III, the following general conclusions can be made.

235

- The six analytical models as formulated, validated, and updated offer useful tools to be used in conjunction with established combustion design methods for the design and development process of turbopropulsion combustors.

- The correlation between model predictions and test measurements is generally good.

- The models have the ability to handle both can and annular combustors of various geometries.

- While the state of development for the models is considered good for a first step, increased usage and reliance will require additional updating and improvements.

- The success of the models is evident in this program through the successful attainment of all design goals in a maximum of one major design iteration for two different concepts. This is certainly promising in light of the intended objective of reducing the time and cost associated with the development of gas turbine combustion systems.

- At this stage of development, the models provide excellent design aids but must be used carefully by the design test engineer in conjunction with traditional empirical methods.

SECTION H-H

237

SECTION AA-AA

CHAMBER ASSEMBLY,
COMBUSTION

3551611

2

239

DETAIL OF

VIEW V

2

244

CHAMBER ASSEMBLY,
COMBUSTION

3581512

SECTION N-N

SECT ON M-M

VIEW V
SCALE 2/1

VIEW L
SCALE 2/1

VIEW K
SCALE 2/1

SECTION T-T

SECTION U-U

VIEW P-P
SCALE 2/1

VIEW **J - J**

SECTION K-K

COMBUSTION CHAMBER-
PLENUM

3551513

2

VIEW F-F

.491-.487 DIA THRU
.810-.830 X 82° DIA
THREAD 1/4 ANPT PER SPEC MIL-P-7105
15 HOLES EQUALLY SPACED

H-H

.766-.747 DIA THRU
10 HOLES EQUALLY SPACED

N

W M-M

TAP DRILL .81-.83 DEEP
1/4-28 UNJF-3B THD
.65 MIN FULL THREAD
5 HOLES

SECTION N-N

3551513

LINER, TRANSITION, INNER

3551522

.044-.049 DIA THRU
20 HOLES
EQUALLY SPACED

.168-.173 DIA THRU
84 HOLES
EQUALLY SPACED

LE REF

TYP

VIEW D

	COOLING SKIRT	HAYNES
	COOLING SKIRT	HAYNES
	FLANGE	HAYNES
	PLATE NUT	HAYNES
	FLANGE	HAYNES
	LINER	HAYNES

OUTER TRANSITION
LINER

355 527

SECTION C-C

6. MAY BE TACK WELDED FOR ASSEMBLY
   PURPOSES PER AIRESEARCH N83 5040

5. APPLY PART NO PER AIRESEARCH MC5014, CL II A

4. 125/ ALL OVER

3. BRAZE PER AIRESEARCH WPS 5027 USING
   BRAZING ALLOY PER AIRESEARCH EMS 54752 TYPE II

1. SHALL CONFORM TO AIRESEARCH /
   SEG001 MACHINED FEATURES

253

1841-79

SECTION I)-I)

.23
.21

.050 8 PLACES
.040

DRAIN 1/240 TOTAL

3551540

| | | RING · INNER | CRES 347 AMS 5646 | |
| | | RING · OUTER | CRES 347 AMS 5646 | |

PARTS LIST

AXIAL SWIRLER

| D | 99193 | 3551540 |